UNIVERSIDAD DE GRANADA

Tesis doctoral

Diciembre 2011

Calibration, Characterization and Analysis of the ALHAMBRA Photometric System

[PhD THESIS]

Teresa Aparicio Villegas

Instituto de Astrofísica de Andalucía (CSIC)

Memoria de Tesis

presentada en la Universidad de Granada

para optar al grado de Doctor en Física

Directores de tesis:

Emilio J. Alfaro Navarro

Mariano Moles Villamate

Editor: Editorial de la Universidad de Granada
Autor: Teresa Aparicio Villegas
D.L.: GR 1732-2012
ISBN: 978-84-9028-042-3

A mis dos Pepes.

Los sueños no desaparecen
siempre que las personas no los abandonan.

- Anónimo -

Las matemáticas son el alfabeto
con el cual Dios ha escrito el Universo.

- Galileo Galilei -

Agradecimientos

Esta Tesis la he realizado rodeada de una gran cantidad de gente que me ha apoyado y ayudado a que se haga posible, por lo cual me siento enormemnete afortunada.

No tengo ninguna duda de que a los primeros que he de agradecerles algo es a mis padres. Aparte de darme la vida y educarme bajo los mejores valores humanos, Teresa y Manolo han sido, son y serán el pilar al que aferrarme en cada paso que doy en mi vida. Generosos, comprensivos, cariñosos y sobretodo, ellos son mis primeros fanes, pues haga lo que haga su orgullo hacia mi me alienta y empuja a seguir alcanzando metas que superar en mi vida. Os quiero y agradezco todo lo que habeis hecho por mi, y espero que de alguna manera os pueda corresponder (siempre lo intento).

Aparte de mis padres, mi familia en general es un gran arbol que siempre me da cobijo. Mi hermano Manolo, que recientemente me ha hecho tita junto con mi adorable cuñada, la Raquel. Chico te agradezco que siempre esteis ahí, que me regañeis cuando me equivoco y me apoyeis cuando tambaleo, además te agradezco muchísimo las llamadas que me has hecho esas mañanas que con miedo a que el cansancio me ganara te pedía que me despertasen, no hay mejor muestra de amor de hermano, y yo también te quiero a ti y a tu nueva familia. Pepe, Rosa, Jesús, Magdalena, Inocencio entro otros tíos y todos mis primos más cercanos, gracias por apoyarme y hacerme sentir tan querida. Y cómo no a mi abuela Lola de 98 años que cada vez que me ve desde hace un año me pregunta cuándo voy a leer la tesis y se emociona de pensar que su nieta va a ser "Doctora", esta tesis también es para ti.

Gracias a Gala, mi compañera incondicional, aquella que me esperaba en casa siempre dándome alegría y amor en todo momento, los malos y los buenos. Ella me ha hecho levantarme más de una mañana cuando las fuerzas me fallaban, me ha limpiado las lágrimas cuando he estado triste, cuando me he sentido sola ella siempre estaba allí, y cuando cantaba de alegría era la primera que bailaba conmigo. Y aunque no sepa leer estas palabras, sé que siempre se sentirá gratamente agradecida por mi parte, esa es la grandeza de los animales.

Doy las gracias a mis dos directores de tesis, Emilio y Mariano, primero por darme la oportunidad de ser becada para realizar una tesis doctoral con vosotros. En especial agradezco a Emilio, con el cual he tenido un trato más directo. Sé que todo lo que has hecho lo has hecho pensando en mi futuro profesional y en la ciencia, eres un ejemplo de científico involucrado, trabajador y fascinado por la Astrofísica, además te has preocupado en introducirme en el mundo científico en general y en el mundo de la fotometría en particular de forma gratuita con la finalidad de poder volar sóla tras la tesis, te lo agradezco muchísimo. Gracias a ambos por la confianza depositada en mi.

Y si tengo algo a mi alrededor, eso es buena gente y buenos amigos. No voy a poder nombrar a todos pero resaltaré algunos que es imposible no nombrarlos. El IAA está lleno de grandes científicos pero también de grandes personas. Mi equipo 547 que me ha sufrido todo este tiempo y también se han reido mucho conmigo; Yoli, siempre me has ayudado desinteresadamente, me has escuchado cuando lo he necesitado y has sido un gran apoyo en muchos momentos, gracias; Gabi, la templanza mejicana, me has dado cariño y consejo, también un gran apoyo que nunca

olvidaré; Domi, esa polaca con una gran sonrisa en la cara, transmites alegría y frescura, gracias también por estar allí. Sois las tres unas bellísimas personas por dentro y por fuera, os echaré de menos. Los radical fruit company, Charly, Dani, Marta y Darío, a cual más especial, me habeis hecho pasar grandes momentos en el instituto y fuera de él, y de veras espero que no se terminen. Beni y Rafa y la nueva incorporación de los chicos "Ubuntu", gracias también por ayudarme siempre con tanta rapidez y efectividad en mis numerosos problemillas informáticos pero sobretodo por esa alegría que me dais siempre, me habeis hecho sentir muy querida y creo también que sois bellísimas personas (Fdo: la chaci). Paco, nuestro Paco, gracias por todas las golosinas y pasteles que nos has acercado al despacho, es una alegría llegar a tu lugar de trabajo y encontrarte allí a alguien tan adorable como tu.

Fuera del instituto también han estado rodeándome, cuidándome y animándome muy buenos amigos; el grupo de los cenutrios, mi buena amiga Gema, grande como ella misma, Oscar el "tóterreno", un gran pequeño hombre, Sergio y Lauri. Inma, mi "amiga del alma", incondicional, y tan especial. Romi, mi ejemplo a seguir en los años. Dani, mi compañero y amigo para siempre. Gracias chicos, vosotros también lo habeis hecho posible. Y muchos otros, Rubén y Susana, Moni, Carmencilla, Mare, Janilla, Manolico, Emma (mi prima)... Gracias a todos.

También agradezco haber trabajado con un grupo de gente tan válida como es el equipo ALHAMBRA. Especial gracias a César y Alberto Molino que me han ayudado y apoyado siempre. Txitxo, Jaime y Chony, Isabel, Pepa, Alberto Fernandez, Jordi, Miguel, Javier entre muchos otros, gracias por hacerme sentir parte de un proyecto tan importante.

Agradezco también a los dos grupos de la misión Gaia con los que he trabajado. En Barcelona, Carme y Carrasco, y en Heidelberg, Coryn, Vivi, Kester, Chao y Rainer. Gracias por acogerme en vuestros centros haciéndome sentir tan agusto, y enseñándome tantas cosas.

También tengo que agradecer haber formado parte del Grupo de Sistemas Estelares. Antonio, Rainer, Meme, Tere, Mayte, Alfredo, Miguel, Nestor, Jesús, y las nuevas incorporaciones. Un gran grupo de trabajo y de personas.

Agradecer cómo no a la Universidad de Granada por permitirme doctorarme en ella, al Ministerio de Educación y Ciencia por concederme la beca, y al CSIC por apoyar y desarrollar centros de investigación como éste.

Y creo que ya está aunque seguro me olvido de alguien, espero me perdoneis en tal caso. En general me he sentido muy agradecida por muchos motivos durante estos 4 años y eso siempre es algo de agradecerle a esta vida.

Resumen

Esta tesis no versa sobre un objeto celeste concreto, ni sobre un instrumento astronómico, ni siquiera sobre un telescopio, versa sobre un objeto singular a caballo ente el concepto y el hecho, trata sobre un sistema fotométrico único: el sistema fotométrico ALHAMBRA.

Creo que hay pocos estudiantes de doctorado que hayan tenido la oportunidad, no de aplicar un sistema fotométrico a un problema astronómico particular, sino de estudiar el propio sistema, caracterizarlo, establecer su calibración en flujo, la comparación con otros sistemas fotométricos y analizar su capacidad para conocer las propiedades físicas de los objetos estelares y del medio interestelar que ha atravesado su luz hasta llegar a nosotros. Pues bien, éstos son los objetivos de la tesis que ahora presento y yo he tenido la fortuna de realizar este trabajo.

El sistema fotométrico ALHAMBRA está constituido por el conjunto de 20 filtros contiguos de banda media, con una anchura similar para todos los filtros de unos 300Å, y que cubren el rango espectral desde 3500Å hasta 9700Å, más los tres clásicos filtros de banda ancha (J, H, Ks) que cubren el rango del infrarrojo cercano hasta 2.2 micras. En este trabajo nos limitamos al análisis del rango óptico. La memoria de la tesis se ha dividido en cuatro capítulos más unas conclusiones.

En el primer capítulo que sirve de introducción al estudio, se introduce el concepto de sistema fotométrico y se repasan las características y propiedades de los más señalados hasta llegar al sistema fotométrico en estudio. Es al comienzo del segundo capítulo donde se describen más ampliamente los objetivos científicos del proyecto ALHAMBRA y cómo en base a estos se diseñó el sistema que ahora estudiamos.

El capítulo segundo está dedicado a la caracterización del sistema fotométrico. Después de una breve compilación de los conceptos básicos de la radiación estelar y su medida, definimos los estimadores de primer y segundo orden de las respuestas del sistema atmósfera+filtro+detector y los calculamos para las cuatro realizaciones de ALHAMBRA. Realizamos una comparación de los mismos y establecemos una definición del sistema en función de una curva de respuesta. A continuación se detalla el conjunto de estrellas estándares seleccionadas y se establece una estrategia de calibración en flujo.

Las ecuaciones de transformación entre el sistema ALHAMBRA y otros sistemas fotométricos se presentan en el capítulo tres. En particular analizamos las relaciones entre ALHAMBRA y Sloan y ALHAMBRA y Gaia. Sloan es el sistema fotométrico en el que se basó el cartografiado SDSS (Sloan Digital Sky Survey) y de gran difusión actual, por el contrario el sistema fotométrico de la misión Gaia es algo por venir, pero que se lleva diseñando y analizando desde hace una década y con el que se obtendrá el mayor catálogo estelar jamás conocido.

La última parte de la memoria de tesis (capítulo 4) analiza las posibilidades que ofrece el sistema fotométrico ALHAMBRA para realizar clasificaciones espectrales y determinar los principales parámetros físicos de las estrellas, tanto internos como externos (T_{eff}, $log(g)$, $[Fe/H]$ y E_{B-V}). Aunque los objetivos científicos del cartografiado sean puramente extragalácticos, se obtendrá también una importante muestra de las poblaciones estelares galácticas. Así, resulta evidente el interés de analizar la capacidad de los "espectros" de baja resolución ALHAMBRA

para obtener estas cuatro variables estelares. Primeramente analizamos el diagrama Q,Q (combinación de colores libre de enrojecimiento) y el diagrama color-color que mejor proporcionan una clasificación espectral preliminar de la población estelar. La construcción de los parámetros Q, lleva implícita el uso de una determinada ley de enrojecimiento interestelar, la elección de tres diferentes conjuntos de datos estelares y la comparación de sus posiciones relativas en el espacio Q,Q nos llevan a elegir la ley que mejor se comporta en este contexto. A continuación analizamos la determinación de los parámetros físicos a partir de relaciones funcionales entre colores, para finalmente proponer una metodología basada en la comparación directa de los 18 Qs consecutivos observables con los derivados de los modelos. Una metodología sugerida por el propio concepto de espectrofotometría. Finalmente se aplica este método a una muestra del catálogo ALHAMBRA.

Las conclusiones y líneas de desarrollo futuro forman el quinto y último capítulo.

Summary

This thesis deals neither with a specific celestial object, nor with an astronomical instrument, nor even with a telescope, but with a singular object halfway between concept and fact, that is, with a unique photometric system: the ALHAMBRA photometric system.

I believe that there are few doctoral students who have had the opportunity, not of applying a photometric system to a particular problem, but of studying the system itself, of characterizing it, establishing its flux calibration, comparing it with other photometric systems, and analyzing its capacity to recognize the physical properties of stellar objects and the interstellar medium that its light has travelled to reach us. So, these are the aims of the thesis that I now present and that I have had the fortune to work on.

The ALHAMBRA photometric system is constituted by the set of 20 contiguous filters of medium bandwidth, with a similar width for all of the filters of around 300Å, and which cover the spectral range from 3500Å up to 9700Å, plus the three classic broad band filters (J, H, Ks) that cover the near infrared range up to 2.2 microns. This work is limited to the analysis of the optical range. The dissertation has been divided into four chapters and a conclusion.

In the first chapter, which serves as an introduction to the study, the concept of the photometric system is introduced, and the characteristics and properties of the most distinguished systems are looked at before arriving at the photometric system under study. It is at the beginning of the second chapter where the scientific objectives of the ALHAMBRA project are described more fully and how, based on these aims, the system was designed.

The second chapter is dedicated to the characterization of the photometric system. After a brief compilation of the basic concepts of stellar radiation and its measurement, we define first- and second-order moments of the atmosphere+filter+detector system responses, and we calculate them for the four ALHAMBRA versions. We carry out a comparison of these and establish a system definition based on a response curve. Then the set of selected standard stars is examined in detail and a flux calibration strategy is ascertained.

The transformation equations between the ALHAMBRA system and other photometric systems are presented in chapter three. In particular we analyze the relations between ALHAMBRA and Sloan, and ALHAMBRA and Gaia. Sloan is the photometric system on which the SDSS (Sloan Digital Sky Survey) is based and is now widespread, whereas the Gaia mission photometric system is still to come, although it has been under design and analysis for more than a decade and upon completion it will provide the largest stellar catalogue ever known.

The last part of the thesis dissertation (chapter 4) analyzes the possibilities that the ALHAMBRA photometric system offers for performing spectral classifications and for determining the principal physical parameters of stars, both internal and external (T_{eff}, $log(g)$, $[Fe/H]$ y E_{B-V}). Although the scientific aims of the mapping survey are purely extragalactic, an important sample of galactic stellar populations will also be obtained. Thus it is evidently of interest to analyze the capacity of the ALHAMBRA low resolution "spectra" to obtain these four stellar variables. Firstly we analyze the Q,Q diagram (reddening-free combination of colors) and the color-color diagram that provides a better preliminary spectral classification of the stellar pop-

ulation. Implicit in the construction of the Q parameters is the use of a determined interstellar reddening law, the choice of three different sets of stellar data, and the comparison of their relative positions in the Q,Q space leads us to choose the law that behaves best in this context. Next we analyze the determining of the physical parameters based on the functional relations between colors, so as finally to propose a methodology based on the direct comparison of the 18 consecutive Qs observable with those derived from the models: a methodology suggested by the very concept of spectrophotometry. Finally this method is applied to a sample from the ALHAMBRA catalogue.

The conclusions and future lines of development form the fifth and last chapter.

Index

1

Introduction

For many centuries the magnitude of a star together with its coordinates have allowed the identification of the stars in the celestial sphere. The first scale of luminosity of the stars was established by the Greek astronomer and mathematician Hipparchus (190 - 120 BC), who ranked the stellar objects in six degrees or magnitude classes according to their brightness, similar to that used today. The brightest stars were assigned a magnitude of 1, the next brightest magnitude 2, and so on to the faintest stars just visible to the unaided eye, which were magnitude 6. He also elaborated the first stellar catalogue with the positions of approximately 850 stars in ecliptic coordinates. However, not until the beginning of the 20th century did astronomers begin to understand that the radiation of celestial objects entails information, not only of the physical nature of the emitter, but also about the properties of the medium that the light passes through between the emitter and the observer. For example, the comparison of the intensity of radiation of an unreddened star in two different regions of the spectrum can provide its temperature. Thus, photometry in several bands gives a quantitative estimation of the spectral distribution of the stars, providing a number of parameters (color indexes or combination of them) which correlate well with the physical quantities describing the energy distribution according to the theory of stellar atmospheres.

A photometric system is defined with a set of filters corresponding to different wavelength ranges, able to the measure absolute fluxes, from which particular properties (such as temperature, gravity, and metallicity) of the emitting objects can be inferred. The first attempts at defining a photometric system that provides a spectral classification of stars led to the need to measure in at least three spectral bands, since the fundamental deviations of the stellar radiation from a Black Body (i.e. the Balmer jump, a depression in the intensity of the continuous spectrum at about 3650Å caused by hydrogen absorption lines, related to the surface temperature of a star) can be determined quantitatively by making use of at least two colors (a color is defined as the difference of two bands measured in magnitudes). The need of incrementing the spectral information, and therefore the discriminant capacity of the photometric system, has led to the increase of the spectral bands and the narrowing of their wavelength range. The result has been a great variety of photometric systems for charac-

terizing and classifying stars. An exhaustive list of photometric systems can be found on the Asiago database on photometric systems (Moro and Munari 2000, Fiorucci and Munari 2002), accessible at the web page `http://ulisse.pd.astro.it/Astro/ADPS/`, or The General Catalogue of Photometric Data (GCPD, Hauck et al. 1990), accessible at the web page `http://obswww.unige.ch/gcpd/gcpd.html`. An explanation of the history and utility of the most relevant photometric systems can be found in Bessell (2005).

Depending on the width of the different bands, the photometric systems are usually classified as: narrow band photometry, with a bandwidth lower than 90Å; intermediate-band photometry, with a bandwidth between 90Å and 300Å; and wide-band photometry with a bandwidth greater than 300Å and lower than 10,000Å. The term of "ultra-broad band" has come to denote those systems with passbands wider than 10,000Å. Each one of these kinds of photometric system has the capacity to determine certain physical properties of the stars, being more effective in a particular range of temperatures and luminosities, and most of them have the capacity of determining and correct from interstellar extinction effects. Another kind of classification of the photometric systems relates to whether they are closed or open. An open system is one whose originators encourage others to duplicate the passbands and detector system and to use the originator's standard stars and reduction system for their photometric programs. A closed system is one where a small group of people control the instrumentation and data reduction and only encourage others to use the results but not to attempt to duplicate the system and observe stars for themselves. For obvious reasons, systematic errors and the data quality are better controlled in a closed system than in an open system. In the past, the main disadvantage of a closed system was that your particular star of interest was often not in the catalog. However, with the advent of large-scale sky surveys to faint magnitudes, it is likely that, photometry for most objects of interest will be provided by closed photometric systems.

One of the earliest and most used photometric systems is the photoelectric UBV system (Johnson & Morgan, 1953). This is a broad-band open system consisting of three bands established especially for the photometric study of stars that are classified in the MK system (two-dimensional classification scheme based on spectral lines sensitive to stellar temperature and surface gravity, which is related to luminosity). The B band was devised to approximate the photographic magnitude, the V band to approximate the visual magnitude, and the system was completed with an ultraviolet magnitude U in order to include the spectral region of the Balmer jump. The transmission curves of the filters are represented in Figure 1.1 and their central wavelengths and the Full Width at Half Maximum (FWHM) of each one are shown below:

Filter	λ_c (nm)	FWHM (nm)
U	358	55
B	439	99
V	545	85

The UBV system was originated with the cooled blue sensitive RCA 1P21 photomultiplier

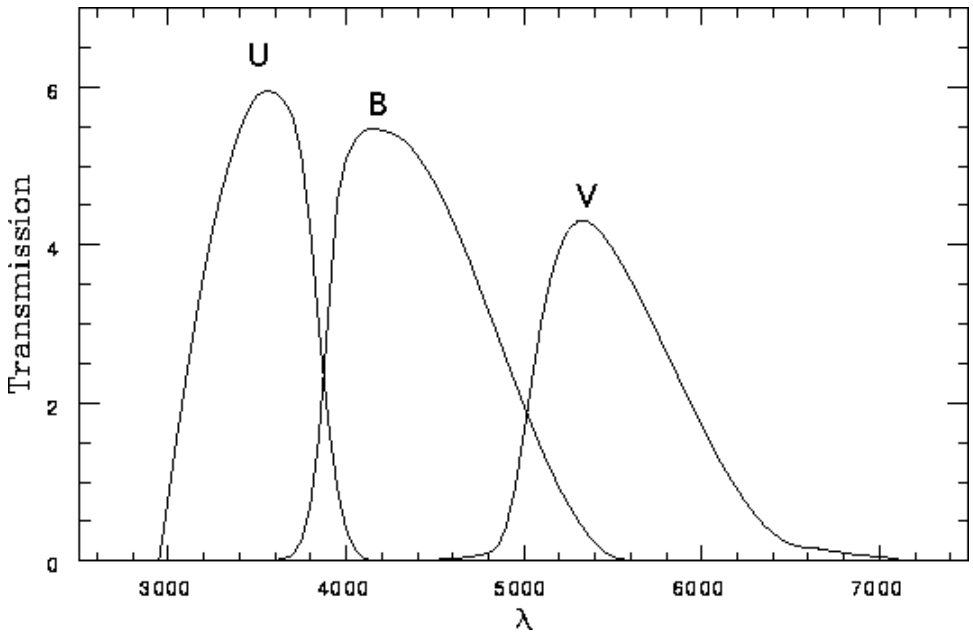

Figure 1.1 Response function in wavelength (Å) of the UBV system. Figure extracted from the GCPD, adapted from Johnson & Morgan(1951).

tube, and although the B and V bands have been well duplicated using redder and more sensitive detectors, the U band has provided difficulties, since the system of U magnitudes depends on zenith distance, on atmospheric transparency and on the observatory latitude.

The color-color diagram formed by the two correlative colors of the system, U-B versus B-V diagram, has been used to distinguish dwarf main-sequence stars, reddened OB stars, weak-line (halo) FG-type stars and evolved K giants. It has also been used for estimation of absolute magnitudes or gravities of solar chemical composition stars with a T_{eff} between 5500 and 8000K (A7-G2 stars). The B-V color was normally used to derive temperature; however, for OB stars the Q method or intrinsic U-B color has obtained better results. The Q method is an excellent technique for correcting for interstellar reddening in OB-type stars. This parameter was introduced by Johnson & Morgan(1953) with the following relation:

$$Q = (U - B) - 0.72(B - V) \tag{1.1}$$

where 0.72 is the value of the slope of the reddening line in the U-B, B-V diagram. Johnson(1958) also established the following relation between the reddening-free Q-parameter and the intrinsic B-V color:

$$(B - V)_0 = -0.009 + 0.337Q \tag{1.2}$$

One disadvantage of the UBV system is the fact that for FGK stars, B-V is sensitive to temperature, metallicity and effective gravity, whereas U-B is sensitive to metallicity and effective gravity, and so the calibration of the diagram in T_{eff} and $log(g)$ depends on metallicity.

This system has remained in use up to the present since it has been used in many astrophysical studies and also for the importance in some analyses of being able to compare measurements through time. However, the choice of the filters was not mainly based on the astrophysical prop-

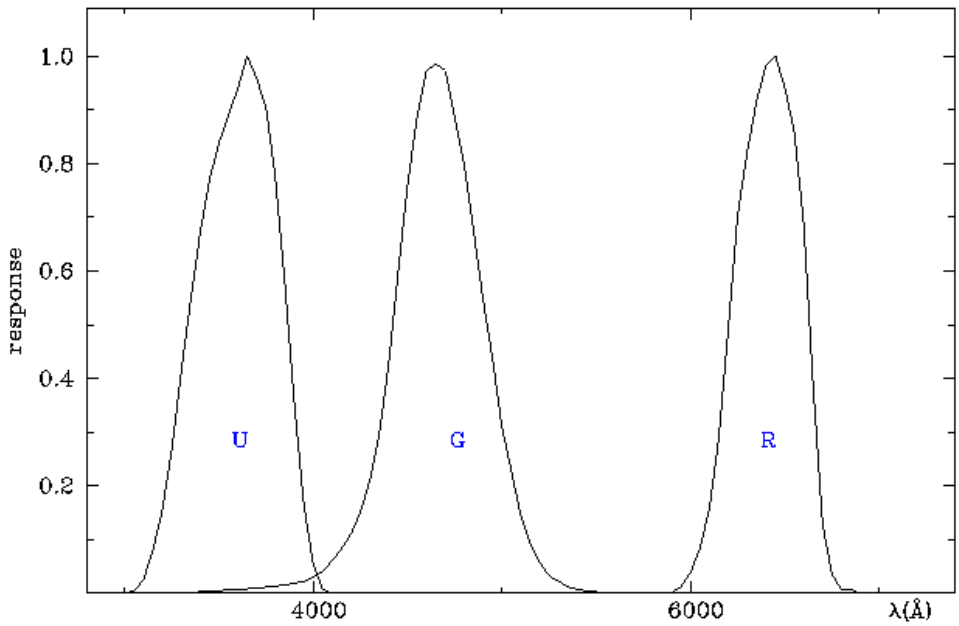

Figure 1.2 Response function in wavelength (Å) of the RGU system. Figure extracted from the Asiago database.

erties of the observed objects but on the availability of glasses to build those filters. In fact, the first photometric system for which bands were selected based only on the properties of the emitters was the RGU photometric system (Becker 1946). This is a broad-band system, photographically defined and specially designed for the study of a high number of weak stars, which allows deep penetration at galactic scales. The bands were selected taking into account the energy distribution in the stellar spectra and the interstellar extinction law. The transmission curves are shown in Figure 1.2, and they have the following central wavelengths and FWHM:

Filter	λ_c (nm)	FWHM (nm)
U	360	53.5
G	467	50
R	641.8	43

Becker was the first to apply a three-color photometry in the study of open clusters. He developed a new method for determining cluster reddening and photometric distances (Becker, 1951). He also suggested a "color-difference" method which is a prototype of the current Q method. Conversely, the G-R index is less sensitive that the B-V index in estimating chemical compositions, since the G filter avoids the 4000-4500Å interval that always contains lines and absorption bands. But, the U-G index appears to be rather more sensitive than the U-B to differences between the energy distributions of a dwarf and a giant, and so the RGU system offers a better separation of the cold giants. However, although the RGU system has been proved to be very effective in the research of galactic structure, this system was from the very beginning a purely photographic system since photoelectric realization of the red magnitude was found to be difficult, and so its application was subordinated to the existence of a sequence of standard stars measured in a photoelectric system, which was usually the UBV system.

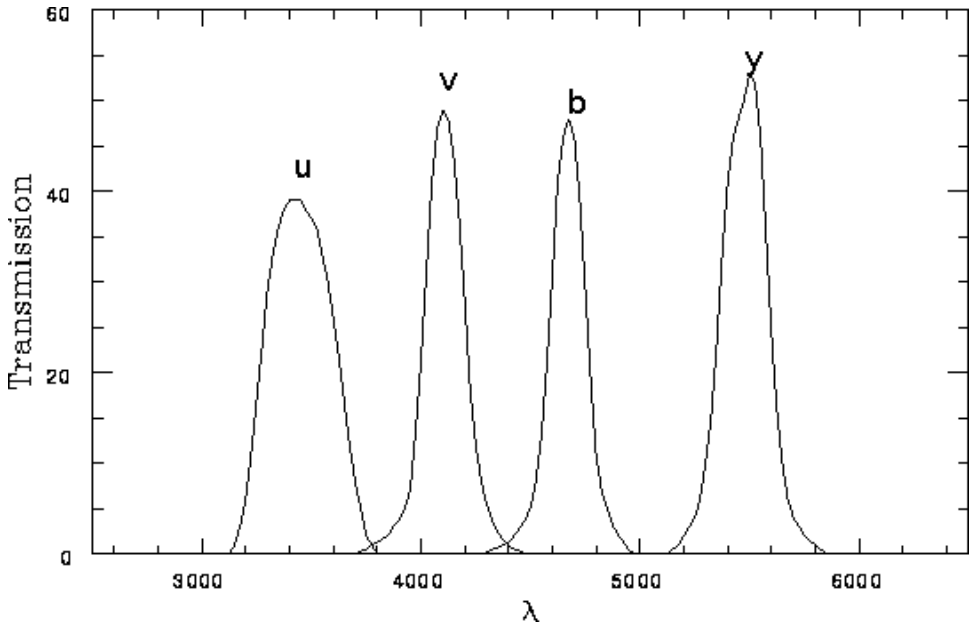

Figure 1.3 Response function in wavelength (Å) of the *uvby* system. Figure extracted from the GCPD, adapted from Crawford & Barnes(1970).

With the appearance of the photomultiplier 1P21 in the mid-1940s, apart from the Johnson & Morgan system, other photoelectric systems emerged, most of them with a selection of the filters based on the properties of the emitter. One of these systems was the devised in 1951 by Strömgren, the open intermediate-band *uvby* system. This set of filters was built specifically in order to characterize B, A and F stars, in particular the measurement of the Balmer line, the metallicity and the effective temperature. The narrower passbands are designed to better determine the Paschen slope, the Balmer jump, and metal-line blanketing, and they do not overlap, unlike the UBV bands. The main characteristics of the filters are in the table below and Figure 1.3 shows their transmission curves.

Filter	λ_c (nm)	FWHM (nm)
u	350	30
v	411	19
b	467	18
y	547	23

The u filter is located in wavelengths lower than the Balmer Jump; the v filter is located in a region with a lot of absorption due to metallic lines and so it is very useful for chemical composition estimations; the b filter is less affected by the metallic elements than the Johnson B, and y is centered as the Johnson V, but it has a narrower bandwidth, so, b-y is a color like B-V but less sensitive to metallicity. The bandwidths adopted are such that the reddening lines are practically straight lines whose slopes only depend upon the interstellar extinction law adopted. Reddening is often better measured through *uvby* photometry than UBV photometry, although for O and B stars the UBV reddening-free Q index is still a powerful tool. To these four filters the reddening-free index $\beta = \beta_w - \beta_n$ was added, which measures the strength of

the Hβ line, in order to obtain luminosities of B stars and to be able to estimate temperatures of late A-type stars, and early FG-type stars.

Some of its indexes are well-known to be related to the different physical parameters, such as:

- $(b-y)_0$ index is particularly insensitive to the abundance of lines in the spectrum and thus provides a sensitive temperature measure for F, G and K stars.

- $c_1 = (u-v) - (v-y)$ is designed to measure the Balmer discontinuity and it is a temperature indicator for B, A type-stars and a surface gravity indicator for late-type stars.

- $m_1 = (v-b) - (b-y)$ is designed to measure the depression owing to metal lines around 4100Å, and so to measure the total intensity of the metal lines in the v band, being especially sensitive to metallicity.

Also reddening-free parameters are used for stellar calibration, such as,

- β, which is a measure of the equivalent width of Hβ, it is a luminosity indicator for O-A stars, and a temperature indicator for A-G stars.

- [u-b] = (u-b) - 1.84(b-y), (Strömgrem 1966), which is a widely used photometric index for the determination of T_{eff} for normal hot stars ($T_{eff} \gtrsim 9500K$) and it is also used for temperature calibrations for Ap stars.

- $[m_1] = m_1 + 0.18$(b-y) and $[c_1] = c_1$ - 0.20(b-y), defined by Strömgren (1966), form a 2D plane widely used for spectral stellar classification. In particular, $[c_1]$ remains an indicator of the Balmer discontinuity.

This photometric system has been highly successful and is in widespread use. Numerous diagrams and calibration equations with these indexes, enable good stellar classifications and physical parameter estimations. An example is the study of halo stars developed by Schuster et al. (2004), where the c_1 versus $b-y$ diagram is used to readily distinguish dwarfs, subgiants, horizontal branch stars and sdOB stars. It has been extended to white dwarfs, K giants and dwarfs, and FGK supergiants but, unfortunately, the width and position of the u and v bands used by different observers have not been the same as those of the original system. This and the restricted color, reddening, and spectral-type range of the original standards, have introduced systematic differences in photometry for stars of different metallicities and luminosities.

Another important medium-band photoelectric system for stellar classification has been the medium-band UPXYZVTS Vilnius photometric system developed by Straižys & Zdanavicius (1965). The Vilnius system is intended for a two-dimensional spectral classification and quantification of stars over the whole stellar temperature range, with interstellar reddening present. Straižys (1963) aimed to select an optimum multicolor system capable of classifying stars of any spectral type, luminosity class, and reddening. The bandpasses were selected based on

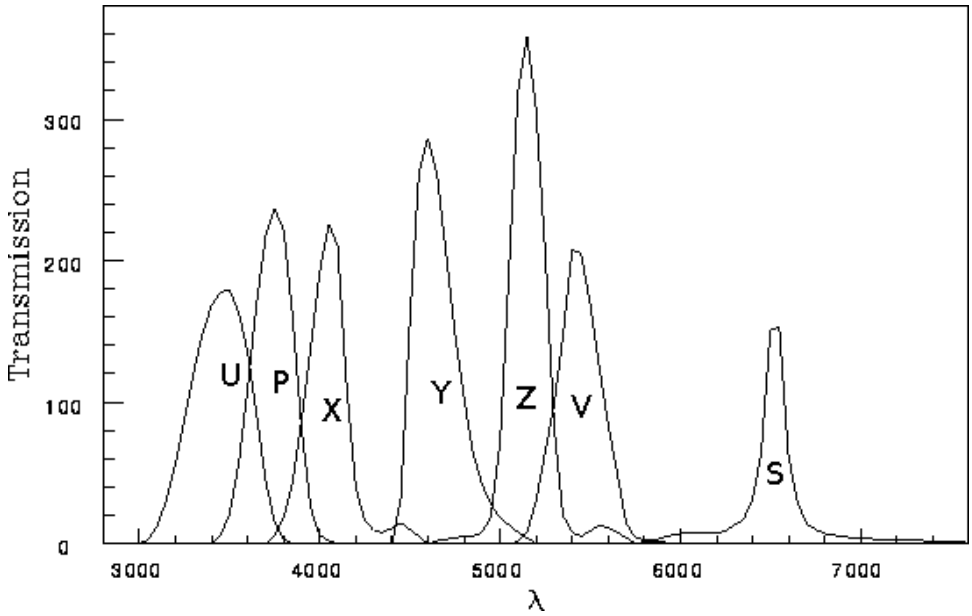

Figure 1.4 Response function in wavelength (Å) of the UPXYZVS system. Figure extracted from the GCPD, adapted from Straižys & Zdanavicius(1970).

spectral energy distribution (SED) of stars of different types and on interstellar extinction law, and making use of synthetic colors and Q, Q diagrams to analyze the relations with the diverse physical stellar parameters. A medium-band filter system was chosen to ensure the possibility of measuring faint stars, since the narrow-band photometric systems are more informative, but their limiting magnitude is too bright for the objectives. Finally the system was formed by eight bands, the transmissions of which are represented in Figure 1.4, and they have the following central wavelengths and FWHM:

Filter	λ_c (nm)	FWHM (nm)
U	345	40
P	374	26
X	405	22
Y	466	26
Z	516	21
V	544	26
T	625	22
S	656	20

For two-dimensional classification of early-type stars the UPXYZ (or V) bandpasses have sufficient information, whereas for late-type star classification the use of the XYZTS bandpasses is enough. T can be omitted if the M-type stars are known, since T is a bandpass within the Ti0 absorption band, and is essentially only for detection of M-type stars or early subclasses. See Straižys (1992) for more detail of the different bands. With the different Q, Q diagrams derived from these bands, it is possible to develop a more complete stellar classification distinguishing all spectral types and most luminosity classes, and deriving peculiarities in reddening and

composition, for instance, the Q_{UPY}, Q_{PYV} diagram is used for photometric classification of B-type stars of solar chemical composition, in spectral types and luminosities. Compared with the Strömgren system, the Vilnius system extends its capacities to cooler spectral types and can detect peculiar stars.

The narrow-band photometric systems are able to obtain more detailed information about the conditions of the stellar atmospheres, however the amount of luminosity received through the narrow filters is very low and as a consequence these systems are only useful for studying bright stars. An example of this kind of system, is the Wing photoelectric system (Wing, 1971), which consists of eight narrow filters in the near-infrared spectral region, developed to classify late-type stars, especially M-type stars and carbon stars. The bandpasses have widths between 40-70Å, and the features measured by each of them are specified on the table below, together with their central wavelengths and FWHMs (the response functions of the system were not published):

Filter	λ_c (nm)	FWHM (nm)	Feature	Contamination
71	711.7	5.3	TiO	CN
75	754.5	5	Continuum (M0-M7)	CN, VO
78	780.6	4.2	Continuum (G,K,C)	TiO
81	812.2	4.3	CN	TiO
104	1039.2	5.5	Continuum	
105	1054.4	5.8	VO	
108	1080	7.4	Continuum (C)	HeI
109	1096.8	7.3	CN	

The system makes it possible to distinguish between oxygen-rich and carbon-rich stars, and to determine temperatures, spectral types, and luminosity classes of M-type giants, supergiants, and dwarfs. Observations of the bands and continuum colors were used to derive abundances for metal-rich globular clusters (Mould & Siegel 1982) and for studies of M supergiants in two-dimensional classifications (White & Wing 1978) among numerous studies of M-type stars. More recently, calibrations of late M dwarfs have been made using IDS and CCD spectrophotometry (Bessel, 1991).

Over the years, the photoelectric photometer, which measured the light intensity of a single object by directing its light on to a photosensitive cell, has largely been replaced with charge-coupled devices (CCD) cameras, which appeared for the first time in the mid-1970s, and which can image multiple objects simultaneously. With the multiband photometry and the use of wide-field two-dimensional detectors, the SED for a high number of celestial objects can be obtained, the photometric redshifts (z) of quasars (QSOs) and galaxies can be measured, or it is also possible to classify galaxies or other kinds of more exotic objects. Thus photometric systems have become a very powerful tool for dealing with a great quantity of astrophysical problems. Furthermore, nowadays extragalactic Astronomy and Cosmology are immersed in a

transition period, with large observational projects, involving many scientists, gaining increasing importance. This implies that the criteria of band selection for the photometric systems used in the surveys have changed from criteria based on stellar atmospheres to objectives more focused on obtaining accurate estimations of redshifts and precise classifications of galaxies, in order to study the large-scale structure of the Universe. The multi-filter imaging and spectroscopic redshift Sloan Digital Sky Survey (SDSS, Fukugita et al. 1996; Smith et al. 2002), with five non-overlapping wide bands (*ugriz*), was the most ambitious astronomical survey ever undertaken. Section 3 presents in detail the characteristics of its photometric system and the main objectives of the survey. COMBO-17 (Wolf et al. 2003), Classifying Objects by Medium-Band Observations in 17 filters, is a sky survey designed to provide a sample of ∼50,000 galaxies and $\lesssim$1000 QSOs with rather precise photometric redshifts. The photometric system consists of 17 optical bands, five broad-band filters (UBVRI) and 12 medium-band filters covering the wavelength range from 4000 to 9300Å. The total system transmission is shown in Figure 1.5, and the central wavelengths and FWHM are presented below:

Filter	λ_c (nm)	FWHM (nm)
U	364	38
B	456	99
V	540	89
R	652	162
I	850	150
1	420	30
2	462	14
3	485	31
4	518	16
5	571	25
6	604	21
7	646	27
8	696	20
9	753	18
10	815	20
11	856	14
12	914	27

Such a filter set provides a redshift accuracy of $\sigma_{z,gal} \approx 0.03$, $\sigma_{z,QSO} \lesssim 0.1$, smoothing the true redshift distribution of the sample only slightly and allowing the derivation of luminosity functions. However, the near-infrared is fundamental for obtaining deeper photo-zs ($z > 0.9$), and the survey only imaged 1 square degree of sky, which is not enough to dissolve the effects of the Cosmic variance, and so insufficient to obtain more realistic results for understanding the large-scale structure of the Universe.

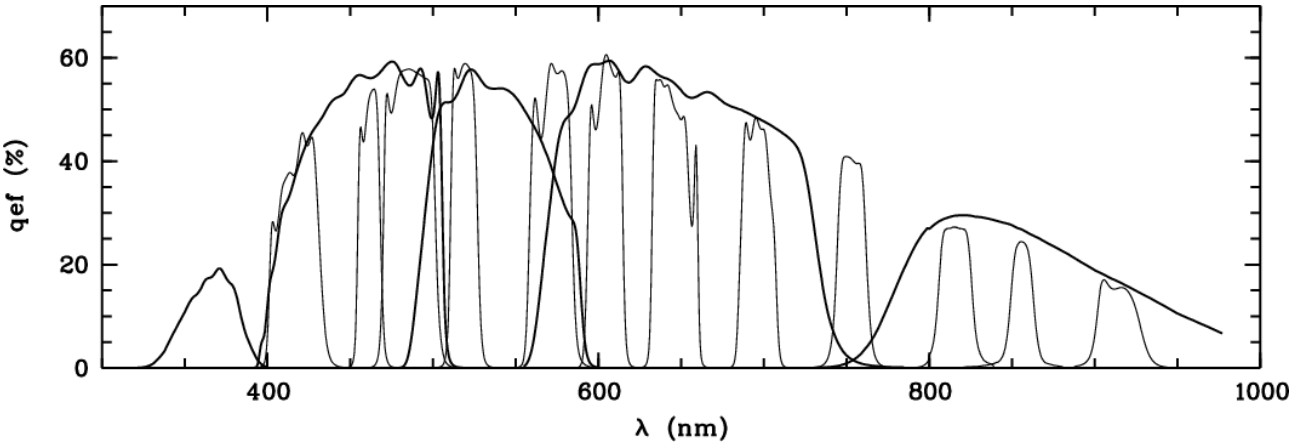

Figure 1.5 Response function in wavelength (nm) of the photometric system of COMBO-17 survey. Figure extracted Wolf et al. (2003).

In 2004, a large group of scientists met to exchange ideas about the possibilities of making a deep study of the cosmic evolution of the Universe. The observational conditions for gathering the data necessary to sample the Universe with enough precision so as to follow its content and properties with z were analyzed, and the Advanced Large, Homogeneous Area Medium Band Redshift Astronomical (ALHAMBRA) project emerged (Moles et al. 2008). Its photometric system consists of 20 constant-width, non-overlapping, medium-band filters in the optical range, with wavelength coverage from 3500Å to 9700Å, and the three classical JHKs bands in the near infrared wavelength range.

This doctoral thesis is centered on the characterization and analysis of the optical system of the ALHAMBRA survey. Chapter 2 of the dissertation presents an introduction to the ALHAMBRA project, the principal scientific objectives, and the global strategy to be applied on the photometric system and the observational system. The 20-band system will be presented with the response curves, and some first and second order moments of these response functions. Furthermore, the set of primary standard stars for the calibration of the system is introduced and the calibration strategy of the system is analyzed with two different methodologies, in order to obtain accurate zero point corrections.

In Chapter 3 the ALHAMBRA system is related to two different photometric systems. Firstly, some transformation equations between the SDSS *ugriz* bands and the 20 ALHAMBRA filters are presented. These equations are elaborated as linear regressions, looking for the best analytical models with the minimum number of coefficients, and they are valid for stellar objects. In general, color transformation for stars are not valid for galaxies since they do not take effects of redshift or intergalactic absorption into account, so colors in the system of observed galaxies at different redshifts are also presented, taking filter SDSS r as reference. However, the validity of the parametric equations on galaxies at z=0 is analyzed as well. Secondly, using the photometry of the Gaia mission some color transformation equations with the ALHAMBRA optical bands are also established. These relations can be helpful for the calibration of the Gaia system enlarging the number of standard stars, and for the stellar parametrization methodology of Gaia to be tested on already observed stars in the ALHAMBRA survey.

In Chapter 4, the system's ability in stellar classification and physical parameter estimation is analyzed. Although the system has been built following some purely extragalactic scientific objectives, the photometry obtained by the optical filters can be considered as a very-low spectroscopy, which means that it is suitable for analyzing its ability in stellar classification. In a first approximation of the problem, Q-parameters are generated in order to obtain a Q,Q diagram capable of classifying most stellar objects to be found in the ALHAMBRA fields into spectral classes. The Q-values entail the use of an extinction law, and which interstellar extinction law fits better with ALHAMBRA photometry, and generates the best discriminant Q,Q diagram for stellar classification, is also analyzed. Estimations of stellar parameters are also developed. Color excess and effective temperature are estimated with two different methodologies, first a parametric approximation and secondly a non-parametric algorithm. For testing the methods, a subset of 288 ALHAMBRA standard stars are used. Finally, a new methodology is developed for estimating all the main physical parameters, that is, T_{eff}, $log(g)$, $[Fe/H]$ and E_{B-V}, for all stellar spectral classes and luminosity types. The method is called the Q Fit Algorithm. To test the method, the subset of 288 standard stars is used again, and then the algorithm is applied to the ALHAMBRA field stars with photometric errors lower than 0.1 magnitudes in all bands. The results are presented with some statistical indexes, and the degenerations shown in some parameters are analyzed more deeply.

Bibliography

Becker, W. 1946, Veröff. Univ. Stremwarte Göttingen 79

Becker, W. 1951, ZAp, 29, 66

Bessell, M. S. 1991, AJ, 101, 662

Bessell, M. S. 2005, ARA&A, 43, 293

Crawford, D. L., & Barnes, J. V. 1970, AJ, 75, 978

Fiorucci, M., & Munari, U. 2002, Ap&SS, 280, 77

Fukugita, M., Ichikawa, T., Gunn, J. E., Doi, M., Shimasaku, K., & Schneider, D. P. 1996, AJ, 111, 1748

Hauck, B., Nitschelm, C., Mermilliod, M., & Mermilliod, J.-C. 1990, A&AS, 85, 989

Johnson, H. L. 1958, Lowell Observatory Bulletin, 4, 37

Johnson, H. L., & Morgan, W. W. 1953, ApJ, 117, 313

Johnson, H. L., & Morgan, W. W. 1951, ApJ, 114, 522

Moles, M., et al. 2008, AJ, 136, 1325

Moro, D., & Munari, U. 2000, A&AS, 147, 361

Mould, J. R., & Siegel, M. J. 1982, PASP, 94, 223

Schuster, W. J., Beers, T. C., Michel, R., Nissen, P. E., & García, G. 2004, A&A, 422, 527

Smith, J. A., et al. 2002, AJ, 123, 2121

Straižys, V. 1963, Vilnius Astronomijos Observatorijos Biuletenis, 6, 1

Straižys, V., & Zdanavicius, K. 1965, Vilnius Astronomijos Observatorijos Biuletenis, 14, 3

Straižys, V., & Zdanavicius, K. 1970, Vilnius Astronomijos Observatorijos Biuletenis, 29, 15

Straižys, V. 1992, Tucson : Pachart Pub. House, c1992.,

Strömgren, B. 1951, AJ, 56, 142

Strömgren, B. 1966, ARA&A, 4, 433

White, N. M., & Wing, R. F. 1978, ApJ, 222, 209

Wing, R. F. 1971, Contributions from the Kitt Peak National Observatory, 554, 145

Wolf, C., Meisenheimer, K., Rix, H.-W., et al. 2003, A&A, 401, 73

2

The ALHAMBRA Photometric System: characterization and zero-point calibration*

The characterization of the optical range of the ALHAMBRA photometric system is presented in this chapter. It consists of 20 contiguous, equal-width, medium-band filters with wavelength coverage from 3500Å to 9700Å. The photometric description of the system is done by presenting the full response curve as a product of the filters, CCD and atmospheric transmission curves, and by using some first and second order moments of this response function. The set of standard stars that defines the system is also introduced, being formed by 31 classic spectrophotometric standard stars that have been used in the calibration of other known photometric systems, and 288 stars, flux calibrated homogeneously, from the Next Generation Spectral Library (NGSL). Finally a strategy to calculate the photometric zero points of the different pointings in the ALHAMBRA project is developed and discussed.

2.1 ALHAMBRA project and its photometric system

The ALHAMBRA (Advanced Large, Homogeneous Area Medium Band Redshift Astronomical) photometric system has been defined in response to scientific objectives included in a scientific project with specific purposes (ALHAMBRA project, Moles et al. 2008). In particular, it has been designed and made, seeking the optimization of specific variables in order to attain a photometric data super-cube, to sample a cosmological fraction of the universe with enough precision to draw an evolutionary track of its content and properties. The global strategy for achieving this aim requires depth, accuracy and spectral coverage to make two objectives possible:

- Obtain spectral energy distributions (SED) with spectral resolution and good enough depth for a physical classification of the objects.
- Estimate the redshifts (z) for the largest possible number of objects and with the greatest

*T. Aparicio Villegas et al. 2010, The Astronomical Journal , 139, 1242

possible accuracy.

We would thus be able to obtain a data set with the accuracy needed for the systematic study of the cosmic evolution of the universe. In particular, it would for example allow us to identify a large number of objects, families or structures at different redshifts (z), and to compare their properties as a function of z, once the physical dispersion of those properties at every z-value has been taken into account. So, it is possible to identify epochs (measured by z) of development of some families of objects or structures, or their disappearance, or even the progressive change in the proportion of a family of objects and the degree of structuring of the universe.

The number of filters, and the width and position of these, have been optimized to obtain at the same time:

- Good precision in z
- Obtaining the largest number of objects with a z more precise that a specific value.
- Being sensitive to not too weak emission lines.

In Benítez et al. (2009) it is proved that these filter system selection criteria are stable and effective for reaching these objectives. Using a sample of spectral energy distributions and galaxy redshifts, based on the redshift catalogue of the Hubble Deep Field, they analyze the behavior of four different filters systems, exploring the impact of factors such as the number of filters, constant vs. logarithmically increasing bandwidth or whether the use of filters with half-band ($\Delta\lambda/2$) overlap improves the photometric redshift estimation, assuming a fixed amount of observing time and with a telescope of 4m. Finally they conclude that the filters system would depend basically on two different aims: obtaining the best photometric accuracy, or getting the largest number of galaxies below a specific error in z. The filters systems that maximize the photometric redshift completeness are formed by 9 bands with logarithmically increasing bandwidth and half-band overlap, but, if a photo-z and SED accuracy better than a certain value are also required, the system should have more than 15 filters of medium bandwidth. It is also shown that a system with 20 constant-width, non-overlapping medium band filters with a uniform transmission would reach a precision of $\delta z = 0.014(1 + z)$ for $I \lesssim 24$ galaxies.

On the other hand, the ALHAMBRA project aims at covering a minimum of 4 square degrees in 8 discontinuous regions of the sky. The choice of the fields was based on the following criteria:

- Low extinction.
- No (or few) bright sources or conspicuous structures.
- High galactic latitude.
- Overlap with other surveys to ensure the possible cross-checking of ALHAMBRA results and maximum complementarity, in particular regarding the largest coverage in wavelength. Only ALHAMBRA-1 does not overlap with other surveys.

Table 2.1 The ALHAMBRA Survey selected fields.

Field name	RA(J2000)	DEC(J2000)	E(B-V)	l	b
ALHAMBRA-1	00 29 46.0	+05 25 28	0.017	113	-57
ALHAMBRA-2/DEEP2	02 28 32.0	+00 47 00	0.031	166	-53
ALHAMBRA-3/SDSS	09 16 20.0	+46 02 20	0.015	174	+44
ALHAMBRA-4/COSMOS	10 00 28.6	+02 12 21	0.018	236	+42
ALHAMBRA-5/HDF-N	12 35 00.0	+61 57 00	0.011	125	+55
ALHAMBRA-6/GROTH	14 16 38.0	+52 25 05	0.007	95	+60
ALHAMBRA-7/ELAIS-N1	16 12 10.0	+54 30 00	0.005	84	+45
ALHAMBRA-8/SDSS	23 45 50.0	+15 34 50	0.027	99	-44

The selected fields are shown in Table 2.1.

This implies the need for a wide-field instrument, associated to a 3-4m telescope that is capable of covering the selected area with the required signal-to-noise ratio, within a reasonable observing time period. For optical range, the Centro Astronómico Hispano-Alemán (CAHA) has the wide-field camera LAICA[1] (Large Area Imager for Calar Alto), which achieves the ideal conditions for the project. It covers a total of 0.25 square degrees and works in the primary focus of the 3.5m telescope. In the same telescope, and also in the primary focus, the OMEGA-2000[2] camera for near infrared (NIR) wavelength range also seems to have the requirements to complete the system in this part of the spectrum with the classical JHKs bands.

LAICA has 4 discontinuous CCDs with 4096×4096 pixels, each one with a pixel-size of 15 microns. Each detector covers an area of one sixteenth degree. The arrangement of the CCDs in the instrument is shown as a true photo in Figure 2.1. In order to get a contiguous field one has to fill in the gaps between the CCDs, i.e. 4 telescope pointings are needed for full coverage of a 1 square degree field. See Figure 2.2 for a graphic representation of the geometry implicit. So, to bring the ALHAMBRA photometric system to fruition, 4 filter sets with the characteristics explained before are required. Each of these sets has to be associated to one of the LAICA detectors, and the survey would observe two pointings in each of the 8 fields in order to complete the 4 square degrees desired.

[1] `http://www.caha.es/CAHA/Instruments/LAICA/index.html`
[2] `http://www.caha.es/CAHA/Instruments/O2000/index.html`

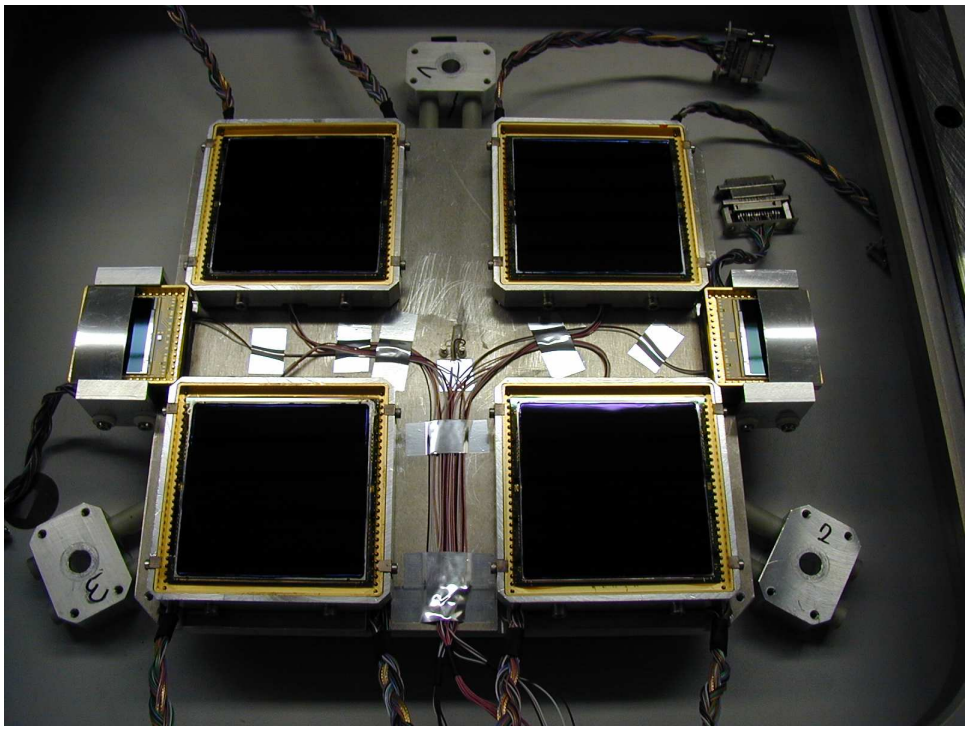

Figure 2.1 Arrangement of the four discontinuous CCDs of LAICA. The spacing between the CCDs is equal to the size of a single CCD minus an overlap of about 100 arcsecs

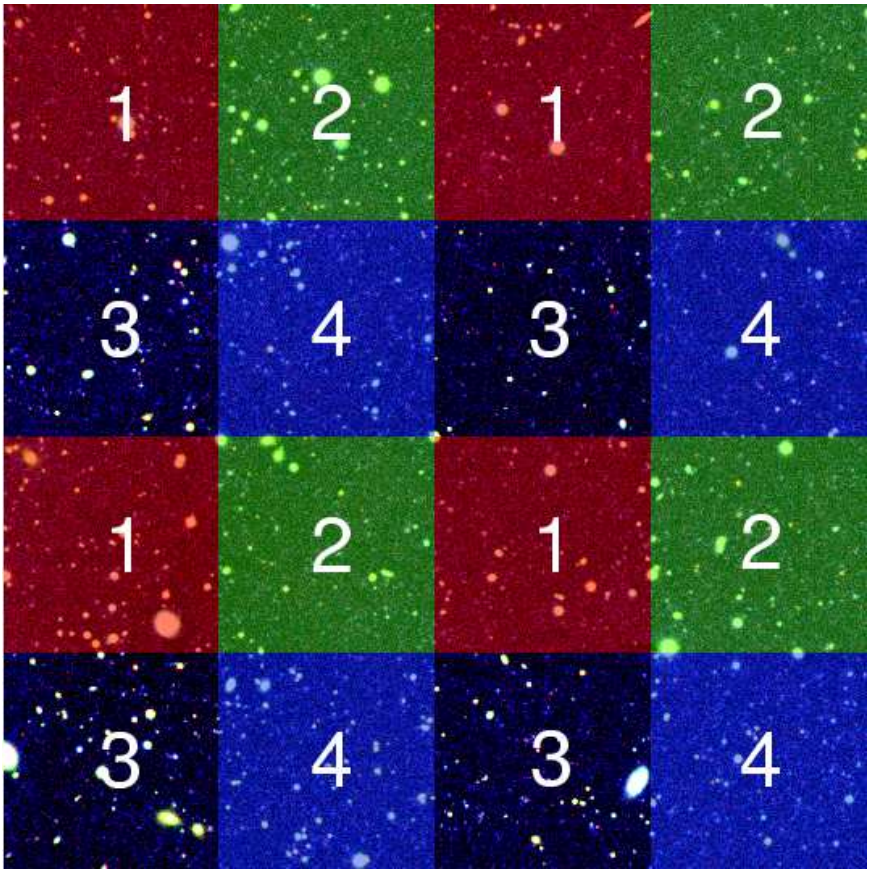

Figure 2.2 A **pointing** is a set of 4 non-contiguous CCDs. A **mosaic** is a set of 4 pointings forming an adjoining image. The graphic shows a mosaic of 4 pointings forming a 1 degree image, where each pointing, numbered from 1 to 4, is formed by the four squares with the same color and marked with the same pointing number.

The filters system was designed taking into account some specific requirements for the response function (constant in most of the spectral range), homogeneity and transmission. In particular, all filters must have steep side slopes, non-overlapping and flat tops, and with a transmission over 70% in all the wavelength range. Obviously, the 4 filters sets should be equivalent within some precise limits. The sets of 20×4 filters were manufactured by BARR Associates.

The transmission curves of the filters are shown in Figure 2.3 for the four filters sets. Each one of these was associated to one of the LAICA CCDs, in such a way that they are always associated to the same position in the instrument. The response curves of the four combinations filter+detector are represented in Figure 2.4. The quantum efficiency of the 4 detectors was provided by the CAHA team and is shown in Figure 2.5.

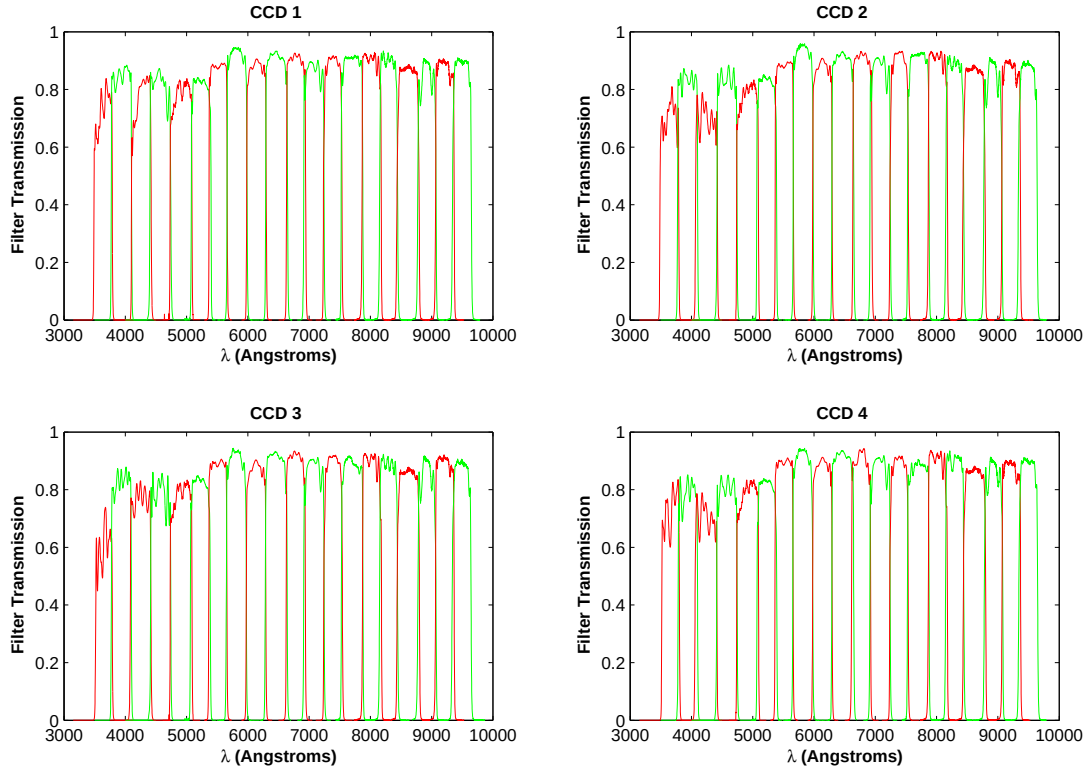

Figure 2.3 Response function in wavelength (Å) of the 4 sets of 20 ALHAMBRA filters for the 4 LAICA CCDs.

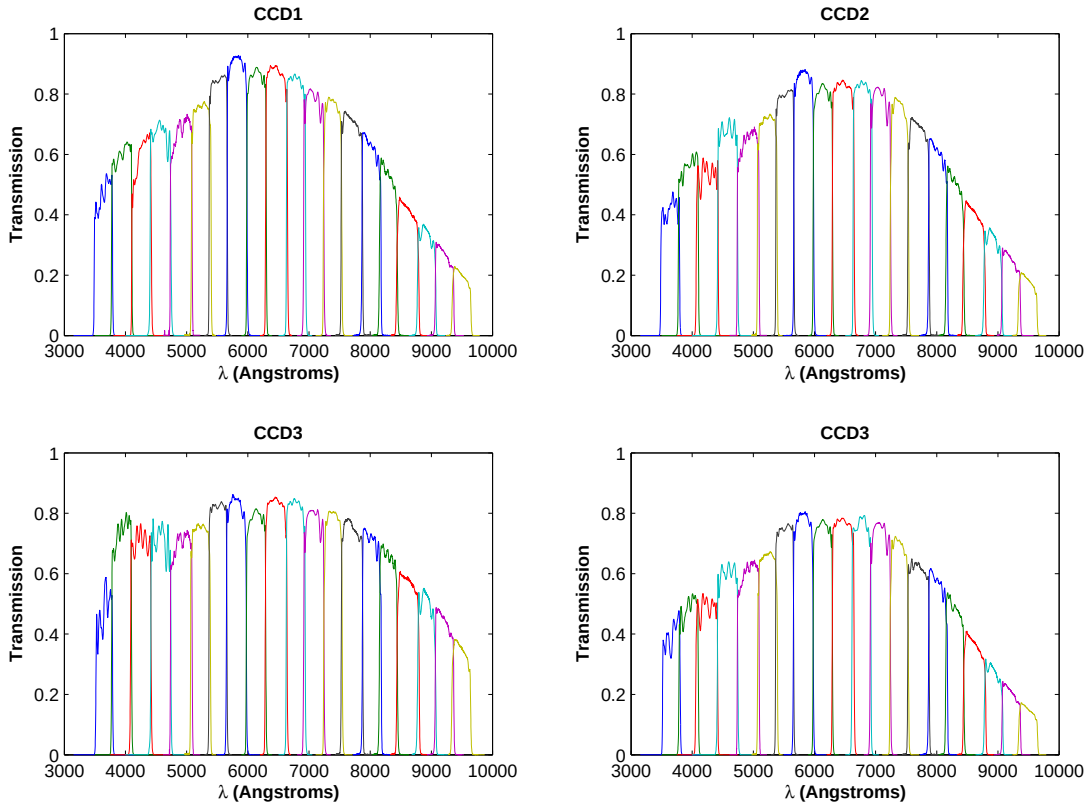

Figure 2.4 Transmission curves in wavelength (Å) of the combination filter+detector for the 4 ALHAMBRA filters sets.

2.2 Basic Definitions on Astronomical Photometry

Supposing that a star is at a distance r from the telescope which has the area ds perpendicular to the line of sight, then considering that there is neither interstellar nor atmospheric extinction, the telescope will receive a quantity of energy such as:

$$dE_\lambda = I_\lambda d\omega dt d\lambda \tag{2.1}$$

being I_λ the *specific intensity* of the radiation of the star, $d\omega$ the solid angle under which the area ds is seen from the star distance r ($d\omega = r^{-2}ds$), and dt y $d\lambda$ the intervals of time and wavelength, respectively. This equation (2.1) represents the definition of the specific intensity.

The amount of energy received in the area ds per unit interval of time is called *radiation flux*

$$dF_\lambda = \frac{dE_\lambda}{dt} = I_\lambda d\omega d\lambda \tag{2.2}$$

and the radiation flux received per unit surface is called *flux density*:

$$dL_\lambda = \frac{dF_\lambda}{ds} = \frac{I_\lambda}{r^2} d\lambda \tag{2.3}$$

For a given star its distance r keeps constant, so the flux density per unit interval of

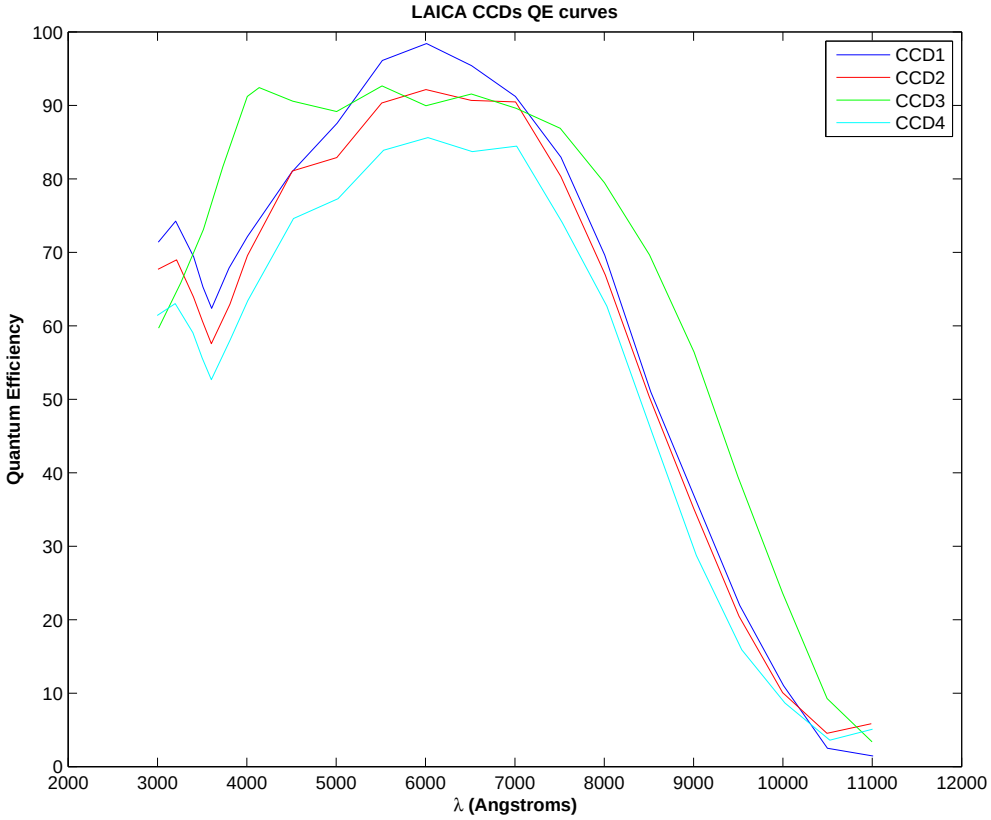

Figure 2.5 Quantum efficiency of the 4 LAICA detectors.

wavelength can be considered as a measure of the specific intensity I_λ which is also called the energy spectral distribution.

Instead of unit wavelength, the unit frequency can be also used taking into account the relation established between I_λ and I_ν given by:

$$I_\nu = I_\lambda \frac{\lambda^2}{c} \tag{2.4}$$

being c the speed of light.

The flux density is also called the *brightness* of an object and is measured in another unit, the *magnitude*. The definition of magnitude was formalized by Robert Pogson in 1856:

$$m = -2.5 \log \frac{L}{L_0} = -2.5 \log L + 2.5 \log L_0 = -2.5 \log L + const \tag{2.5}$$

where L_0 is a constant that defines the zero-point of a magnitude scale, and the coefficient -2.5 is called the *Pogson's ratio*. The sign "minus" indicates that the magnitudes decrease with increasing brightness. The magnitude of a star would then depend on the intrinsic luminosity and the distance of the star.

We define the *monochromatic magnitude* as:

$$m_{mon} = -2.5 \log L_\lambda + const \tag{2.6}$$

where L_λ is the brightness of the star at a wavelength λ.

If the response function of a detector is S_λ, then the determined magnitudes are called *heterochromatic* and are defined as follows:

$$m_{het} = -2.5 \log \frac{\int L_\lambda S_\lambda d\lambda}{\int S_\lambda d\lambda} + const \tag{2.7}$$

We are able to compare the brightness of the same star in different wavelengths or frequencies. Let m_1 and m_2 be the monochromatic magnitudes of a star at λ_1 and λ_2, respectively, then the expression:

$$m_1 - m_2 = -2.5 \log \frac{L_{\lambda_1}}{L_{\lambda_2}} \tag{2.8}$$

is called *color index*. In the case of heterochromatic magnitudes with responses S_{1_λ} and S_{2_λ}, the color index is defined as:

$$m_1 - m_2 = -2.5 \log \frac{\int L_\lambda S_{1_\lambda} d\lambda}{\int L_\lambda S_{2_\lambda} d\lambda} + const \tag{2.9}$$

where

$$const = 2.5 \log \frac{\int S_{1_\lambda} d\lambda}{\int S_{2_\lambda} d\lambda} \tag{2.10}$$

the value of this index directly shows how many magnitudes the star is brighter in one wavelength compared with another wavelength. Furthermore, the color index does not depend on the distance of the star r since, in the monochromatic case, using equation (2.3) we have that

$$m_1 - m_2 = -2.5 \log \frac{L_{\lambda_1}}{L_{\lambda_2}} = -2.5 \log \frac{\frac{I_{\lambda_1}}{r^2}}{\frac{I_{\lambda_2}}{r^2}} = -2.5 \log \frac{I_{\lambda_1}}{I_{\lambda_2}} \tag{2.11}$$

where I_λ is the specific intensity at a wavelength λ; it is equivalently proved for the heterochromatic case.

On the other hand, the *synthetic magnitudes* are those derived by convolving model atmosphere fluxes or observed spectrophotometric fluxes with the transmission of the response function of a system, normally obtained by multiplying together the filter transmission, the reflectivity of the telescope mirror, the quantum efficiency of the detector used and the transmission of the Earth's atmosphere for an airmass of (at least) 1.0. However, in the telescope the magnitude measured is the *instrumental magnitude* that is defined according to the number of counts scored by the detector, such as:

$$m_{inst} = -2.5 \log n_\lambda \tag{2.12}$$

being n_λ the rate of detected photons. The synthetic and the instrumental magnitudes are related by the *instrumental zero point* (zp) by the following way:

$$m_{synt} = m_{inst} + zp \tag{2.13}$$

and so, this parameter makes possible to obtain the magnitude in the desired system from the instrumental magnitude measured with the telescope.

So far, non interstellar extinction has been taken into account. Considering now that the radiation of the star passes through an absorbing medium and the radiation of the initial intensity $I_{0\lambda}$ crosses a dust cloud of optical thickness x. Then the received radiation has the intensity:

$$I_\lambda = I_{0\lambda} e^{-k_\lambda x} \tag{2.14}$$

where k_λ is the extinction coefficient at the wavelength λ. The value:

$$\tau_\lambda = e^{-k_\lambda} = \frac{I_\lambda}{I_{0\lambda}} \tag{2.15}$$

characterizes the transmission of light by a unit quantity of interstellar matter (x=1) and varies from 0 (total absorption) to 1 (total transparency).

If the radiation of a star passes through an interstellar cloud of unit optical thickness (x=1), then magnitudes m_1 and m_2 will turn into $m_1 + e_1$ and $m_2 + e_2$ respectively, being e_1 and e_2 the extinctions at the wavelengths correponding to the magnitudes when x=1. Then, the color index would be:

$$(m_1 + e_1) - (m_2 + e_2) = m_1 - m_2 + (e_1 - e_2) \tag{2.16}$$

This additional reddening given by the absorbing interstellar cloud is called *color excess*:

$$E_{m_1 - m_2} = e_1 - e_2 \tag{2.17}$$

The color excess caused by x units of absorbing matter (extinction) is:

$$E^x_{m_1 - m_2} = xe_1 - xe_2 = xE^{(x=1)}_{m_1 - m_2} \tag{2.18}$$

The photometric systems with more than two colors (three bands) can generate an important parameter, the *color excess ratio*. Considering three different magnitudes of the system, m_1, m_2 and m_3, we can plot a color-color diagram with $m_1 - m_2$ versus $m_2 - m_3$. In this figure the unreddened stars form a definite sequence, and when there is interstellar reddening, each star in the diagram moves along the reddening line with slope

$$\chi = \frac{E_{m_1 - m_2}}{E_{m_2 - m_3}} \tag{2.19}$$

This cocient just depends on the properties of the interstellar medium; however, when heterochromatic magnitudes are used, there could be a slightly dependency on the stellar spectral

type.

Then, with this ratios and two color indexes one can generate a Q-parameter by,

$$Q_{m_1 m_2 m_3} = (m_1 - m_2) - \frac{E_{m_1-m_2}}{E_{m_2-m_3}}(m_2 - m_3) \tag{2.20}$$

This parameters have an important property: they are independent of interstellar reddening as well as of the distance of the star. Indeed, this Q-parameter is the ordinate of the point at which the reddening line of a star intersects the axis $m_2 - m_3 = 0$.

2.2.1 System of magnitudes in a photometric system

A photometric system is defined by a set of filters that can have narrow, intermediate or wide bandwidth as explained in Chapter 1, and by a system of magnitudes based on the value of L_0 from the definition (2.5). Thus three types of photometric systems can be considered according to the definition of this zero point:

- **ST System** : L_0 is the flux density of *Vega* at $\lambda = 5500$Å.
- **AB System** : L_0 is the flux density of *Vega* at $\lambda = 5500$Å in frequency.
- **VEGA System** : L_0 is defined basing on the spectral energy distribution of *Vega*, being *Vega* magnitudes in all the filters of the photometric system equal to 0.

Photometric systems anchored to a VEGA magnitude system can present in their magnitudes small differences since they are based on the absolute flux calibration of *Vega* star, and this has several available spectra with different calibrations and so they can slightly differ. AB magnitudes and VEGA magnitudes can be related by the lineal relation:

$$mag_{AB}(Obj) = mag_{VEGA}(Obj) + mag_{AB}(Vega) \tag{2.21}$$

that is, the AB magnitude of an object in a system is the VEGA magnitude of that object plus the AB magnitude of *Vega* in that system.

With these definitions we are already prepared to start with the own characterization of the ALHAMBRA optical photometric system.

2.3 Characterization of the optical ALHAMBRA photometric system

As explained in the previous section, the ALHAMBRA photometric system has been defined as specified in Benítez et al. (2009), as a system of 20 constant-width, non-overlapping, medium-band filters in the optical range (with wavelength coverage from 3500Å to 9700Å). However, due to the geometry of LAICA and its four CCDs, it is necessary that one of the filters sets be the standard system from which the characterization and calibration of the optical photometric system is based. Considering that the four systems are equivalent between some strict limits, the standard ALHAMBRA photometric system is chosen to be the one at position 3 of the instrument, that is, the 20 filters set associated to CCD3. The characterization of the photometric system, however, is presented here for the four sets of filters and CCDs.

The definition of the system is given by the response curve defined by the product of three different transmission curves: the filter set, detector and atmospheric extinction at 1.2 air masses, based on the CAHA monochromatic extinction tables (Sánchez et al. 2007). The graphic representation of the optical ALHAMBRA photometric system is shown in Figure 2.6. Numerical values of these response curves can be found at the web page `http://alhambra.iaa.es:8080`.

First and second order moments of the transmission functions of the different 20 filters are also of interest. We will characterize the filter systems using their isophotal wavelengths, full width half-maxima, and other derived quantities as follows. Let E_λ be the spectral energy distribution of an astronomical source and S_λ the response curve of a filter in the photometric system, defined as:

$$S_\lambda = T_t(\lambda)T_f(\lambda)T_a(\lambda), \tag{2.22}$$

where T_t is the product of the throughput of the telescope, instrument and quantum efficiency of the detector, T_f is the filter transmission and T_a is the atmospheric transmission. Following the definition in Golay (1974), assuming that the function E_λ is continuous and that S_λ does not change sign in a wavelength interval $\lambda_a - \lambda_b$, the mean value theorem states that there is at least one λ_i inside the interval $\lambda_a - \lambda_b$ such that:

$$E_{\lambda_i} \int_{\lambda_a}^{\lambda_b} S_\lambda d\lambda = \int_{\lambda_a}^{\lambda_b} E_\lambda S_\lambda d\lambda \tag{2.23}$$

implying,

$$E_{\lambda_i} = \langle E_\lambda \rangle = \frac{\int_{\lambda_a}^{\lambda_b} E_\lambda S_\lambda d\lambda}{\int_{\lambda_a}^{\lambda_b} S_\lambda d\lambda}, \tag{2.24}$$

where λ_i is the *isophotal wavelength* and $\langle E_\lambda \rangle$ denotes the mean value of the intrinsic flux above the atmosphere over the wavelength interval (see also Tokunaga & Vacca 2005). Tables

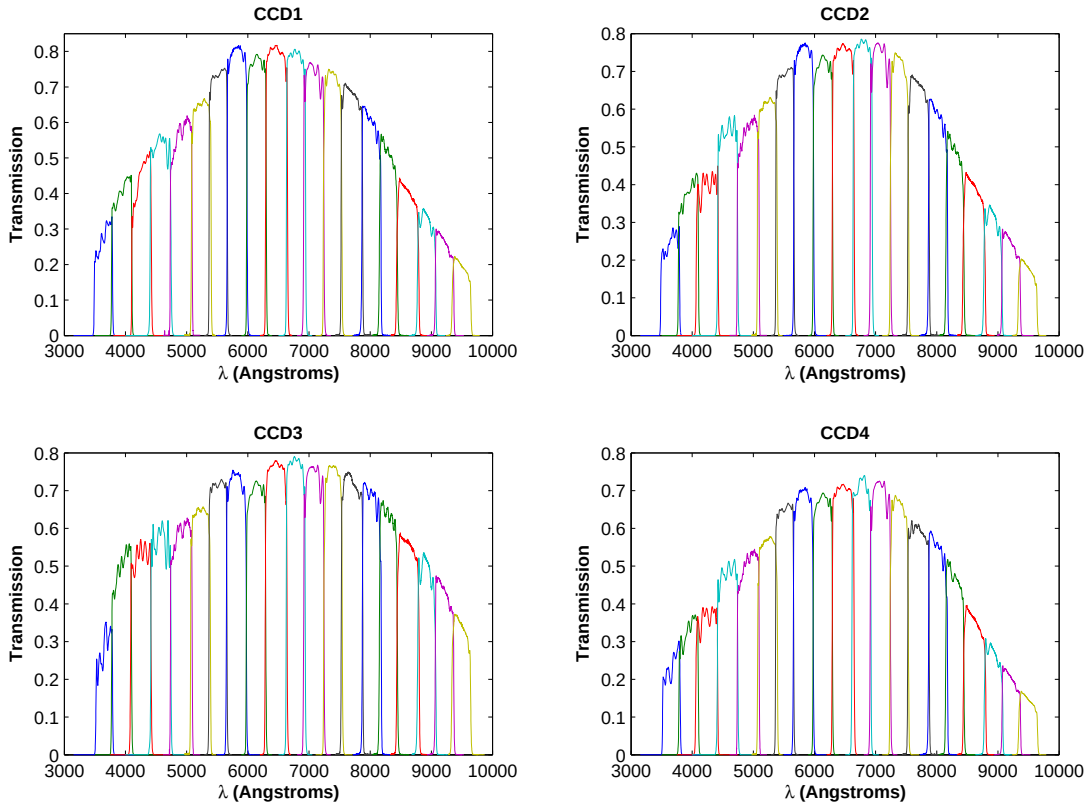

Figure 2.6 Response functions of the ALHAMBRA photometric system filters including atmospheric transmission at 1.2 air masses at the altitude of Calar Alto Observatory.

2.2-2.5 show the isophotal wavelengths of the ALHAMBRA filters using the spectrum of *Vega* as reference. The absolute calibrated spectrum has been taken from the STScI Observatory Support Group web page[3], as the file $alpha\_lyr\_stis\_004.fits$. This spectrum is a combination of modeled and observed fluxes consisting of STIS CCD fluxes from 3500Å-5300Å, and a Kurucz model with $T_{eff} = 9400K$ (Kurucz 2005) from 5300Å to the end of the spectral range. The isophotal wavelengths were calculated using formula 2.24.

The determination of the isophotal wavelengths of a star in a photometric system can be complex, especially for the filters that contain conspicuous stellar absorption lines. In Figure 2.7 the response functions of the standard ALHAMBRA photometric system is represented together with the spectrum of *Vega* superimposed on the transmission curves, in such a way that it easily allows one to detect the filters with some of these kinds of lines. For example, filter A394M is extremely sensitive to the Balmer jump and filter A425M encompasses the two prominent H_γ and H_δ lines, at 4340Å and 4101Å respectively. At 4861Å, H_β is in filter A491M, and at 6563Å H_α falls on filter A646M. The Paschen series, from 8208Å at filter A829M, appears associated to the four reddest ALHAMBRA filters (A861M, A892M, A921M and A948M).

However, this quantity depends on the spectral energy distribution of the emitter or the atmospheric absorption, thus for the same filter it will be different for each kind of source. The

[3] `http://www.stsci.edu/hst/observatory/cdbs/calspec.html`

isophotal wavelength can be approximated by other central parameters that only depend on the photometric system, such as the wavelength-weighted average or the frequency-weighted average (written as $c\nu^{-1}$):

$$\lambda_m = \frac{\int \lambda S_\lambda d\lambda}{\int S_\lambda d\lambda} \tag{2.25}$$

$$\nu_m = \frac{\int \nu S_\nu d(\ln \nu)}{\int S_\nu d(\ln \nu)}, \tag{2.26}$$

or by the effective wavelength as defined by Schneider et al.(1983):

$$\lambda_{eff} = exp[\frac{\int d(\ln \nu) S_\nu \ln \lambda}{\int d(\ln \nu) S_\nu}] \tag{2.27}$$

which is halfway between the wavelength-weighted average and the frequency-weighted average (Fukugita et al. 1996).

The root mean square (rms) fractional widths of the filters, σ, defined as:

$$\sigma = \sqrt{\frac{\int d(\ln \nu) S_\nu [\ln(\frac{\lambda}{\lambda_{eff}})]^2}{\int d(\ln \nu) S_\nu}} \tag{2.28}$$

is useful in calculating the sensitivity of the effective wavelength to spectral slope changes:

$$\delta\lambda_{eff} = \lambda_{eff}\sigma^2\delta n, \tag{2.29}$$

where n is the local power-law index of the SED ($f_\nu\ \nu^n$), and the effective band width, δ, is given by:

$$\delta = 2(2\ln 2)^{1/2}\sigma\lambda_{eff}. \tag{2.30}$$

We also calculate the flux sensitivity quantity Q, defined as

$$Q = \int d(\ln \nu) S_\nu, \tag{2.31}$$

which allows a quick approximation to the response of the system to a source of known flux in the following way:

$$N_e = AtQf_{\nu_{eff}}h^{-1}, \tag{2.32}$$

where N_e is the number of photoelectrons collected with a system of effective area A integrating for a time t on a source of flux f_ν, and h is the Planck constant. For example, the number of photoelectrons collected using the ALHAMBRA photometric system, in 1 $arcsec^2$, integrating for a time of 5000 seconds on a source of AB=23 mag$\cdot arcsec^{-2}$ in filter A491M, is 1.54×10^4 photoelectrons.

Tables 2.2-2.5 show the values of these parameters calculated for each of the filters sets in the ALHAMBRA photometric system.

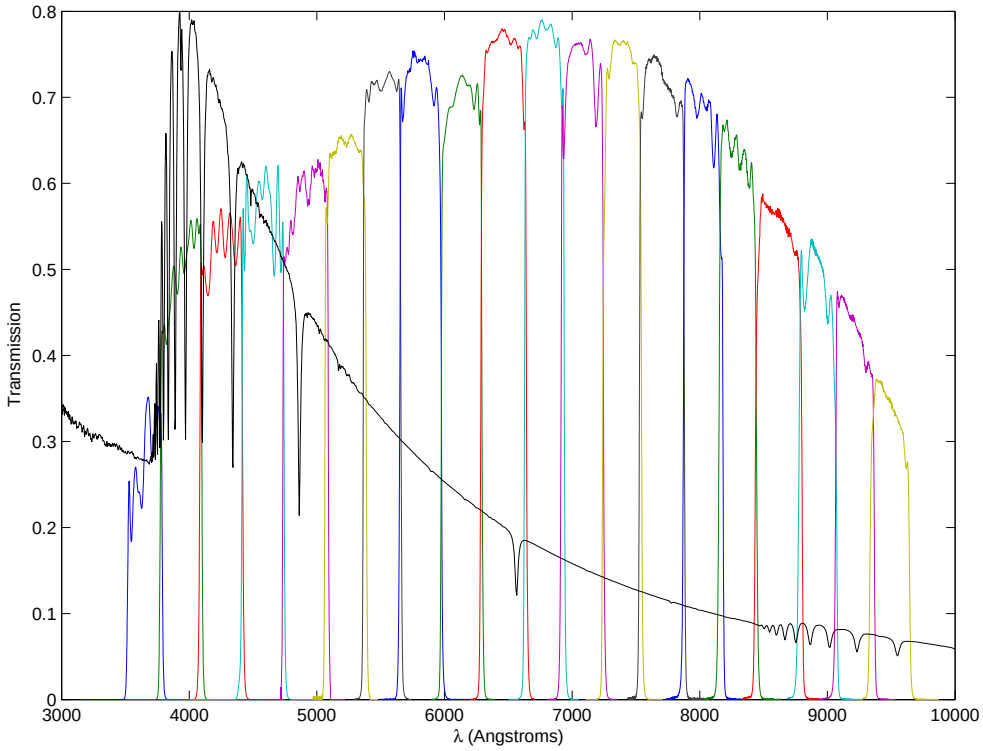

Figure 2.7 Response functions of the standard ALHAMBRA photometric filters system including atmospheric transmission at 1.2 air masses at the altitude of Calar Alto Observatory. This also represents the spectrum of *Vega* superimposed on the transmission curves. The flux of *Vega* has been normalized and properly scaled to make the graphic possible. Figure from Aparicio Villegas et al. (2010).

Table 2.2 Representative parameters of the ALHAMBRA photometric system filters: CCD1

Filter	λ_{iso} [1] (nm)	F_λ ($erg/s/cm^2/$Å)	*Vega* AB Magnitude	λ_m [2] (nm)	$c\nu_m^{-1}$ [3] (nm)	λ_{eff} [4] (nm)	σ	Q	FWHM (nm)	δ
A366M	330.9	3.329e-09	0.97	365.1	364.7	364.8	0.0238	0.0227	30.8	204.8
A394M	398.5	6.851e-09	0.03	394.5	394.0	394.2	0.0244	0.0343	33.6	227.1
A425M	430.9	6.782e-09	-0.14	427.4	426.9	427.1	0.0215	0.0338	32.4	216.1
A457M	456.5	6.137e-09	-0.18	457.3	456.9	456.9	0.0216	0.0402	34.6	232.9
A491M	500.7	4.726e-09	-0.05	491.7	491.2	491.4	0.0209	0.0412	35.8	241.6
A522M	524.0	4.107e-09	-0.04	523.9	523.6	523.7	0.0178	0.0398	32.4	219.1
A551M	551.6	3.541e-09	0.01	551.8	551.5	551.6	0.0156	0.0396	29.9	203.1
A581M	582.2	3.013e-09	0.07	582.5	582.2	582.3	0.0162	0.0447	32.7	222.3
A613M	614.0	2.564e-09	0.13	614.3	613.9	614.0	0.0150	0.0400	32.1	217.4
A646M	650.7	2.119e-09	0.23	646.9	646.6	646.7	0.0159	0.0441	36.1	243.1
A678M	678.7	1.890e-09	0.24	678.8	678.5	678.6	0.0133	0.0364	31.2	213.3
A708M	707.2	1.666e-09	0.29	707.7	707.4	707.5	0.0135	0.0347	33.3	225.6
A739M	738.3	1.458e-09	0.34	738.6	738.4	738.5	0.0116	0.0292	30.1	202.7
A770M	770.1	1.277e-09	0.39	769.8	769.6	769.6	0.0132	0.0311	35.4	239.4
A802M	801.5	1.126e-09	0.44	801.5	801.3	801.4	0.0113	0.0235	31.5	214.2
A829M	829.3	1.014e-09	0.48	829.3	829.1	829.2	0.0103	0.0182	29.7	201.2
A861M	861.5	8.943e-10	0.54	860.9	860.6	860.7	0.0120	0.0168	35.8	244.0
A892M	905.7	8.695e-10	0.50	891.8	891.6	891.7	0.0096	0.0109	29.8	202.8
A921M	919.5	8.225e-10	0.48	920.7	920.5	920.6	0.0096	0.0087	29.9	207.2
A948M	950.4	7.502e-10	0.52	948.6	948.4	948.5	0.0093	0.0063	30.4	208.1

1. Isophotal wavelength defined in equation (2.24)
2. Wavelength-weighted average
3. Inverse of frequency-weighted average
4. Effective wavelength defined in equation (2.27)

Note. — Columns 2 to 4 represent the isophotal wavelengths, flux densities and AB magnitudes of *Vega* in the ALHAMBRA photometric system.

Table 2.3 Representative parameters of the ALHAMBRA photometric system filters: CCD2

Filter	λ_{iso} [1] (nm)	F_λ ($erg/s/cm^2/$Å)	*Vega* AB Magnitude	λ_m [2] (nm)	$c\nu_m^{-1}$ [3] (nm)	λ_{eff} [4] (nm)	σ	Q	FWHM (nm)	δ
A366M	371.8	3.352e-09	0.97	364.8	364.4	364.5	0.0245	0.0208	31.8	210.3
A394M	398.5	6.851e-09	0.02	394.6	394.1	394.2	0.0242	0.0317	33.2	224.7
A425M	430.9	6.782e-09	-0.13	425.0	424.5	424.7	0.0245	0.0338	35.8	244.9
A457M	457.5	6.107e-09	-0.18	458.2	457.8	457.9	0.0208	0.0390	33.2	224.7
A491M	500.2	4.718e-09	-0.05	492.0	491.6	491.7	0.0208	0.0392	35.8	241.5
A522M	522.4	4.145e-09	-0.04	522.9	522.6	522.6	0.0178	0.0377	32.6	219.2
A551M	551.6	3.541e-09	0.01	551.7	551.4	551.5	0.0156	0.0374	29.8	203.0
A581M	582.2	3.013e-09	0.07	582.3	582.0	582.1	0.0162	0.0423	32.6	221.8
A613M	613.4	2.573e-09	0.13	613.8	613.5	613.6	0.0150	0.0373	32.0	216.4
A646M	650.7	2.119e-09	0.23	647.0	646.7	646.8	0.0160	0.0417	35.7	243.2
A678M	678.7	1.890e-09	0.24	678.9	678.7	678.7	0.0133	0.0355	31.2	213.3
A708M	707.9	1.661e-09	0.29	707.8	707.5	707.6	0.0135	0.0349	33.4	225.1
A739M	739.0	1.453e-09	0.34	738.8	738.6	738.7	0.0116	0.0289	30.1	201.7
A770M	770.0	1.277e-09	0.39	769.9	769.7	769.8	0.0131	0.0299	35.2	236.9
A802M	801.5	1.126e-09	0.44	801.5	801.3	801.3	0.0114	0.0229	31.7	214.4
A829M	829.3	1.014e-09	0.48	829.1	828.9	829.0	0.0103	0.0174	29.0	200.8
A861M	861.5	8.943e-10	0.54	860.4	860.1	860.2	0.0120	0.0163	35.8	243.7
A892M	905.7	8.695e-10	0.50	891.2	890.9	891.0	0.0096	0.0104	29.5	201.2
A921M	919.5	8.225e-10	0.48	920.6	920.5	920.5	0.0096	0.0081	31.8	207.3
A948M	950.4	7.502e-10	0.52	947.9	947.7	947.7	0.0093	0.0058	30.5	207.3

1. Isophotal wavelength defined in equation (2.24)
2. Wavelength-weighted average
3. Inverse of frequency-weighted average
4. Effective wavelength defined in equation (2.27)

Note. — Columns 2 to 4 represent the isophotal wavelengths, flux densities and AB magnitudes of *Vega* in the ALHAMBRA photometric system.

Table 2.4 Representative parameters of the ALHAMBRA photometric system: CCD3

Filter	λ_{iso} [1] (nm)	F_λ ($erg/s/cm^2/$Å)	*Vega* AB Magnitude	λ_m [2] (nm)	$c\nu_m^{-1}$ [3] (nm)	λ_{eff} [4] (nm)	σ	Q	FWHM (nm)	δ
A366M	373.8	3.354e-09	0.96	366.4	366.0	366.1	0.0216	0.0211	27.9	186.2
A394M	398.5	6.851e-09	0.02	394.4	393.9	394.1	0.0239	0.0414	33.0	222.2
A425M	430.9	6.782e-09	-0.13	425.3	424.9	424.9	0.0229	0.0419	34.2	229.8
A457M	456.8	6.117e-09	-0.18	457.8	457.4	457.5	0.0209	0.0412	33.2	224.9
A491M	500.8	4.726e-09	-0.05	491.7	491.2	491.3	0.0208	0.0426	35.6	241.2
A522M	522.4	4.145e-09	-0.04	522.6	522.3	522.4	0.0178	0.0395	32.6	218.9
A551M	551.0	3.547e-09	0.01	551.2	550.9	551.0	0.0156	0.0385	29.7	202.1
A581M	581.1	3.031e-09	0.07	581.2	580.9	580.9	0.0161	0.0407	32.4	221.1
A613M	613.4	2.573e-09	0.13	613.6	613.4	613.4	0.0149	0.0364	32.0	216.2
A646M	650.8	2.119e-09	0.23	646.4	646.0	646.1	0.0159	0.0419	35.7	241.5
A678M	678.1	1.896e-09	0.24	678.2	678.0	678.1	0.0133	0.0355	31.4	211.9
A708M	707.9	1.661e-09	0.29	707.9	707.7	707.8	0.0135	0.0347	33.2	225.3
A739M	739.1	1.453e-09	0.34	739.3	739.1	739.2	0.0117	0.0302	30.4	203.3
A770M	770.1	1.277e-09	0.39	770.2	769.9	769.9	0.0132	0.0329	35.4	239.2
A802M	802.4	1.123e-09	0.44	802.2	801.9	802.0	0.0111	0.0263	31.2	210.5
A829M	830.2	1.012e-09	0.48	829.5	829.3	829.4	0.0103	0.0226	29.6	202.1
A861M	861.5	8.943e-10	0.54	861.6	861.3	861.4	0.0121	0.0233	36.9	246.4
A892M	884.3	8.703e-10	0.50	891.9	891.7	891.8	0.0095	0.0162	30.3	200.2
A921M	936.2	8.197e-10	0.48	920.9	920.7	920.8	0.0096	0.0143	30.8	207.8
A948M	950.4	7.502e-10	0.52	948.3	948.2	948.2	0.0093	0.0109	31.9	208.1

1. Isophotal wavelength defined in equation (2.24)
2. Wavelength-weighted average
3. Inverse of frequency-weighted average
4. Effective wavelength defined in equation (2.27)

Note. — Columns 2 to 4 represent the isophotal wavelengths, flux densities and AB magnitudes of *Vega* in the ALHAMBRA photometric system.

Table 2.5 Representative parameters of the ALHAMBRA photometric system: CCD4

Filter	λ_{iso} [1] (nm)	F_λ ($erg/s/cm^2/$Å)	*Vega* AB Magnitude	λ_m [2] (nm)	$c\nu_m^{-1}$ [3] (nm)	λ_{eff} [4] (nm)	σ	Q	FWHM (nm)	δ
A366M	377.3	3.334e-09	0.92	367.1	366.7	366.8	0.0232	0.0187	28.6	200.3
A394M	381.4	6.972e-09	0.01	395.0	394.6	394.7	0.0233	0.0266	32.4	216.8
A425M	430.6	6.854e-09	-0.13	424.2	423.7	423.8	0.0244	0.0308	36.4	244.2
A457M	457.9	6.107e-09	-0.18	458.2	457.8	457.9	0.0212	0.0354	33.8	228.7
A491M	500.2	4.718e-09	-0.05	492.3	491.8	491.9	0.0208	0.0368	36.1	241.5
A522M	522.7	4.128e-09	-0.04	523.3	522.9	523.1	0.0177	0.0344	32.7	218.1
A551M	551.0	3.547e-09	0.01	551.3	551.0	551.1	0.0156	0.0350	29.8	202.3
A581M	581.6	3.022e-09	0.07	581.7	581.4	581.4	0.0161	0.0382	32.7	220.1
A613M	613.4	2.573e-09	0.13	613.7	613.4	613.4	0.0149	0.0348	31.9	215.8
A646M	650.7	2.119e-09	0.23	646.9	646.6	646.7	0.0159	0.0388	35.9	243.1
A678M	676.7	1.908e-09	0.24	676.9	676.6	676.7	0.0133	0.0327	31.2	211.6
A708M	707.2	1.666e-09	0.29	707.7	707.4	707.5	0.0135	0.0328	33.4	224.8
A739M	738.3	1.458e-09	0.34	738.6	738.4	738.4	0.0116	0.0265	30.3	202.7
A770M	770.1	1.277e-09	0.39	769.9	769.6	769.7	0.0132	0.0271	35.1	239.8
A802M	801.5	1.126e-09	0.44	801.4	801.2	801.2	0.0112	0.0212	31.4	211.6
A829M	829.3	1.014e-09	0.48	829.0	828.8	828.9	0.0105	0.0169	30.2	204.7
A861M	861.5	8.943e-10	0.54	861.1	860.8	860.9	0.0121	0.0149	37.2	245.9
A892M	905.7	8.695e-10	0.50	892.1	891.9	891.9	0.0097	0.0089	29.8	203.8
A921M	919.5	8.225e-10	0.48	920.9	920.7	920.8	0.0095	0.0066	30.1	206.9
A948M	950.4	7.502e-10	0.52	948.6	948.4	948.4	0.0093	0.0047	30.4	208.3

1. Isophotal wavelength defined in equation (2.24)
2. Wavelength-weighted average
3. Inverse of frequency-weighted average
4. Effective wavelength defined in equation (2.27)

Note. — Columns 2 to 4 represent the isophotal wavelengths, flux densities and AB magnitudes of *Vega* in the ALHAMBRA photometric system.

2.4 Standard Stars System

So far we have defined the ALHAMBRA photometric system by the response curves of the combination of the filter+detector+atmosphere transmissions, but any photometric system needs a set of photometric-standard stars, and the choice of a magnitude system which gives a structure to the system. A standard star is a flux calibrated stellar spectrum in such a way that the values of its magnitudes in different photometric systems are well known, so, in other words, we need to anchor the system to a set of stars whose magnitudes in the 20 filter system are known, then we can compare the amount of light received from other objects observed by the ALHAMBRA survey to a standard star in order to determine the exact brightness, or stellar magnitude, of the object.

To calibrate the ALHAMBRA photometric system we have chosen two different sets of primary standard stars. The first one is a set of 31 classic spectrophotometric standard stars from several libraries such as Oke & Gunn (1983), Oke (1990), Massey & Gronwall (1990) and Stone (1996), together with the main standard stars adopted by the Hubble Space Telescope (Bohlin, 2007), and the SDSS standard $BD+174708$ (Tucker et al. 2001). This set was chosen in order to anchor the ALHAMBRA photometric system to standards that have been used on important photometric systems such as the SDSS, for which we have established transformation equations, as explained in the following chapters. These objects are stars with no detected variability within a few milli-magnitudes scale, available high-resolution spectra ($\leq$ 5 Å), and flux calibrated with errors lower than 5%. These standard stars are spread out all over the sky and are bright, but they do not cover all the spectral types, being mostly white dwarfs and main sequence A-type stars.

The second set of primary standard stars is formed by 288 stars from a recent spectral library, the HST/STIS Next Generation Spectral Library[4] (NGSL), (Gregg et al. 2004). This spectral library has been developed at the Space Telescope Science Institute and it consists of 378 high signal-to-noise stellar spectra. Our set of spectra is observed spectra with good spectral resolution, all of them obtained and flux calibrated homogeneously in a wavelength range covering from 2000Å to 10,200Å. This set of stars presents a wide range of values of T_{eff}, $log(g)$ and metallicity ($3440K \leq T_{eff} \leq 44500K$, $0.45 \leq log(g) \leq 7.5$ and $-3 \leq [Fe/H] \leq 0.7$), and a range of E(B-V) values between 0 and 0.6; they include several hot white dwarfs, and a great number of peculiar stars of different spectral types. These stellar objects represent a potential set of spectrophotometric standards, being valuable in the study of atmosphere parameters using model atmosphere fluxes. Coordinates and physical properties of the majority of these stars can be found at `http://archive.stsci.edu/prepds/stisngsl/`. These 288 stars together with the 31 classic spectrophotometric standards define the set of primary standards of the ALHAMBRA photometric system.

Magnitudes in the ALHAMBRA photometric system are set on the AB magnitude system (Oke & Gunn 1983), a monochromatic (f_ν) system in which the magnitude is directly related to physical units:

[4] `http://lifshitz.ucdavis.edu/~mgregg/gregg/ngsl/ngsl.html`

$$AB_\nu = -2.5\ \log f_\nu - 48.60, \tag{2.33}$$

where the constant comes from the expression

$$48.6 = -2.5 \log F_0, \tag{2.34}$$

and $F_0 = 3.63 \times 10^{-20} erg/cm^2/s/Hz$ is the flux of *Vega* at $\lambda = 5500$Å used by those authors. The parameter f_ν is the flux per unit frequency of an object in $erg/cm^2/s/Hz$.

The AB magnitudes will be estimated as follows:

$$m_\nu = -2.5\ \log \frac{\int f_\nu S_\nu\, d(\log \nu)}{\int S_\nu\, d(\log \nu)} - 48.6 \tag{2.35}$$

where S_ν is the response function of the system corresponding to the atmosphere-telescope-filter-detector combination.

Synthetic AB magnitudes in the standard ALHAMBRA system of these stars are presented in two tables, Table A.1 and Table A.2 of the Appendix. Nine stars (AGK81D266, BD17D4708, BD28D4211, BD75D325, FEIGE 110, FEIGE 34, G191B2B, HZ 44, P041C) are common to both sets. Magnitudes in the ALHAMBRA photometric system for these nine stars derived from the two different sources show differences lower than a few milli-magnitudes over the whole filter set, indicating that both groups of standard stars are anchored to the same physical system. However, once we have established the similitude and stability of the photometric zero points for both sets of standards, we will base the further analysis on the NGSL catalogue, which shows a higher degree of internal homogeneity, both in wavelength and flux calibrations.

Table 2.6 Synthetic ALHAMBRA AB magnitudes of the 31 spectrophotometric primary standard stars. Complete table in Appendix (Table A.1).

Star	A366M	A491M	A613M	A770M	A921M
g191b2b	11.04	11.57	11.99	12.45	12.82
bd75d325	8.77	9.32	9.75	10.21	10.58
feige34	10.40	10.97	11.38	11.80	12.11
p041c	13.40	12.13	11.84	11.73	11.72
alpha_lyr	0.96	-0.05	0.13	0.39	0.48

Table 2.7 Synthetic ALHAMBRA AB magnitudes of the 288 primary standard stars from the NGSL. Complete table in Appendix (Table A.2).

Star	A366M	A491M	A613M	A770M	A921M
BD17d4708	10.45	9.57	9.34	9.25	9.24
Feige110	11.15	11.62	12.05	12.47	12.82
G188-22	11.11	10.24	9.98	9.83	9.87
HD086986	9.13	7.94	8.02	8.14	8.16
HD204543	10.23	8.56	7.99	7.63	7.52

2.4.1 Comparison between the magnitudes of the four CCDs ALHAMBRA systems

A comparison of the three non-standard ALHAMBRA photometric systems and that chosen as the standard, has been performed first using the *Vega* spectrum above. We calculated the absolute differences between the AB magnitudes of the star in each one of the three replicas and the standard ALHAMBRA value, detecting that filter A366M shows the maximum absolute difference (up to 0.05 magnitudes). In the case of filter A394M there is a maximum of 0.02 magnitudes offset, filter A425M has a 0.01 magnitudes offset, and the rest of the filters have smaller differences.

Filter	CCD1	CCD2	CCD3	CCD4	Δmax
A366M	0.97	0.97	0.96	0.92	0.05
A394M	0.03	0.02	0.02	0.01	0.02
A425M	-0.14	-0.13	-0.13	-0.13	0.01

Secondly, we have developed a statistical analysis on the distribution of differences, using synthetic AB magnitudes of the 288 standard stars from the NGSL. Table 2.8 shows the result of this analysis. Once again filter A366M presents the largest difference in magnitude, reaching up to 0.0689 magnitudes for some stars in the sample. For the whole sample, the median of the differences in absolute value between AB magnitudes in the standard ALHAMBRA photometric system in filter A366M, and those determined from the three replicas is 0.0174 magnitudes, with a rms (calculated through MAD, median absolute deviation) of 0.0088. In the other filters the median of the absolute differences is less than 0.01 magnitudes, becoming smaller as we move to redder wavelengths.

Table 2.8 Analysis of the four instances of the ALHAMBRA system used with the LAICA camera

Filter	ΔMax	Median	RMS
A366M	0.0689	0.0174	0.0088
A394M	0.0236	0.0064	0.0053
A425M	0.0592	0.0058	0.0073
A457M	0.0148	0.0028	0.0025
A491M	0.0133	0.0011	0.0013
A522M	0.0325	0.0022	0.0021
A551M	0.0092	0.0008	0.0009
A581M	0.0110	0.0024	0.0019
A613M	0.0052	0.0003	0.0003
A646M	0.0085	0.0012	0.0007
A678M	0.0247	0.0009	0.0007
A708M	0.0031	0.0002	0.0001
A739M	0.0228	0.0009	0.0006
A770M	0.0042	0.0003	0.0003
A802M	0.0134	0.0006	0.0006
A829M	0.0016	0.0003	0.0003
A861M	0.0133	0.0009	0.0007
A892M	0.0034	0.0002	0.0003
A921M	0.0013	0.0003	0.0001
A948M	0.0028	0.0005	0.0003

Note. — The first column is the list of ALHAMBRA filters; the second is the maximum absolute difference between standard ALHAMBRA AB magnitudes and the magnitudes obtained from the three filter-detector replicas at each ALHAMBRA filter; the third represents the median of the former absolute differences; the fourth is the median absolute deviation of the distribution.

2.5 Calibration methods of the ALHAMBRA system: Zero point determination strategy

Having obtained the set of synthetic magnitudes of the standard primary stars, the calibration of the ALHAMBRA survey would then pass through the observation of a subset of standard stars per night, with different air masses and different exposition times, which would allow us to correct from atmospheric extinction and obtain the calibration equations of the system that subsequently would be applied to the observed ALHAMBRA fields in those observational campaigns, and at the same time they would fix the instrumental ALHAMBRA magnitudes of the standard primary stars. This is the direct and classic procedure in the definition of a photometric system and its application to the photometric calibration of the instrumental magnitudes of the problematic objects. This calibration strategy was manifest in a set of observational campaigns due to be carried out with the spectrograph "Albireo"at the Sierra Nevada Observatory (OSN). However, the number of stars then currently observed did not allow us to cover all ALHAMBRA fields with the suitable spectral coverage. Moreover, taking into account the observational strategy of the ALHAMBRA cartography and the total telescope time that was assigned for it, the photometric calibration of the ALHAMBRA fields with this calibration strategy proved to be absolutely impossible to perform, as it would have multiplied the telescope time by a factor of at least 1.5.

The need to calibrate the huge amount of instrumental magnitudes that the ALHAMBRA pipeline was proportioning made us consider an indirect calibration strategy. Therefore, the zero point calibration of the observed fields in the ALHAMBRA survey was carefully considered until we found a strategy robust and general enough to be applied to the whole survey and to all kind of astronomical objects. We tackled the issue in different ways, reaching a strategy with which zero points of ALHAMBRA fields are determined to an error below a few hundredths of magnitude for the whole range of spectral types in the sample. The different strategies considered before the final method was determined are explained below.

2.5.1 Calibration based on Sloan Digital Sky Survey transformation equations

In a first approximation to the problem, a strategy based on the Sloan Digital Sky Survey[5] (SDSS), which is a well-known astronomical project that has obtained deep multi-color images covering more than a quarter of the sky, was considered. Its photometric system is formed by five non-overlapping color bands (*ugriz*) that cover the complete optical range from 3000Å to 11.000Å (Fukugita et al. 1996; Smith et al. 2002). This idea has been used with other classic photometric systems, such as the UBVRI Johnson-Cousins system (Cousins 1976), and it consists of establishing transformation equations between the system we want to calibrate and the SDSS photometric system; then, in the fields with SDSS photometry, we can obtain the AB ALHAMBRA magnitudes of our objects from these transformation equations, and finally these stars will be used as secondary standard stars, as replacements for the primary standard

[5] `http://www.sdss.org`

stars in the system calibration. The only difference with regard to other systems is that to estimate the transformation equations we use synthetic magnitudes instead of observational magnitudes. A more detailed description of the SDSS system is presented in Chapter 3, where it is explained how these transformation equations between both systems were developed.

The calibration strategy entails the following steps:

1 Selection of stars inside the ALHAMBRA fields. In this sample, we take only those stellar objects with a photometry more precise than a certain value, and then we look for those with SDSS photometry. The SDSS photometry from the SDSS-DR6 catalogue was used for the purpose.

2 Obtaining the ALHAMBRA photometry of these stars through the application of the transformation equations between both systems. We called these magnitudes "transformed" ALHAMBRA magnitudes to avoid confusions.

3 For the same set of stars, analysis of the differences between the instrumental ALHAMBRA magnitudes provided by the pipeline, and those determined from the transformations of the SDSS photometry. Determination of the zero points in each filter as a central value of this distribution of differences.

To test the designed methodology, the photometry of the ALHAMBRA field 8 pointing 1 and field 7 pointing 3 were used. The instrumental ALHAMBRA magnitudes we considered here are the magnitudes called AUTO of SExtractor. To select the stellar objects in the ALHAMBRA catalogue, we use a morphologic parameter of SExtractor (Bertin & Arnouts 1996) that gives the probability of an object being a star based on the morphology of the object in the DEEP image that is an image formed by the combination of the 23 ALHAMBRA filters. Thus, we select the objects in the catalogue with a parameter value higher than 0.9. In the ALHAMBRA field stars sample we take the stars with SDSS photometry, and in this subset we choose only the stars with photometric errors below 0.05 magnitudes, in both the instrumental ALHAMBRA magnitudes as well as in the SDSS magnitudes, and labeled with good photometric quality in their measurements. The stars from the SDSS catalogue in the studied region were selected through a SQL request included on the Sloan project web page[6]. The search of common stars was carried out with a code implemented in Matlab, with a tolerance of 10^{-4} degrees. Once we had the common stars in both surveys, the transformed ALHAMBRA magnitudes were determined and the differences between these and the instrumental magnitudes were calculated. The data obtained were refined of outliers with a Chebyshev filter:

$$|x_i - \bar{x}| < k * \sigma \tag{2.36}$$

where $\bar{x}$ is the central value of the differences, k is a constant, in particular we take $k = 3$, and σ is the MAD of the data.

[6] `http://cas.sdss.org/dr6/en/tools/search/sql.asp`

In the resulting distribution of differences (in the sense of instrumental minus transformed AB magnitude), we noticed a systematic structure which depended on the magnitude of the stars, the differences of the brighter stars being higher than the weaker ones, up to one magnitude ahead in some filters. To show this phenomenon, in Figure 2.8 we plot the magnitude differences for filter A394M versus the SDSS magnitude u, for the sample of field stars in field 8 pointing 1 using the method presented above.

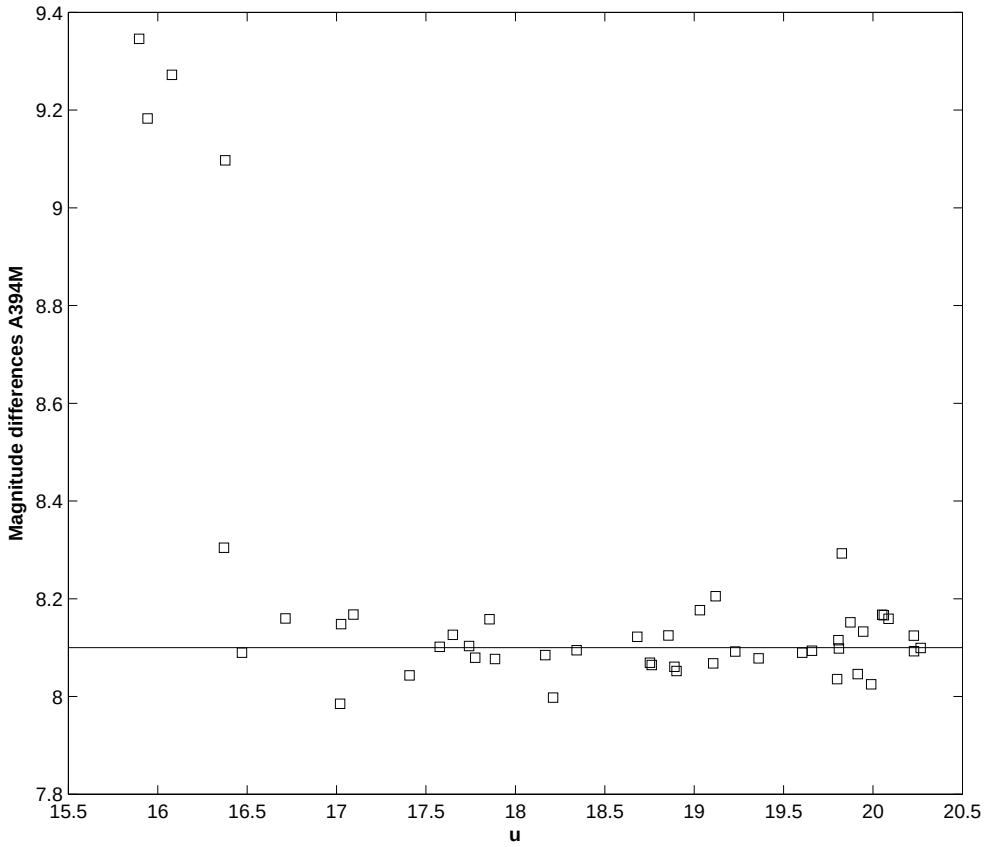

Figure 2.8 Magnitude differences in filter A394M versus SDSS magnitude u, for the field stars in the ALHAMBRA field 8 pointing 1 with SDSS photometry, and with photometric errors lower than 0.05 magnitudes in all bands of both photometric systems. These are differences between the instrumental magnitude of the stars and the magnitude obtained from the ALHAMBRA-SDSS transformation equations. The horizontal line represents the zero-point solution determined with this methodology.

However, this anomalous result seems not to be limited to the pair ALHAMBRA-SDSS systems, but is also found in other photometric systems that use transformation equations to calibrate the zero points from data of the SDSS. A particular example can be seen in Chonis & Gaskell (2008) with the UBVRI Johnson-Cousins system. Figure 2.9 shows the differences between the calibrated U magnitude for a set of Landolt stars and the magnitude from the application of some transformation equations, versus the SLOAN u magnitude (this figure is taken from Chonis & Gaskell, 2008). It is obvious that there is a different distribution of

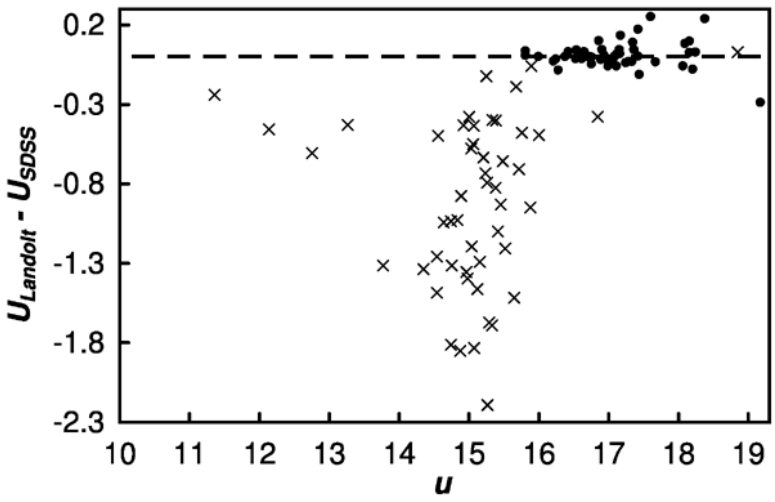

Figure 2.9 Differences between calibrated U magnitudes from Landolt standard stars, and the magnitudes obtained from the transformations equations between the UBVRI system and the SDSS system. The discontinuous line represents the zero point determined from the weakest stars. Figure taken from Chonis & Gaskell (2008).

the zero points in those stars brighter than $u = 16$. In the case of the ALHAMBRA system, the differences are also presented for stars brighter than $u = 16$. Those authors proposed some possible explanations to account for the observed systematic differences, in particular the saturation of Sloan stars in the brightest magnitudes, but we consider that a detailed discussion of the precision and accuracy of the brightest stars photometry in the SDSS catalogue is beyond the scope of our work.

From a functional point of view, the conclusion we came to was that the calibration of the zero point had to be based only on the weakest Sloan stars, within a certain range of precision. Empirically, we checked that the simplest criterion for the choice of the secondary standard stars in the ALHAMBRA system was to have a transformed A366M magnitude greater than 16, and photometric errors lower than 0.05 magnitudes were also needed.

Table 2.9 presents the photometric zero points from field 8 pointing 1 and field 7 pointing 3 with this methodology and their corresponding errors (measure of the precision of the median).

Table 2.9 Photometric zero points of ALHAMBRA field 8 pointing 1 (columns 2-3) and ALHAMBRA field 7 pointing 3 (columns 4-5) from the calibration method based on the transformation equations of the SDSS system. In the first case, field 8 pointing 1, the number of stars considered to determine the zero points is 17. In the case of the field 7 pointing 3 there are 14 stars.

Filter	ZP (F8P1)	Error	ZP (F7P3)	Error
A366M	7.60	0.061	7.64	0.067
A394M	8.09	0.047	7.29	0.048
A425M	9.16	0.043	8.59	0.038
A457M	8.74	0.036	8.18	0.041
A491M	8.73	0.017	8.72	0.030
A522M	8.51	0.034	7.89	0.040
A551M	8.59	0.018	7.83	0.023
A581M	8.69	0.035	8.67	0.036
A613M	8.52	0.017	8.70	0.025
A646M	8.6	0.026	8.82	0.017
A678M	8.57	0.037	8.11	0.039
A708M	8.42	0.031	8.46	0.035
A739M	8.87	0.023	8.34	0.018
A770M	7.97	0.028	7.87	0.017
A802M	8.44	0.036	7.65	0.025
A829M	8.43	0.034	7.31	0.046
A861M	8.13	0.021	7.38	0.027
A892M	7.22	0.029	6.52	0.026
A921M	6.59	0.049	6.62	0.052
A948M	5.95	0.035	6.21	0.035

2.5.2 New Calibration Strategy

In order to overcome the troubles derived from a direct comparison between instrumental and standard ALHAMBRA values obtained from SDSS-to-ALHAMBRA transformations, we decided to study other methods for the determination of the zero points of the system. After an exhaustive analysis, taking into account the peculiarities of our system, we found a strategy that is robust and general enough to be applied to the whole survey and to all kinds of astronomical objects, and which determines the zero points of the ALHAMBRA fields with an error below or equal to a few hundredths of magnitude for the whole range of spectral types in the sample. This method makes use of the set of standard stars from the NGSL, and entails the following steps:

1. The first task, as in the former methodology, is to perform an exhaustive selection of field stars found in the ALHAMBRA sources catalogue for each field. We select objects morphologically classified by SExtractor as stellar objects at the three reddest filters, A892M, A921M, and A948M. It is possible that the pipeline may recognize the nucleus of a distant galaxy as a star in the bluest filters, while in the reddest ones it is classified as an extensive object, so we focus primarily on classification in the reddest filters. Among these, we select the stars with low photometric error (less than 0.15 magnitudes) in all ALHAMBRA bands. As an example, in Figure 2.10 we show the objects selected from field 8 pointing 1, where it can be seen that the great majority of these stars are main sequence stars of late spectral types.

2. Using this set of stars we look for those that have SDSS *ugriz* photometry as well as photometric errors lower than 0.15. We select SDSS stars in the studied region from the SDSS DR7 catalogue, using the SkyServer Tools offered on its web page[7]. Amongst the different types of search requests we choose the more complete SQL Search, where one can search for the needed objects directly from the DR7 database. The search of common stars was carried out with a code implemented in Matlab, with a tolerance of 10^{-4} degrees.

3. Then, for each stellar object, we find the star (within the 288 NGSL objects) that best fits with its SDSS photometry. The *ugriz* synthetic magnitudes for the NGSL stars were obtained from the filters and detector set that formed the SDSS standard system given by Smith et al. (2002), USNO, located in the US Naval Observatory 1m telescope. Then, for each field star, we look for the NGSL star that minimizes the variance of the differences between its SDSS (synthetic) magnitudes and the SDSS (observed) magnitudes of the field star. This idea is based on the fact that the apparent magnitudes of two physically identical stars, which are at different distances in an empty space, only differ in a constant term for every magnitude, which is equal to the difference of the geometric distance module of both stars ($\delta v = 5\log(\frac{r_2}{r_1})$), and consequently the former variance is

[7] `http://cas.sdss.org/dr7/en/tools/search/radial.asp`

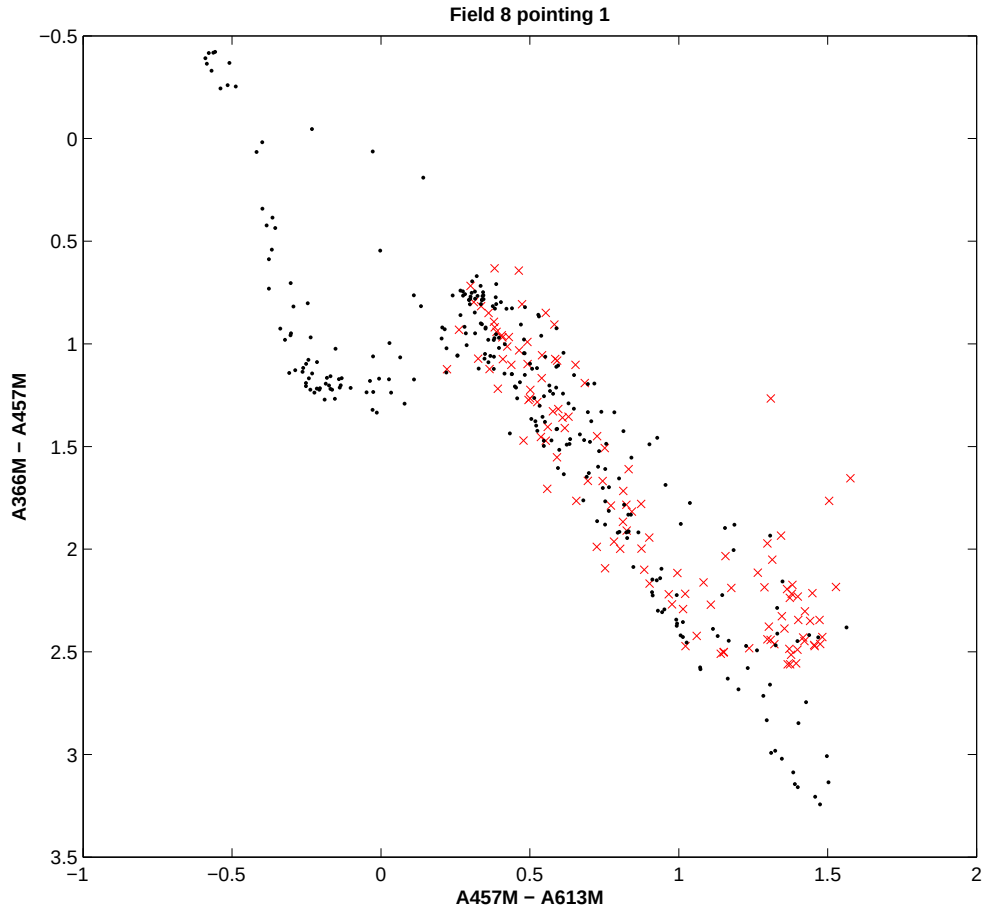

Figure 2.10 ALHAMBRA color-color diagram. Black points represent the 288 stars from the Next Generation Spectral Library, and red crosses represent the field stars in field 8 pointing 1 of the ALHAMBRA survey. Figure from Aparicio Villegas et al. (2010).

clearly null. Finally, the ALHAMBRA AB magnitudes assigned to the field star are the ALHAMBRA AB magnitudes of the NGSL star plus the difference of the distance module, calculated with the average difference of the Sloan magnitudes of both stars. In Figure 2.11 we show, as an example, the spectrum of the star HD160346 in AB magnitudes, together with the instrumental magnitudes plus the zero points of a field star fitted with this NGSL star in the algorithm, and also its SDSS photometry.

4. The distribution of the differences between instrumental magnitudes and synthetic AB magnitudes of all the field stars is refined from outliers with a Chebyshev filter:

$$|x_i - \bar{x}| < k * \sigma \tag{2.37}$$

where $\bar{x}$ is the central value of the differences, k is a constant, in particular we take $k = 3$, and σ is the MAD of the data. The zero point is determined as the central value of this distribution of differences.

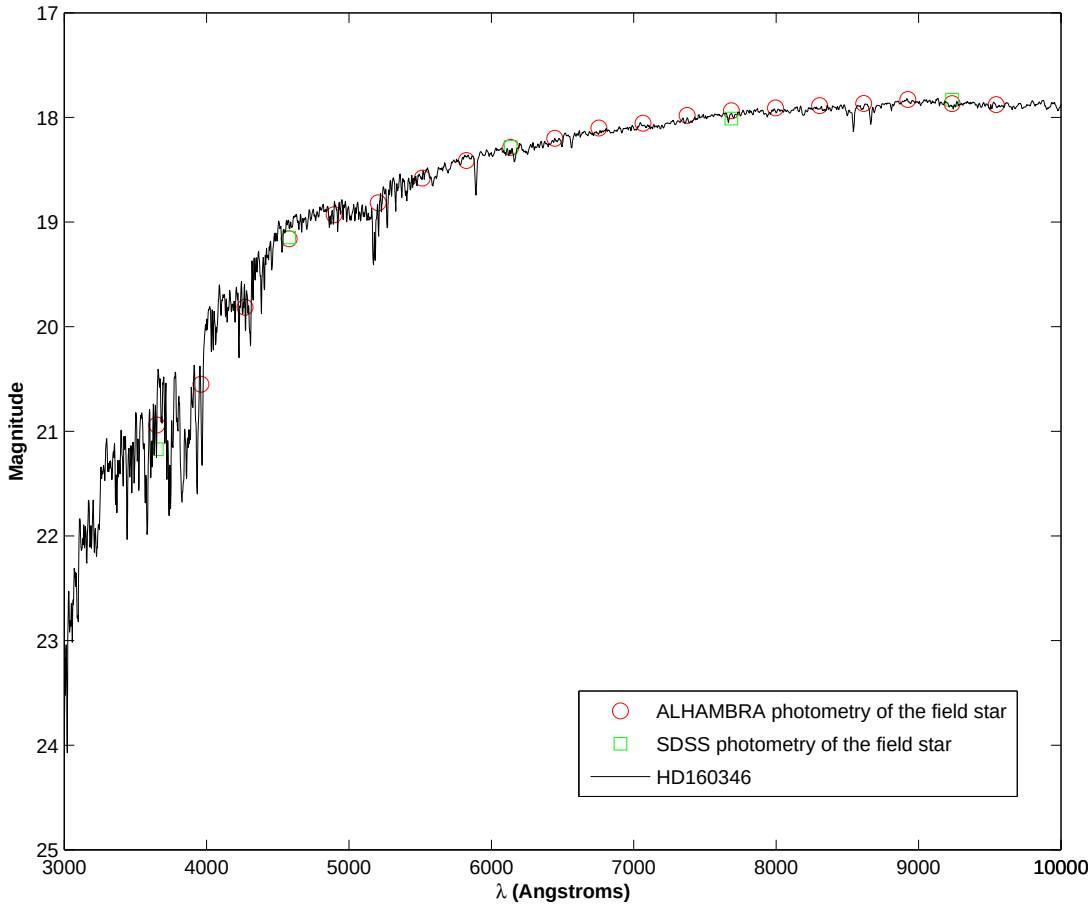

Figure 2.11 Spectrum in AB magnitudes of the star HD160346, belonging to the set of NGSL standard stars. The spectrum is scaled so that this object is the best fit for the zero point determination to the star at RA = 356.3323 and DEC = 15.5486. The red circles are the instrumental magnitudes of the field star plus the zero points determined with our final strategy, and the green squares are its SDSS photometry. Figure from Aparicio Villegas et al. (2010).

Table 2.10 Photometric zero points for ALHAMBRA field 8 pointing 1 (columns 2-3) and field 7 pointing 3 (columns 4-5). 94 stars are considered to determine the zero points of the field 8 pointing 1, and 43 stars in field 7 pointing 3.

Filter	ZP (F8P1)	Error	ZP (F7P3)	Error
A366M	7.42	0.011	7.51	0.036
A394M	8.31	0.008	8.34	0.028
A425M	8.48	0.007	8.52	0.016
A457M	8.67	0.009	8.75	0.016
A491M	8.73	0.004	8.74	0.013
A522M	8.52	0.005	8.52	0.012
A551M	8.59	0.004	8.60	0.011
A581M	8.67	0.006	8.69	0.013
A613M	8.47	0.004	8.45	0.013
A646M	8.59	0.004	8.58	0.009
A678M	8.54	0.005	8.50	0.010
A708M	8.37	0.004	8.35	0.008
A739M	8.84	0.004	8.84	0.007
A770M	7.96	0.003	7.99	0.007
A802M	8.41	0.004	8.40	0.007
A829M	8.41	0.005	8.40	0.008
A861M	8.11	0.004	8.10	0.008
A892M	7.21	0.004	7.21	0.009
A921M	6.59	0.006	6.60	0.010
A948M	5.98	0.006	5.94	0.011

Table 2.10 shows the main characteristics of the photometric zero points of the ALHAMBRA field 8, pointing 1 and field 7, pointing 3, as an example of the results obtained when applying this strategy. Comparing with the same table in the previous section (Table 2.9), the fact that the errors of the zero points have decreased with this new method stands out; these errors are measures of the errors of the medians that form the zero points. Moreover, the systematic structures we were able to appreciate when determining the zero points using transformation equations from Sloan photometry, do not appear in the distribution of differences between synthetic and instrumental magnitudes with this strategy. Figure 2.12 shows this distribution for filter A457M versus the SDSS u magnitude, where it can be seen that the brightest stars now present a zero point in keeping with the average zero points of the whole sample, even though the photometric errors are greater.

In order to test this methodology, we developed an algorithm based on the idea of Zhou et al. (1999), who calculate the zero points of the BATC 15 photometric system from instrumental colors, previously fitting the field stars to stellar models from a mixture of different libraries including the theoretical SEDs of Kurucz (1992, 1993) and the observational SEDs of Gunn & Stryker (1983) and Straižys & Sviderskiene (1972). The zero points are determined with an algorithm of convergence calling subroutines of MINUIT package (James 1994) from the

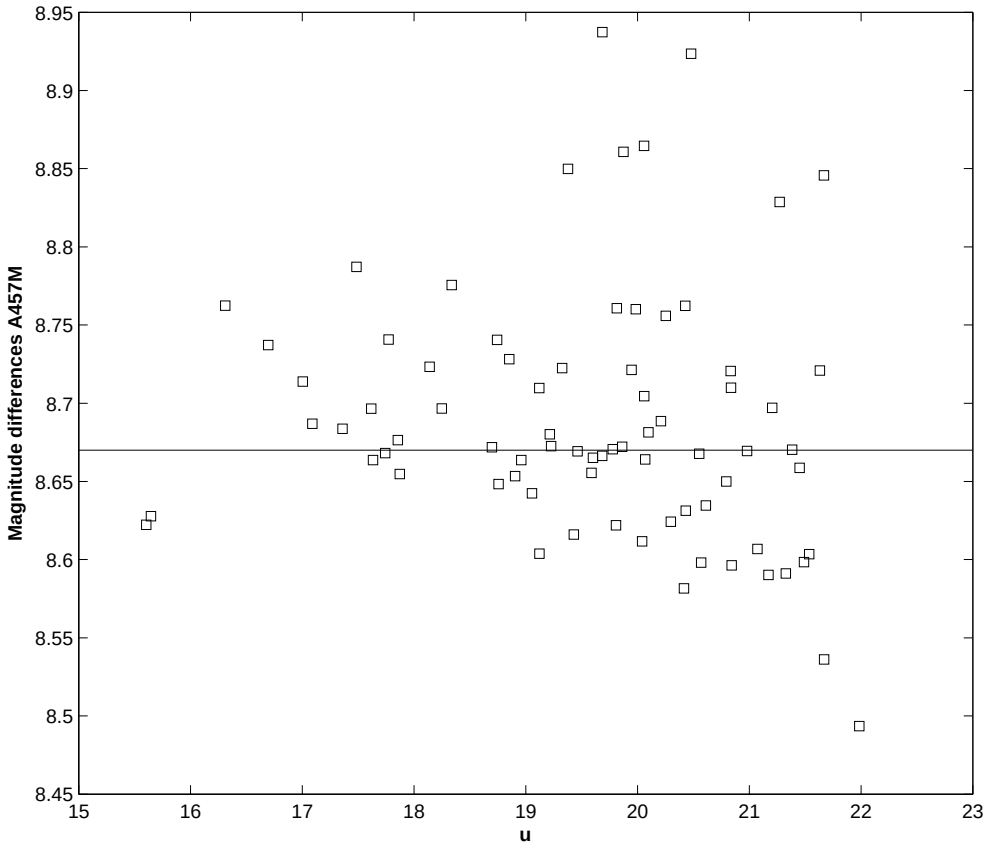

Figure 2.12 Magnitude differences in filter A457M versus SDSS magnitude u, for the field stars in the ALHAMBRA field 8 pointing 1. These are differences between the instrumental magnitude of the stars and the magnitude obtained from the ALHAMBRA-SDSS transformation equations. The horizontal line represents the zero-point solution determined with this methodology.

CERNLIB software. In our case, the standard stars from the NGSL were used to fit the field stars, and in the algorithm we call subroutines of the PyMinuit package (an extension module for Python that passes low-level MINUIT functionality to Python functions). We compare the results from our method and the results from this algorithm, and they differ in at the most 6 hundredths of magnitudes in all ALHAMBRA filters, except in A366M and A394M where the differences reach 1 tenth. So we can conclude that the method applied is robust and reliable.

Bibliography

Aparicio Villegas, T., Alfaro, E. J., Cabrera-Caño, J., et al. 2010, AJ, 139, 1242

Benítez, N., et al. 2009, ApJ, 692, L5

Bertin, E., & Arnouts, S. 1996, A&AS, 117, 393

Bohlin, R. C. 2007, The Future of Photometric, Spectrophotometric and Polarimetric Standardization, 364, 315

Chonis, T. S., & Gaskell, C. M. 2008, AJ, 135, 264

Cousins, A. W. J. 1976, MmRAS, 81, 25

Fukugita, M., Ichikawa, T., Gunn, J. E., Doi, M., Shimasaku, K., & Schneider, D. P. 1996, AJ, 111, 1748

Golay, M. 1974, Astrophysics and Space Science Library, 41,

Gregg, M. D., et al. 2004, Bulletin of the American Astronomical Society, 36, 1496

Gunn, J. E., & Stryker, L. L. 1983, ApJS, 52, 121

James, F. 1994, MINUIT: Function Minimization and Error Analysis (CERN Program Libr. Long Writeup D506) (version 94.1; Geneva: CERN)

Kurucz, R. L. 1992, The Stellar Populations of Galaxies, 149, 225

Kurucz, R. 1993, ATLAS9 Stellar Atmosphere Programs and 2 km/s grid. Kurucz CD-ROM No. 13. Cambridge, Mass.: Smithsonian Astrophysical Observatory, 1993., 13,

Kurucz, R. L. 2005, Memorie della Societa Astronomica Italiana Supplement, 8, 14

Massey, P., & Gronwall, C. 1990, ApJ, 358, 344

Moles, M., et al. 2008, AJ, 136, 1325

Oke, J. B., & Gunn, J. E. 1983, ApJ, 266, 713

Oke, J. B. 1990, AJ, 99, 1621

Sánchez, S. F., Aceituno, J., Thiele, U., Pérez-Ramírez, D., & Alves, J. 2007, PASP, 119, 1186

Schneider, D. P., Gunn, J. E., & Hoessel, J. G. 1983, ApJ, 264, 337

Smith, J. A., et al. 2002, AJ, 123, 2121

Stone, R. P. S. 1996, ApJS, 107, 423

Straižys, V., & Sviderskiene, Z. 1972, Vilnius Astronomijos Observatorijos Biuletenis, 35, 3

Tokunaga, A. T., & Vacca, W. D. 2005, PASP, 117, 1459

Tucker, D. L., Smith, J. A., & Brinkmann, J. 2001, The New Era of Wide Field Astronomy, 232, 13

Zhou, X., Chen, J., Xu, W., Zhang, M., Jiang, Z., Zheng, Z., & Zhu, J. 1999, PASP, 111, 909

3

ALHAMBRA transformations with other Photometric Systems*

To begin this chapter, some relations between the ALHAMBRA photometric system and the Sloan Digital Sky Survey filter system are presented. Transformation equations for stars are developed based on the 288 NGSL stars, and later the validity of these when they are applied to galaxies is analyzed. Several tables with ALHAMBRA colors of different kinds of observed galaxies, at different redshifts, are also elaborated, using an empirically calibrated library, and taking SDSS filter r as reference. Secondly, the filter system of the Gaia mission is connected to the ALHAMBRA photometry by some transformation equations, valid for stars, and generated with the same strategy as with the SDSS system. Finally, cubic transformation models from ALHAMBRA to Gaia photometry (and vice versa) are developed using the same method the Gaia team used between Sloan and Gaia filters, in order to make possible a comparison between the ALHAMBRA and SDSS systems in establishing some relations with Gaia photometry.

3.1 Sloan Digital Sky System

The Sloan Digital Sky Survey (SDSS) is a multi-filter imaging and spectroscopic redshift survey that, over eight years of operations (SDSS-I, 2000-2005; SDSS-II, 2005-2008), obtained deep, multi-color images covering more than a quarter of the whole sky and created 3-dimensional maps containing more than 930,000 galaxies and more than 120,000 quasars.

The survey was begun in 2000, and for 5 years it imaged more than 8,000 square degrees of the sky with photometric observations of around 500 million objects, and it obtained spectra of galaxies and quasars (more than 1 million objects) selected from 5,700 square degrees of that imaging. The main galaxy sample has a median redshift of z = 0.1; there are redshifts for luminous red galaxies as far as z = 0.6, for quasars as far as z = 5; and the imaging survey has been involved in the detection of quasars beyond a redshift z = 6. In the year 2006 the survey entered a new phase, the SDSS-II, by extending observations to explore the structure

*Partially included in: T. Aparicio Villegas et al. 2010, The Astronomical Journal , 139, 1242

and stellar composition of the Milky Way, through the SEGUE Project (Sloan Extension for Galactic Understanding and Exploration), and the Sloan Supernova Survey, which watches after supernova Ia events to measure the distances to far objects. SDSS is continuing with the Third Sloan Digital Sky Survey (SDSS-III), a program of four new surveys using SDSS facilities. SDSS-III began observations in July 2008 and released its first public data as Data Release 8, which includes all photometric observations that will be taken with the SDSS imaging camera, covering 14,555 square degrees on the sky (just over 35% of the full sky). SDSS-III will continue operating and releasing data through 2014.

The SDSS uses a dedicated 2.5-meter telescope at Apache Point Observatory, New Mexico, equipped with two powerful special-purpose instruments; a CCD camera, specially designed to take wide field (3 degrees in diameter) images using a 5x6 mosaic of 2048x2048 CCD's, in five wavelength bands; and a pair of spectrographs fed by optical fibers measures spectra of more than 600 galaxies and quasars in a single observation. The telescope uses the drift scanning technique, so the telescope is fixed and makes use of the Earth's rotation to record small strips of the sky. This method allows consistent astrometry over the widest possible field and precision remains unaffected by telescope tracking errors.

3.1.1 Filter system

The SDSS photometric system is formed by five non-overlapping wide bands (*ugriz*) that cover the complete optical range from 3000Å to 11,000Å (Fukugita et al. 1996; Smith et al. 2002). The effective wavelengths, defined by Schneider et al. (1983), equation (2.27), and the full width half-maxima of the filters are shown in the following table:

Filter	λ_{eff} (nm)	FWHM (nm)
u	354.0	59.9
g	477.0	137.9
r	622.2	138.2
i	763.2	153.5
z	904.9	137.0

The response curves of the standard SDSS system are shown in Figure 3.1, where the transmission of the ALHAMBRA photometric system is also superimposed, thus obtaining a visual comparison of both systems. The SDSS response functions correspond to the product of three different transmissions: USNO filters and detector which formed the standard system given by Smith et al. (2002), and atmospheric transmission at 1.2 airmasses at the altitude of Calar Alto Observatory. The magnitude system that the SDSS adopted is the AB magnitude system defined by Oke & Gunn (1983), the same as in the ALHAMBRA system.

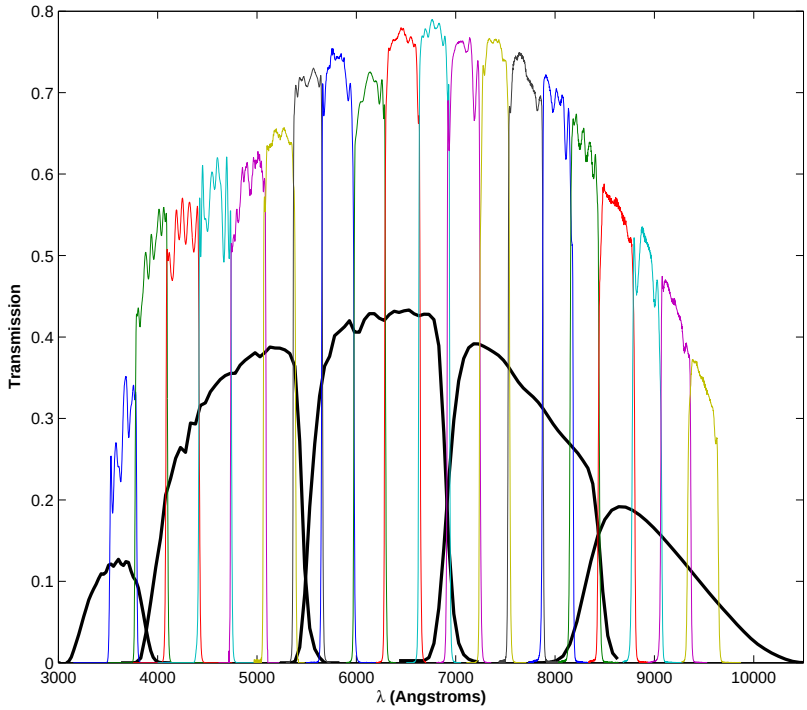

Figure 3.1 Response functions of the SDSS standard system (USNO) and the standard ALHAMBRA photometric system, both with atmospheric transmission at 1.2 airmasses at the altitude of Calar Alto Observatory. Figure from Aparicio Villegas et al. (2010).

Based on the proximity of their effective wavelengths, the ALHAMBRA filters which better correspond to the 5 SDSS bands are the following:

SDSS Filter	λ_{eff} (nm)	ALHAMBRA Filter	λ_{eff} (nm)
u	354.0	A366M	366.1
g	477.0	A491M	491.3
r	622.2	A613M	613.4
i	763.2	A770M	769.9
z	904.9	A921M	920.7

In this way, a zero-order approximation to the SDSS photometric system could be given by the ALHAMBRA colors A366M-A491M (corresponding to the u-g SDSS color), A491M-A613M (g-r color), A613M-A770M, (r-i color) and A770M-A921M (i-z color).

However, the different widths of the filters in the two systems have to be taken into account (see Figure 3.1 for a graphic comparison). The ALHAMBRA photometric system uses medium-band filters ($\approx$ 31 nm wide), so they are more sensitive to discontinuities in the spectral energy distribution. On the contrary, the SDSS wide-band filters transmit more energy, permitting the detection of fainter objects, but showing more difficulties in the interpretation and analysis of the information derived from their photometric measurements.

3.1.2 ALHAMBRA-SDSS transformations

The transformation equations from SDSS magnitudes to the ALHAMBRA photometric system (and vice versa) have been calculated using synthetic AB magnitudes for the subset of the ALHAMBRA primary standards from the NGSL. The *ugriz* synthetic magnitudes were obtained from the filters and detector set, following the SDSS standard system given by Smith et al. (2002, USNO), located in the US Naval Observatory 1m telescope.

The elaboration of the linear model, used to obtain the magnitudes in the ALHAMBRA photometric system from SDSS photometry, has been developed using the statistical software **R** [1], in particular the statistical task called "Backward Stepwise Regression" that uses the Bayesian Information Criterion (BIC), a tool for model selection defined as:

$$BIC = -2 \ln\ L + k\ \ln(n) \tag{3.1}$$

where L is the maximized value of the likelihood function for the estimated model, k the number of free parameters to be estimated, and n is the sample size (number of observations).

The transformation equations are, in general, valid for the range of stellar parameters covered by the selected 288 NGSL stars (see section 2.4). Table 3.1 shows the coefficients of the transformation from SDSS magnitudes to ALHAMBRA photometry. In the first column the dependent variables of the linear regression are listed, composed of a color formed with an ALHAMBRA band minus a SDSS band; the independent variables are correlative SDSS colors. The last column represents the residual standard error of each fit, that is, the expected error in a single estimation. The bluest filters are more sensitive and so they present higher errors in the models, tailing off with the most central wavelengths of the spectrum.

The use of colors in the linear model as dependent and independent variables is not arbitrary, indeed they are chosen instead of using magnitudes in order to force the sum of the linear model coefficients to be 1, a necessary condition when we are comparing magnitudes and not colors, as we explain below. From a model such as,

$$Alh_i = \sum_j a_{ij} \cdot Sloan_j + b_i \tag{3.2}$$

it follows that the same star observed (using any photometric system) at different distances would have the same magnitudes plus a single constant equal for all filters, μ, so the equations should verify,

$$\begin{aligned} Alh_i + \mu &= \textstyle\sum_j a_{ij} \cdot (Sloan_j + \mu) + b_i = \\ &= \textstyle\sum_j a_{ij} \cdot Sloan_j + b_i + (\sum_j a_{ij}) \cdot \mu \end{aligned} \tag{3.3}$$

which implies that the coefficients in the transformation equations should satisfy that the sum

[1] `http://www.r-project.org`

Table 3.1 Coefficients of the transformation equations from SDSS to ALHAMBRA photometry

	Synthetic					
	∅	u-g	g-r	r-i	i-z	Error
A366M - i	-0.0209	0.9813	0.7946	1.0889		0.038
A394M - i	-0.1997	0.4183	1.9673	0.8166	-0.8552	0.097
A425M - i	-0.0639	0.1475	1.4885	0.8921		0.058
A457M - i	-0.0094		1.0195	1.0358	0.1799	0.037
A491M- i	0.0240		0.6274	1.2114	0.1969	0.024
A522M - i	-0.0239		0.6204	1.0030		0.028
A551M - g	-0.0093	-0.0108	-0.6518	0.1231	-0.0975	0.010
A581M - g	-0.0029	-0.0018	-0.9166	0.2327	-0.0547	0.007
A613M - g	-0.0009	0.0129	-1.0759	0.1896		0.009
A646M - g	-0.0023	0.0159	-1.0349	-0.2544		0.011
A678M - g	0.0131	0.0077	-1.2133	-0.1184	0.1035	0.022
A708M - g	-0.0155	0.0218	-1.1169	-0.4915		0.014
A739M - g	-0.0096	-0.0104	-0.9076	-1.1087	0.0677	0.006
A770M - g	0.0165	-0.0068	-1.0636	-0.9769		0.007
A802M - g	-0.0005	0.0139	-1.0063	-1.2263	-0.1022	0.006
A829M - g	0.0036	0.0199	-1.0274	-1.2496	-0.2488	0.006
A861M - g	0.0159	0.0211	-1.0723	-1.0679	-0.6102	0.011
A892M - g	0.0171	-0.0192	-1.0259	-1.0268	-0.8638	0.015
A921M - g	0.0055	-0.0163	-0.9414	-1.0725	-1.1318	0.019
A948M - g	0.0221		-0.9802	-0.9667	-1.4006	0.021

Note. — Last column represents the residual standard error of each fit, that is the expected error in a single estimation.

of all the coefficients is equal to 1. With this in mind, the equations can be posed as:

$$Alh_i - Sloan_k = \sum_{j=1}^{4} c_{ij} \cdot (Sloan_j - Sloan_{j+1}) + d_i \tag{3.4}$$

where $Sloan_k$ is any of the five SDSS bands, and so we avoid that condition and the systematic errors that this entails.

Table 3.2 shows the coefficients of the inverse transformation equations, from ALHAMBRA photometry to SDSS magnitudes, obtained with the same procedure. For each SDSS filter minus one of the ALHAMBRA filters, the column below shows the coefficients of each one of the 19 ALHAMBRA colors, plus the independent term. The last row gives the residual standard error of each fit.

Table 3.2 Coefficients of the transformation equations from ALHAMBRA to SDSS photometry

	Synthetic				
	u - A522M	g - A613M	r - A522M	i - A522M	z - A613M
∅	-0.0247	0.0197	-0.0006	-0.0002	-0.0116
A366M - A394M	1.0741				
A394M - A425M	1.2574	0.0467		-0.0142	-0.0337
A425M - A457M	0.9768	0.2250		0.0177	
A457M - A491M	1.4529	0.2282	-0.0535	-0.0336	
A491M - A522M	0.8850	0.4580			
A522M - A551M		0.6206	-1.0334	-1.0117	
A551M - A581M		1.4129	-0.8928	-0.9767	
A581M - A613M		1.3538	-0.5793	-0.9498	
A613M - A646M			-0.3299	-0.9424	-0.9459
A646M - A678M	-0.2832		-0.1895	-0.9525	-0.9399
A678M - A708M	1.9317			-1.0060	-1.0696
A708M - A739M	-1.6333	-0.4194	-0.2017	-0.8624	-1.0935
A739M - A770M	-1.7633		-0.1224	-0.5364	-0.7336
A770M - A802M		0.6199		-0.2679	-1.0201
A802M - A829M	2.5577	1.2026	0.3267		-0.5209
A829M - A861M		-0.2826			-1.0507
A861M - A892M					-0.5793
A892M - A921M	-1.2739	-0.2896	-0.0429		
A921M - A948M					-0.7648
Error	0.0253	0.0121	0.0035	0.0024	0.0102

Note. — Last row gives the residual standard error of each fit.

3.1.3 Redshift Galaxy templates

Color transformations for stars, in general, would not offer accurate results for galaxies, especially when the effects of redshift and intergalactic absorption are taken into account. It is therefore desirable to describe the colors of observed galaxies at different redshifts in the system, as accurately as possible. To do so, we use the empirically calibrated library of Benítez et al. (2004). We generate estimated colors for the galaxies in the library in redshift intervals of 0.05, using the SDSS filter r as reference for all the ALHAMBRA medium-band filters. All colors correspond to the AB system, and were calculated using the functions included in the module bpz_tools from the BPZ package (Benítez 2000) which offers an accuracy similar to that of SYNPHOT (Baggett et al. 1997). We present here the tables for the E/S0, Sbc, Im, SB2, SB3 and Scd templates for the ALHAMBRA photometric system (Tables A.3 to A.5 in the Appendix). These lists allow us to determine the k-correction in a easy way, by estimating spectral indices at observing frequencies other than the rest frequency. The k-values enable the correction of the magnitude (or color) of a galaxy in a certain wavelength range from the redshift effects, so it is possible to compare the measures through the same filter of objects at

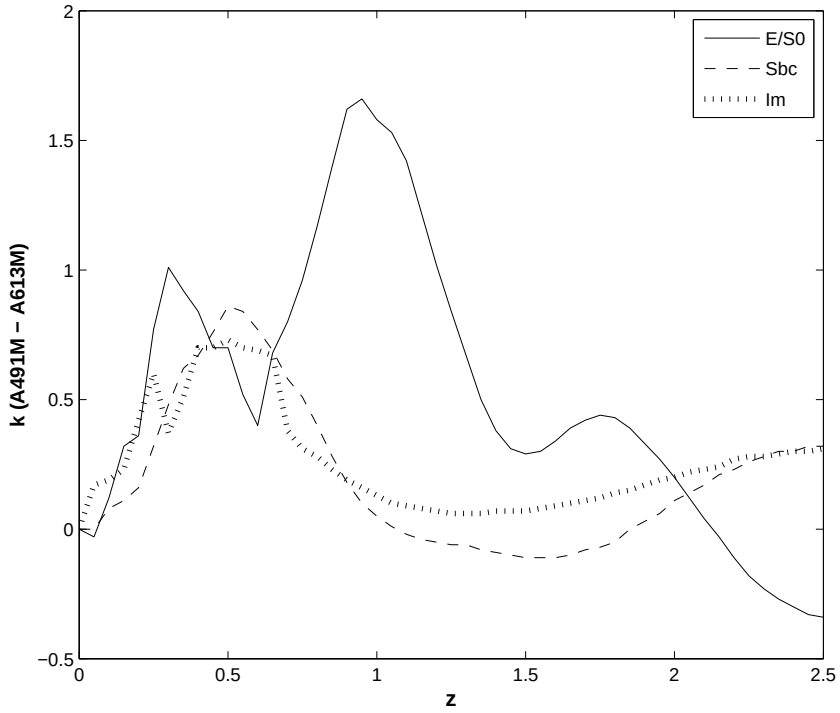

Figure 3.2 k-correction for different values of redshift (z) for ALHAMBRA color A491M-A613M and three galaxy templates. Figure from Aparicio Villegas et al. (2010).

different redshifts. By way of example, Figure 3.2 and Figure 3.3 represent the variation of the k-correction for two ALHAMBRA colors, A491M-A613M and A770M-A921M respectively, versus different values of z for the E/S0, Sbc, Im galaxy templates.

These tables must be used with caution, since it is obvious that a few templates cannot represent all the possible variations of real galaxy spectra. Nevertheless, they also serve as a guide to transform galaxy colors between different photometric systems for a given spectral type and redshift. To this end, we need to find the closest possible match in redshift and spectral type in the electronic tables, using as many colors as possible. Then we look up the corresponding color in the table corresponding to the spectral type and filter of interest, using interpolation between spectral types and redshifts if needed.

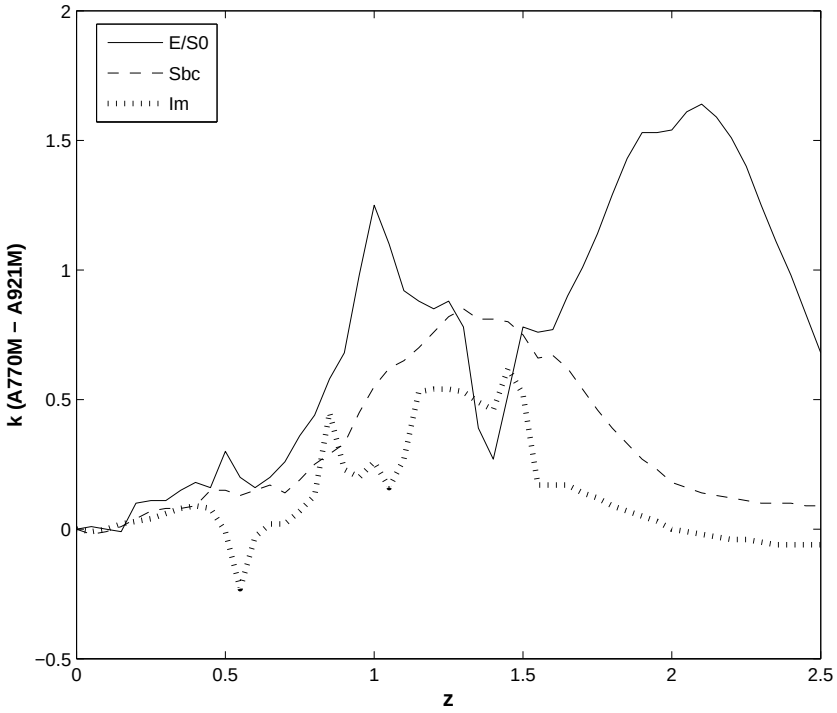

Figure 3.3 k-correction for different values of redshift (z) for ALHAMBRA color A770M-A921M and three galaxy templates. Figure from Aparicio Villegas et al. (2010).

Table 3.3 Multi-instrument colors of the E/S0 galaxy template from Benitez et al. (2004) in the ALHAMBRA system (AB mag) and SDSS r (AB mag). Complete table in Appendix (Table A.3).

z	A366M-r	A491M-r	A613M-r	A770M-r	A921M-r
0.00	2.26	0.55	-0.01	-0.41	-0.66
0.25	3.00	1.32	-0.01	-0.58	-0.94
1.00	3.47	2.26	0.12	-0.88	-2.38
1.50	1.69	1.06	0.21	-1.98	-3.01
2.25	1.17	0.47	0.09	-0.83	-2.48

Table 3.4 Multi-instrument colors of the Sbc galaxy template from Benitez et al. (2004) in the ALHAMBRA system (AB mag) and SDSS r (AB mag). Complete table in Appendix (Table A.4).

z	A366M-r	A491M-r	A613M-r	A770M-r	A921M-r
0.00	1.64	0.45	0.01	-0.33	-0.55
0.25	2.28	0.76	0.00	-0.44	-0.73
1.00	1.03	0.56	0.07	-1.17	-1.94
1.50	1.22	0.34	0.01	-0.49	-1.46
2.25	1.92	0.69	-0.01	-0.34	-0.67

Table 3.5 Multi-instrument colors of the Im galaxy template from Benitez et al. (2004) in the ALHAMBRA system (AB mag) and SDSS r (AB mag). Complete table in Appendix (Table A.5).

z	A366M-r	A491M-r	A613M-r	A770M-r	A921M-r
0.00	0.75	-0.00	-0.00	-0.19	-0.30
0.25	1.20	0.43	-0.17	-0.13	-0.28
1.00	0.27	0.15	0.02	-0.63	-1.00
1.50	0.42	0.07	0.00	-0.13	-0.76
2.25	0.95	0.27	-0.01	-0.09	-0.16

Table 3.6 Multi-instrument colors of the SB2 galaxy template from Benitez et al. (2004) in the ALHAMBRA system (AB mag) and SDSS r (AB mag). Complete table in Appendix.

z	A366M-r	A491M-r	A613M-r	A770M-r	A921M-r
0.00	0.54	-0.34	0.24	-0.02	-0.25
0.25	1.00	0.44	-0.51	0.21	0.01
1.00	0.13	0.08	0.08	-0.45	-0.62
1.50	0.06	0.12	-0.06	-0.02	-0.71
2.25	0.56	0.01	-0.00	-0.03	-0.06

Table 3.7 Multi-instrument colors of the SB3 galaxy template from Benitez et al. (2004) in the ALHAMBRA system (AB mag) and SDSS r (AB mag). Complete table in Appendix.

z	A366M-r	A491M-r	A613M-r	A770M-r	A921M-r
0.00	1.15	0.32	0.09	-0.11	-0.45
0.25	1.05	0.49	-0.04	-0.27	-0.40
1.00	0.36	0.21	-0.02	-0.42	-0.96
1.50	0.31	0.20	-0.02	-0.24	-0.50
2.25	0.74	0.22	-0.00	-0.11	-0.26

Table 3.8 Multi-instrument colors of the Scd galaxy template from Benitez et al. (2004) in the ALHAMBRA system (AB mag) and SDSS r (AB mag). Complete table in Appendix.

z	A366M-r	A491M-r	A613M-r	A770M-r	A921M-r
0.00	1.31	0.30	0.00	-0.22	-0.27
0.25	1.60	0.62	-0.05	-0.34	-0.53
1.00	0.61	0.40	0.01	-0.73	-1.35
1.50	0.74	0.13	0.01	-0.39	-0.94
2.25	1.41	0.48	-0.01	-0.15	-0.38

3.1.4 Validity of the transformation equations on galaxies

Although the transformation equations presented in section 3.1.2 are calculated to be applied to stellar objects, a quick test has been carried out to see how they work for galaxy templates at z=0. Using tables X, Y and Z from the Appendix, ALHAMBRA colors of the E/S0, Sbc and Im galaxy templates are obtained. Applying the transformation equations to their ALHAMBRA colors, SDSS colors are determined, and these were compared with two different results presented by Fukugita et al.(1995), where they obtained synthetic colors from the convolution of Kennicutt's (1992) spectrophotometric atlas with the response functions of the SDSS photometric system, and Shimasaku et al.(2001), where SDSS colors of a sample of observed galaxies are presented. As Figure 3.4 shows, the values obtained by the ALHAMBRA-SDSS transformation equations are within the observed range of SDSS galaxy colors, taking into account the typical uncertainty in the colors that define a class of morphological type.

The validity of these transformation equations for galaxies depends on the proximity of their spectral energy distributions to the SED of the stars used in the elaboration of the equations, in our case, the 288 stars from the NGSL. Thus, in a color-color diagram, the smaller the distance of the galaxy to the distribution of the stars, the higher the confidence level will be when applying the transformation equations to this galaxy. Figure 3.5 shows two ALHAMBRA color-color diagrams where the same previous three galaxy templates are presented at different redshift values. E/S0 and Sbc galaxies at z=0 are quite close to the stellar distribution, while Im galaxies at z=0 are too blue, and slightly offset from the distribution of the stellar colors.

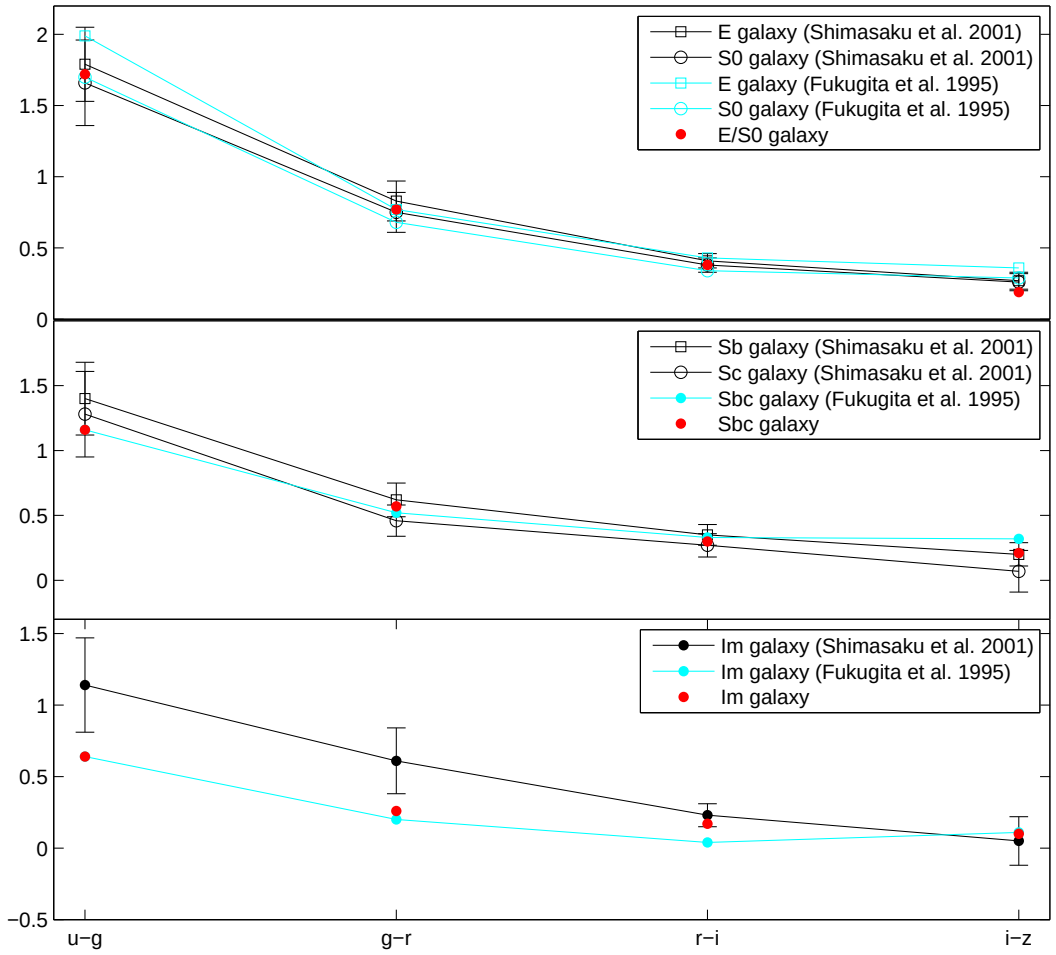

Figure 3.4 SDSS colors for three galaxies of different spectromorphological types. Black symbols are colors obtained from Shimasaku et al.(2001) with a rms error bar, blue ones are obtained from Fukugita et al.(1995), and red points are the colors obtained by applying the transformation equations of section 3.1.2 to the ALHAMBRA photometry of these three galaxy templates (Benítez et al. 2004). Figure from Aparicio Villegas et al. (2010).

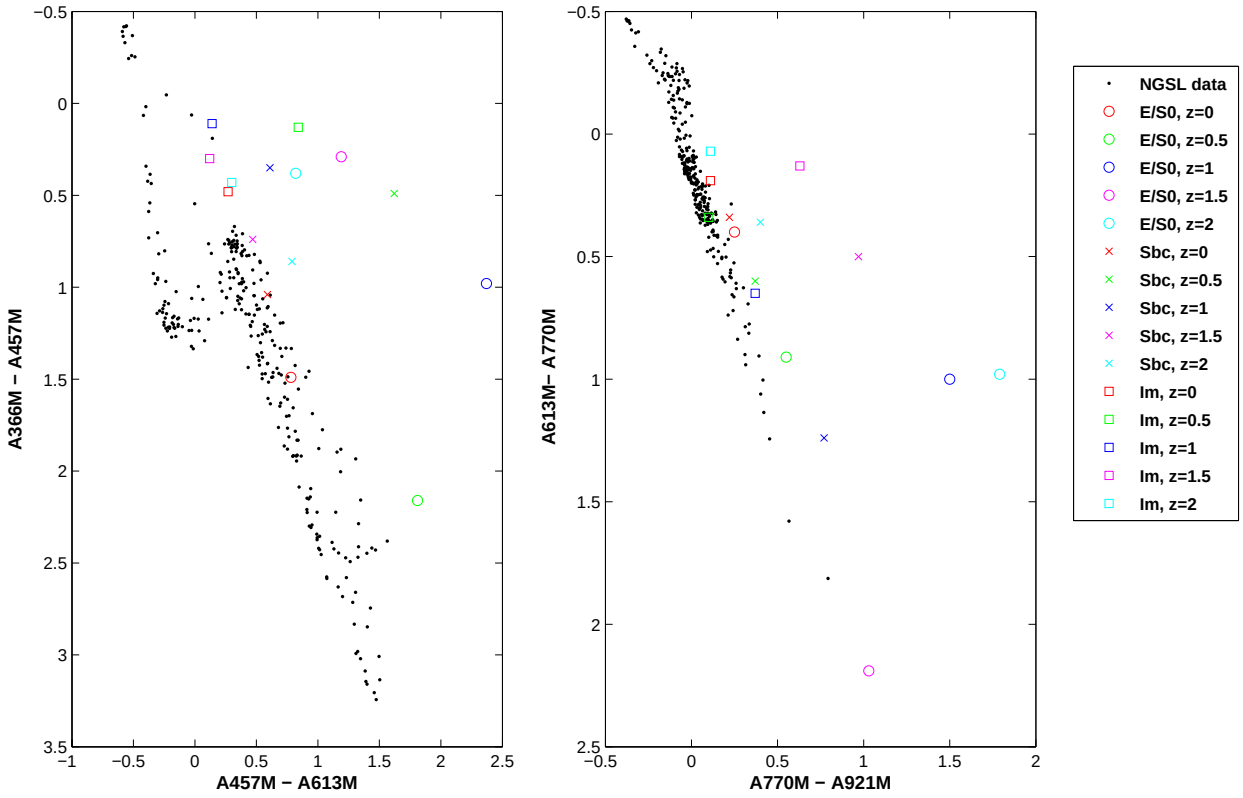

Figure 3.5 ALHAMBRA color-color diagrams. Black points are the set of primary standard stars from the NGSL. Circles represent E/S0 galaxy templates, crosses are Sbc galaxy templates and squares represent Im galaxy templates, all of them from Benítez et al.(2004). Different colors show different values of z. Figure from Aparicio Villegas et al. (2010).

3.2 Gaia mission

The Gaia (Global Astrometric Interferometer for Astrophysics) mission was approved in 2000 as the cornerstone of the ESA program Horizon 2000+, and the satellite is scheduled for launch in 2012. The main objective of Gaia is observing the physical characteristics, kinematics and distribution of a great fraction of the stellar content of the Milky Way, thus clarifying its dynamics and structure and, consequently, its formation and evolutionary history. The understanding of our galaxy would of course help us to understand other similar spiral galaxies, providing for the first time quantitative tests for galactic formation models.

Gaia will survey the sky in a similar way to the Hipparcos mission (Perryman et al. 1997; ESA 1997), obtaining astrometry (position, proper motion and parallax), photometry (between about 300 y 1100 nm) and spectra (between 848-874 nm in order to determine radial velocities) of more than a billion of stars: that means almost 1% of our galaxy, apart from stars from galaxies of the Local Group, other galaxies, quasars and Solar system objects. For 5 years Gaia will observe all the celestial objects of a visual magnitude brighter than around V=20 mag (25 depending on the spectral type of the star). The astrometry precision is expected to be about 7 μas to V=10, 12-25 μas to V = 15 and 100-300 μas to V=20 (depending on the spectral type). The photometry will reach the same completeness limit. The radial velocities will be obtained for about 100-150 million stars with a magnitude lower than V=17 mag with precisions of about 1-15 kms^{-1}, depending on the apparent magnitude and the spectral type of the star and the density of the sky (Katz et al. 2004; Wilkinson et al. 2005).

More details of the characteristics of the Gaia mission can be found in the "Red Book" of the mission (GAIA Study Report, ESA (2000)). Documentation about the satellite can be found at `http://www.rssd.esa.int/index.php?project=GAIA`.

3.2.1 Gaia observational system

Gaia makes use of two different instruments for its observations. First, Gaia will provide the spectral energy distribution of every object sampled by a spectrophotometric instrument that will provide low resolution spectra in the blue and red part of the wavelength range. In this way, the observed objects will be classified, parametrized (for instance, determination of effective temperature, surface gravity, metallicity, and interstellar reddening, for stars) and monitored for variability. Secondly, radial velocities will also be acquired through Doppler-shift measurements from high-resolution spectra by the Radial Velocity Spectrometer (RVS). These high-resolution spectra will also provide astrophysical information, such as interstellar reddening, atmospheric parameters, elemental abundances for different chemical species, and rotational velocities for stars brighter than $V \simeq 13$ magnitudes.

The integrated flux of the low-resolution blue photometer (BP) and red photometer (RP) spectra will yield G_{BP} and G_{RP} magnitudes as two broad passbands in the ranges 330-680 nm and 640-1000 nm, respectively. A graphic representation of the transmission of BP and RP overlapped with the ALHAMBRA photometric system is shown in Figure 3.6. The radial velocity instrument (RVS) will disperse light in the 847-874 nm range (region of the CaII triplet)

and the integrated flux of the resulting spectrum can be seen as measured with a photometric medium band yielding G_{RVS} magnitudes. In addition, from measurements of unfiltered (white) light in the Astrometric Field, from about 350 to 1000 nm, Gaia will yield G-magnitudes that will be monitored through the mission for variability. Therefore, four passbands and their corresponding magnitudes can be associated with the Gaia instruments: the very broad band G, two broad bands, G_{BP} and G_{RP}, and the medium band G_{RVS}. A more detailed description of the four bands can be found in Jordi et al.(2010).

The main aim of BP and RP photometric observations is the classification of the sources by estimating the astrophysical characteristics, such as effective temperature, surface gravity, and chemical composition for all stars. Once the astrophysical parameters are determined, age and mass will enable the chemical and dynamical evolution of the Galaxy over a wide range of distances to be described. The white light observations, G band photometry described by Jordi et al.(2006), will yield the best signal-to noise ratio and hence is the most suitable for variability detection. Gaia spectroscopic data processing has as its main goal to derive radial velocities and rotation velocities for all the stars observed with the RVS (up to magnitude 16-17), and atmospheric parameters and element abundances for the brightest part of the Gaia survey. In addition, the Radial Velocity Spectrometer multi-epoch observations are well suited for the identification, classification and characterization of the many types of double, multiple and variable stars.

The mean wavelength and the full width half-maxima of the different bands are shown in the following table:

Band	λ_m (nm)	FWHM (nm)
G	673	440
G_{BP}	532	253
G_{RP}	797	296
G_{RVS}	860	28

Gaia integrates astrometry, photometry, and spectroscopy in two main telescopes and only one focal plane as explained in Lindegren (2010). Sixty-two CCDs are used in the Astrometic Field, while BP and RP spectra are recorded in strips of 7 CCDs each. Twelve CCDs are used in the RVS instrument. Every CCD will have its own QE curve and there will be pixel-to-pixel sensitivity variations.

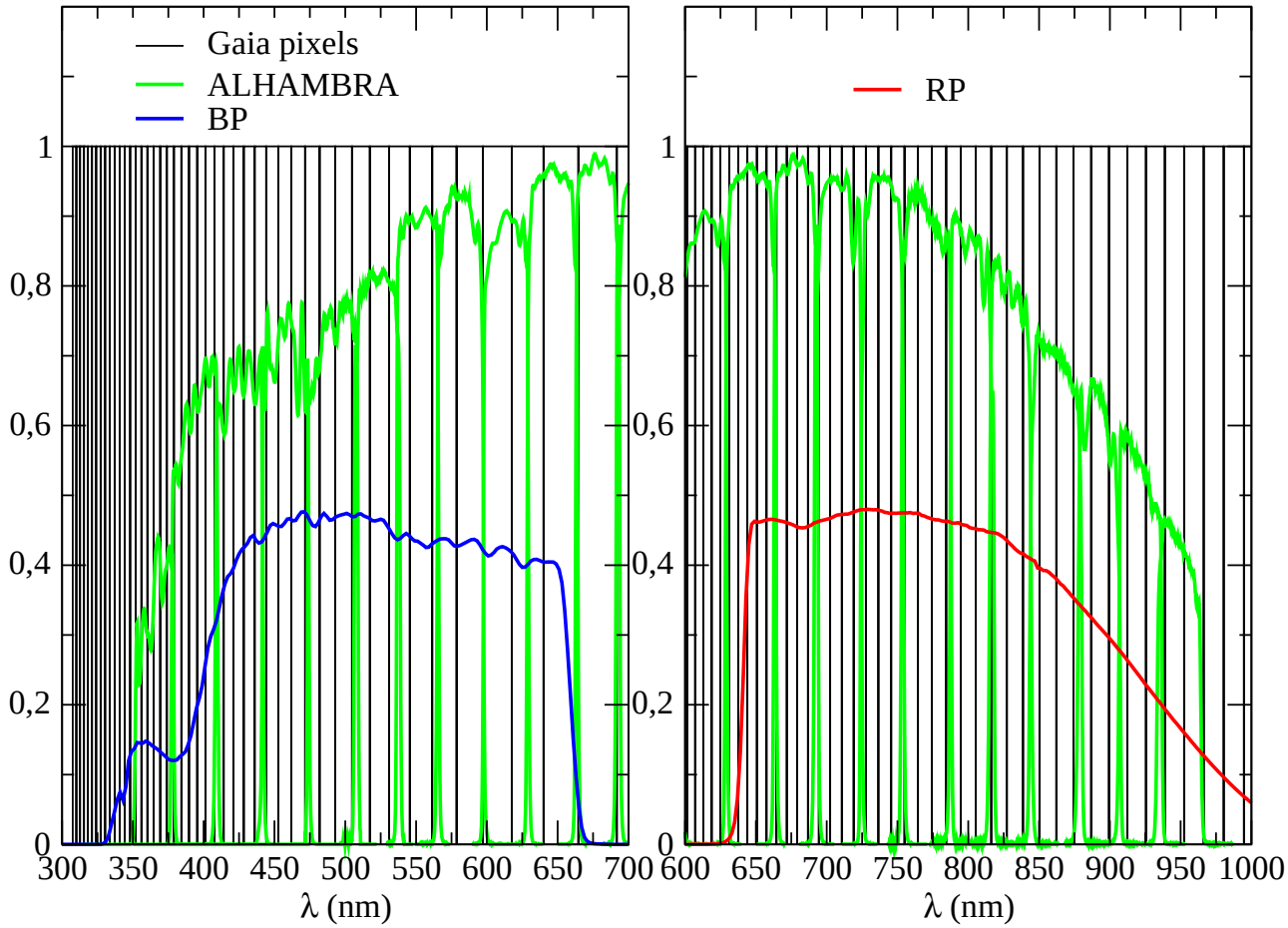

Figure 3.6 BP (blue) and RP (red) Gaia passbands overlapped with ALHAMBRA passbands (green). In black, the size of the pixels in Gaia BP/RP spectra are plotted.

3.2.2 ALHAMBRA-Gaia transformations

The optical ALHAMBRA survey could enlarge the number of standard stars for the calibration of the Gaia photometric system, and so it could help on its validation of flux scale. Moreover, establishing some relations between Gaia photometry and ALHAMBRA bands, the techniques developed for stellar classification and physical parameters estimation in the ALHAMBRA system could be applied to the huge amount of stars that will be observed with the satellite.

In this sense, linear transformation equations between both photometric systems have been calculated using synthetic magnitudes (AB magnitude in the ALHAMBRA system and VEGA magnitudes in Gaia photometry) for the 288 stars from the NGSL. The models are built with the same methodology and with the same tools as in Section 3.1.2. The equations of the transformation from ALHAMBRA to Gaia photometry are formed with the 19 correlative ALHAMBRA colors as independent variables, and a color formed with a Gaia band minus an ALHAMBRA band as dependent variables. The reverse relations are formed in the same way as before, with the corresponding Gaia colors (G-BP and BP-RP) as independent variables and the ALHAMBRA band - Gaia band colors as dependent ones. The elaboration of the linear model has been developed using the statistical task Backward Stepwise Regression, in the statistical software **R**, and the Bayesian Information Criterion is used to optimize the minimum number of variables with the minimum error in the model. Table 3.9 and 3.10 show the coefficients of these transformation equations.

The RVS Gaia band is directly related to the ALHAMBRA band A861M, so the bright sources sample of the ALHAMBRA survey could be useful to the Gaia spectroscopic data processing, that is, precisely the data obtained with Radial Velocity Spectrometer (RVS). Table 3.9 also shows the relation between RVS-A861M and the 19 correlative ALHAMBRA colors, where it can be noticed that the greatest information in the model is given by the color A861M-A892M, with a coefficient in the model much greater than almost the rest of the coefficient corresponding to different colors. At the bottom of Table 3.9 the linear relation between RVS an A861M is also shown.

In Jordi et al.(2010) they establish cubic models between *griz* SDSS bands and Gaia bands using g-r, g-i, r-i and g-z SDSS colors. The same type of models between ALHAMBRA photometry and Gaia bands are also developed using the ALHAMBRA bands which better correspond to the Sloan ones basing on the proximity of their effective wavelengths ($g \sim A491M$, $r \sim A613M$, $i \sim A770M$ and $z \sim A921M$). These equations are based on the theoretical stellar spectra of BaSeL 3.1 (Westera et al. 2002) that is the same library they used for the SDSS-Gaia transformations. The models were built during a visit to the Departament d'Astronomia i Meteorologia (Universitat de Barcelona) where the Gaia team in charge of the photometry of the mission is located, led by Carme Jordi. Comparing the relations between SDSS and Gaia (see Jordi et al. 2010) with that elaborated with these ALHAMBRA bands, it is notable that models elaborated with ALHAMBRA photometry have the same value of sigma or even lower than the values in the model with Sloan bands. Table 3.11 presents the coefficients of these ALHAMBRA-Gaia cubic models.

Table 3.9 Coefficients of the transformation equations from ALHAMBRA to GAIA photometry.

	Synthetic			
	RVS - A861M	G - A522M	BP - A613M	RP - A457M
∅	-0.4811	-0.0809	0.0284	-0.3591
A366M - A394M	-0.0052		0.0717	
A394M - A425M				-0.0486
A425M - A457M		0.1209	0.1970	0.0671
A457M - A491M		-0.3795		-0.1189
A491M - A522M				
A522M - A551M		-1.4843	-0.3694	-0.0966
A551M - A581M			1.5768	
A581M - A613M			1.6242	0.2492
A613M - A646M				0.1790
A646M - A678M				0.2202
A678M - A708M				
A708M - A739M		-2.0004	-0.8307	
A739M - A770M	0.0573			0.5568
A770M - A802M	0.1111		0.5354	0.6840
A802M - A829M		2.6308	2.4129	0.7444
A829M - A861M	-0.0787	-0.6084	-0.8026	0.6532
A861M - A892M	0.1335			-0.0897
A892M - A921M	-0.0594			-0.0796
A921M - A948M				
Error	0.0024	0.0339	0.0284	0.0048

$$RVS = -0.4694 + 0.9987 \cdot A861M$$
$$rms = 0.0056$$

Table 3.10 Coefficients of the transformation equations from GAIA to ALHAMBRA photometry.

	Synthetic			
	∅	G-BP	BP-RP	Error
A366M - RP	0.4276	-3.5908	0.6905	0.3925
A394M - RP	-0.1020	-2.1733	1.2864	0.2762
A425M - RP	-0.1505	-1.7268	1.0148	0.1467
A457M - RP	-0.1657	-0.8905	0.9574	0.0638
A491M- RP	-0.0622	-1.3332	0.5043	0.0351
A522M - RP	-0.0234	-1.0528	0.4889	0.0421
A551M - RP	0.0392	-0.9244	0.3438	0.0277
A581M - RP	0.0865	-1.3313		0.0430
A613M - RP	0.1325	-1.3939	-0.1480	0.0456
A646M - RP	0.0865	-1.3313		0.0430
A678M - BP	0.2082	-0.8263	-1.0384	0.0294
A708M - BP	0.2422	-1.4002	-1.3855	0.0448
A739M - BP	0.2670	-0.9515	-1.2676	0.0210
A770M - BP	0.3074		-0.9403	0.0136
A802M - BP	0.3710	-0.2391	-1.1365	0.0125
A829M - BP	0.4066		-1.0873	0.0183
A861M - BP	0.4544		-1.1449	0.0181
A892M - BP	0.4985		-1.1890	0.0143
A921M - BP	0.5078	0.1253	-1.1868	0.0239
A948M - BP	0.5281	0.2469	-1.1432	0.0348

Table 3.11 Coefficients of the transformation equations from Gaia to ALHAMBRA photometry, based on the models from Gaia to Sloan photometry developed in Jordi et al.(2010).

		$(A491M - A770M)$	$(A491M - A770M)^2$	$(A491M - A770M)^3$	σ
$G - A491M$	-0.0925	-0.4275	-0.1119	0.0048	0.09
$G - G_{\rm RVS}$	0.4062	0.7859	-0.1116	0.0046	0.09
$G-$BP	-0.1424	-0.3921	-0.0323	0.0012	0.11
$G-$RP	0.2675	0.5537	-0.0827	0.0044	0.04
$A491M - G_{\rm RVS}$	0.4987	1.2134	0.0003	-0.0001	0.10
$A491M-$BP	-0.0499	0.0354	0.0796	-0.0035	0.11
$A491M-$RP	0.3601	0.9812	0.0292	-0.0004	0.10
BP-RP	0.4100	0.9458	-0.0504	0.0031	0.14
		$(A491M - A613M)$	$(A491M - A613M)^2$	$(A491M - A613M)^3$	σ
$G - A491M$	-0.0650	-0.7818	-0.4098	0.0422	0.26
$G - G_{\rm RVS}$	0.3623	1.4849	-0.3893	0.0298	0.12
$G-$BP	-0.1180	-0.7306	-0.1276	0.0161	0.22
$G-$RP	0.2346	1.0397	-0.2767	0.0249	0.06
$A491M - G_{\rm RVS}$	0.4273	2.2667	0.0205	-0.0124	0.32
$A491M-$BP	-0.0530	0.0512	0.2822	-0.0261	0.06
$A491M-$RP	0.2996	1.8214	0.1332	-0.0173	0.30
BP-RP	0.3526	1.7703	-0.1490	0.0087	0.27
		$(A613M - A770M)$	$(A613M - A770M)^2$	$(A613M - A770M)^3$	σ
$G - A491M$	-0.1107	-0.8741	-0.6949	0.0947	0.38
$G - G_{\rm RVS}$	0.4653	1.6777	-0.5386	0.0527	0.07
$G-$BP	-0.1678	-0.8302	-0.1991	0.0233	0.14
$G-$RP	0.3082	1.1645	-0.3721	0.0419	0.04
$A491M - G_{\rm RVS}$	0.5760	2.5518	0.1563	-0.0419	0.34
$A491M-$BP	-0.0571	0.0439	0.4959	-0.0713	0.26
$A491M-$RP	0.4189	2.0386	0.3229	-0.0528	0.39
BP-RP	0.4760	1.9946	-0.1730	0.0186	0.17
		$(A491M - A921M)$	$(A491M - A921M)^2$	$(A491M - A921M)^3$	σ
$G - A491M$	-0.0949	-0.3325	-0.0630	0.0023	0.10
$G - G_{\rm RVS}$	0.4090	0.5892	-0.0614	0.0018	0.07
$G-$BP	-0.1434	-0.2936	-0.0209	0.0009	0.09
$G-$RP	0.2707	0.4132	-0.0452	0.0017	0.03
$A491M - G_{\rm RVS}$	0.5039	0.9217	0.0017	-0.0005	0.12
$A491M-$BP	-0.0485	0.0388	0.0421	-0.0014	0.13
$A491M-$RP	0.3656	0.7457	0.0178	-0.0006	0.09
BP-RP	0.4141	0.7069	-0.0242	0.0008	0.10

Bibliography

Aparicio Villegas, T., Alfaro, E. J., Cabrera-Caño, J., et al. 2010, AJ, 139, 1242

Baggett, S., Casertano, S., Gonzaga, S., & Ritchie, C. 1997, Instrument Science Report (WFCP2 97-10; Baltimore: STScI)

Benítez, N. 2000, ApJ, 536, 571

Benítez, N., et al. 2004, ApJS, 150, 1

ESA 1997, VizieR Online Data Catalog, 1239, 0

Fukugita, M., Shimasaku, K., & Ichikawa, T. 1995, PASP, 107, 945

Fukugita, M., Ichikawa, T., Gunn, J. E., Doi, M., Shimasaku, K., & Schneider, D. P. 1996, AJ, 111, 1748

Jordi, C., Høg, E., Brown, A. G. A., et al. 2006, MNRAS, 367, 290

Jordi, C., Gebran, M., Carrasco, J. M., et al. 2010, A&A, 523, A48

Katz, D., Munari, U., Cropper, M., et al. 2004, MNRAS, 354, 1223

Kennicutt, R. C., Jr. 1992, ApJS, 79, 255

Lindegren, L. 2010, IAU Symposium, 261, 296

Oke, J. B., & Gunn, J. E. 1983, ApJ, 266, 713

Perryman, M. A. C., Lindegren, L., Kovalevsky, J., et al. 1997, A&A, 323, L49

Schneider, D. P., Gunn, J. E., & Hoessel, J. G. 1983, ApJ, 264, 337

Shimasaku, K., et al. 2001, AJ, 122, 1238

Smith, J. A., et al. 2002, AJ, 123, 2121

Westera, P., Lejeune, T., Buser, R., Cuisinier, F., & Bruzual, G. 2002, A&A, 381, 524

Wilkinson, M. I., Vallenari, A., Turon, C., et al. 2005, MNRAS, 359, 1306

4

Stellar Physics with the ALHAMBRA Photometric System

As mentioned in the introductory chapter of this thesis, Chapter 1, photometry provides a quantitative low spectral resolution spectroscopy. This assertion could seem simply a good advertising slogan when we work with photometry with three wide bands such as the UBV and RGU systems, designed and developed in the fifties of the last century, but it becomes in a well-defined reality when we move to narrow band and go above, e.g., 10 filters to cover the optical wavelength range, where the estimated spectral resolution, R, would be about 5.5.

The ALHAMBRA photometric system is defined by 20 contiguous, equal-width filters ($\sim$30nm) that cover the optical wavelength range between 3500Å and 9700Å. ALHAMBRA was specifically designed to obtain a large-scale extragalactic survey, providing the morphologic type and redshift of about one million galaxies. However, it is clear that the "spectra" obtained for the field stellar objects will provide important information on the physical properties of the stars, the interstellar medium that their light passes through and the structure of the galactic halo.

The spectrum of a star is characterized by three internal physical properties, $log(g)$, T_{eff} and metallicity, and by one external property, the reddening. Therefore the first question to be answered is: how can we extract this information from the observed "spectra"?

We can consider that historically there has been a unique approximation to the problem, the establishment of functional relations between colors or color combinations and the physical properties of stars. This could be limited to spectral type groups and/or luminosity classes or subsets of themselves. Examples of this procedure can be found for OB-type stars in the UBV system in Johnson & Morgan (1953), and for several spectral types and luminosity classes in the Strömgren $uvbyH\beta$ system (Strömgren 1951, Crawford 1966, Balona 1984, 1994), etc. However, two new factors make us consider a change of orientation to the problem. The simulation of stellar spectra from evolutionary models has already become an almost-routine task with high precision in the estimated fluxes, and photometry is more and more a low-resolution spectroscopy. So the direct comparison between models and photometry seems to be a viable

solution that needs a more detailed study. In this chapter we deal with the problem of the determination of the stellar physical properties from both perspectives.

4.1 Stellar classification: Diagram of reddening-free Q-parameters

Our first step in performing a stellar spectral classification is to generate a diagram formed by two reddening-free Q-parameters, that enables an approximation to the spectral type of the stars. This kind of parameters was originally defined by Johnson & Morgan (1953) for the UBV system, and in the same way, the definition for the ALHAMBRA system would be:

$$Q_{ijkl} = (m_i - m_j) - \frac{E_{ij}}{E_{kl}}(m_k - m_l) \tag{4.1}$$

where m_i is the AB magnitude in the ALHAMBRA band i estimated as in equation 2.35, and E_{ij}/E_{kl} is the color excess ratio, which only depends on the interstellar extinction law.

To generate these parameters we not only consider the 19 correlative colors from the 20 ALHAMBRA bands but the 190 colors you can get from all the combinations of these. Moreover, as we can see in the definition of the reddening-free Q-parameters, an extinction law must also be taken into account, and indeed, it takes an important role in this task, since it can be easily checked that the extinction law used gives significantly different results in the Q,Q diagrams. So, different extinction laws were tested to generate these Q-parameters. We computed the extinction coefficients of eight Milky Way extinction laws using the on-line application York Extinction Solver[1] (YES, McCall, M. L. 2004). The extinction laws tested were Cardelli et al. (1989), Fitzpatrick (1999), McCall (1982), Nandy et al. (1975), O'Donnell (1994), Prevot et al. (1984), Savage & Mathis (1979) and Schild (1977). All the coefficients are obtained using a value of the ratio of total-to-selective absorption R_V=3.1, since it is the standard value for the diffuse interstellar medium (ISM). After, these coefficients for the ALHAMBRA bands are obtained as follows: first BaSeL spectra are reddened with a value of $E_{B-V} = 1$ and the reddened magnitudes are obtained for each band; then, $A(\lambda)s$ are estimated as the differences between the unreddened and reddened colors, and considering that E(B-V)=1 we get an estimate of the extinction law for the 20 ALHAMBRA bands.

We apply this methodology to the O-B-type stars in BaSeL 2.2 models. The stars of O-B spectral type have few absorption lines due to their high temperatures, and so they are usually used to define extinction coefficients. With this distribution of differences the outliers are removed with a Chebyshev filter (see definition 2.36) using the MAD and $k = 3$. For the band where the color excess, $E_{\lambda_i - \lambda_{i+1}}$, has the minimum MAD, $A(\lambda_i)$ is determined as the median of the differences between the magnitudes in that band with reddening and the unreddened ones,

$$A(\lambda_i) = median_i(m_{i_1} - m_{i_0}), i = 1 : 20 \tag{4.2}$$

and from this coefficient and the list of color excesses in each band the rest of $A(\lambda)$s are obtained.

[1] `http://cadcwww.hia.nrc.ca/yes`

The differences between these coefficients and those obtained from YES are of some hundredths of magnitudes, with the highest differences in the bluest filters.

4.1.1 Data

Three different kinds of data are used and compared simultaneously in the Q,Q diagrams:

1. The theoretical stellar spectra library BaSeL 2.2 (Lejeune et al. 1998). Main sequence stars with $log(g) = 4.5$ are selected, covering all spectral classes from O- to M-type stars, and metallicities varying from -5 to 1.

2. The subset of primary standard stars of the ALHAMBRA photometric system formed by 288 stars from the NGSL. They are observed spectral energy distributions with synthetic AB ALHAMBRA magnitudes, and they are the basis of the zero point calibration of the photometric system (see section 2.5.2). The range of values of T_{eff}, $log(g)$, [Fe/H], and color excess E_{B-V} is presented in section 2.4.

3. Observed AB ALHAMBRA colors from field stars of the ALHAMBRA project (Table 2.1). Only stars with a photometric error lower than 0.15 in all ALHAMBRA magnitudes are considered.

Therefore, Q,Q diagrams for different interstellar extinction laws can be compared, and the most suitable diagram can be chosen functionally, in the sense of being the one in which the three data sets take up similar positions. In the same way, these diagrams have been generated for different pairs of Q-parameters.

4.1.2 Q,Q diagram and extinction law

The extinction law of Nandy et al. is the one that fits best with theoretical colors, synthetic colors and observed colors, in the Q,Q diagrams. Figure 4.1 shows the extinction laws of Nandy et al. and Cardelli et al. for the whole optical range covered by the 20 ALHAMBRA filters. Table 4.1 shows the values of the Nandy et al. extinction coefficients for each one of the 20 ALHAMBRA filters.

The Q,Q diagram empirically chosen for the preliminary stellar spectral classification is formed by $Q_{1,3,12}$ versus $Q_{2,16,19}$ where:

$$Q_{1,3,12} = (A366M - A425M) - \frac{E_{A366M,A425M}}{E_{A425M,A708M}}(A425M - A708M) \tag{4.3}$$

$$Q_{2,16,19} = (A394M - A829M) - \frac{E_{A394M,A829M}}{E_{A829M-A921M}}(A829M - A921M) \tag{4.4}$$

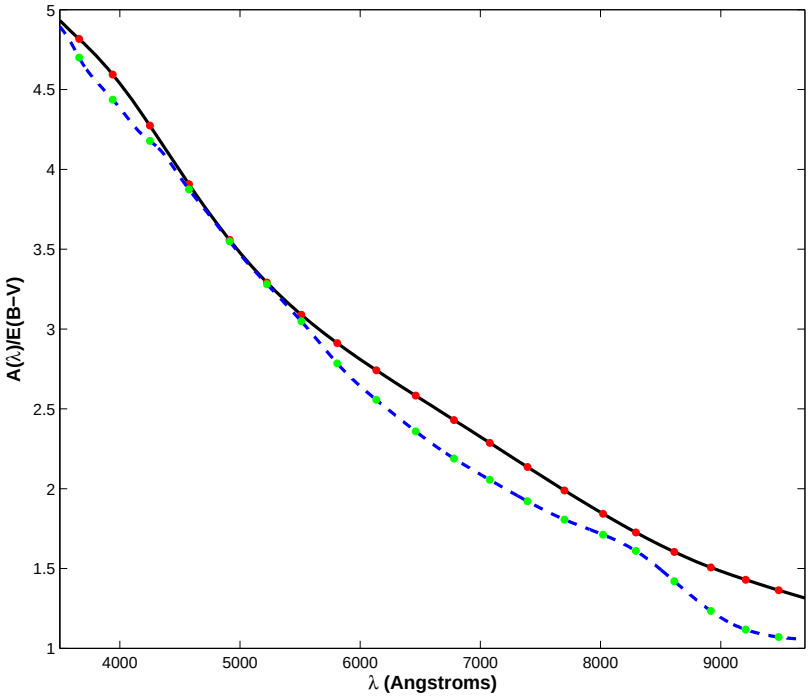

Figure 4.1 The black line represents the Cardelli et al. (1989) extinction law and the blue discontinuous line represents the Nandy et al. (1975) extinction law. The points show the extinction coefficients at the effective wavelengths of the 20 different ALHAMBRA filters.

Table 4.1 Extinction coefficients obtained from synthetic ALHAMBRA photometry and the Nandy et al. (1975) extinction law.

Filter	$A(\lambda)/E_{B-V}$	$A(\lambda)/A(V)$
A366M	4.71	1.52
A394M	4.43	1.43
A425M	4.18	1.35
A457M	3.87	1.25
A491M	3.55	1.14
A522M	3.28	1.06
A551M	3.04	0.98
A581M	2.78	0.90
A613M	2.56	0.82
A646M	2.36	0.76
A678M	2.19	0.70
A708M	2.06	0.66
A739M	1.92	0.62
A770M	1.81	0.58
A802M	1.71	0.55
A829M	1.61	0.52
A861M	1.42	0.46
A892M	1.24	0.40
A921M	1.12	0.36
A948M	1.07	0.34

Figure 4.2 shows this diagram for two different extinction laws, at the left side the Q-values are generated with the Fitzpatrick extinction law and the diagram at the right corresponds to the Nandy et al. extinction law. BaSeL models are represented by points and the stars from the NGSL by squares; each color in the diagram represents one spectral type from O- to M-type stars, the white dwarfs or O-type subdwarfs being marked in yellow, which are:

- Agk+81266 (sdOB)
- BD+284211 (Op White dwarf)
- Feige110 (DA[2] White dwarf)
- Feige34 (DO[3] White dwarf)
- G191b2b (DAw White dwarf)
- HD149382 (sdOB)
- HZ44 (B2 White dwarf)

Comparing both diagrams we can easily see how the same Q, Q diagram can be quite different depending on the extinction law used, and how the diagram with Nandy et al. presents greater facility for differentiating between the diverse spectral types, and in particular it seems to be more discriminating than other laws among the K- to F-type stars. Synthetic Q-parameters of the NGSL stars fit quite well with the position of the BaSeL models, according to each spectral type. Certain dispersion in some NGSL stars with respect to the BaSeL sample can be noticed in the graph. This is due to the different luminosity classes that can be found in the NGSL stars while in the graph only BaSeL models with $log(g) = 4.5$ are represented; indeed, different luminosity-type from main sequence stars in the same temperature range implies more dispersion in the point cloud of each spectral type.

The great majority of stars expected to be found in the ALHAMBRA fields are main sequence stars and giants of late spectral types. Figure 4.3 shows the same diagram generated with Nandy et al. extinction law, where BaSeL models of the two different luminosity classes are represented. The black points correspond to main sequence stellar models (log(g) = 4, 4.5, 5), and red circles represent red giant models, selected by $T_{eff} < 6000$k and $-0.5 \leq log(g) \leq 3.5$. Both luminosity classes coincide in the same position over the diagram, according to the temperature range.

[2]DA White dwarf is a hydrogen-rich atmosphere white dwarf, indicated by strong Balmer hydrogen spectral lines.

[3]DO White dwarf is a helium-rich atmosphere white dwarf, indicated by ionized helium, He II, spectral lines.

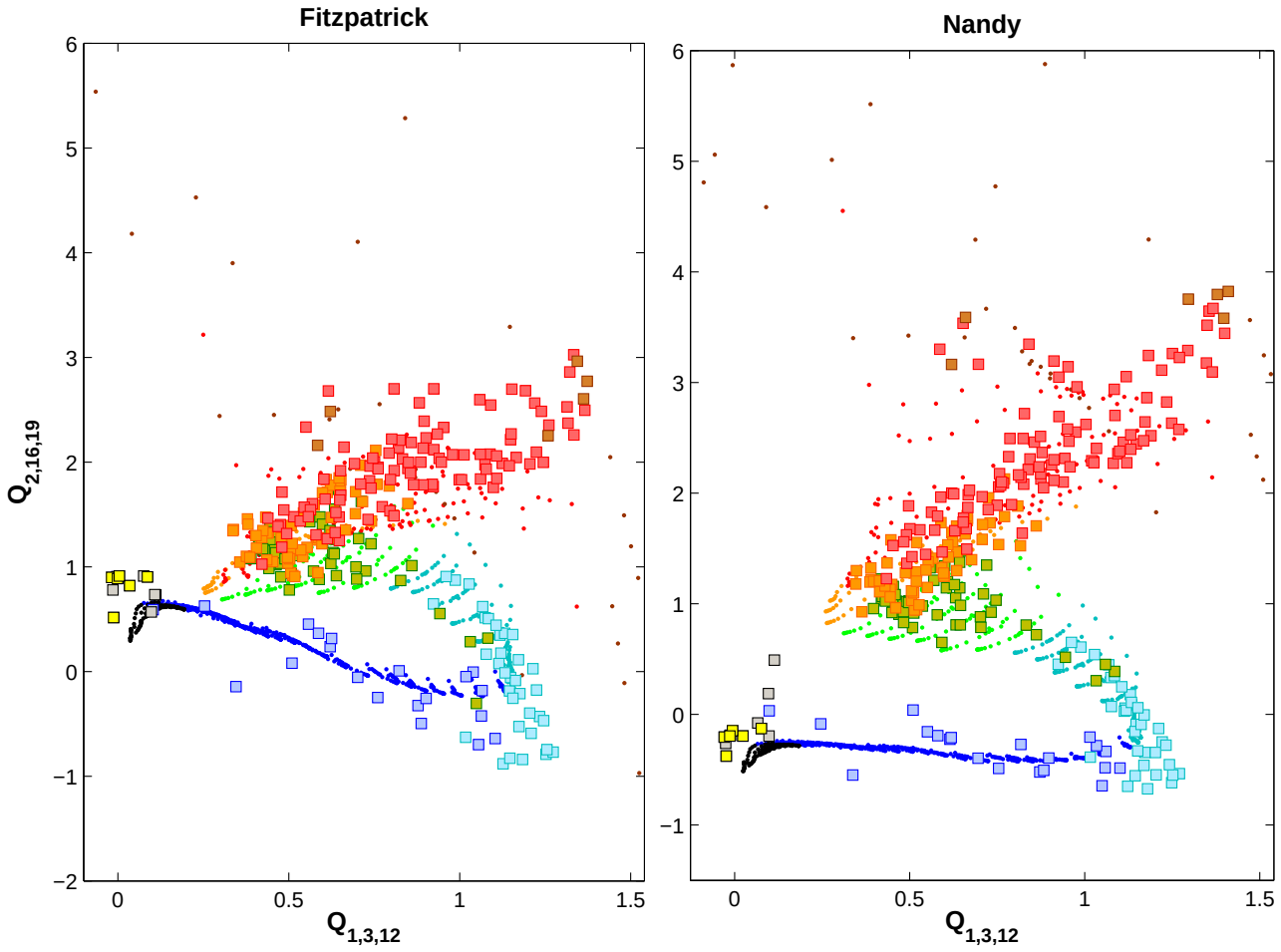

Figure 4.2 $Q_{1,3,12}$,$Q_{2,16,19}$ diagram for spectral classification. The left diagram corresponds to Q-values generated with the Fitzpatrick (1999) extinction law, and the diagram on the right corresponds to the Nandy et al. (1975) extinction law. The points are models from BaSeL 2.2 library. The squares are the NGSL stars. Each different color corresponds to a different spectral type: black O-, blue B-, cyan A-, green F-, orange G-, red K-, brown M-type stars and yellow squares are white dwarfs or subdwarfs of spectral type O and B.

With this Q,Q diagram we can elaborate a relation between the effective temperature of a star and the mean values of $Q_{1,3,12}$ and $Q_{2,16,19}$, based on the values of BaSeL models. Table 4.2 shows these values for each interval of temperature, and their graphic representation is shown in Figure 4.4 with red markers on the Q,Q diagram. The dispersion in the Q,Q average values increases while the temperature decreases, as can be appreciated in Fig. 4.2, the coldest stars (G,K,M) being those with more dispersion, since the selected Qs are in these cases also sensitive to metallicity, and not only representative of the temperature. In Fig. 4.4, the blue points to the left of the red markers represent stars with low metallicity (-3.5 to -5) and the blue points to the right are stars with $[Fe/H] = 1$, of the different spectral types. The blue points are not represented for O- to B-type models since these Qs are not sensitive to metallicity in these kinds of stars.

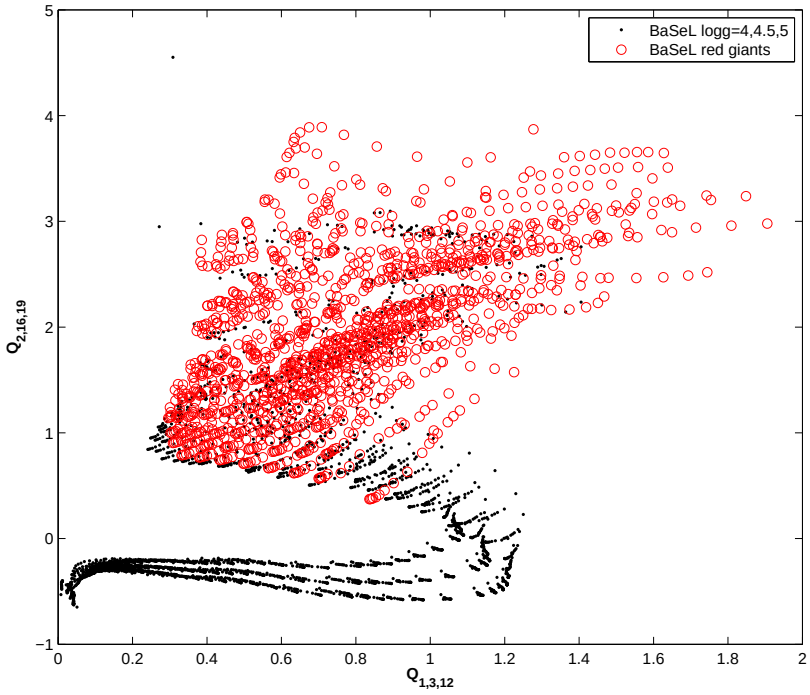

Figure 4.3 $Q_{1,3,12}$,$Q_{2,16,19}$ diagram for spectral classification with the Nandy et al. (1975) extinction law. The black points are main sequence BaSeL models ($log(g) = 4, 4.5, 5$) while the red circles correspond to red giants models.

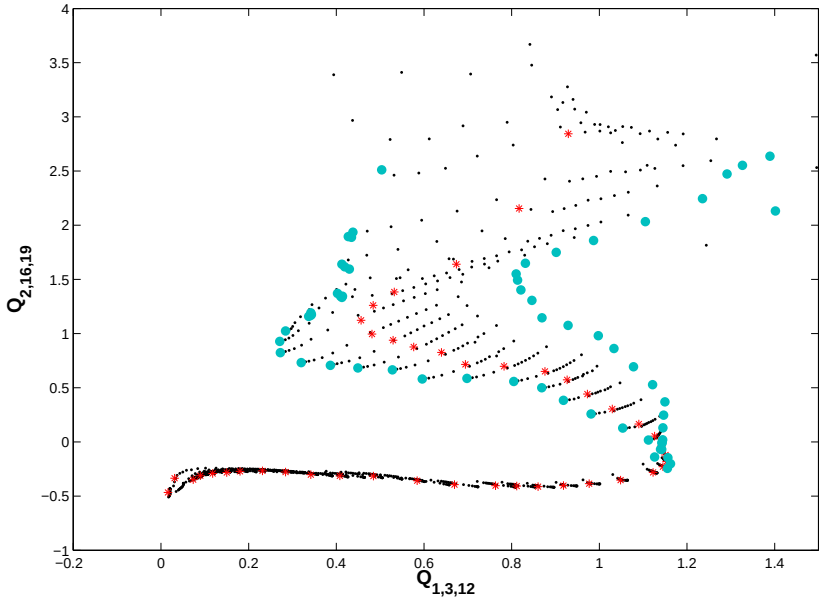

Figure 4.4 Q,Q diagram for spectral classification. The points are data from BaSeL library. The red markers are the average values of $Q_{1,3,12}$ and $Q_{2,16,19}$ for each interval of effective temperature. The blue points to the left of the red markers are stars with low metallicity (-3.5 to -5), and the blue points to the right are stars with $[Fe/H] = 1$ of the several spectral types.

Table 4.2 Average values of $Q_{1,3,12}$ and $Q_{2,16,19}$ for different effective temperatures.

Temperature (K)	$Q_{1,3,12}$	$Q_{2,16,19}$	Temperature (K)	$Q_{1,3,12}$	$Q_{2,16,19}$
O			B		
30,000	0.1501	-0.2830	11,500	0.9231	-0.3933
33,000 - 31,000	0.0736	-0.3478	11,000	0.9816	-0.3833
37,500 - 34,000	0.0160	-0.4665	10,500	1.0501	-0.3470
40,000	0.0899	-0.3118	10,000	1.1209	-0.2728
A			12,000	0.8640	-0.4058
7,500	0.8923	0.6653	12,500	0.8135	-0.3989
7,750	0.9392	0.5848	13,000	0.7637	-0.3923
8,000	0.9852	0.4504	14,000	0.6683	-0.3812
8,250	1.0412	0.3094	15,000	0.5844	-0.3580
8,500	1.1002	0.1667	16,000	0.5431	-0.3072
8,750	1.1313	0.0566	17,000	0.4948	-0.3070
9,000	1.1433	-0.0404	18,000	0.4536	-0.2995
9,250	1.1516	-0.1188	19,000	0.4160	-0.3006
9,500	1.1542	-0.1792	20,000	0.3819	-0.3004
9,750	1.1454	-0.2264	21,000	0.3493	-0.2953
F			22,000	0.3179	-0.2868
6,000	0.5108	1.0512	23,000	0.2886	-0.2695
6,250	0.5563	0.9835	24,000	0.2608	-0.2532
6,500	0.6017	0.9114	25,000	0.2345	-0.2561
6,750	0.6630	0.8540	26,000	0.2103	-0.2532
7,000	0.7161	0.7376	27,000	0.1896	-0.2544
7,250	0.8017	0.7162	28,000	0.1708	-0.2601
M			29,000	0.1542	-0.2610
2,000	1.6338	8.1695	G		
2,200	1.8060	7.6693	5,250	0.5818	1.4757
2,350	0.9500	5.9000	5,500	0.5240	1.3426
2,500	1.9171	5.2137	5,750	0.4901	1.1922
2,800	1.5761	4.9184	K		
3,000	1.1715	3.9388	3,750	0.9380	2.8609
3,200	1.2272	3.3932	4,000	0.9601	2.7817
3,350	1.7300	2.2650	4,250	0.8604	2.1016
3,500	0.8900	3.3932	4,500	0.8010	1.8306
			4,750	0.8010	1.8306
			5,000	0.6817	1.6399

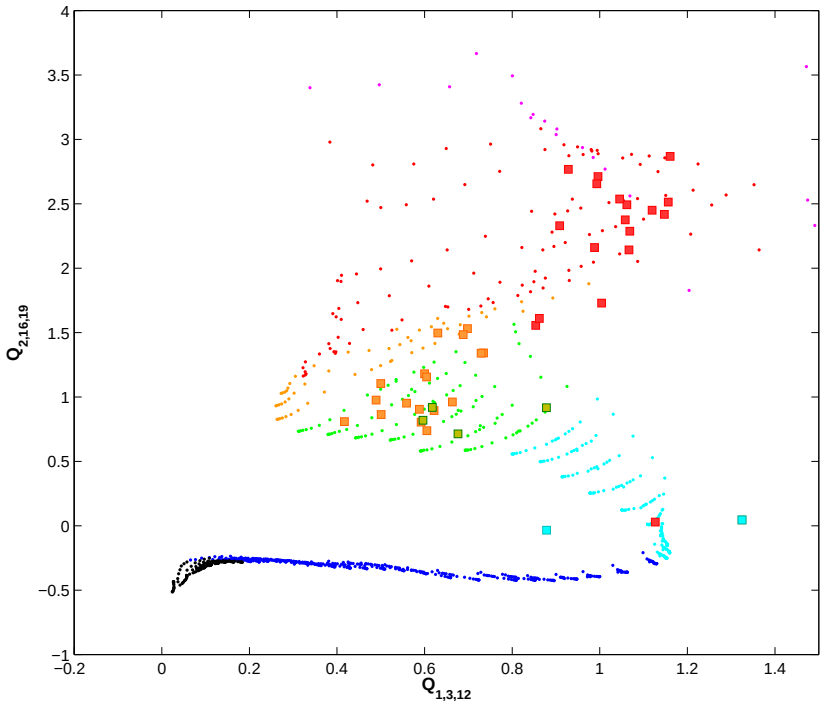

Figure 4.5 $Q_{1,3,12}$,$Q_{2,16,19}$ diagram. The points are BaSeL models, the squares represent 41 ALHAMBRA field stars with estimated spectral types. Different colors correspond to different spectral types as in Figure 4.2.

In Figure 4.5 the same diagram is shown but where squares represent Q-values of 41 stars of the ALHAMBRA survey, observed in different fields of the project. They were selected from the whole star catalogue for having SDSS photometry and estimations of their physical parameters from their SDSS spectra, and so the spectral type they show in the graph specified with the different colors is the spectral type of the associated SDSS star. The mean of the photometric errors in the 20 bands of these stars is lower than 1 hundredth magnitude, except in the bands A366M, A394M and A948M, which have a mean of 0.03, 0.01 and 0.01 magnitudes, respectively. The matching was carried out with a code implemented in Matlab, with a tolerance of 10^{-4} degrees, and the SDSS parameters were taken from the DR7 release. The RMSE of the right ascension (RA) in the internal astrometric solutions for LAICA images, has a mean of 0.029 *arcsec* with a standard deviation of 0.014, and a mean of 0.022 *arcsec* with a standard deviation of 0.006 in the case of the declination (DEC).

The majority of these stars are in the expected positions compared with the positions of BaSeL models of the same spectral types, with some dispersion possibly due to photometric errors.

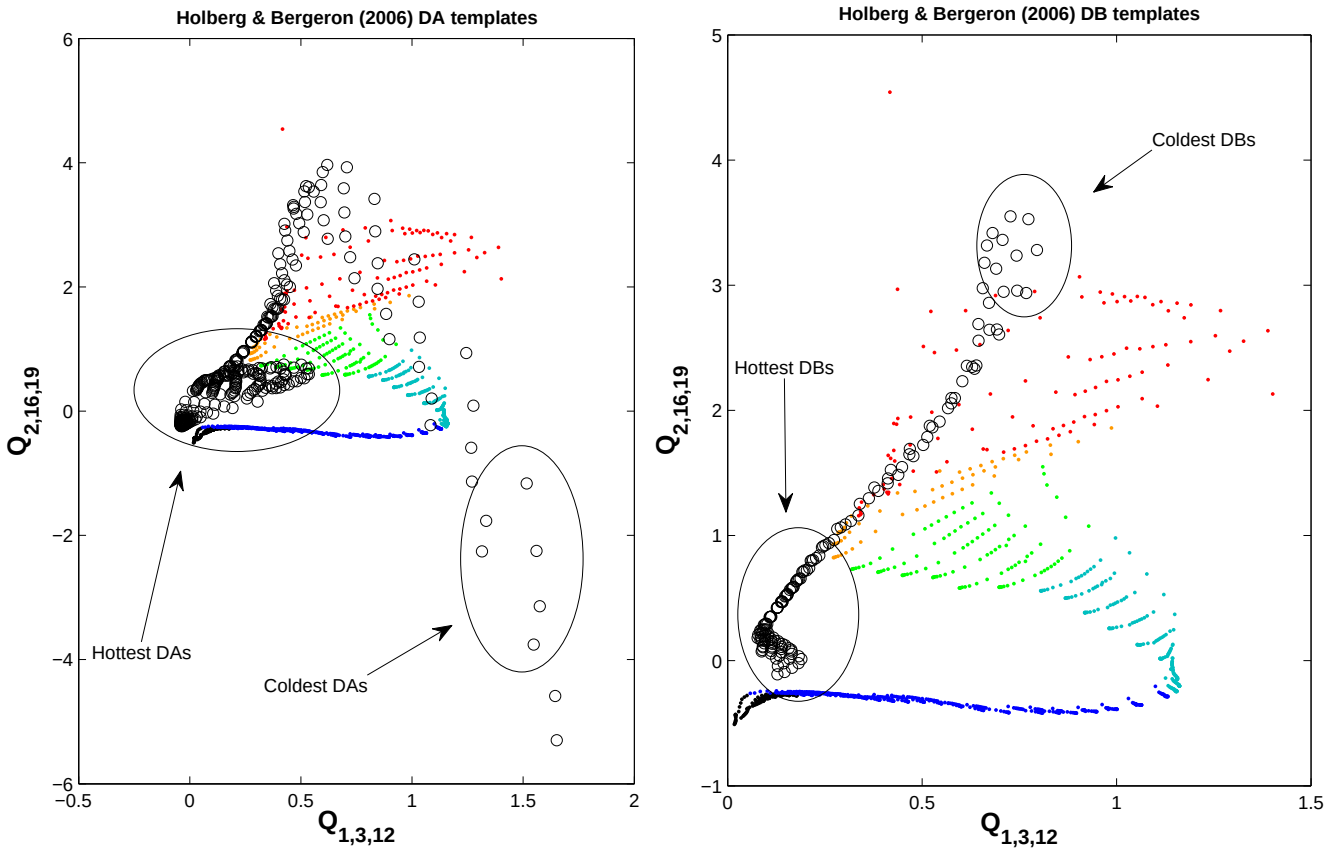

Figure 4.6 Same Q,Q diagram with BaSeL models in colored points, and DA and DB hot white dwarfs models from Holberg & Bergeron (2006) in black circles.

Figure 4.6 shows templates of DA and DB[4] white dwarfs from Holberg & Bergeron (2006) with black circles, and it can be seen that hot white dwarf models are mostly over the O-B model cloud, and they spread all over the diagram while the temperature is decreasing, the coldest white dwarfs ($\sim$ 3500k) coinciding with the K-M-type main sequence stars. DA templates, the graph on the left, can reach low temperatures of 1500K , these models are the circles marked as "Coldest DAs" in the plot.

Notwithstanding, Matute et al. (2012) (in referee), show the abilities of the ALHAMBRA survey in assigning accurate photo-z's to Blazars (BLAGN)/ QSOs based on their ALHAMBRA very-low-resolution optical-NIR spectroscopy, and they present estimations of the number of QSOs presented in the ALHAMBRA fields 2 to 8. Figure 4.7 represents, in the same Q, Q diagram, some QSO models from the SWIRE template library (Polletta et al. 2007), used in Matute et al. to detect these kinds of objects. In particular two templates of moderately luminous AGNs representing Seyfert 1.8 and Seyfert 2 galaxies, three optically-selected 1-type QSOs with different values of infrared/optical flux ratios, one 2-type QSO obtained by combining the observed optical/near-IR spectrum of the red quasar FIRST J013435.7-093102 (Gregg et al. 2002) and the rest-frame IR data from the quasars in the Palomar-Green sample with consistent optical SEDs, two composite (AGN+SB) empirical templates created to fit the SEDs

[4]DB White dwarf is a helium-rich atmosphere white dwarf, indicated by neutral helium, He I, spectral lines.

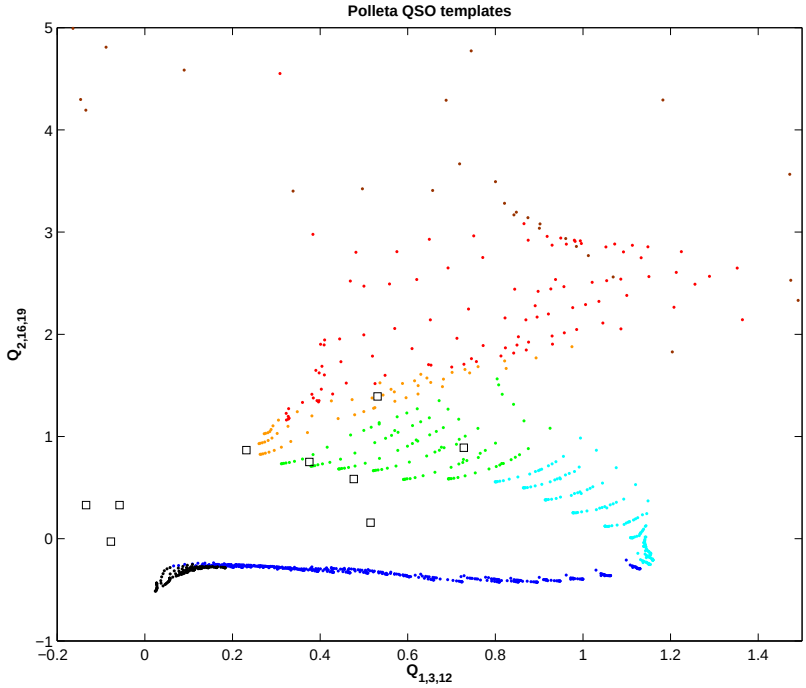

Figure 4.7 Same Q,Q diagram with QSO models (squares).

of two objects, the heavily obscured BAL QSO Mrk 231 (Berta 2005) and the Seyfert 2 galaxy IRAS 19254-7245 South (Berta et al. 2003), and finally a starburst template corresponding to the SED of NGC 6240. Looking at the Q,Q diagram, the three 1-type QSOs are the ones situated over the O-type stars: the one over the blue points is the AGN+SB template corresponding to the Mrk 231 QSO. The 2-type QSO and the two Seyferts are situated on the left edge of the F-G-type stars. The AGN+SB template corresponding to the Seyfert 2 IRAS 19254-7245 South is over the G-type stars, and the NGC 6240 template is over the F-type stars. Thus, a priori, this diagram is not useful for selecting white dwarfs or QSOs mixed among the stars, but, in the case an ALHAMBRA field star is located in the diagram above the O-B-type star line (black and blue points), it can be considered a good candidate to be a hot white dwarf or 1-type QSO, since we do not expect to have such hot stars on these fields and the position coincides with these kinds of objects.

In summary, a Q,Q diagram such as the one analyzed here is not discriminating for all the point-like objects that can be found in the ALHAMBRA survey, but if we just consider the stars, this diagram provides us a first evaluation of their spectral types.

4.1.3 Color-color Diagram

Another tool to detect possible hot white dwarfs, QSOs or another kind of objects such as dM/WD binaries or RR Lyrae-type stars, is a color-color diagram. Following Sesar et al. (2007), the (A366M-A491M) vs. (A491M-A613M) color-color diagram (corresponding to the

effective wavelengths closest to the u-g and g-r colors in the SDSS) can be divided into six characteristic regions, each dominated by a particular type of object specified in the box at the right side in Figure 4.8. The 41 same field stars are represented in blue points with error bars indicating the uncertainties in the corresponding colors. These objects are selected in the SDSS catalogue as "normal" stellar objects, and as it was expected most of the objects are classified in the diagram as stars and just two of them are close to the border between main-sequence stars and high redshift QSOs. There are two stars in the region of the RR Lyrae-type stars; the most distant one to the main locus of the stars is classified in the SIMBAD Astronomical Database[5] as a Horizontal Branch star which agrees with the position found in the diagram; SIMBAD Database does not have any object at the coordinates of the other star (within a radius of 2 *arcmin*), the closest star is a low-mass star at 159.44 *arcsec*.

To generate the graph, the magnitudes of the stars are dereddened with the color excesses estimated for the SDSS stars, and in order to define the regions with the best precision, some linear relations between the u-g and g-r colors and the ALHAMBRA (A366M-A491M) and (A491M-A613M) colors are established and applied to the SDSS diagram of Sesar et al. (2007):

$$A366M - A491M = 1.00(u - g) - 0.03 \ (RSE = 0.04) \tag{4.5}$$

$$A491M - A613M = 0.75(g - r) - 0.01 \ (RSE = 0.03) \tag{4.6}$$

These equations are built with synthetic ALHAMBRA and SDSS magnitudes of the 288 primary NGSL stars.

4.2 Reddening estimation

In the previous section, reddening-free Q parameters were used to obtain a first approximation for stellar classification with the ALHAMBRA photometric system. However, these indexes entail the use of an extinction law that, in most cases, represents an interpolation among a few measured values, which implies the probable existence of systematic errors. A possible way to overcome this would be to obtain accurate estimations of the color excess from the objects' own colors, and so determine the rest of the main physical stellar parameters directly from the dereddened colors. Two different ways to deal with this task have been considered and tested.

4.2.1 Parametric approximation

In order to obtain parametric models to estimate the color excess E_{B-V} from ALHAMBRA colors, firstly, theoretical spectra of BaSeL 2.2 library are reddened with the Nandy et al. extinction law for the values of E_{B-V} = 0.05, 0.1, 0.25, 0.4, 0.5, 0.6, 0.75, 0.9 and 1. Models with $log(g)$=4.5 of all the spectral types are selected to optimize the regressions, and in order to obtain more accurate E_{B-V} estimations the sample is divided in four temperature ranges:

[5] `http://simbad.u-strasbg.fr/simbad/`

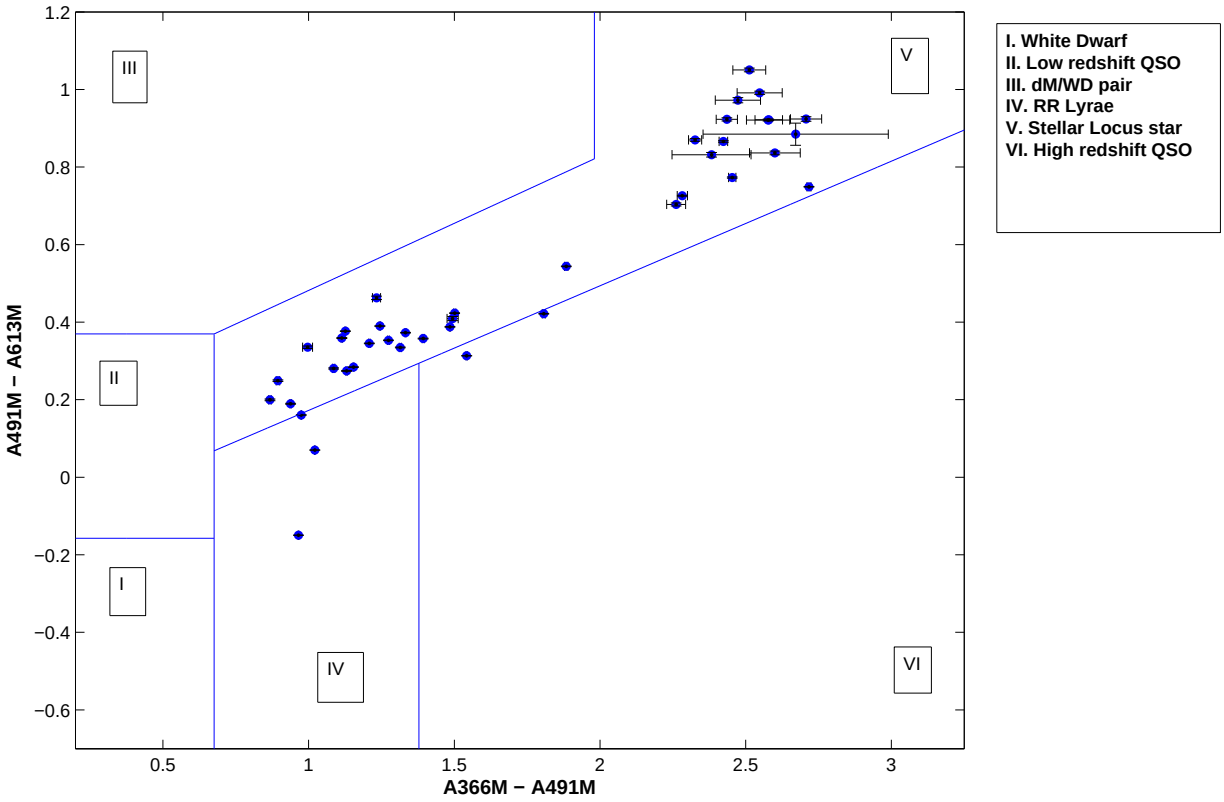

Figure 4.8 Color-color diagram with six characteristic regions, each dominated by a particular type of object specified in the box at the right side. The blue points with photometric error bars represent 41 ALHAMBRA field stars.

1. O-B-type stars ($T_{eff} > 10,000K$)
2. A-F-type stars ($6000K < T_{eff} \leq 10,000K$)
3. G-K-type stars ($3700K < T_{eff} \leq 6000K$)
4. M-type stars ($T_{eff} \leq 3700K$)

The statistical software **R** is used to elaborate the regressions, in particular the statistical task "Backward Stepwise Regression" and the tool called Bayesian Information Criterion (BIC) for model selection (see definition 3.1). Among the 190 ALHAMBRA colors, we look for the subset of colors that best correlates with the color excess in each of the temperature ranges, that is, the colors with the highest coefficient of determination, R^2, together with the smallest residual standard error (RSE) in the linear regression model with E_{B-V}. Then, with these subsets, we consider linear or quadratic regression models with one or more colors in order to obtain the model with less error and the minimum number of coefficients in it. Finally, the best relations found for each interval of temperature are the following:

1. E_{B-V}=0.43+3.04(A457M-A491M)
   R^2=0.99, RSE=0.015
2. E_{B-V}=-0.28+0.64(A366M-A646M)-2.28(A425M-A457M)
   R^2=0.99, RSE=0.016
3. E_{B-V}=0.07-0.07(A366M-A770M)-3.05(A802M-A948M)+8.52(A829M-A892M)
   R^2=0.99, RSE=0.029
4. E_{B-V}=-0.70-0.78(A366M-A491M)+1.21(A394M-A921M)-0.56(A457M-A646M)-0.88(A613M-A829M)
   R^2=0.96, RSE=0.068

These models entail the propagation of two kinds of errors, the error of the equations, estimated with the values of the RSE, and the photometric errors of the colors presented in each model. The RSEs of the regression models are higher in the coldest stars, being the equations for M-type stars the greatest of which is 0.068 magnitudes. So, even if the photometric errors of the magnitudes are lower than 0.1 magnitudes, the equations will provide E_{B-V} estimations with uncertainties well above a few tenths of magnitudes. Since the ALHAMBRA field stars are expected to have a E_{B-V} lower than 0.1, the expected estimates from these equations would reach relative errors over 100%.

Among the 288 NGSL primary stars there are 216 with an estimation of their E_{B-V} in the literature, and only 12 stars have a value of $E_{B-V} > 0.1$. The white dwarfs and OB-type subdwarfs have been left out since the BaSeL 2.2 library does not have any spectral model of them and so the equations do not have to work properly on these kinds of object. If the parametric models are applied to these 12 stars the results can be summarized in the following figures:

$\overline{\lvert\delta(E_{B-V})\rvert}$	0.113±0.04
$\overline{\delta(E_{B-V})}$	-0.084±0.05

$\overline{\lvert\delta(E_{B-V})\rvert}$ being the mean of the differences between the color excess of the stars from the literature and the estimations from the parametric models in absolute values, and $\overline{\delta(E_{B-V})}$ the mean of the same differences without absolute values. If the stars with a $E_{B-V} < 0.1$ are included in the sample, a total of 216 stars, the results are:

$\overline{\lvert\delta(E_{B-V})\rvert}$	0.148±0.01
$\overline{\delta(E_{B-V})}$	-0.145±0.01

In both cases, the values estimated of E_{B-V} seem to be overestimated on average. However, in the second case the value of $\overline{\delta(E_{B-V})}$ is much bigger, which implies a greater bias in the estimations of the color excess. Figure 4.9 shows a graphic representations of the results, where the residuals, in the sense of E_{B-V} from the literature minus E_{B-V} estimated by the equations, are shown versus the $log(T_{eff})$ of the stars. The residuals are higher in the coldest stars (stars with spectral type later than F), that in average correspond to the stars with E_{B-V} close to 0. The residuals get smaller with temperature increase, as expected because the RSEs of the equations for the coldest stars ($log(T_{eff}) < 3.75$) are greater than for hot stars. Furthermore, the graphic shows that this methodology leads to high systematic errors for late spectral type stars, which are those that mainly populate the ALHAMBRA fields.

An application of these formulae to those ALHAMBRA field point-like objects with photometric errors less than 0.1 magnitudes in the 20 bands is developed. These objects are selected as point-like objects from the whole catalogue with geometric criteria up to magnitude 25 in the A646M band, so among them there can be distant galaxies or QSOs. There are 2477 objects with these photometric errors among the 27,009 geometrically considered as point-like objects. Since the equations need a previous spectral-type classification of the objects, the $Q_{1,3,12}$, $Q_{2,16,19}$ diagram is used to gain an approximation of their temperatures and so to be able to apply the parametric models to them, but some of these objects have positions on the Q,Q diagram too far from the point cloud of BaSeL models and so the estimation of their spectral type is not possible. Thus, the equations are only applied to the 2420 stars with "good" positions on the Q,Q diagram. Figure 4.10 shows a histogram of the E_{B-V}s obtained for these ALHAMBRA field point-like objects where a bias in the estimated color excesses is appreciable. The mean and the median of the color excesses are very close being:

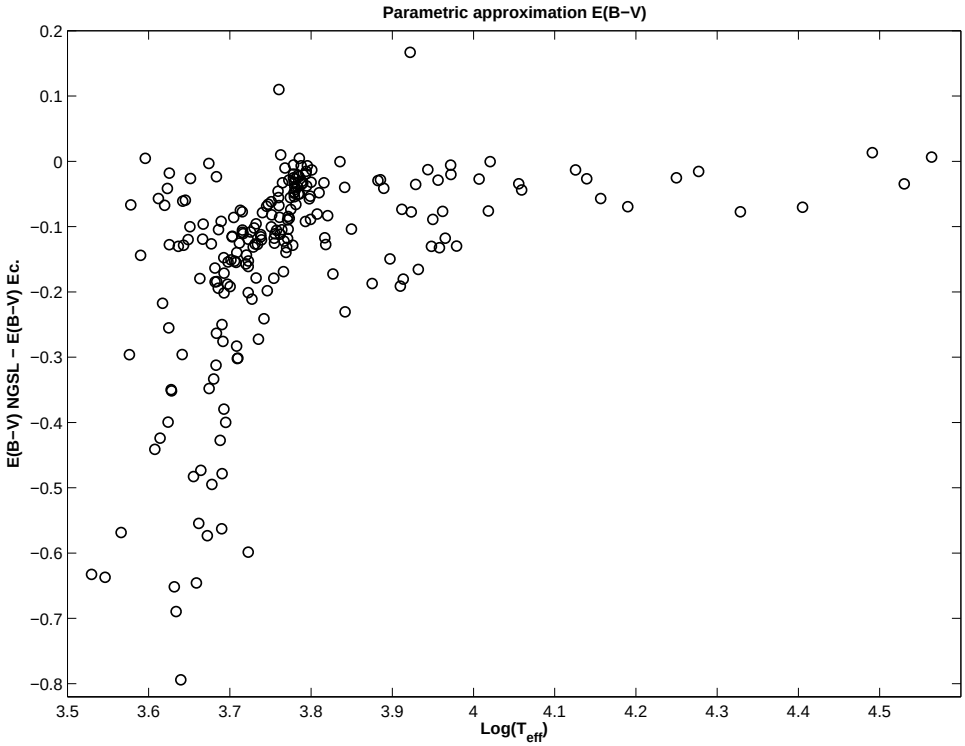

Figure 4.9 $log(T_{eff})$ vs. E_{B-V} residuals from the parametric approximations

$Median(E_{B-V})$	0.278 ± 0.005[1]
$Mean(E_{B-V})$	0.274 ± 0.008[2]

1. MAD divided by the square root of the number of elements

2. Standard deviation divided by the square root of the number of elements

The ALHAMBRA stars from the fields detailed in Table 2.1 are expected to have a mean and median of E_{B-V} much lower than the values obtained from the equations (the expected values of the main physical parameters of these stars are presented in detailed in section 4.5.6). Even if we correct the bias obtained with the NGSL, $\overline{\delta(E_{B-V})} = -0.145$, the final values are too high ($Mean(E_{B-V}) = 0.129$). So this result is consistent with the conclusions we have explained before for the results this methodology offers.

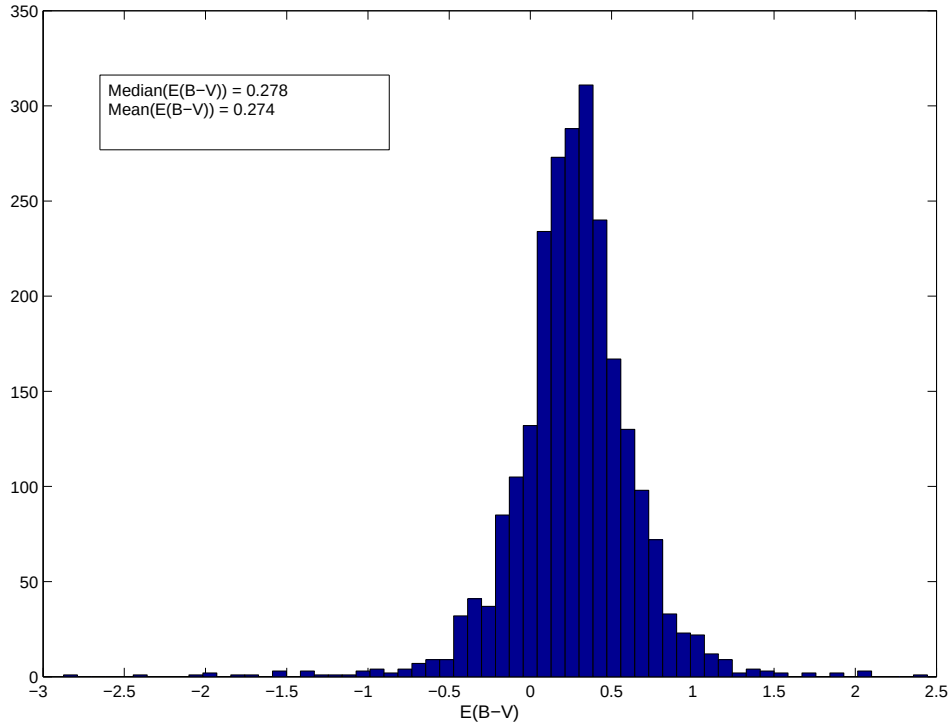

Figure 4.10 Frequency histogram of the E_{B-V} of 2477 ALHAMBRA field stars, with photometric errors of less than 0.1 magnitudes in the 20 magnitudes, obtained by the parametric equations. The mean and median of the color excesses are shown in a text box.

4.2.2 Support Vector Machine E_{B-V} estimation

More recently, new methods have been proposed to extract the physical information of the stars from photometric observations. These are more automatic algorithms without too much supervision from the astrophysicist, but which enable dealing with large samples of stars at the same time, and they are statistically robust enough to find quite accurate results.

The Support Vector Machine (SVM) is a useful technique for data classification. Its theory was initially developed by V. Vapnik (1998) and it is based on what is called Statistical Learning Theory. It involves separating data into training and testing sets. Each instance in the training set contains one "value" (i.e. the class labels) and several "attributes" (i.e. the features or observed variables). The goal of SVM is to produce a model (based on the training data) which predicts the target values of the test data given only the test data attributes. In particular, having a set of data so that each one of them belongs to one of two categories, then SVM looks for a hyperplane that manages to optimally separate the data of one category from the others. In SVM, the optimum hyperplane is the one that has the largest distance (margin) to the nearest training data points of any class. The vector formed by the nearest points to the hyperplane is called "support vector". Often, the sets for discrimination are not linearly separable through an optimum hyperplane in the original finite dimensional space, i.e. there are more than two categories to classify, or maybe the data set cannot be completely separated. In these cases, the initial space is mapped into a much higher-dimensional feature space, where

the data can be linearly separated. The transformation of the data from an initial space to another with a higher dimension is achieved by the kernel function, that is, an internal product in the feature space that has its equivalent in the initial space. Analytically, given a training set of instance-label pairs $(xi; yi)$; i = 1,...,l where $xi \in R^n$ and $y \in 1, -1^l$, the support vector machines (Boser et al., 1992; Cortes and Vapnik, 1995) require the solution to the following optimization problem:

$$\min_{w,b,\xi} w^T w + C \sum_{i=1}^{l} \xi_i \tag{4.7}$$

subject to,

$$y_i(w^T \phi(x_i) + b) \geq 1 - \xi_i, \xi_i \geq 0 \tag{4.8}$$

Here the training vectors xi are mapped into a higher (maybe infinite) dimensional space by the function ϕ. $C > 0$ is the penalty parameter of the error term and $K(x_i, x_j) \equiv \phi(x_i)^T \phi(x_j)$ is the kernel function.

The main differences of the SVM versus Artificial Neural Networks (ANN), is that ANNs use empirical risk minimization, whilst SVMs use structural risk minimization, which minimizes a superior limit to the expected risk, instead of minimizing the error over the test data. Moreover, while the ANN can have multiple local minima, the solution to an SVM is global and unique. On the other hand, one of the main problems with the SVMs is the "overtraining", which happens when the model classifies correctly on the test data, but is unsuccessful on new data, meaning a bad generalization of the model.

Using the SVM implementation in the statistical software **R**, estimations of the color excess of stars were determined from ALHAMBRA colors. A radial basis function (RBF) such as:

$$K(x_i, x_j) = exp(-\gamma \|x_i - x_j\|^2), \gamma > 0. \tag{4.9}$$

is used as kernel function, where γ is the kernel parameter, and the model generated is based on the theoretical spectra of the BaSeL 2.2 library, reddened with the Nandy et al. extinction law, with E_{B-V} = 0.05, 0.1, 0.25, 0.4, 0.5, 0.6, 0.75, 0.9, 1, and taking as attributes the 19 correlative ALHAMBRA colors. From the same library, the training subset and the test subset are randomly selected, and after elaborating the best model, it can be applied to 216 NGSL stars (rejecting the White Dwarfs and the sdOB-type stars again). An advantage of the SVM algorithm is that it is not necessary to know the spectral type of the stars a priori. The results have the following statistical indicators:

$\lvert\overline{\delta(E_{B-V})}\rvert$	0.095±0.005
$\overline{\delta(E_{B-V})}$	-0.032±0.008

Figure 4.11 shows a graphic representation of the results, in the same way as Fig. 4.9. It seems that, although the SVM algorithm makes use of 19 colors instead of the, at most, 4 colors used in each estimation by the equations, the residuals are higher in the parametric approximations, which means that the equations have a greater intrinsic error than the SVM algorithm. Furthermore, in the graph we can notice that the distribution of residuals in this case presents less bias in the coldest stars compared with the previous case. However the dispersion in the E_{B-V} estimations of the stars with $T_{eff} < 3.85$ is here also greater than the dispersion of the hottest stars.

The same SVM model is applied to the ALHAMBRA field point-like objects, with photometric errors lower than 0.1 magnitudes in the 20 bands (2477 objects). Figure 4.12 shows the histogram of the E_{B-V}s obtained with this algorithm. The mean and median of these values are:

$Median(E_{B-V})$	0.021 ± 0.01[1]
$Mean(E_{B-V})$	0.019 ± 0.01[2]

1. MAD divided by the square root of the number of elements

2. Standard deviation divided by the square root of the number of elements

Both values have decreased regarding the mean and median obtained with the parametric equations. Indeed, these values are closer to the real values expected to be found in the ALHAMBRA field stars, taking into account the characteristic of the selected fields (Table 2.1). Comparing histograms 4.10 and 4.12 we can also notice here less bias and less dispersion with regard to the average values.

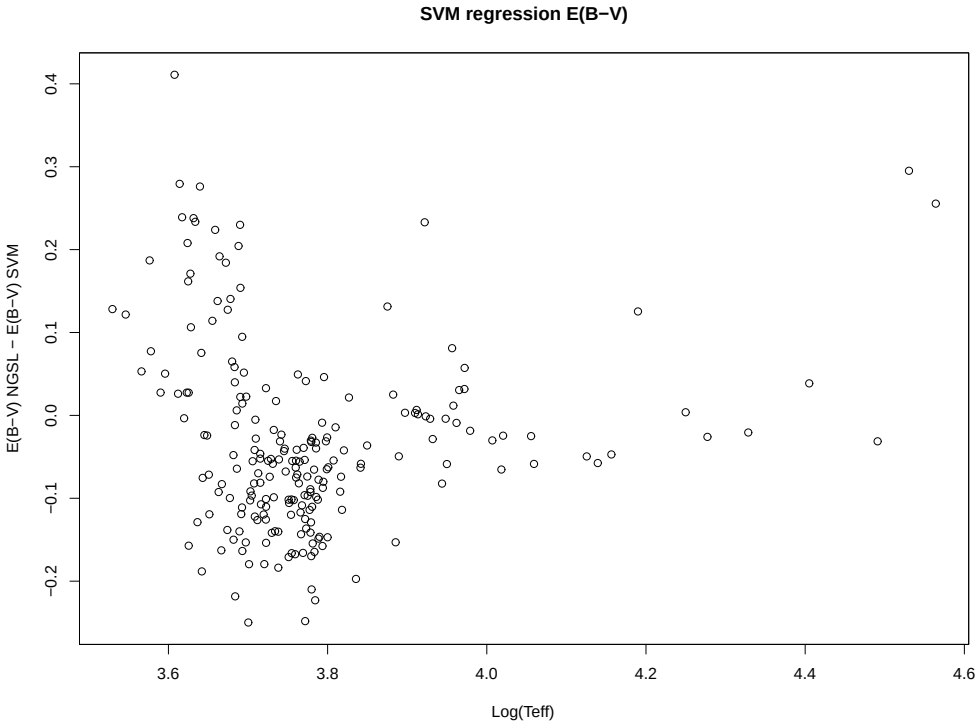

Figure 4.11 $log(T_{eff})$ vs. E_{B-V} residuals from the SVM.

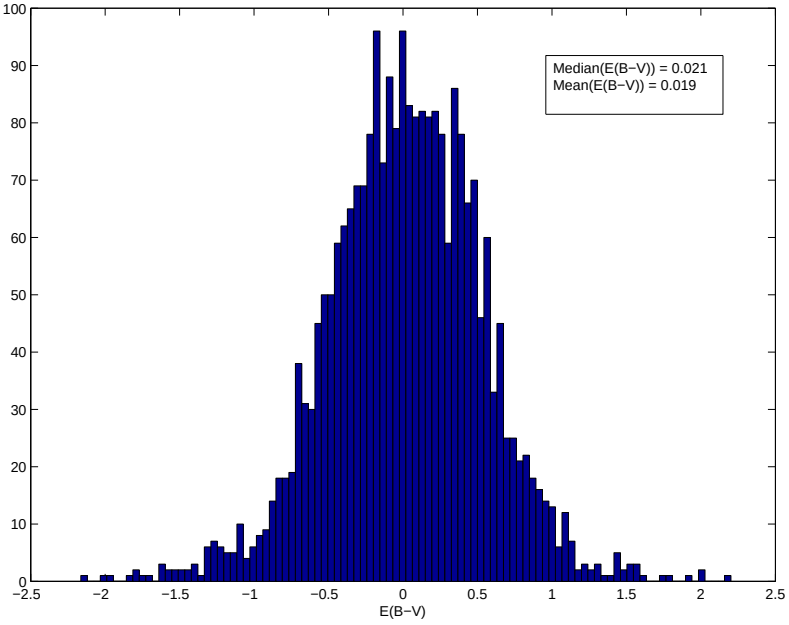

Figure 4.12 Frequency histogram of the E_{B-V} of the ALHAMBRA field stars, with photometric errors lower than 0.1 magnitudes in the 20 bands, obtained by the SVM algorithm. The mean and median of the color excesses are shown in a text box.

4.3 Effective Temperature estimation

The effective temperature of a star is the temperature of a black body with the same luminosity per surface area (F_{Bol}) as the star, and it is defined according to the Stefan-Boltzmann law $F_{Bol} = \sigma T_{eff}^4$ (σ is called the Stefan-Boltzmann constant). Precise determinations of effective temperature of stars are decisive for several reasons, not only for direct applications such as comparisons of isochrone calculations to observed color-magnitude diagrams, but also for different indirect applications, e.g. determinations of chemical abundances. Photometric indexes of the stars have a crucial role when determining their effective temperatures, since the variation of the colors of the stars is a direct consequence of their surface temperatures.

As with the color excess, several tools are used to try to determine the effective temperature of the stars with the best possible accuracy, and making use of the ALHAMBRA photometric indexes. Parametric and non-parametric temperature approximations are presented below.

4.3.1 Color Parametric Approximation of T_{eff}

We look for the best relation between T_{eff} and some intrinsic ALHAMBRA colors, or a combination of several of them, trying to find the best analytical relation with the minimum number of colors, and covering the maximum number of stellar spectral types. We use all the BaSeL 2.2 theoretical spectra, and consider the 190 possible ALHAMBRA colors to find the best model, making use of the Bayesian information criterion (BIC) in the statistical software **R**. Finally we divide the sample into two ranges of temperature since the behavior in front of the different colors varies in both groups of stars:

1. $log(T_{eff}) \geq$3.9, corresponding to the intrinsic color $(A522M - A948M)_0 \leq$-0.29
2. $log(T_{eff}) <$3.9, corresponding to the intrinsic color $(A522M - A948M)_0 >$-0.29

This correspondence between T_{eff} of the stars and the color $(A522M - A948M)_0$ is established making use again of BaSeL spectra. In both cases, the best analytical relation with effective temperature is formed with an ALHAMBRA color in a quadratic model such as:

1. For stars with $(A522M - A948M)_0 \leq$-0.29 :

   $log(T_{eff})$=1.71$(A522M - A829M)_0^2$ + 1.04$(A522M - A829M)_0$ + 4.07

   R^2=0.99 , Residual Standard Error = 0.02

2. For stars with $(A522M - A948M) >$ -0.29 :

   $log(T_{eff})$=0.02$(A457M - A646M)_0^2$ - 0.18$(A457M - A646M)_0$ + 3.84

   R^2=0.97 , Residual Standard Error = 0.02

These relations are valid for all spectral types and luminosity classes included in the BaSeL 2.2 library. In order to apply these equations correctly, it is necessary to deredden the magnitudes of the stars since they use intrinsic colors. So, considering the color excesses obtained from the literature of the NGSL stars, it is possible to deredden their magnitudes and so to apply the equations to them. Not all of the 288 stars have any value of its E_{B-V} in the literature, and the white dwarfs and the sdOB-type stars have to be rejected (in principle the relations do not have to work well on them), so in total there are 216 stars to test the equations. The results are the following:

$\overline{\lvert\delta(T_{eff})\rvert}$	574.54±151[1] (K)
$\overline{\delta(T_{eff})}$	-265.80±155[1] (K)
$\overline{\lvert\delta(T_{eff})/T_{eff}\rvert}$	0.054±0.007[1] (K)

1. Standard deviation divided by the square root of the number of elements

$\overline{|\delta(T_{eff})|}$ being the mean of the differences between the temperature of the stars from the literature and the estimations from the parametric models in absolute values; $\overline{\delta(T_{eff})}$ is the mean of the same differences without absolute values, which indicates that the temperatures obtained are overestimated in average. The mean is also present of the relative differences in absolute value that shows most residuals are within a 5%. Figure 4.13 shows the relative differences of the temperatures in two plots, at the top there are the stars with $T_{eff} < 10,000$K and at the bottom the stars with $T_{eff} \geq 10,000$K; there are not significant differences between the residuals of both groups of stars.

There are three stars that have greater residuals than the average, painted in the graphic with red circles. These stars are the following:

- HD141851, classified as double or multiple star of spectral type A3Vn
- HD048279, classified as a star in double system of spectral type O8V
- HD034078, classified as a double or multiple star of spectral type O9.5Ve

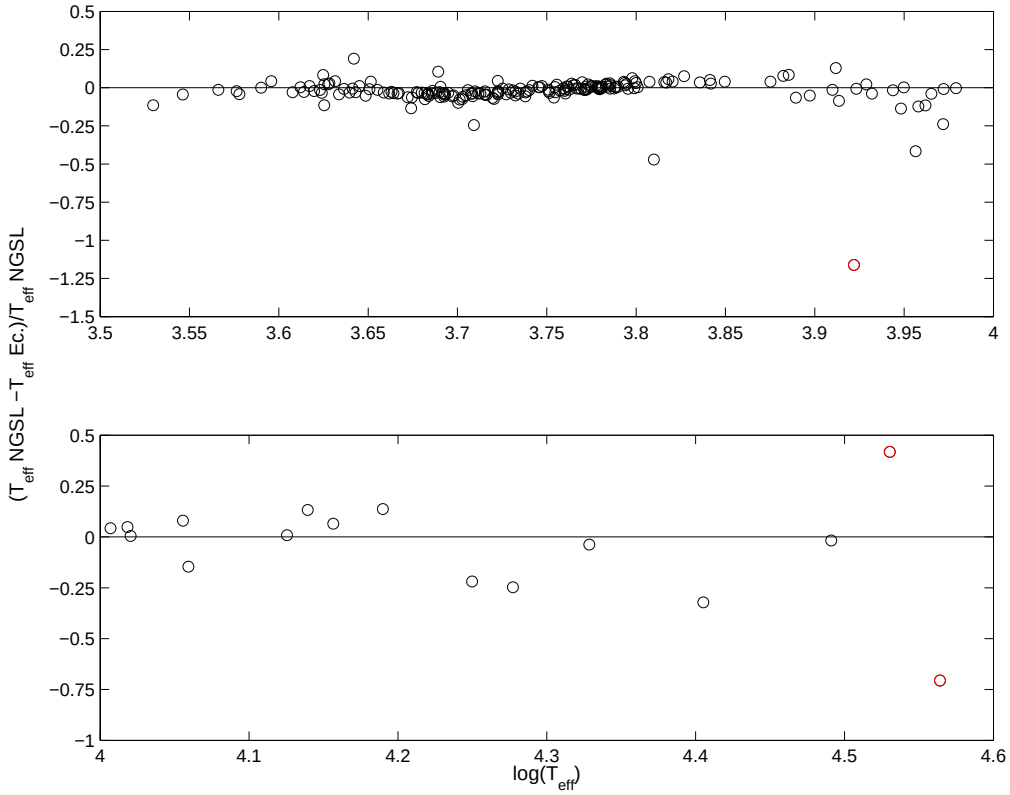

Figure 4.13 $log(T_{eff})$ vs. T_{eff} relative residuals from the parametric approximation of T_{eff} with colors.

4.3.2 *Q* Parametric Approximation of T_{eff}

The same methodology of the previous subsection can be applied on Q parameters in order to find parametric models to estimate the T_{eff} of the stars. Considering all the combinations of the 190 ALHAMBRA colors, 1140 Q-values are generated using the Nandy et al. extinction law on their definition (see formula 4.1), and synthetic ALHAMBRA photometry of BaSeL 2.2 spectra. The models are divided in the same two temperature ranges as with the color equations, and the best relations found, in the sense of minimum Residual Standard Error (RSE) and maximum coefficient of determination, R^2, with the minimum of Q-parameters in the linear regression model, are the followings:

1. For stars with $log(T_{eff})$ ≥3.9 :

   $log(T_{eff})$ = -1.09·$Q_{1,5,6}$ + 0.44·$Q^2_{1,5,6}$ - 0.09·$Q_{2,17,19}$ + 4.55

   R^2=0.98 , Residual Standard Error = 0.03

2. For stars with $log(T_{eff})$ <3.9 :

   $log(T_{eff})$ = -0.14·$Q_{6,16,18}$ + 0.01·$Q^2_{6,16,18}$ - 0.02·$Q_{1,7,8}$ + 3.81

R^2=0.91 , Residual Standard Error = 0.04

being,

$$Q_{1,5,6} = (A366M - A491M) - \frac{E_{A366M,A491M}}{E_{A491M,A522M}}(A491M - A522M) \tag{4.10}$$

$$Q_{2,17,19} = (A394M - A861M) - \frac{E_{A394M,A861M}}{E_{A861M,A921M}}(A861M - A921M) \tag{4.11}$$

$$Q_{6,16,18} = (A522M - A829M) - \frac{E_{A522M,A829M}}{E_{A829M,A892M}}(A829M - A892M) \tag{4.12}$$

$$Q_{1,7,8} = (A366M - A551M) - \frac{E_{A366M,A551M}}{E_{A551M,A581M}}(A551M - A581M) \tag{4.13}$$

The main advantage of these models is the fact of not depending on the color excess of the objects. Here we use the Q,Q diagram to classify the stars in the two subsets according to their temperatures. Having the $Q_{1,3,12}$,$Q_{2,16,19}$ values of a NGSL star, we look for the $Q_{1,3,12}$,$Q_{2,16,19}$ pair in Table 4.2 which minimizes the euclidean distance of both, and we consider the effective temperature corresponding to those Q,Q values. Applying these Q parametric models on the 281 NGSL stars (rejecting again the White Dwarfs and the sdOB-type stars), the temperatures estimated have the following representative figures:

$\lvert\overline{\delta(T_{eff})}\rvert$	695.26±120[1] (K)
$\overline{\delta(T_{eff})}$	23.60±127[1] (K)
$\lvert\overline{\delta(T_{eff})/T_{eff}}\rvert$	0.084±0.005[1] (K)

1. Standard deviation divided by the square root of the number of elements

In this case the residuals have more dispersion than in the previous case, and the relative differences indicate that the errors are within a 8.4%. The value of $\overline{\delta(T_{eff})}$ is closer to 0 than in the former case; furthermore it is positive, what means that the temperatures are not systematically overestimated.

Figure 4.14 shows the residuals of these equations in the same way as Fig. 4.13. The top graph shows a bias in the distribution of differences in the stars with $3.65 < log(T_{eff}) < 3.8$ which is dependent on the temperature of the objects. There are three stars that stand out for their high residuals compared with the average, and they are represented with red circles in the graphic. These are:

- HD164402, classified as a spectroscopic binary of spectral type B0Iab/Ib (bottom graph).
- HD034078, classified as a double or multiple star of spectral type O9.5Ve (bottom graph). This star is wrongly classified in the Q,Q diagram, since, although it is over the black

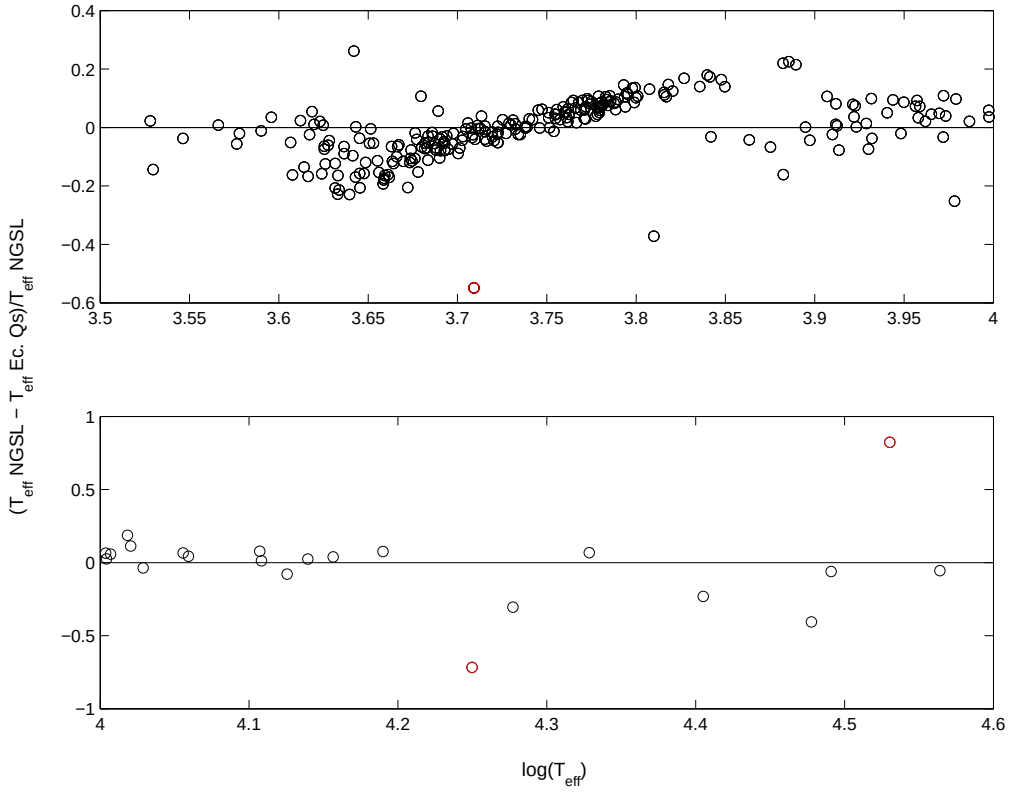

Figure 4.14 $log(T_{eff})$ vs. T_{eff} relative residuals from the parametric approximation of T_{eff} with Q-parameters.

point cloud (corresponding to the O-type stars), its $Q_{1,3,12}$,$Q_{2,16,19}$ values are closer to the values of a star with a temperature of 6500K (see Figure 4.2), and the equations give a temperature of 6015K.

- V* BN Vul, classified as a variable star of RR Lyrae type and spectral type A9.2 D (top graph); however, the values of effective temperature found in the literature do not correspond with its spectral type, having a mean temperature of 5119K. In the Q,Q diagram it is classified as a star with $T_{eff} = 8000K$ and the temperature obtained with the equations is of 7928K, which corresponds to an A-type star. If the intrinsic color $(A522M - A948M)_0$ is used to classify the stars in the two subsets (as we did for the color equations), then this star is included in the group of cold stars, so it is a late A-type star but its SED must be similar to a late-type star maybe due to its low-metallicity ($[Fe/H] = -1.3$).

4.4 SVM T_{eff} estimations

Using the SVM algorithm, a model is elaborated to predict the T_{eff} of the stellar objects with BaSeL 2.2 synthetic photometry. The model is applied to the unreddened magnitudes of the same subset of NGSL stars as in the previous subsection, and the residuals have the following statistical indicators:

$\lvert\overline{\delta(T_{eff})}\rvert$	541.61±107[1] (K)
$\overline{\delta(T_{eff})}$	-273.28±112[1] (K)
$\lvert\overline{\delta(T_{eff})/T_{eff}}\rvert$	0.052±0.006[1] (K)

1. Standard deviation divided by the square root of the number of elements

The results are statistically equivalent to the previous estimations, and particularly similar to the approximations from the color equations. The residuals are within a 5%, and the temperatures are overestimated in average in about 300K.

Figure 4.15 shows the relative residuals of these results. If we compare both plots, the corresponding to the coldest stars at the top and to the hottest stars at the bottom, we can see that the residuals are higher in the second group of stars. It is also remarkable that the structure showed in the Q parametric approximations is not present in the results with the SVM algorithm.

The outliers from the distribution of residuals are marked in red circles. The stars with the greatest differences between their temperature values from the literature and the values estimated with SVM are:

- HD141851, classified as a double or multiple star of spectral type A3Vn
- HD037202, classified as a Be star of spectral type B2IV
- HD164402, classified as a spectroscopic binary of spectral type B0Iab/Ib

there being two stars in common with the outliers from the former methods of T_{eff} calibration.

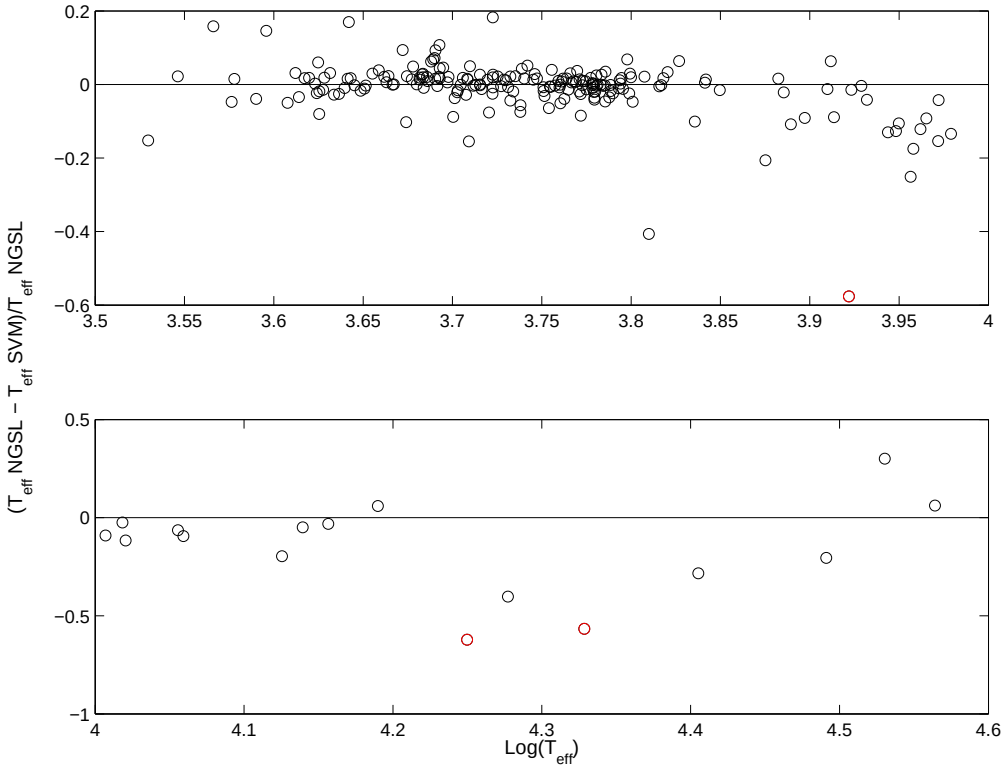

Figure 4.15 $log(T_{eff})$ vs. T_{eff} relative residuals from the SVM estimation of T_{eff}.

4.5 Stellar classification and physical parameter estimation: *Q* Fit Algorithm

The methodology developed, Q Fit Algorithm (QFA), leads to the $T_{\rm eff}$, $log(g)$, $[Fe/H]$ and E_{B-V} estimation of a great variety of spectral and luminosity classes, from O- to M-type stars and including hot white dwarfs and chemically peculiar stars. The method is based on reddening-free Q-parameters and the core of the algorithm is based on the following steps:

1. Generation of 18 independent Q-parameters from ALHAMBRA photometry: theoretical spectra and observed spectra.

2. Estimation of main physical parameters, T_{eff}, $log(g)$ and $[Fe/H]$, comparing observations with predictions from models.

3. Estimation of E_{B-V} from 19 correlative ALHAMBRA colors.

However, other factors have to be taken into account to get the most accurate estimation of the possible parameters with this methodology, such us zero point corrections for the synthetic ALHAMBRA photometry of BaSeL models, or checking the dependence of the method on the extinction law used to generate the Q-values and to estimate the color excess of the stars. To test the methodology we use the NGSL primary stars before applying it to the ALHAMBRA field stars. The physical parameters of these stars are obtained from the literature, indeed,

most of them are well known stars and so one can easily find several values of their T_{eff}, $log(g)$, $[Fe/H]$ and color excess; the mean of these parameter distributions is compared with the values estimated in the algorithm. A more detailed description of each step of the algorithm is presented as follows.

4.5.1 Generation of 18 independent Q parameters

Since the optical photometric system is formed by 20 bands, 18 independent correlative Q-parameters can be generated, taking for their definition three correlative bands, instead of taking four different bands, so if we enumerate the ALHAMBRA magnitudes with the 20 different bands, such us, m_i, $i = 1 : 20$, the Q-values are defined as:

$$Q_{ijk} = (m_i - m_j) - \frac{E_{ij}}{E_{jk}}(m_j - m_k), i = 1 : 18, j = i + 1, k = i + 2 \tag{4.14}$$

We generate these values for theoretical spectra from the BaSeL 2.2 library. Since we are not expecting to observe stars with very low metallicity, and among the NGSL stars there are no stars with a metallicity lower than -3, we select BaSeL models with $[Fe/H]$ higher or equal to -3 to optimize the algorithm. Conversely, the same 18 Q-parameters are generated for the 288 NGSL stars. Among these stars there are some hot white dwarfs, so to be able to classify them, white dwarf models have to be introduced into the algorithm; in particular, we generate the Q-values for the models from Holberg & Bergeron (2006).

4.5.2 Estimation of main physical parameters, T_{eff}, $log(g)$ and $[Fe/H]$

Considering the 18-dimensional euclidean space formed by 18 independent Q-parameters for each object, we look for the model that minimizes the euclidean distance between both, the star and the model. The physical parameters of the model (T_{eff}, $log(g)$ and $[Fe/H]$ in the case of BaSeL models, and T_{eff}, $log(g)$ in the case of the white dwarf stars) are directly associated to the star. In this fit, and again with the objective of getting the most accurate estimation possible, we do a minimization of this distance including some weights for the different Q-values, focusing on the different bands that conform the Q-parameters, in particular, giving less weight in the minimization to the $Q_{A366MA394MA425M}$, $Q_{A394MA425MA457M}$, $Q_{A861MA892MA921M}$ and $Q_{A892MA921MA948M}$, that is, the two bluest Qs and the two reddest ones. The reason for giving less significance to these Qs and not others is because the colors (A366M-A394M), (A394M-A425M), (A921M-A948M), and (A921M-A948M) present the highest offsets with the synthetic photometry of the models, which can reach a difference of 10^{-2} magnitudes on average. The weights we give to the different bands are proportional to these offsets. Figure 4.16 shows an example of this fit. The star we try to classify is HD117880. The graphic shows the 18 Q-values of the star in red crosses and of the model in black circles. The values are generated using the Nandy et al. extinction law. The x axis represents just the number of the Q-parameters in increasing order. At the top of the graph the physical parameters of the stars obtained from the literature are shown on the left, and on the right the parameters of the model are found,

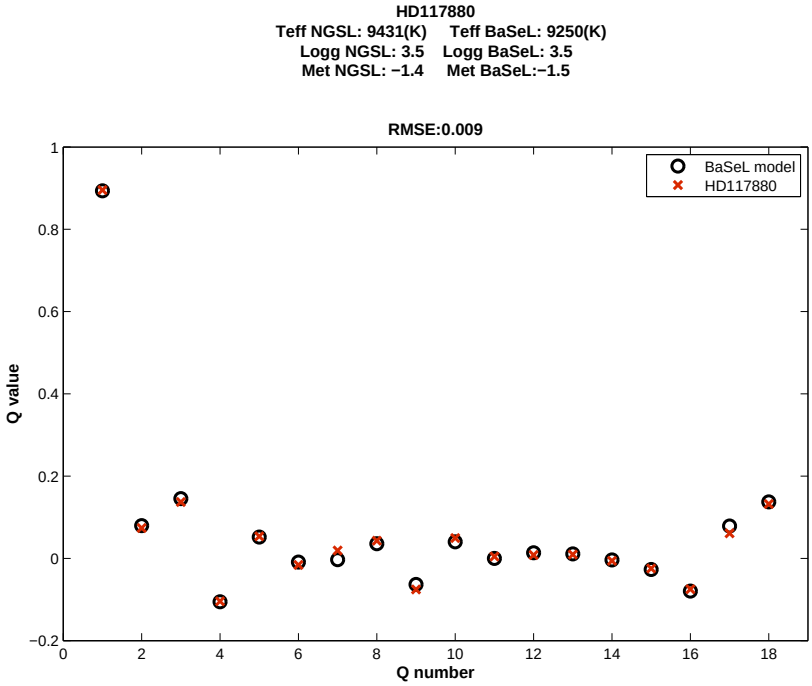

Figure 4.16 Example of Q fit. The graphic shows the 18 Q-values of the star HD117880 with red crosses and the values of the BaSeL model that minimizes the euclidean distance with black circles. At the top of the graphic the physical parameters of the object are shown, on the left the parameters from the literature and on the right the parameters from the QFA. The Root Mean Square Error (RMSE) of the fit is also shown.

that is, the parameters associated to the star by the algorithm. The root mean square error (RMSE) of the fit is also shown.

4.5.3 Estimation of E_{B-V}

For the estimation of E_{B-V} we proceed as follows. From the synthetic photometry of the model, we have 19 unreddened ALHAMBRA colors:

$$m_{0i} - m_{o(i+1)}, i = 1 : 19 \tag{4.15}$$

Thus, with the reddened colors of the star, we can determine the color excess in each band as the difference between the unreddened color of the model and the color of the star:

$$E(m_i - m_{i+1}) = (m_{1i} - m_{1(i+1)}) - (m_{0i} - m_{0(i+1)}), i = 1 : 19 \tag{4.16}$$

We can then generate 19 values of E_{B-V} from each different color excess adopting an extinction law. The E_{B-V} associated to the star would be the median of these 19 values:

$$E_{B-V} = median_i(\alpha_i \cdot E(m_i - m_{i+1})), i = 1 : 19 \tag{4.17}$$

Returning to the former example, Figure 4.17 shows the color fit for the same star, HD117880. The graph plots the 19 values of the colors of the star with red crosses, already dereddened

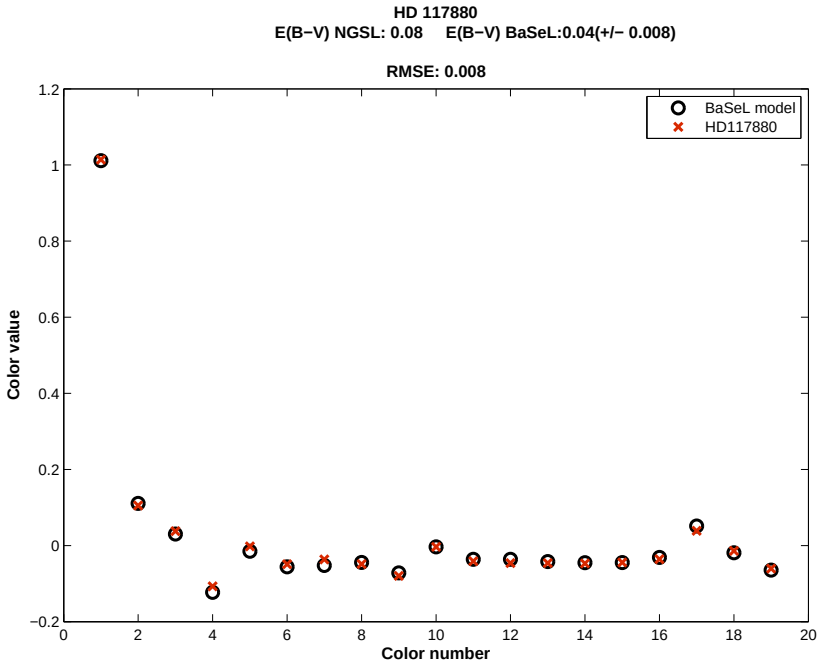

Figure 4.17 Example of color fit. The graphic shows the 19 ALHAMBRA color values of the star HD117880, already dereddened with the E_{B-V} obtained from the method, with red crosses, and the color values of the BaSeL model with black circles. At the top of the graph the color excess from the literature of the object is shown on the left and on the right the E_{B-V} obtained from the fit and its error. The RMSE of the fit is also shown.

with the color excess obtained as explained before, and the unreddened 19 colors of the model with black circles. At the top, we can see the value of E_{B-V} compiled from the literature, and the value obtained with our method plus the error of it, that is the MAD of the distribution of color excesses divided by the root square of the number of elements (19 in this case). Again, the RMSE of this fit is shown.

4.5.4 Zero point corrections

In order to improve the parameter estimation with this methodology, we correct synthetic photometry of the theoretical spectra from BaSeL with the synthetic photometry of our primary standard stars. To apply the offsets, we execute the algorithm on the 288 NGSL stars and BaSeL models, and once we have the results we select the stars with a RMSE in the Q fit less or equal to 0.03, rejecting also the white dwarfs, resulting in 216 stars on average, depending on the extinction law used in the algorithm (in particular 217 stars are selected when using Nandy et al. 1975, 214 stars with Cardelli et al. 1989 and 218 with the Fitzpatrick 1999 extinction law). With each of these stars and their model associated in the algorithm, and for each one of the 19 colors, we can determine the differences between the colors of both, and the zero point corrections will be the mean of these differences. The parameter estimation with the algorithm is more accurate in most cases with these corrections, in the sense of getting lower average

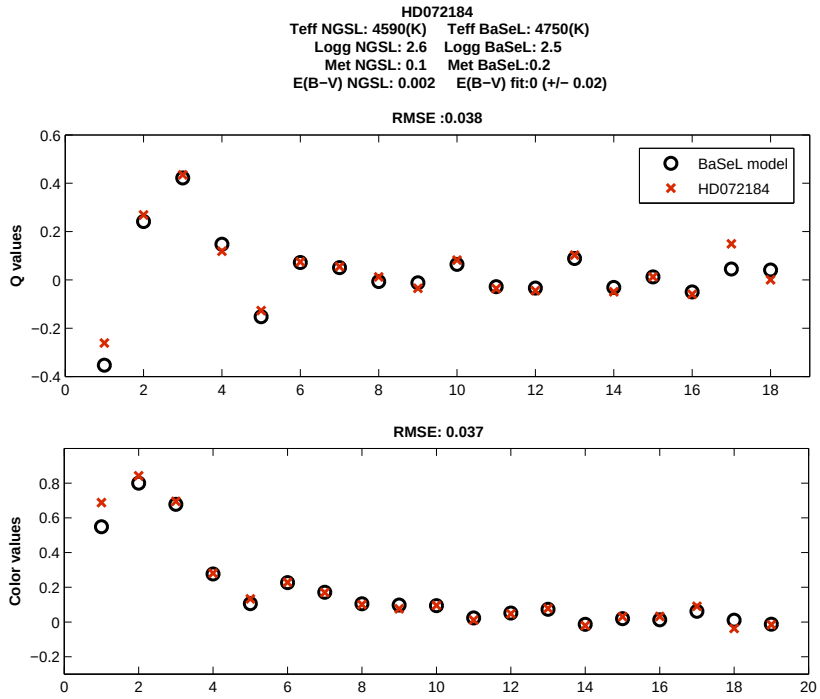

Figure 4.18 Example of Q fit (plot at the top) and color fit (plot at the bottom) of a cold star of spectral type K. The graphics are as previous plots. The RMSE of both fits are higher comparing with the previous example, although the spectral classification of the star seems to be precise; the increment of the RMSEs is due to the complexity of the distribution of Q and color values.

RMSE of the fits for all the different spectral types; and even though, in some cases, there is a better approximation of the physical parameters compared with those from the literature, and never worse than before correcting, especially, and as a direct consequence, there are better estimations of the color excess. Particularly of interest for us, we also manage to obtain lower RMSE in the fits of the coldest stars, G- to M-type stars, which are the types of stars that we expect to observe in the ALHAMBRA fields. The RMSE of the fits gives information of how good the estimation of the parameters is, that at the same time depends on how dense the grid of models in the library used is. These RMSEs are also related with the spectral type of the star, in such a way that cold stars will have on average higher RMSEs of the fits because they have more complex Q distribution or SED, and the range of values of Qs or colors is wider than in the hottest stars (see Figure 4.18).

4.5.5 Extinction law

As we checked in section 4.1, the Q-parameters are very sensitive to the extinction law that is used in their definition, so it was appropriate to test this methodology with different extinction laws and see how the results varied in each case. From the former study of the Q,Q diagrams, we saw that Nandy best fitted with our data, followed by Cardelli and Fitzpatrick. We therefore checked the validity of the methodology with these three extinction laws. The results are shown in Table 4.3 with several statistical indicators; the color excesses determined in the algorithm

are obtained as the median of the 19 values of E_{B-V} that can be attained from the color fit, and so the MAD of this distribution can also be calculated. The mean of all these 288 MADs is shown in the first row and its standard deviation in the second. Focusing on the mean, we can see that Nandy et al. and Cardelli et al. have a lower value on this estimator, although the difference with Fitzpatrick is not significant. This parameter gives an estimate of the internal precision of the extinction law in the estimation of the color excess. The third row is the mean of the differences in absolute values between the color excesses compiled from the literature, and the color excesses obtained in the algorithm; here, Nandy shows the lowest value with 0.52 magnitudes. The next row is the mean of the same differences but now without absolute values. Rows 5 and 6 are equal to the two previous ones but applied to effective temperature, and the next shows the relative differences between T_{eff}s in absolute values. The following rows are the means of differences with and without absolute values applied to $log(g)$ and $[Fe/H]$. There are not significant enough differences in any of the indicators to declare that one law is more appropriate than the others in this particular case, so we can conclude that any of the three extinction laws can be adopted on this algorithm and with our data. Table 4.4 shows rows 4, 6, 8, 10 of Table 4.3 for hot, intermediate and cold stars, separately. Below, the results of the QFA for the NGSL stars are shown in more detail for the Nandy et al. extinction law.

Results of Q Fit Algorithm for 288 NGSL stars and with the Nandy extinction law

Figures from 4.19 to 4.23 show the residuals of T_{eff}, $log(g)$, $[Fe/H]$ and E_{B-V} respectively, with different kinds of plots. The parameter that presents most dispersion is the metallicity, as can be appreciated in Fig. 4.22, and in Figure 4.21 it can be appreciated that the greatest dispersion is present in the estimations for hot stars ($log(T_{eff}) > 3.8$). On the other hand, the different estimations of $[Fe/H]$ found for a single star in the several catalogs found in the literature have, in most cases, a range of values that is also quite wide. Figure 4.19 shows the residuals of the temperature estimations. Here we can not see any systematic structure dependent on T_{eff} in any temperature range, and the residuals are within a 7% (see Table 4.3).

In several stars we can find typical cases of degeneracy in the spectral classification. For instance, there is a tendency of overestimating the color excess for cold spectral types, and for hot stars the estimations are on average underestimated; intermediate stars have the most accurate estimation of the color excess. In cold K-to M-type stars, there are several stars with $log(g)$ wrongly estimated although the rest of the parameters are corrected, and normally it happens that the main sequence star is fitted with a giant star. An example of this is shown in Figure 4.24 with a M2.0V star. In O-, B- and hot A-type stars, however, the degeneracy that can be found is in metallicity, such that a solar metallicity star is fitted with a very low metallicity hot star, as in the case of HD027295 (Figure 4.25) which is fitted in the algorithm with a B star with $[Fe/H]$=-3 while in the literature it has a $[Fe/H]$=-0.6. The photometry of these stars does not have enough information to be discriminating on metallicity, as is shown in Figure 4.26 where the 18 Q values are shown for the star HD004727 in red, together with the same values of two BaSeL models in black and light blue. The black line corresponds to the SED

Table 4.3 Statistical indicators of the QFA results, applied to the 288 NGSL stars and with BaSeL models corrected by photometric zero points, and three different extinction laws: Nandy et al. (1975), Cardelli et al. (1989) and Fitzpatrick(1999).

	Nandy	Cardelli	Fitzpatrick
$Mean(MAD(E_{B-V})/\sqrt{n})$ [1]	0.018	0.018	0.019
$Std(MAD(E_{B-V})/\sqrt{n})$ [2]	0.016	0.016	0.016
$\lvert\overline{\delta(E_{B-V})}\rvert$	0.052±0.004	0.057±0.005	0.055±0.005
$\overline{\delta(E_{B-V})}$	-0.024±0.005	-0.030±0.006	-0.029±0.006
$\lvert\overline{\delta(T_{eff})}\rvert$	564.51±81	592.79±81	534.81±71
$\overline{\delta(T_{eff})}$	-434.18±84	-401.38±85	-374.73±74
$\lvert\overline{\delta(T_{eff})/T_{eff}}\rvert$	0.069±0.005	0.072±0.005	0.068±0.006
$\lvert\overline{\delta(log(g)))}\rvert$	0.50±0.03	0.49±0.03	0.49±0.03
$\overline{\delta(log(g)))}$	0.007±0.04	-0.02±0.04	0.01±0.04
$\lvert\overline{\delta([Fe/H]))}\rvert$	0.49±0.03	0.48±0.03	0.50±0.03
$\overline{\delta([Fe/H]))}$	-0.14±0.04	-0.13±0.04	-0.13±0.04

1,2. n is the number of elements in the distribution of color excesses, in our case n=19

of the model that minimizes the euclidean distance with the star, and the blue one corresponds to the second closest model (this fit is done with BaSeL spectra without corrections). Although the T_{eff} and $log(g)$ are similar or even the same, the metallicity of these two models are quite different in spite of the small differences that can be found between them in the Qs distribution. Sometimes, the degeneracies are in all parameters (see Figure 4.27).

For a more detailed idea of the results, Table A.9 in the Appendix shows the physical parameters of the 288 stars with their spectral type and luminosity class. For each parameter, the estimation compiled from the literature is presented followed by the estimation with the QFA; in the case of the effective temperature it is also shown the temperatures obtained by the color parametric equations, with unredden colors by the color excesses obtained in the QFA; if any of the parameters has not been found it will be written "Nan". The estimations of the E_{B-V} appears with their MADs, which gives a measure of the precision of the final color excess. The spectral types and luminosity classes of the stars are obtained from the SIMBAD Astronomical Database.

Table 4.4 Statistical indicators of the QFA results, applied to the 288 NGSL stars and with BaSeL models corrected by photometric zero points, and three different extinction laws, Nandy et al. (1975), Cardelli et al. (1989) and Fitzpatrick(1999), for hot, intermediate and cold stars. Errors are standard deviations of the differences divided by the square root of the number of elements.

Nandy			
	O- to B-	A- to F-	G- to M-
$\overline{\delta(E_{B-V})}$	0.047±0.03	-0.011 ±0.007	-0.040±0.006
$\overline{\delta(T_{eff}))}$	-2304±906	-254.5±67	-274.8±25
$\overline{\delta(log(g)))}$	-0.38±0.13	-0.14±0.05	0.14±0.06
$\overline{\delta(Fe/H))}$	0.44±0.27	0.17±0.08	-0.36±0.04
Cardelli			
	O- to B-	A- to F-	G- to M-
$\overline{\delta(E_{B-V})}$	0.049±0.03	-0.011±0.007	-0.051±0.008
$\overline{\delta(T_{eff}))}$	-1631±954	-283.6±68	-296.5±35
$\overline{\delta(log(g)))}$	-0.26±0.15	-0.14±0.04	0.08±0.06
$\overline{\delta(Fe/H))}$	0.42±0.26	0.24±0.08	-0.37±0.03
Fitzpatrick			
	O- to B-	A- to F-	G- to M-
$\overline{\delta(E_{B-V})}$	0.043±0.03	-0.009±0.007	-0.048±0.008
$\overline{\delta(T_{eff}))}$	-1528±842	-257.4±69	-286.4±37
$\overline{\delta(log(g)))}$	-0.29±0.15	-0.12±0.04	0.12±0.06
$\overline{\delta(Fe/H))}$	0.39±0.25	0.22±0.08	-0.36±0.03

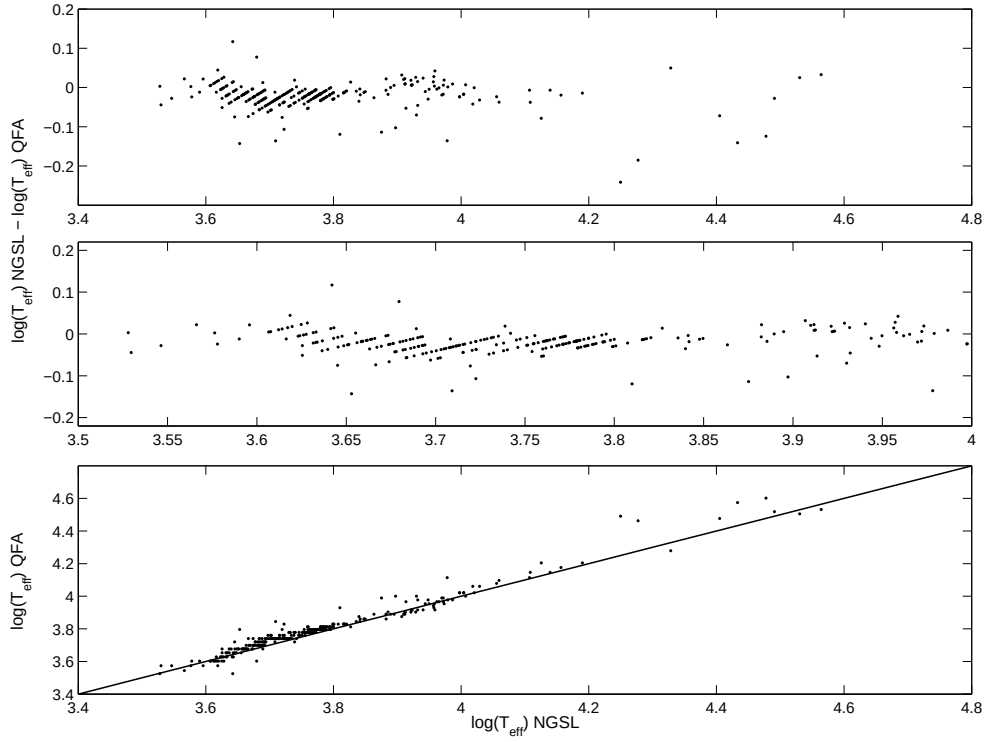

Figure 4.19 Results of the QFA with the Nandy et al. extinction law for effective temperature. The top graph shows the relative differences vs. the effective temperatures from the literature. The middle graph is the same plot but only for stars with $T_{eff} < 10,000$K. The bottom graph represents the effective temperatures from the QFA vs. the temperatures from the literature.

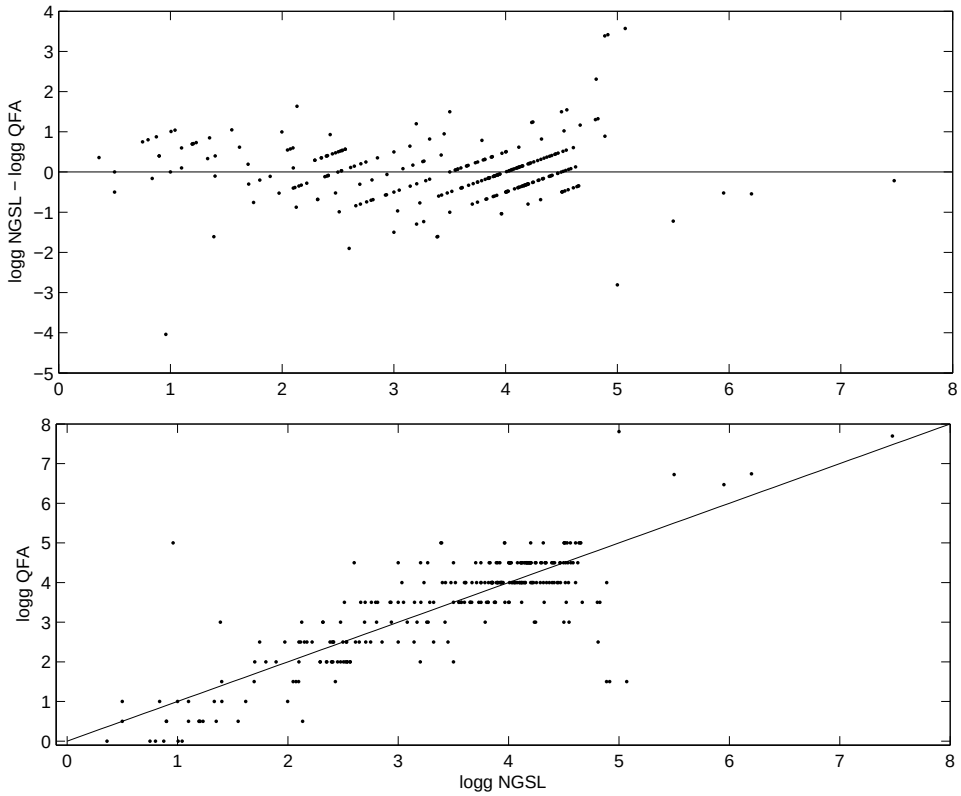

Figure 4.20 $log(g)$ residuals from the Q Fit Algorithm with the Nandy extinction law.

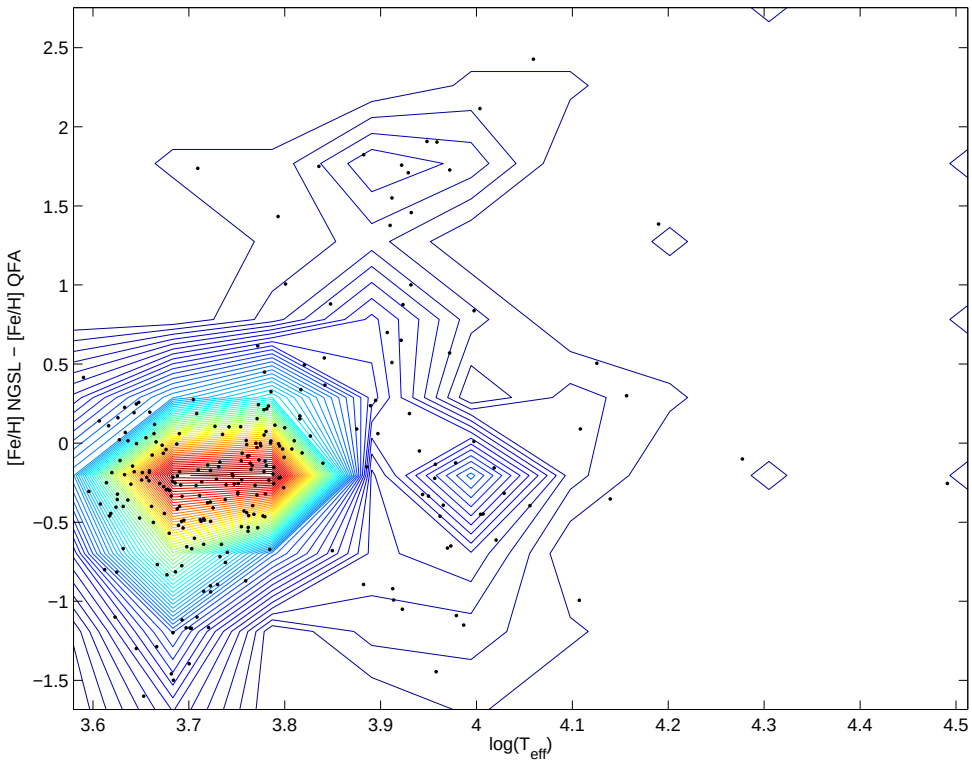

Figure 4.21 Contour plot of QFA $[Fe/H]$ vs. $log(T_{eff})$ from the literature, from the algorithm with the Nandy extinction law.

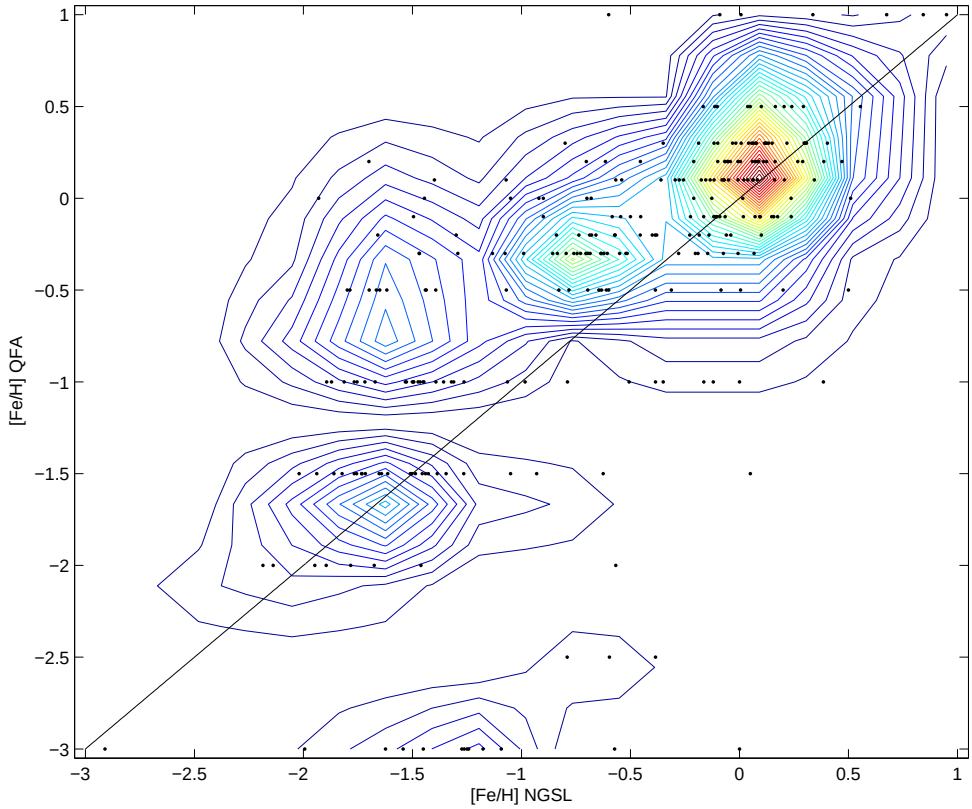

Figure 4.22 Contour plot of QFA $[Fe/H]$ vs. $[Fe/H]$ from the literature, from the algorithm with the Nandy extinction law.

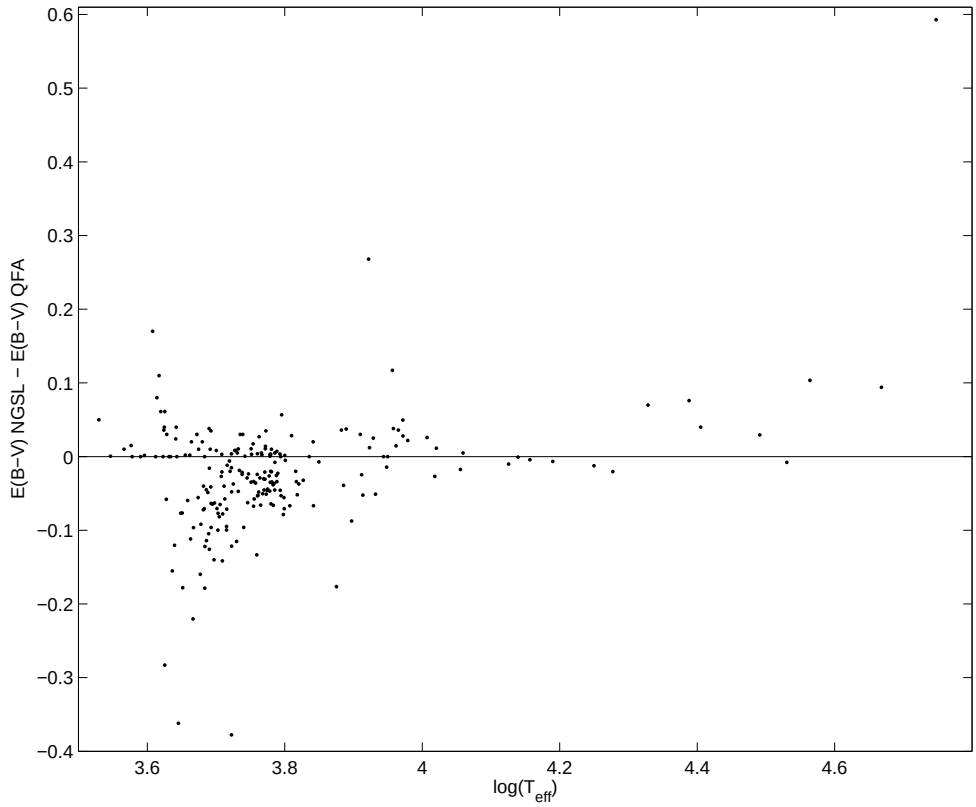

Figure 4.23 E_{B-V} residuals vs. $log(T_{eff})$ from the QFA with the Nandy extinction law.

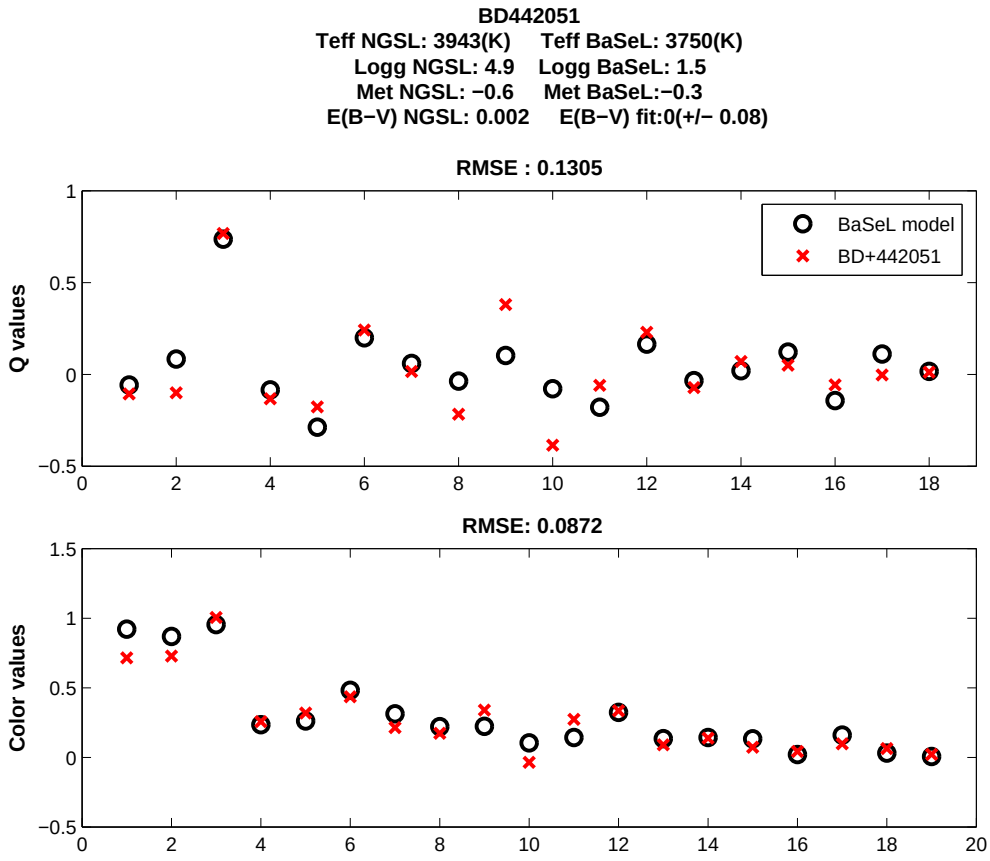

Figure 4.24 Example of $log(g)$ degeneracy in the QFA with the NGSL stars. The graphic shows the 18 Q-values (on top) and 19 colors (at the bottom) of the star BD+442051 with red crosses, and the values of the model associated from BaSeL with black circles. At the top of the graph the physical parameters of the object are shown, on the left the parameters from the literature and on the right the parameters from the BaSeL model.

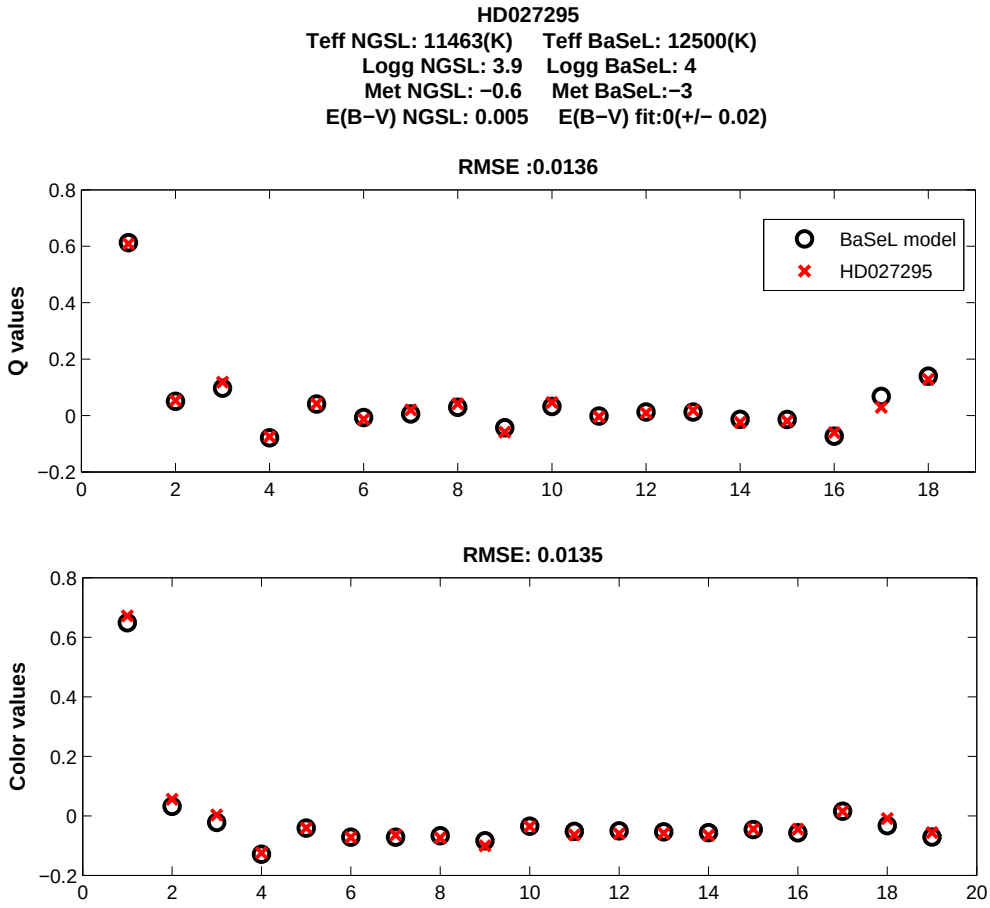

Figure 4.25 Example of $[Fe/H]$ degeneracy in the QFA with the NGSL stars. The graphic shows the 18 Q-values (on top) and 19 colors (at the bottom) of the star HD027295 with red crosses and the values of the model associated from BaSeL with black circles. At the top of the graph the physical parameters of the object are shown, on the left the parameters from the literature and on the right the parameters from the BaSeL model.

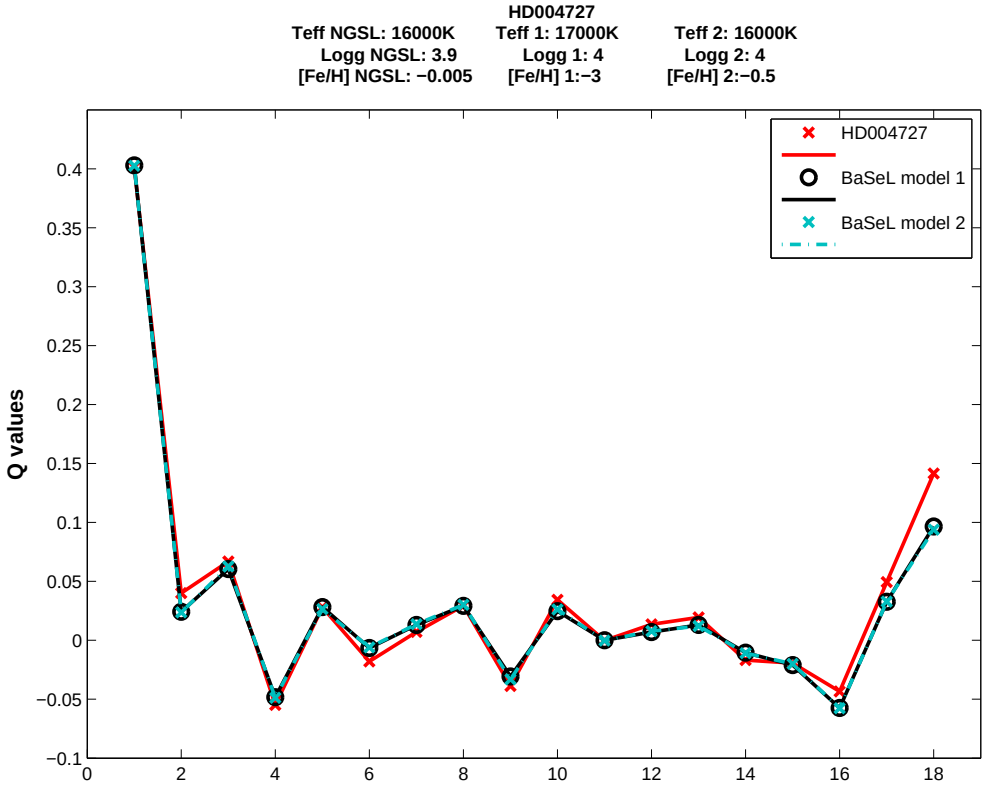

Figure 4.26 Example of $[Fe/H]$ degeneracy in the QFA with the NGSL stars. The graphic shows the 18 Q-values of the star HD002747 in red, the values of the first closest model in black, and the values of the second closest model in light blue. At the top of the graph the main physical parameters of the object are shown, on the left the parameters from the literature and on the right the parameters from the BaSeL models.

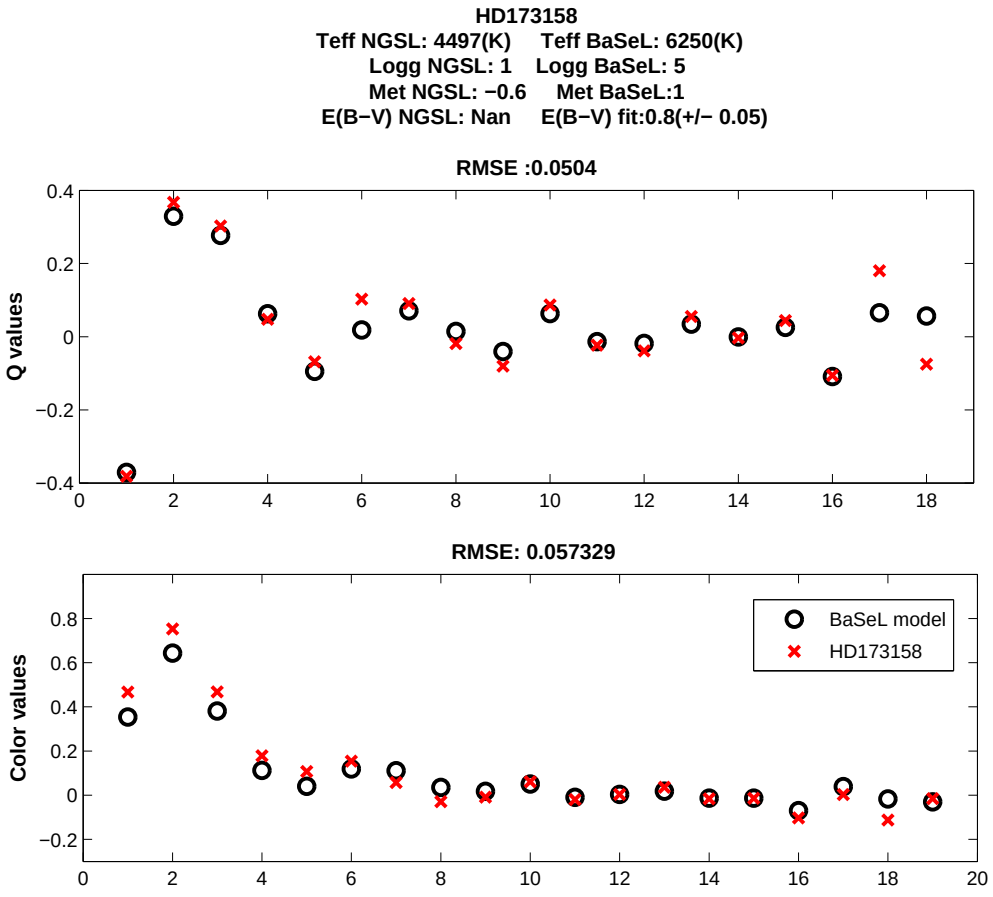

Figure 4.27 Example of degeneracy in the QFA with the NGSL stars. The graphic shows the 18 Q-values (on top) and 19 colors (at the bottom) of the star HD173158 with red crosses and the values of the model associated from BaSeL with black circles. At the top of the graph the physical parameters of the object are shown, on the left the parameters from the literature and on the right the parameters from the BaSeL model.

4.5.6 QFA and the stars in the ALHAMBRA survey. Preliminary Results

Using the Nandy et al. extinction law, the Q Fit Algorithm has been applied to the ALHAMBRA field point-like objects with photometric errors in the 20 bands lower than 0.1 magnitudes. The fits have been obtained in the same way as with the NGSL stars without taking into account the photometric errors. The only factor changed in the methodology has been the estimation of the color excesses, being calculated as the median of the values of E_{B-V} from the 15 intermediate colors, rejecting the color excesses obtained from the colors A366M-A394M, A394M-A425M, A892M-A921M, A921M-AA948M, since statistically they have higher errors than the rest of the colors and it has been checked that the color excesses obtained taking into account the 19 colors have more dispersion than without them. Among the field point-like objects there could be distant QSOs, so, in order to be able to detect them among the real stars, some QSO models from the SWIRE template library (see subsection 4.1.2) have been added to the BaSeL stellar models and the white dwarfs templates.

Finally, 288 objects have been fitted as white dwarfs, and 165 objects are classified as QSOs. Among the white dwarfs, 152 have temperatures below 10,000K. Figures 4.28, 4.31, 4.32 and 4.34 show histograms for the four parameters. The median and mean of the different astrophysical parameters estimated are corrected by the biases that appear with the NGSL stars in the case of the Nandy et al. extinction law (Table 4.3), and they are shown in the table below:

$Median(E_{B-V})$	0.037±0.004[1]
$Mean(E_{B-V})$	0.142±0.005[2]
$Median(T_{eff})$	5316±84[1]
$Mean(T_{eff})$	7440±139[2]
$Median(log(g))$	4.5±0.04[1]
$Mean(log(g))$	4.12±0.05[2]
$Median([Fe/H])$	-0.64±0.02[1]
$Mean([Fe/H])$	-0.79±0.02[2]

1. MAD divided by the square root of the number of elements

2. Standard deviation divided by the square root of the number of elements

As can be seen in the table, the average of the objects found in this sample are main sequence cold stars with low metallicity, and also low values of color excess. Figure 4.28 shows the histogram of the estimated effective temperatures. The most probable value is clearly situated over 5000-6000K. However there is a subset of about 400 stars in the sample with temperature values greater than 10,000K, not all of them classified as hot white dwarfs as can be appreciated in Figure 4.29, where temperature is represented with $log(g)$ in a bivariate histogram. These such hot stars are not expected to be observed in the ALHAMBRA survey, since most stars in the halo are late-type stars. We could consider then that these stars are not correctly classified, indeed, we think these stars could be hot white dwarfs classified in

the algorithm as O-type stars. Figure 4.30 shows the Q spectrum of the star HD048279 in red, the spectrum of a O-type star model from BaSeL 2.2 ($T_{eff} = 35,000K$, $log(g) = 5$ and $[Fe/H] = -1$) in black, and the spectrum of a DA model in blue with $T_{eff} = 60,000K$ and $log(g) = 6.24$. The NGSL star is correctly classified as an O-type star in the QFA, but the blue and the black spectra are very similar (except in the two first Qs) and in the case the star has higher photometric errors the fit can be mistaken, and this case can be generalized.

Figure 4.32 shows the histogram of $[Fe/H]$ values. The distribution is centered in values of metallicity of 0 and -0.5. There are around 200 stars with very low metallicities ($[Fe/H] = -2.5, -3$) the majority of them being G-type stars as can be observed in the bivariate histogram T_{eff}, $[Fe/H]$ showed in Figure 4.33.

Figure 4.34 represents a histogram of the color excesses obtained in the algorithm. The distribution is clearly centered in 0, although there is a subset of stars with $E_{B-V} > 0.2$. These stars have overestimated values of this parameter since the ALHAMBRA fields have low extinction. These objects could have in the fit a case of degeneracy such as the explained with the NGSL stars, where a late spectral type is classified as a hotter star with a high value of color excess.

To see whether this medians of the parameters are close to the expected values for the ALHAMBRA field stars we perform a stellar population simulation with the models built by Robin et al. (2003). The ALHAMBRA star sample is spread out over 7 different ALHAMBRA fields, so we consider the average values of longitude and latitude for these ($l = 140°$, $b = 49°$), and a limit magnitude of V=19 to build the model (the central value of the magnitude A551M in the sample is 19). We consider all the stellar objects that can be found at those coordinates, and a distance interval from 0 up to 50 kpc. In this way we obtain some statistical indicators of the main characteristics of the stellar population this model assumes to have, among them the median of the four main physical parameters:

$Median(E_{B-V})$	0.026
$Median(T_{eff})$	5012
$Median(log(g))$	4.61
$Median([Fe/H])$	-0.38

Compared with the results of this stellar population model, the average values of the main physical properties of the ALHAMBRA stars obtained by the Q Fit algorithm seem really to be in keeping with the expected values in these fields.

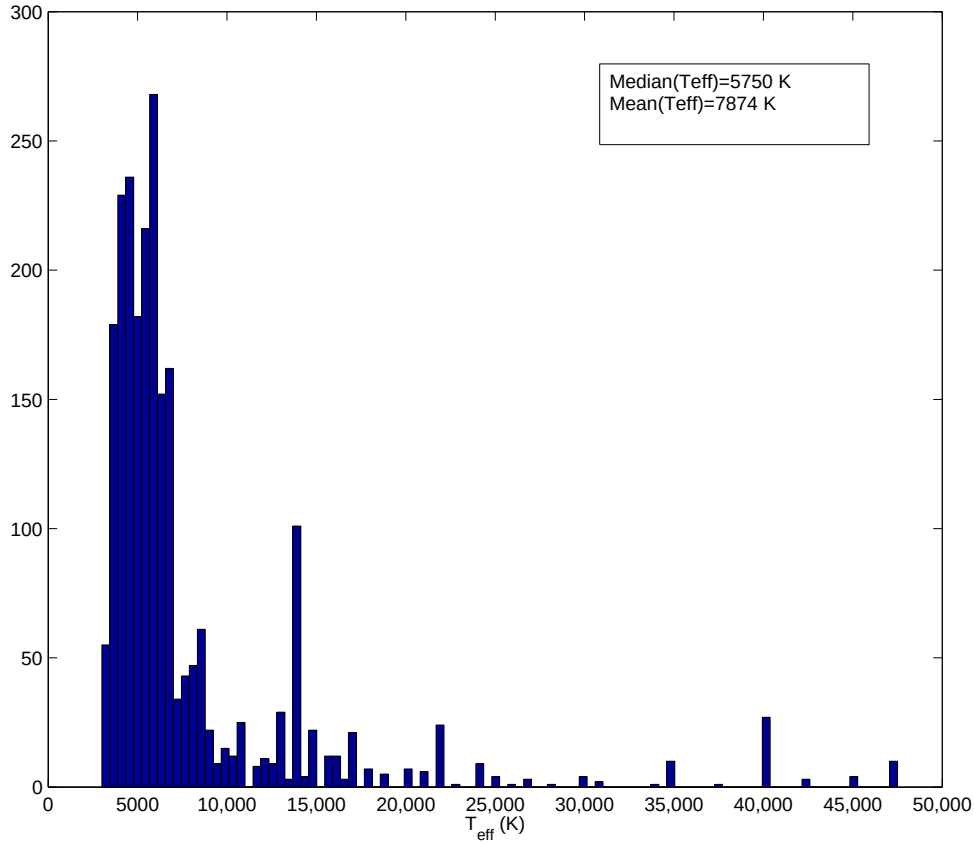

Figure 4.28 Frequency histogram of the T_{eff} of the ALHAMBRA field stars, with photometric errors less than 0.1 magnitudes in the 20 magnitudes, obtained by the QFA. The mean and median of the color excesses are shown in a text box.

Anyway, this is a crude way to have a preliminary conclusion of the object we find in the ALHAMBRA fields. The QFA can be adapted to objects with higher photometric errors, and it could be interesting to analyze the results it would provide in the cases the objects do not have photometric measures of the 20 bands. Moreover, it could also be applied to determine one specific astrophysical parameter, studying a priori which colors have the most significant information about it, and giving more weight to these bands in the fits. This Ph.D. Thesis does not delve deeper into this algorithm, but this is considered a future work of special importance.

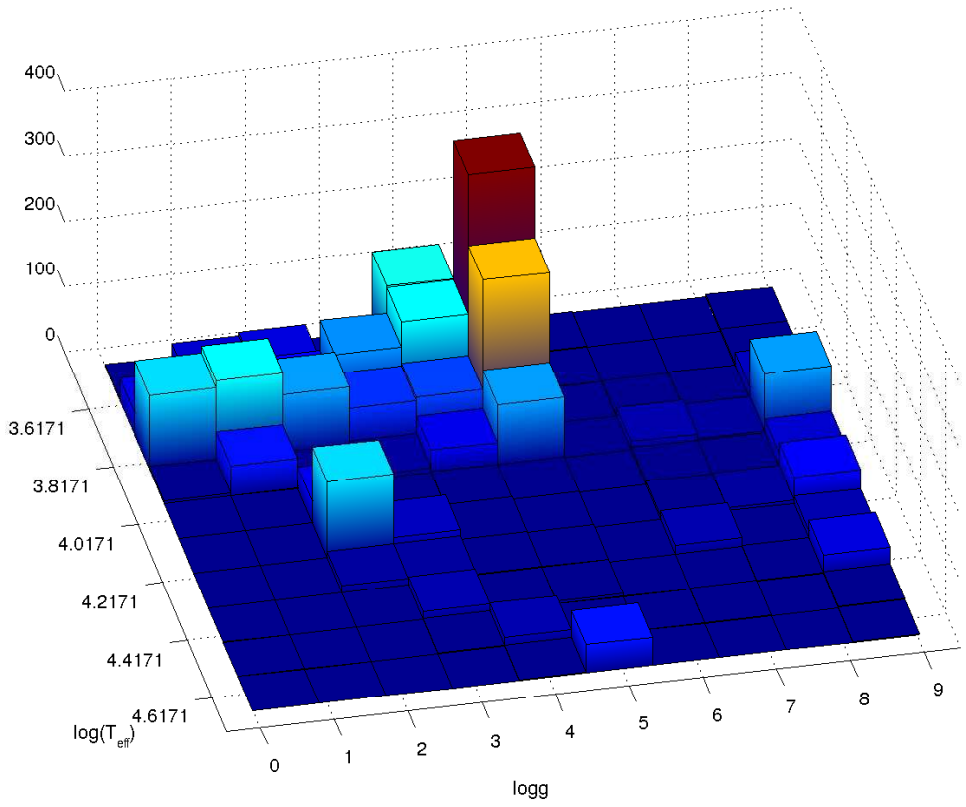

Figure 4.29 Bivariate histogram of the T_{eff} and $log(g)$ of the ALHAMBRA field stars, with photometric errors less than 0.1 magnitudes in the 20 magnitudes, obtained by the QFA.

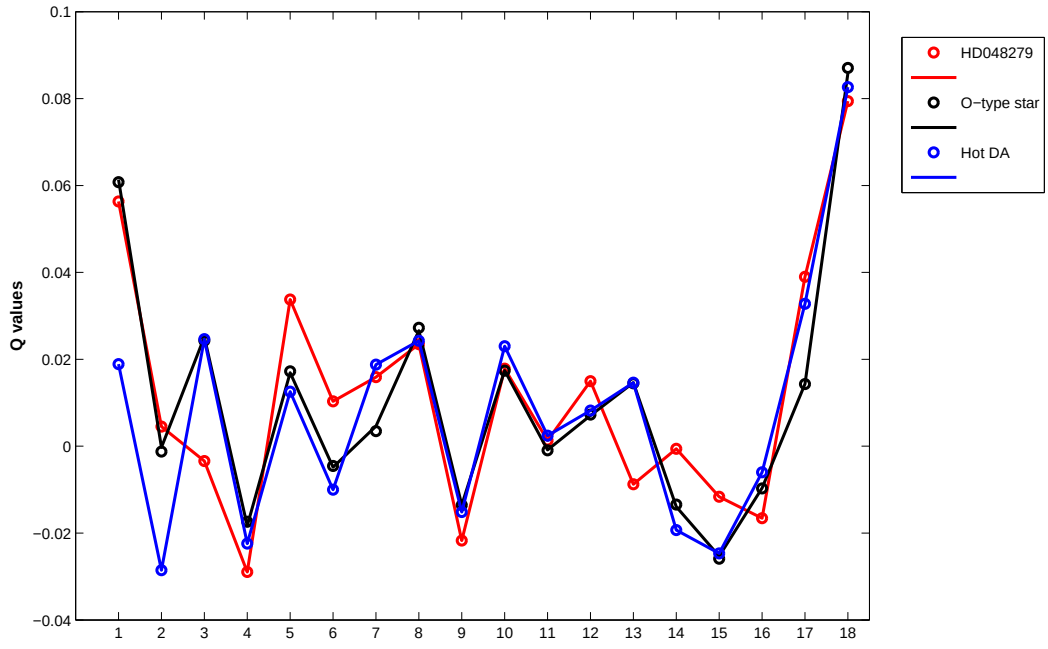

Figure 4.30 The graphic shows the 18 Q-values of the star HD048279 in red, the values of a O-type star model in black, and the values of a hot DA white dwarf in blue.

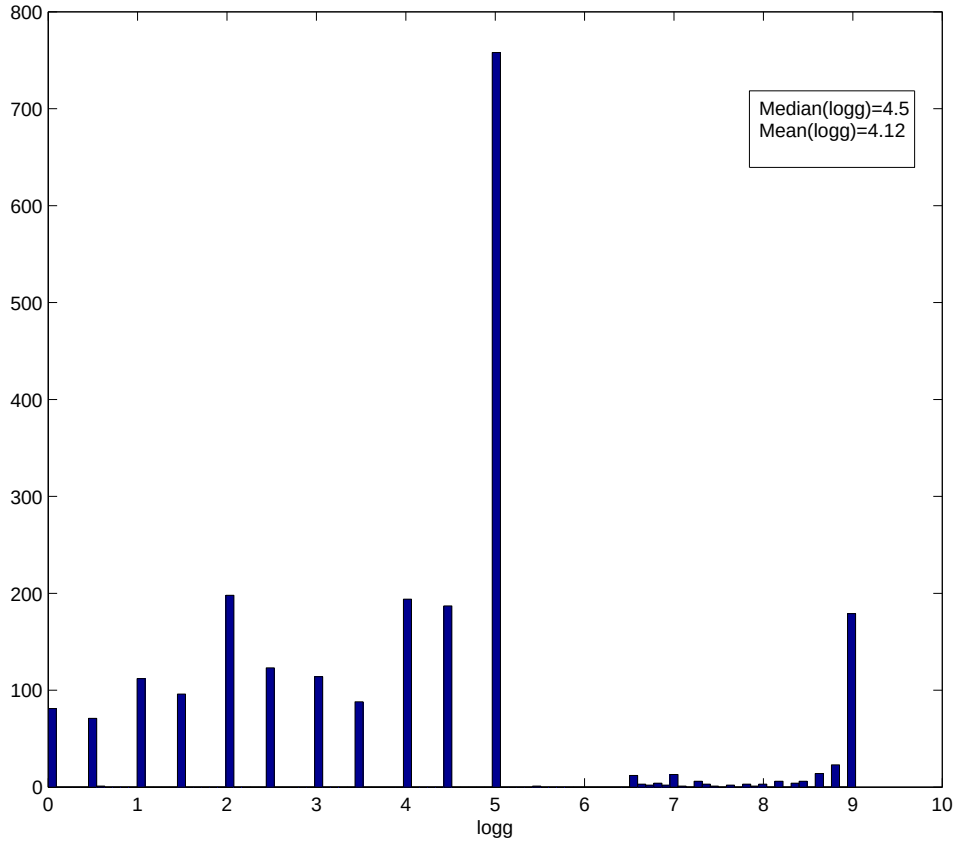

Figure 4.31 Frequency histogram of the $log(g)$ of the ALHAMBRA field stars, with photometric errors less than 0.1 magnitudes in the 20 magnitudes, obtained by the QFA. The mean and median of the color excesses are shown in a text box.

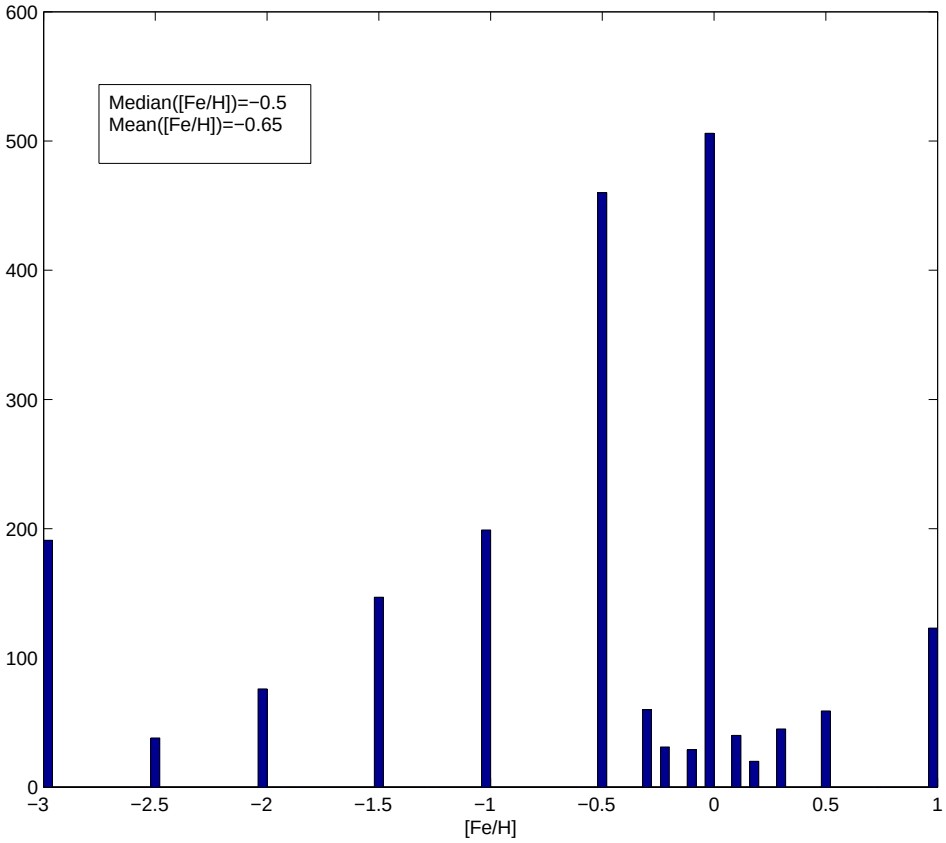

Figure 4.32 Frequency histogram of the $[Fe/H]$ of the ALHAMBRA field stars, with photometric errors less than 0.1 magnitudes in the 20 magnitudes, obtained by the QFA. The mean and median of the color excesses are shown in a text box.

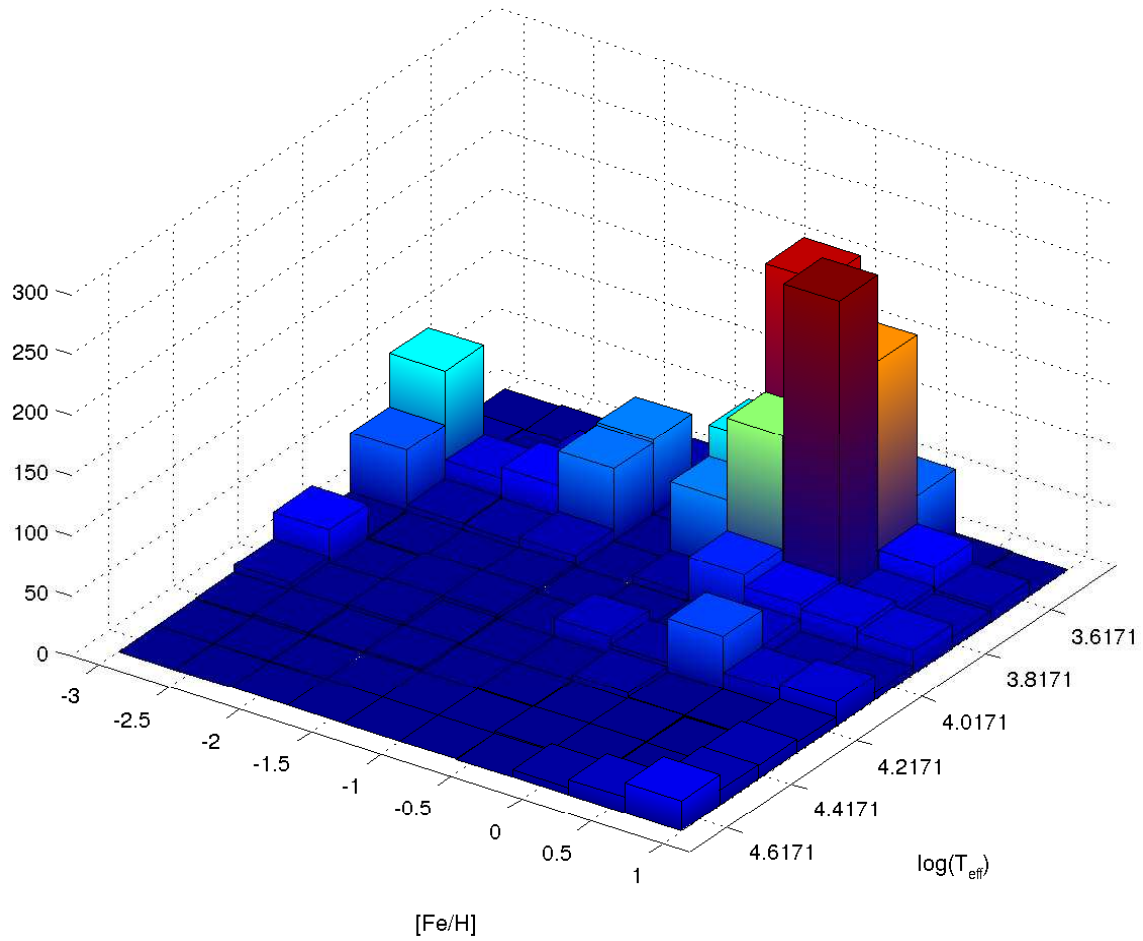

Figure 4.33 Bivariate histogram of the T_{eff} and $[Fe/H]$ of the ALHAMBRA field stars, with photometric errors less than 0.1 magnitudes in the 20 magnitudes, obtained by the QFA.

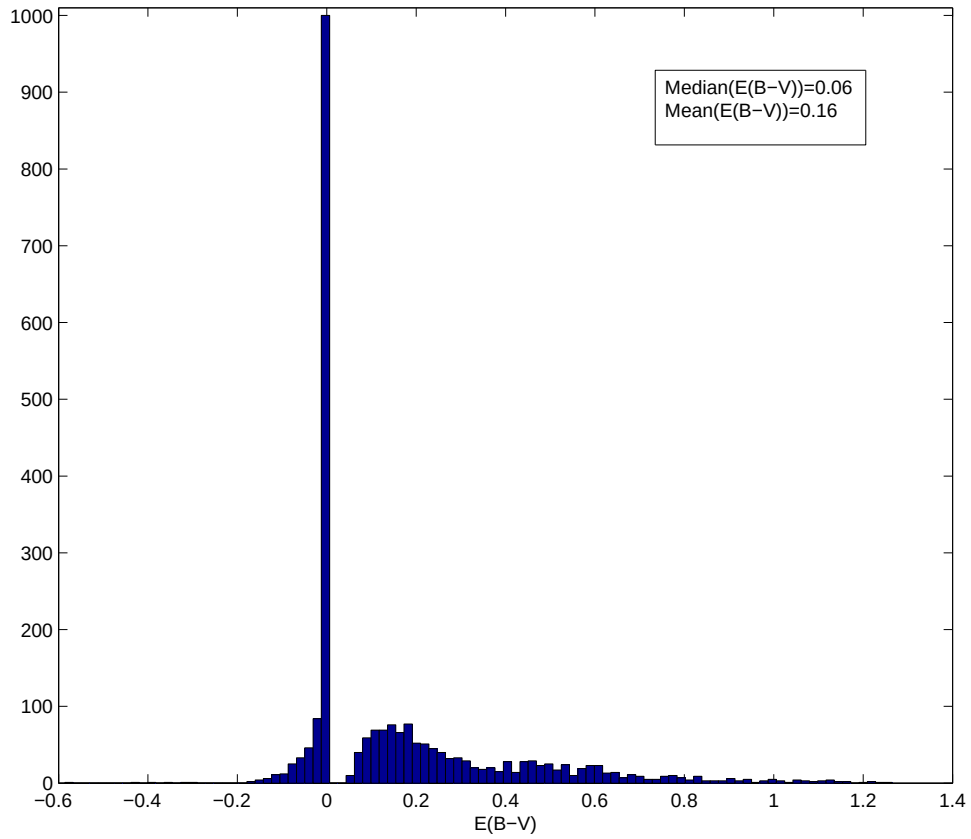

Figure 4.34 Frequency histogram of the E_{B-V} of the ALHAMBRA field stars, with photometric errors less than 0.1 magnitudes in the 20 magnitudes, obtained by the QFA. The mean and median of the color excesses are shown in a text box.

Bibliography

Balona, L. A. 1984, MNRAS, 211, 973

Balona, L. A. 1994, MNRAS, 268, 119

Berta, S., Fritz, J., Franceschini, A., Bressan, A., & Pernechele, C. 2003, A&A, 403, 119

Berta, S. 2005, Ph.D. Thesis,

B. E. Boser, I. Guyon, and V. Vapnik. A training algorithm for optimal margin classifiers. In *Proceedings of the Fifth Annual Workshop on Computational Learning Theory*, pages 144-152. ACM Press, 1992.

Cardelli, J. A., Clayton, G. C., & Mathis, J. S. 1989, ApJ, 345, 245

C. Cortes and V. Vapnik. Support-vector network. *Machine Learning*, 20:273-297, 1995.

Crawford, D. L. 1966, Spectral Classification and Multicolour Photometry, 24, 170

Fitzpatrick, E. L. 1999, PASP, 111, 63

Gregg, M. D., Lacy, M., White, R. L., et al. 2002, ApJ, 564, 133

Holberg, J. B., & Bergeron, P. 2006, AJ, 132, 1221

Johnson, H. L., & Morgan, W. W. 1953, ApJ, 117, 313

Lejeune, T., Cuisinier, F., & Buser, R. 1998, A&AS, 130, 65

Matute, I., et al. 2011, A&A, in referee

McCall, M. L. 1982, University of Texas Publications in Astronomy, 20, 1

McCall, M. L. 2004, AJ, 128, 2144

Nandy, K., Thompson, G. I., Jamar, C., Monfils, A., & Wilson, R. 1975, A&A, 44, 195

O'Donnell, J. E. 1994, ApJ, 422, 158

Polletta, M., Tajer, M., Maraschi, L., et al. 2007, ApJ, 663, 81

Prevot, M. L., Lequeux, J., Prevot, L., Maurice, E., & Rocca-Volmerange, B. 1984, A&A, 132, 389

Robin, A. C., Reylé, C., Derrière, S., & Picaud, S. 2003, A&A, 409, 523

Savage, B. D., & Mathis, J. S. 1979, ARA&A, 17, 73

Schild, R. E. 1977, AJ, 82, 337

Sesar, B., Ivezić, Ž., Lupton, R. H., et al. 2007, AJ, 134, 2236

Strömgren, B. 1951, AJ, 56, 142

V.N. Vapnik. Statistical Learning Theory. John Wiley & Sons, Inc, 1998

5

Conclusions

In this thesis we present a characterization of the optical range of the ALHAMBRA photometric system, and we analyze its abilities in stellar spectral classification. In the following we summarize the main conclusions obtained:

1. The four filter sets of the ALHAMBRA photometric system have been characterized with the response curves obtained from the product of the transmission of the filters, detectors and atmospheric extinction, and some first and second order moments of same response functions.

2. The variations in magnitude of these four sets of filters have been analyzed through synthetic photometry of a subset of the primary standard stars of the system.

3. The set of primary standard stars has been presented together with the magnitude system anchored to the ALHAMBRA system, which also represents part of the characterization of the photometric system.

4. Of the four filter+detector systems, that at position 3 of the instrument (LAICA) has been chosen to be the standard ALHAMBRA photometric system; that is, the 20 filters set associated to CCD3.

5. Two different strategies have been developed for the photometric calibration of the system. Between both, the methodology finally chosen is the one which avoids systematic errors and is robust enough to be applied to all kind of astronomical objects in the ALHAMBRA survey, obtaining zero points for the ALHAMBRA fields with errors lower than a few hundredths of magnitude.

6. Transformation equations between the ALHAMBRA photometry and the Sloan Digital Sky Survey (SDSS) filters and Gaia photometric system are elaborated using equivalent strategies.

7. The analysis of the abilities of the ALHAMBRA optical photometric system on stellar spectral classification and the determination of the main physical parameters has been tackled from two points of view:

   - The use of a set of colors or lineal combinations of them that characterize the representative physical properties of well-defined stellar groups.

   - By the direct comparison of the ALHAMBRA photometry and synthetic spectra derived from evolutionary atmospheric models.

8. In this thesis, for the first time the comparison of observed Q "spectra" with the same type of theoretical synthetic spectra is proposed in order to obtain estimates of the main physical stellar parameters (T_{eff}, $log(g)$, $[Fe/H]$ y E_{B-V}) for all kinds of stellar objects that can be found in the ALHAMBRA fields. This methodology is based on the idea that the observations with this filter system can be considered very low resolution spectroscopy.

9. We analyze and compare the results from the different methods of stellar parametrization applied to a sample of standard stars of the system.

10. The Q Fit Algorithm is also applied to a subset of the ALHAMBRA field stars.

11. Apart from obtaining these clear objectives, during the four years I have increased my training and knowledge in the basic concepts of stellar radiation, the more recent photometric and spectrophotometric techniques, the models of stellar evolution, and the theory and experience of the statistical classification as well as the manipulation of large databases.

    I have had the opportunity of working with the Gaia group led by Carme Jordi at the UB (Universidad de Barcelona) and with the Gaia group led by Coryn Bailer-Jones at the Max Planck Institute of Astronomy (MPIA) in Heidelberg (Germany), having taken great advantage of both opportunities.

    I have actively participated in the scientific activities of the ALHAMBRA group and currently I am involved in the development of a new sky survey project, the J-PAU survey, that is an extension of the ALHAMBRA project, and which is being carried out by CEFCA (Centros de Estudios de Física del Cosmos de Aragón) in Teruel. I have also been a member of the "Stellar System Group" in the Instituto de Astrofísica de Andalucía (IAA) and the "REG" (Red para la Explotación científica de Gaia) and I have actively participated in congresses organized by both groups.

    Furthermore, I am the first author of the paper "The ALHAMBRA Photometric System" (Aparicio Villegas et al. 2010) published in the Astronomical Journal, where we present the main results related in Chapter 2 and 3. I participate in two papers as a collaborator, Bongiovanni et al.(2010) and Matute et al. 2011 (in referee). And a proceeding with referee called "Stellar Physics with the ALHAMBRA Photometric System" has been published at the end of this year in the Journal of Physics: Conference Series (Aparicio

Villegas et al. 2011), where a preliminary result of the Q Fit Algorithm (described in Chapter 4) is presented, and a more extended paper is in preparation.

Conclusiones

En esta Tesis presentamos una caracterización del rango óptico del sistema fotométrico ALHAMBRA, y analizamos sus capacidades para la clasificación espectral de estrellas. A continuación se resume las principales conclusiones obtenidas:

1. Los cuatro conjuntos de filtros del sistema fotométrico ALHAMBRA han sido caracterizados con las curvas respuesta obtenidas del producto de la transmisión de filtros, detectores y extinción atmosférica, y algunos momentos de primer y segundo orden de las mismas.
2. Las variaciones en magnitud de estos cuatro conjuntos de filtros han sido analizadas a través de la fotometría sintética de un subconjunto de las estrellas primarias estándares del sistema.
3. El conjunto de las estrellas primarias estándares ha sido presentado junto con el sistema de magnitudes anclado al sistema ALHAMBRA, lo que también representa parte de la caracterización del sistema fotométrico.
4. De los cuatro sistemas filtros+detector, se elige como el sistema fotométrico ALHAMBRA estándar al que está en la posición 3 del instrumento (LAICA), esto es, los filtros asociados al CCD3.
5. Han sido desarrolladas dos estrategias distintas para la calibración fotométrica del sistema. Entre ambas, la metodología finalmente elegida es la que evita errores sistemáticos y es suficientemente robusta para ser aplicada a todos los objetos astronómicos en el cartografiado ALHAMBRA, obteniendo puntos cero para los campos ALHAMBRA con errores por debajo de unas pocas centésimas de magnitud.
6. Se han elaborado ecuaciones de transformación entre la fotometría ALHAMBRA y los filtros del Sloan Digital Sky Survey (SDSS) y el sistema fotométrico de la misión Gaia, utilizando estrategias equivalentes.
7. El análisis de las capacidades del sistema fotométrico ALHAMBRA en la parte óptica del espectro en la clasificación espectral de estrellas y la determinación de los principales parámetros físicos estelares, han sido abordados desde dos puntos de vista:

   - El uso de colores o combinación lineal de los mismos que caracterizan propiedades físicas representativas de grupos estelares bien definidos.

   - A través de la comparación directa de la fotometría ALHAMBRA y espectros sintéticos derivados de modelos evolutivos atmosféricos.
8. En esta tesis se propone por primera vez la comparación de "espectros" Q con espectros teóricos sintéticos del mismo tipo para estimar los principales parámetros físicos (T_{eff}, $log(g)$, $[Fe/H]$ y E_{B-V}) para todos los tipos de objetos estelares que podemos encontrar en los campos ALHAMBRA. Esta metodología está basada en la

idea de que las observaciones con este tipo de sistema de filtros puede ser considerada como una espectroscopía de muy baja resolución.

9. Analizamos y comparamos los resultados de los diferentes métodos de parametrización estelar aplicado a una muestra de estrellas estándares del sistema.

10. El algoritmo de ajustes con *Qs* también es aplicado a un subconjunto de estrellas de campo ALHAMBRA.

11. Aparte de alcanzar estos objetivos cientÃficos, durante los cuatro años he aumentado mi conocimiento y experiencia en los conceptos básicos de radiación estelar, las técnicas fotométricas y espectroscópicas más recientes, los modelos de evolución estelar, y la teoría y práctica en la clasificación estadística así como en la manipulación de grandes bases de datos.

    He tenido la oportunidad de trabajar con el grupo de Gaia liderado por Carme Jordi en la Universidad de Barcelona (UB) y con el grupo de Gaia liderado por Coryn Bailer-Jones en el Max Planck Institute of Astronomy (MPIA) en Heidelberg (Alemania), habiendo aprovechado gratamente ambas oportunidades.

    He participado activamente en las actividades científicas del grupo ALHAMBRA y actualmente estoy involucrada en el desarrollo de un nuevo proyecto de cartografiado del cielo, el proyecto J-PAU, que es una extensión del proyecto ALHAMBRA y que se está llevando a cabo por el CEFCA (Centros de Estudios de Física del Cosmos de Aragón) en Teruel. También he sido miembro del "Grupo de Sistemas Estelares " del Instituto de Astrofísica de Andalucía (IAA) y la "REG" (Red para la Explotación científica de Gaia), y he participado activamente en congresos organizados por ambos grupos.

    Además, soy la primera autora del artículo "The ALHAMBRA Photometric System" (Aparicio Villegas et al. 2010) publicado en el Astronomical Journal, donde se presentan los principales resultados expuestos en los capítulos 2 y 3. He participado en dos artículos como colaboradora, Bongiovanni et al.(2010) y Matute et al. 2011 (en arbitraje). También soy primera autora de un artículo titulado "Stellar Physics with the ALHAMBRA Photometric System" que ha sido publicado a finales del año 2011 en el Journal of Physics: Conference Series (Aparicio Villegas et al. 2011), donde se presenta un resultado preliminar del *Q* Fit Algorithm (descrito en el Capítulo 4), y un artículo más detallado está siendo preparado.

A

APPENDIX

Table A.1 Synthetic ALHAMBRA magnitudes of the 31 spectrophotometric primary standard stars.

Star	Alh 1	Alh 2	Alh 3	Alh 4	Alh 5	Alh 6	Alh 7	Alh 8	Alh 9	Alh10
HZ4	14.71	14.66	14.49	14.26	14.51	14.39	14.47	14.55	14.63	14.85
G191b2b	11.04	11.18	11.32	11.41	11.58	11.68	11.79	11.89	12.00	12.12
IB227	15.42	15.39	15.26	15.07	15.34	15.23	15.29	15.37	15.46	15.67
GD71	12.47	12.58	12.65	12.69	12.88	12.94	13.04	13.15	13.25	13.39
HZ2	13.71	13.71	13.67	13.59	13.79	13.78	13.87	13.96	14.04	14.20
BD75d325	8.76	8.90	9.05	9.19	9.32	9.43	9.55	9.65	9.75	9.87
Agk81d266	11.16	11.29	11.44	11.56	11.71	11.83	11.93	12.04	12.15	12.27
GD108	13.20	13.15	13.19	13.27	13.42	13.49	13.58	13.67	13.75	13.86
Feige34	10.39	10.52	10.68	10.81	10.97	11.09	11.18	11.28	11.38	11.49
HD9521	6.43	6.46	6.56	6.69	6.79	6.90	7.00	7.09	7.18	7.28
HZ21	13.91	14.03	14.19	14.36	14.49	14.59	14.71	14.79	14.89	15.01
Feige66	9.92	9.98	10.08	10.17	10.31	10.41	10.52	10.62	10.71	10.84
Feige67	11.04	11.17	11.33	11.47	11.62	11.73	11.84	11.95	12.05	12.18
GD153	12.71	12.83	12.94	12.99	13.18	13.26	13.36	13.46	13.57	13.69
HZ43	12.21	12.34	12.47	12.55	12.73	12.82	12.92	13.03	13.14	13.26
HZ44	10.98	11.11	11.23	11.35	11.47	11.57	11.67	11.77	11.87	11.99
GRW70d5824	12.59	12.61	12.54	12.46	12.68	12.66	12.75	12.84	12.93	13.10
P041c	13.42	13.02	12.55	12.26	12.13	12.05	11.96	11.88	11.84	11.81
BD33d2642	10.62	10.45	10.51	10.58	10.66	10.74	10.81	10.89	10.97	11.06
P177d	14.96	14.55	14.07	13.76	13.62	13.53	13.44	13.34	13.29	13.26
P330e	14.38	14.01	13.59	13.29	13.15	13.06	12.96	12.88	12.83	12.79
Alpha_lyr	0.98	0.03	-0.14	-0.18	-0.05	-0.04	0.01	0.07	0.13	0.23
LDS749b	14.44	14.46	14.45	14.53	14.59	14.62	14.68	14.77	14.79	14.83
G93-48	12.75	12.72	12.59	12.46	12.69	12.65	12.74	12.84	12.91	13.12
BD28d4211	9.73	9.88	10.03	10.15	10.29	10.41	10.52	10.63	10.74	10.85
BD25d4655	9.01	9.11	9.23	9.37	9.47	9.58	9.69	9.81	9.90	10.01
BD17d4708	10.47	10.04	9.79	9.65	9.57	9.49	9.43	9.38	9.34	9.32
NGC7293	12.71	12.87	13.02	13.18	13.35	13.46	13.57	13.69	13.79	13.91
ITT9491	14.02	13.99	13.98	14.01	14.01	14.04	14.08	14.14	14.16	14.21
Feige110	11.14	11.25	11.37	11.48	11.62	11.73	11.84	11.95	12.05	12.17

Star	Alh11	Alh12	Alh13	Alh14	Alh15	Alh16	Alh17	Alh18	Alh19	Alh20
HZ4	14.82	14.85	14.92	14.98	15.05	15.10	15.17	15.23	15.29	15.35
GD50	14.48	14.56	14.64	14.70	14.79	14.85	14.91	14.98	—	—
G191b2b	12.20	12.29	12.37	12.46	12.54	12.61	12.69	12.76	12.82	12.89
IB227	15.64	15.66	15.72	15.79	15.83	15.89	15.94	15.99	—	—
GD71	13.45	13.53	13.61	13.69	13.77	13.84	13.92	13.98	14.05	14.11
HZ2	14.20	14.26	14.32	14.39	14.46	14.51	14.58	14.63	—	—
BD75d325	9.96	10.04	10.12	10.21	10.28	10.37	10.42	10.50	10.58	10.64
Agk81d266	12.35	12.44	12.53	12.61	12.69	12.76	12.84	12.91	12.99	13.05
GD108	13.91	13.98	14.06	14.12	14.19	14.25	14.31	14.38	—	—
Feige34	11.58	11.65	11.72	11.79	11.87	11.93	11.99	12.05	12.11	12.16
HD9521	7.36	7.44	7.52	7.59	7.67	7.73	7.80	7.86	7.92	7.98
HZ21	15.09	15.18	15.26	15.34	15.42	15.51	15.57	15.65	15.73	15.79
Feige66	10.90	10.98	11.06	11.14	11.21	11.27	11.34	11.40	—	—
Feige67	12.25	12.33	12.42	12.49	12.57	12.64	12.71	12.78	—	—
GD153	13.77	13.85	13.93	14.02	14.09	14.17	14.24	14.31	14.38	14.44
HZ43	13.34	13.42	13.51	13.59	13.67	13.74	13.82	13.89	13.95	14.02
HZ44	12.07	12.15	12.24	12.33	12.40	12.48	12.55	12.63	12.69	12.77
GRW70d5824	13.12	13.18	13.25	13.32	13.39	13.46	13.53	13.59	13.65	13.72
P041c	11.76	11.75	11.74	11.73	11.71	11.72	11.74	11.71	11.72	11.725
BD33d2642	11.13	11.19	11.26	11.33	11.39	11.45	11.52	11.55	—	—
P177d	13.21	13.19	13.17	13.15	13.14	13.14	13.15	13.12	13.12	13.12
P330e	12.74	12.72	12.71	12.69	12.67	12.67	12.68	12.66	12.66	12.67
Alpha_lyr	0.25	0.30	0.35	0.40	0.46	0.49	0.55	0.52	0.50	0.54
LDS749b	14.93	14.97	14.99	15.06	15.11	15.14	15.19	15.23	—	—
G93-48	13.09	13.12	13.22	13.29	13.35	13.39	13.47	13.54	—	—
BD28d4211	10.94	11.03	11.11	11.20	11.28	11.36	11.43	11.51	11.58	11.65
BD25d4655	10.09	10.16	10.24	10.33	10.41	10.47	10.55	10.61	—	—
BD17d4708	9.29	9.27	9.26	9.25	9.24	9.24	9.25	9.24	9.24	9.25
NGC7293	14.00	14.08	14.49	14.27	14.33	14.40	14.49	14.57	—	—
ITT9491	14.24	14.28	14.32	14.36	14.42	14.45	14.50	14.54	—	—
Feige110	12.24	12.32	12.39	12.47	12.56	12.62	12.69	12.78	12.82	12.89

Table A.2 ALHAMBRA magnitudes of the 288 stars from the NGSL

Star name	Alh1	Alh2	Alh3	Alh4	Alh5	Alh6	Alh7	Alh8	Alh9	Alh10	Alh11	Alh12	Alh13	Alh14	Alh15	Alh16	Alh17	Alh18	Alh19	Alh20
Agk81d266	11.17	11.30	11.43	11.56	11.71	11.82	11.93	12.04	12.15	12.27	12.35	12.44	12.53	12.61	12.69	12.76	12.84	12.91	12.98	13.05
BD+413306	10.59	10.20	9.62	9.17	9.02	8.95	8.78	8.66	8.58	8.51	8.44	8.40	8.36	8.32	8.30	8.28	8.29	8.24	8.24	8.26
BD-122669	11.09	10.57	10.39	10.27	10.27	10.21	10.19	10.16	10.14	10.14	10.11	10.10	10.10	10.11	10.13	10.14	10.17	10.17	10.20	10.25
BD092860	12.03	11.57	11.27	11.05	10.91	10.82	10.72	10.63	10.57	10.52	10.46	10.43	10.40	10.39	10.37	10.36	10.37	10.35	10.35	10.39
BD174708	10.38	9.98	9.77	9.61	9.54	9.47	9.41	9.35	9.31	9.30	9.25	9.24	9.22	9.22	9.22	9.23	9.25	9.24	9.26	9.31
BD17d4708	10.45	10.04	9.81	9.64	9.57	9.49	9.43	9.38	9.34	9.33	9.29	9.27	9.26	9.25	9.24	9.24	9.25	9.24	9.24	9.25
BD292091	11.25	10.96	10.73	10.54	10.43	10.35	10.28	10.21	10.15	10.11	10.06	10.03	10.01	9.99	9.99	9.99	10.01	10.00	10.02	10.05
BD423607	10.98	10.68	10.48	10.31	10.22	10.14	10.08	10.03	9.99	9.96	9.92	9.90	9.89	9.89	9.89	9.89	9.91	9.89	9.92	9.95
BD442051	12.10	11.39	10.66	9.66	9.40	9.08	8.65	8.43	8.26	7.92	7.95	7.68	7.34	7.25	7.12	7.04	7.00	6.90	6.84	6.82
BD511696	10.93	10.63	10.34	10.10	9.98	9.89	9.80	9.72	9.66	9.62	9.56	9.53	9.50	9.48	9.47	9.46	9.49	9.47	9.49	9.52
BD592723	11.32	10.94	10.75	10.60	10.52	10.44	10.38	10.32	10.26	10.23	10.17	10.15	10.13	10.12	10.12	10.11	10.13	10.12	10.15	10.19
BD720094	10.85	10.45	10.25	10.11	10.04	9.98	9.93	9.88	9.83	9.80	9.75	9.72	9.70	9.69	9.69	9.69	9.72	9.71	9.73	9.76
BD_28d4211	9.74	9.88	10.02	10.16	10.29	10.40	10.52	10.62	10.73	10.85	10.94	11.03	11.12	11.20	11.28	11.36	11.43	11.51	11.58	11.65
BD_75d325	8.77	8.91	9.05	9.19	9.32	9.43	9.55	9.64	9.75	9.87	9.95	10.04	10.12	10.21	10.28	10.37	10.43	10.50	10.58	10.64
CD-259286	11.84	11.18	10.96	10.80	10.71	10.62	10.56	10.50	10.45	10.41	10.36	10.34	10.32	10.31	10.29	10.29	10.30	10.28	10.30	10.33
CD-3018140	10.85	10.43	10.23	10.09	10.03	9.96	9.92	9.88	9.85	9.84	9.80	9.79	9.78	9.78	9.79	9.79	9.82	9.82	9.84	9.88
CD-621346	11.35	10.91	10.57	10.23	10.06	9.97	9.87	9.79	9.72	9.66	9.60	9.56	9.53	9.50	9.49	9.47	9.47	9.44	9.44	9.46
Feige110	11.15	11.25	11.37	11.48	11.62	11.73	11.84	11.95	12.05	12.17	12.23	12.32	12.40	12.47	12.56	12.62	12.69	12.77	12.82	12.89
Feige34	10.40	10.52	10.67	10.82	10.97	11.08	11.18	11.28	11.38	11.49	11.58	11.66	11.73	11.80	11.87	11.93	11.99	12.05	12.11	12.16
G019-013	10.47	9.89	9.02	8.25	8.14	8.01	7.62	7.40	7.25	7.11	7.02	6.92	6.82	6.74	6.69	6.66	6.65	6.58	6.57	6.59
G021-024	11.93	11.30	10.37	9.48	9.33	9.16	8.72	8.48	8.32	8.15	8.07	7.95	7.82	7.73	7.67	7.64	7.63	7.57	7.55	7.56
G029-023	11.16	10.76	10.55	10.39	10.31	10.24	10.17	10.11	10.05	10.03	9.97	9.96	9.94	9.93	9.93	9.93	9.95	9.94	9.97	10.02
G114-26	10.59	10.24	10.01	9.84	9.76	9.69	9.62	9.56	9.50	9.47	9.41	9.39	9.36	9.35	9.35	9.35	9.36	9.35	9.38	9.42
G115-58	12.94	12.52	12.29	12.13	12.06	11.98	11.92	11.87	11.80	11.78	11.73	11.70	11.68	11.67	11.67	11.66	11.69	11.70	11.69	11.70
G12-21	11.10	10.73	10.49	10.31	10.22	10.15	10.08	10.02	9.97	9.94	9.88	9.86	9.84	9.83	9.82	9.83	9.85	9.85	9.87	9.90
G13-35	10.58	10.20	9.98	9.83	9.75	9.68	9.63	9.59	9.54	9.52	9.47	9.45	9.44	9.43	9.43	9.43	9.45	9.44	9.45	9.48
G169-28	12.07	11.75	11.47	11.26	11.15	11.07	11.00	10.92	10.87	10.84	10.79	10.76	10.74	10.73	10.71	10.72	10.74	10.73	10.74	10.78
G17-25	11.03	10.73	10.30	9.93	9.78	9.68	9.53	9.42	9.33	9.27	9.20	9.15	9.10	9.07	9.05	9.03	9.03	9.00	9.01	9.03
G18-39	11.37	10.99	10.76	10.59	10.51	10.44	10.38	10.33	10.28	10.25	10.19	10.16	10.14	10.13	10.13	10.13	10.14	10.13	10.15	10.19
G18-54	11.80	11.42	11.18	10.99	10.89	10.81	10.73	10.67	10.61	10.57	10.51	10.48	10.45	10.43	10.43	10.42	10.45	10.44	10.45	10.49
G180-24	10.81	10.44	10.20	10.03	9.95	9.88	9.83	9.78	9.73	9.70	9.64	9.62	9.60	9.58	9.58	9.58	9.60	9.59	9.61	9.64
G187-40	11.45	11.15	10.89	10.68	10.57	10.49	10.42	10.35	10.30	10.26	10.21	10.18	10.16	10.15	10.15	10.15	10.17	10.16	10.19	10.22
G188-22	11.11	10.74	10.50	10.32	10.24	10.16	10.10	10.03	9.98	9.95	9.89	9.86	9.84	9.83	9.83	9.83	9.85	9.84	9.87	9.90
G188-30	12.20	11.92	11.59	11.30	11.16	11.07	10.97	10.90	10.83	10.77	10.72	10.69	10.65	10.63	10.61	10.61	10.61	10.59	10.59	10.62
G191b2b	11.04	11.17	11.30	11.41	11.57	11.67	11.78	11.88	11.99	12.11	12.20	12.28	12.37	12.45	12.53	12.60	12.68	12.75	12.82	12.88
G192-43	11.28	10.88	10.66	10.50	10.42	10.35	10.30	10.24	10.20	10.18	10.14	10.12	10.10	10.10	10.11	10.11	10.14	10.13	10.15	10.20
G194-22	10.55	10.20	9.98	9.81	9.74	9.67	9.62	9.58	9.55	9.53	9.49	9.47	9.46	9.46	9.46	9.47	9.49	9.50	9.52	9.56
G196-48	11.44	11.07	10.83	10.64	10.53	10.45	10.37	10.30	10.24	10.20	10.14	10.11	10.08	10.06	10.05	10.05	10.07	10.05	10.07	10.11
G20-15	11.79	11.40	11.14	10.93	10.80	10.68	10.58	10.48	10.40	10.35	10.27	10.22	10.18	10.16	10.13	10.11	10.13	10.10	10.10	10.14
G202-65	11.89	11.43	11.24	11.12	11.11	11.07	11.05	11.02	11.01	11.03	11.00	11.01	11.01	11.02	11.04	11.05	11.08	11.08	11.10	11.15

Table A.2 Continuation

Star name	Alh1	Alh2	Alh3	Alh4	Alh5	Alh6	Alh7	Alh8	Alh9	Alh10	Alh11	Alh12	Alh13	Alh14	Alh15	Alh16	Alh17	Alh18	Alh19	Alh20
G231-52	11.49	11.23	10.92	10.67	10.53	10.43	10.34	10.25	10.18	10.14	10.08	10.05	10.01	9.99	9.99	9.98	9.99	9.97	9.99	10.02
G234-28	12.03	11.65	11.42	11.25	11.16	11.09	11.02	10.96	10.91	10.88	10.82	10.79	10.77	10.76	10.75	10.75	10.77	10.78	10.79	10.82
G24-3	11.42	11.06	10.82	10.66	10.57	10.49	10.43	10.36	10.31	10.27	10.20	10.17	10.14	10.13	10.12	10.12	10.13	10.12	10.14	10.16
G243-62	13.05	12.67	12.08	11.61	11.44	11.36	11.16	11.03	10.94	10.86	10.77	10.72	10.67	10.62	10.59	10.56	10.56	10.50	10.48	10.49
G260-36	13.19	12.70	12.00	11.43	11.25	11.19	10.98	10.84	10.75	10.67	10.58	10.55	10.50	10.45	10.44	10.43	10.43	10.38	10.40	10.42
G262-14	12.91	12.58	12.08	11.67	11.53	11.44	11.27	11.16	11.06	10.98	10.90	10.84	10.78	10.74	10.71	10.69	10.69	10.65	10.65	10.67
G63-26	13.37	12.99	12.77	12.60	12.52	12.44	12.39	12.34	12.28	12.25	12.19	12.16	12.15	12.13	12.14	12.14	12.18	12.16	12.16	12.17
G88-27	11.68	11.29	11.06	10.90	10.82	10.76	10.70	10.65	10.60	10.58	10.53	10.51	10.49	10.49	10.49	10.48	10.50	10.49	10.50	10.54
GJ825	9.91	9.23	8.38	7.44	7.26	7.02	6.56	6.30	6.11	5.86	5.81	5.61	5.37	5.28	5.18	5.14	5.12	5.04	5.01	5.01
GL109	13.90	13.11	12.44	11.49	11.20	10.80	10.46	10.29	10.16	9.58	9.65	9.22	8.66	8.58	8.35	8.24	8.22	8.09	8.02	8.00
GL15B	11.41	10.70	9.98	8.99	8.74	8.49	8.08	7.74	7.55	7.16	7.19	6.89	6.56	6.42	6.24	6.17	6.14	6.05	6.00	6.00
HD000319	7.00	6.10	5.90	5.80	5.89	5.87	5.90	5.93	5.97	6.05	6.05	6.09	6.12	6.16	6.20	6.23	6.26	6.24	6.24	6.28
HD001461	8.00	7.61	7.10	6.74	6.60	6.52	6.41	6.32	6.28	6.25	6.20	6.20	6.19	6.16	6.17	6.16	6.18	6.14	6.15	6.16
HD002857	10.96	10.00	9.85	9.78	9.85	9.84	9.87	9.90	9.92	9.98	9.97	10.00	10.03	10.06	10.10	10.12	10.14	10.10	10.12	10.17
HD004727	4.58	4.18	4.19	4.24	4.37	4.43	4.51	4.57	4.64	4.72	4.75	4.81	4.87	4.92	4.99	5.04	5.11	5.12	5.17	5.24
HD004813	6.28	5.89	5.56	5.34	5.26	5.20	5.13	5.06	5.02	5.00	4.95	4.94	4.93	4.93	4.93	4.93	4.97	4.95	4.98	5.03
HD005256	10.35	9.97	9.49	9.10	8.93	8.84	8.72	8.62	8.55	8.49	8.43	8.40	8.37	8.35	8.33	8.31	8.32	8.28	8.28	8.30
HD005395	6.82	6.32	5.66	5.12	4.87	4.73	4.57	4.44	4.35	4.28	4.21	4.18	4.14	4.09	4.08	4.05	4.03	3.97	3.98	3.99
HD005544	10.38	9.74	8.90	8.24	7.94	7.78	7.57	7.40	7.30	7.21	7.11	7.08	7.03	6.95	6.96	6.92	6.88	6.79	6.82	6.83
HD005916	8.79	8.35	7.79	7.31	7.09	6.96	6.81	6.69	6.61	6.53	6.45	6.41	6.37	6.32	6.30	6.28	6.27	6.21	6.23	6.23
HD006229	10.17	9.71	9.30	8.95	8.77	8.65	8.53	8.43	8.36	8.31	8.25	8.22	8.19	8.16	8.14	8.11	8.11	8.06	8.05	8.06
HD006734	8.32	7.91	7.32	6.85	6.66	6.55	6.39	6.27	6.17	6.09	6.00	5.97	5.92	5.87	5.86	5.84	5.85	5.80	5.83	5.85
HD006755	9.13	8.74	8.40	8.09	7.92	7.79	7.68	7.57	7.48	7.40	7.32	7.27	7.22	7.19	7.16	7.15	7.15	7.13	7.13	7.16
HD008724	10.35	9.86	9.35	8.90	8.62	8.44	8.26	8.10	7.97	7.86	7.75	7.68	7.61	7.56	7.51	7.48	7.46	7.41	7.40	7.43
HD009051	10.54	10.14	9.72	9.34	9.14	9.01	8.87	8.74	8.65	8.57	8.48	8.44	8.39	8.35	8.33	8.30	8.30	8.26	8.28	8.31
HD010780	7.43	7.00	6.41	5.96	5.80	5.72	5.57	5.46	5.39	5.33	5.26	5.23	5.20	5.17	5.16	5.15	5.16	5.11	5.12	5.14
HD012533	5.65	4.89	3.84	2.97	2.56	2.36	2.09	1.90	1.77	1.65	1.51	1.49	1.41	1.29	1.32	1.28	1.24	1.13	1.19	1.22
HD015089	5.58	4.74	4.54	4.44	4.54	4.57	4.60	4.62	4.67	4.77	4.77	4.81	4.87	4.91	4.97	5.02	5.08	5.07	5.08	5.14
HD016031	10.76	10.36	10.15	9.99	9.92	9.85	9.81	9.76	9.72	9.70	9.65	9.63	9.62	9.62	9.62	9.62	9.63	9.61	9.63	9.67
HD017072	7.97	7.51	7.15	6.88	6.73	6.64	6.54	6.45	6.38	6.32	6.24	6.20	6.16	6.13	6.11	6.09	6.10	6.07	6.08	6.10
HD017361	7.24	6.59	5.76	5.10	4.81	4.67	4.46	4.29	4.18	4.09	3.98	3.95	3.90	3.81	3.82	3.80	3.77	3.69	3.73	3.75
HD017925	8.08	7.61	6.96	6.45	6.27	6.18	5.99	5.84	5.75	5.67	5.59	5.56	5.52	5.48	5.47	5.46	5.48	5.44	5.46	5.49
HD018078	9.55	8.55	8.36	8.22	8.26	8.28	8.24	8.20	8.23	8.30	8.27	8.30	8.33	8.36	8.38	8.42	8.43	8.37	8.37	8.41
HD018769	7.00	6.12	5.90	5.77	5.87	5.87	5.89	5.91	5.94	6.01	5.98	6.01	6.04	6.08	6.12	6.16	6.20	6.19	6.20	6.25
HD018907	7.58	7.19	6.67	6.26	6.08	5.97	5.82	5.70	5.61	5.54	5.46	5.42	5.37	5.33	5.31	5.29	5.29	5.25	5.26	5.29
HD019019	8.10	7.73	7.37	7.12	7.03	6.97	6.89	6.81	6.76	6.74	6.68	6.67	6.65	6.64	6.65	6.65	6.68	6.66	6.69	6.74
HD019308	8.82	8.44	7.97	7.63	7.50	7.42	7.32	7.22	7.17	7.12	7.06	7.05	7.03	7.01	7.01	7.01	7.04	7.02	7.05	7.09
HD019445	8.92	8.59	8.38	8.22	8.14	8.07	8.01	7.97	7.92	7.88	7.83	7.81	7.79	7.78	7.78	7.77	7.78	7.77	7.79	7.83
HD019656	7.31	6.71	5.88	5.21	4.91	4.76	4.55	4.38	4.27	4.18	4.07	4.05	3.99	3.91	3.92	3.90	3.88	3.81	3.86	3.89
HD019787	6.81	6.22	5.45	4.86	4.60	4.47	4.29	4.14	4.03	3.95	3.84	3.82	3.77	3.69	3.70	3.68	3.67	3.59	3.65	3.67

Table A.2 Continuation

Star name	Alh1	Alh2	Alh3	Alh4	Alh5	Alh6	Alh7	Alh8	Alh9	Alh10	Alh11	Alh12	Alh13	Alh14	Alh15	Alh16	Alh17	Alh18	Alh19	Alh20
HD020039	10.44	10.07	9.60	9.21	9.04	8.94	8.81	8.71	8.65	8.59	8.53	8.50	8.47	8.43	8.42	8.40	8.40	8.36	8.35	8.36
HD020630	6.32	5.94	5.45	5.11	4.98	4.91	4.81	4.71	4.65	4.61	4.55	4.53	4.51	4.48	4.47	4.47	4.49	4.46	4.47	4.50
HD021742	10.06	9.57	8.93	8.42	8.25	8.18	8.02	7.89	7.81	7.74	7.66	7.64	7.61	7.56	7.56	7.55	7.56	7.51	7.53	7.56
HD022049	5.76	5.30	4.63	4.11	3.93	3.86	3.66	3.51	3.42	3.34	3.25	3.22	3.17	3.13	3.11	3.11	3.12	3.07	3.09	3.12
HD022484	5.57	5.16	4.77	4.50	4.39	4.32	4.25	4.19	4.15	4.14	4.10	4.10	4.09	4.08	4.08	4.08	4.10	4.07	4.07	4.09
HD023439	9.65	9.32	8.84	8.44	8.29	8.22	8.06	7.95	7.88	7.81	7.74	7.70	7.65	7.62	7.60	7.58	7.58	7.54	7.55	7.56
HD025329	10.24	9.93	9.39	8.91	8.73	8.62	8.44	8.32	8.21	8.13	8.04	7.99	7.93	7.89	7.86	7.84	7.84	7.80	7.81	7.84
HD025893	9.08	8.64	8.04	7.59	7.42	7.34	7.18	7.04	6.96	6.90	6.82	6.79	6.76	6.71	6.70	6.70	6.71	6.68	6.70	6.73
HD025975	8.30	7.78	7.08	6.53	6.30	6.19	6.01	5.87	5.78	5.70	5.62	5.59	5.55	5.49	5.49	5.48	5.48	5.43	5.47	5.50
HD026297	9.90	9.30	8.64	8.12	7.81	7.61	7.41	7.23	7.09	6.96	6.84	6.76	6.68	6.61	6.56	6.53	6.51	6.46	6.45	6.46
HD027295	5.96	5.29	5.24	5.23	5.36	5.40	5.47	5.54	5.61	5.71	5.75	5.81	5.87	5.93	5.99	6.04	6.08	6.07	6.08	6.13
HD028946	9.62	9.22	8.67	8.24	8.08	8.01	7.87	7.76	7.69	7.63	7.55	7.52	7.49	7.46	7.45	7.44	7.46	7.41	7.44	7.47
HD028978	6.73	5.73	5.58	5.51	5.62	5.62	5.65	5.68	5.73	5.82	5.82	5.87	5.91	5.96	6.01	6.06	6.10	6.06	6.08	6.14
HD029574	11.39	10.63	9.84	9.23	8.83	8.55	8.28	8.06	7.88	7.72	7.56	7.45	7.34	7.25	7.17	7.11	7.07	6.98	6.95	6.94
HD030834	8.28	7.53	6.47	5.62	5.24	5.03	4.71	4.48	4.32	4.16	4.01	3.94	3.84	3.73	3.70	3.65	3.61	3.52	3.54	3.55
HD031219	9.46	9.06	8.62	8.34	8.24	8.16	8.08	8.00	7.96	7.94	7.89	7.89	7.88	7.87	7.87	7.89	7.93	7.91	7.94	7.98
HD033793	12.19	11.52	10.81	9.76	9.49	9.21	8.74	8.46	8.29	8.02	8.04	7.79	7.49	7.39	7.27	7.19	7.15	7.05	6.99	6.97
HD034078	6.25	6.13	6.09	6.06	6.03	5.97	5.94	5.93	5.92	5.92	5.89	5.89	5.89	5.90	5.91	5.92	5.94	5.94	5.96	6.01
HD034797	6.78	6.26	6.23	6.24	6.36	6.41	6.47	6.53	6.60	6.70	6.74	6.81	6.87	6.94	7.00	7.05	7.10	7.10	7.12	7.17
HD036702	11.01	10.33	9.65	9.12	8.76	8.52	8.30	8.12	7.96	7.83	7.70	7.61	7.53	7.46	7.41	7.37	7.35	7.29	7.28	7.30
HD037202	2.76	2.54	2.60	2.69	2.78	2.86	2.95	3.04	3.11	3.12	3.26	3.33	3.40	3.46	3.52	3.55	3.59	3.61	3.63	3.72
HD037216	9.51	9.12	8.57	8.16	8.00	7.91	7.78	7.68	7.61	7.56	7.50	7.48	7.46	7.43	7.42	7.42	7.44	7.41	7.44	7.47
HD037763	8.06	7.35	6.48	5.76	5.48	5.37	5.12	4.94	4.83	4.74	4.63	4.61	4.55	4.46	4.47	4.44	4.41	4.33	4.37	4.38
HD037828	9.40	8.85	8.11	7.53	7.20	7.01	6.81	6.65	6.52	6.41	6.30	6.23	6.16	6.09	6.04	6.00	5.97	5.89	5.88	5.86
HD038237	8.28	7.43	7.19	7.07	7.14	7.12	7.14	7.17	7.20	7.28	7.27	7.31	7.34	7.38	7.42	7.45	7.48	7.46	7.46	7.50
HD038510	9.35	8.96	8.66	8.43	8.32	8.24	8.17	8.11	8.08	8.05	8.02	8.01	7.99	7.99	7.99	7.98	8.00	7.97	7.98	8.00
HD039587	5.64	5.28	4.89	4.62	4.51	4.44	4.35	4.28	4.22	4.18	4.12	4.10	4.08	4.06	4.06	4.05	4.08	4.06	4.08	4.12
HD039833	9.04	8.66	8.20	7.89	7.77	7.70	7.60	7.51	7.45	7.41	7.35	7.32	7.31	7.28	7.27	7.27	7.31	7.28	7.30	7.33
HD040573	8.22	7.39	7.27	7.24	7.38	7.40	7.46	7.51	7.57	7.66	7.66	7.71	7.75	7.80	7.85	7.90	7.94	7.92	7.93	7.98
HD041357	6.53	5.69	5.44	5.29	5.34	5.32	5.32	5.31	5.32	5.36	5.33	5.35	5.36	5.38	5.41	5.44	5.48	5.46	5.48	5.52
HD041661	8.62	8.06	7.75	7.56	7.50	7.45	7.39	7.33	7.31	7.29	7.24	7.24	7.24	7.23	7.24	7.25	7.29	7.27	7.29	7.33
HD041667	10.61	10.15	9.54	9.05	8.80	8.64	8.47	8.33	8.21	8.11	8.00	7.93	7.86	7.80	7.76	7.72	7.71	7.66	7.65	7.67
HD044007	9.68	9.25	8.86	8.49	8.28	8.13	7.99	7.88	7.77	7.68	7.59	7.53	7.48	7.43	7.40	7.37	7.37	7.32	7.33	7.35
HD045282	9.30	8.94	8.62	8.34	8.18	8.08	7.97	7.88	7.80	7.74	7.67	7.64	7.60	7.58	7.56	7.54	7.55	7.52	7.54	7.58
HD047839	4.09	4.13	4.24	4.35	4.47	4.57	4.68	4.79	4.86	4.95	5.02	5.08	5.15	5.22	5.30	5.35	5.43	5.48	5.55	5.64
HD048279	7.99	7.93	7.93	7.93	7.92	7.90	7.91	7.92	7.95	8.00	8.02	8.05	8.09	8.13	8.15	8.18	8.21	8.23	8.26	8.30
HD050420	7.46	6.58	6.32	6.17	6.18	6.14	6.12	6.10	6.09	6.11	6.06	6.07	6.08	6.08	6.09	6.11	6.12	6.08	6.09	6.13
HD055496	10.35	9.94	9.36	8.86	8.62	8.47	8.32	8.20	8.10	8.02	7.93	7.89	7.83	7.77	7.77	7.75	7.73	7.67	7.72	7.74
HD057727	7.07	6.60	5.96	5.47	5.25	5.13	4.98	4.83	4.74	4.67	4.58	4.55	4.50	4.45	4.45	4.43	4.44	4.38	4.41	4.44
HD058551	7.61	7.19	6.89	6.69	6.61	6.54	6.48	6.43	6.41	6.40	6.36	6.36	6.36	6.35	6.36	6.36	6.38	6.36	6.37	6.39

Table A.2 Continuation

Star name	Alh1	Alh2	Alh3	Alh4	Alh5	Alh6	Alh7	Alh8	Alh9	Alh10	Alh11	Alh12	Alh13	Alh14	Alh15	Alh16	Alh17	Alh18	Alh19	Alh20
HD060319	10.01	9.63	9.34	9.11	9.01	8.94	8.87	8.81	8.78	8.76	8.72	8.71	8.69	8.69	8.69	8.68	8.70	8.67	8.68	8.71
HD061064	6.40	5.79	5.46	5.26	5.20	5.14	5.09	5.05	5.04	5.04	5.01	5.02	5.03	5.03	5.04	5.05	5.08	5.06	5.07	5.09
HD062412	7.93	7.39	6.67	6.12	5.87	5.75	5.58	5.44	5.35	5.27	5.18	5.15	5.10	5.04	5.04	5.02	5.00	4.94	4.97	4.99
HD063077	6.50	6.13	5.82	5.57	5.46	5.39	5.32	5.26	5.22	5.20	5.15	5.14	5.13	5.11	5.11	5.11	5.12	5.10	5.11	5.13
HD063791	9.72	9.26	8.79	8.38	8.16	8.00	7.84	7.71	7.60	7.50	7.39	7.33	7.26	7.21	7.17	7.13	7.13	7.09	7.08	7.09
HD064412	9.97	9.61	9.27	9.00	8.88	8.80	8.71	8.64	8.60	8.58	8.53	8.52	8.51	8.50	8.50	8.49	8.51	8.48	8.48	8.50
HD065228	5.88	5.32	4.82	4.51	4.34	4.25	4.14	4.04	3.99	3.94	3.86	3.83	3.81	3.78	3.76	3.76	3.78	3.74	3.75	3.78
HD065354	10.85	10.01	8.84	7.84	7.38	7.12	6.76	6.52	6.35	6.19	6.02	5.97	5.85	5.72	5.70	5.64	5.57	5.44	5.46	5.44
HD065714	8.28	7.71	6.93	6.37	6.11	5.98	5.81	5.66	5.57	5.49	5.39	5.37	5.32	5.24	5.26	5.24	5.22	5.14	5.20	5.22
HD067390	10.65	9.92	9.64	9.48	9.46	9.42	9.39	9.37	9.36	9.39	9.36	9.38	9.40	9.41	9.43	9.44	9.47	9.44	9.45	9.48
HD068988	9.65	9.26	8.77	8.44	8.32	8.25	8.15	8.05	7.99	7.95	7.89	7.87	7.85	7.83	7.83	7.84	7.87	7.84	7.87	7.91
HD071160	11.81	10.96	9.80	8.83	8.45	8.23	7.89	7.66	7.51	7.36	7.22	7.16	7.04	6.92	6.91	6.85	6.79	6.68	6.69	6.68
HD072184	8.68	7.99	7.15	6.46	6.18	6.04	5.81	5.64	5.54	5.47	5.37	5.36	5.31	5.23	5.26	5.22	5.19	5.10	5.14	5.15
HD072324	8.80	8.23	7.47	6.88	6.61	6.47	6.29	6.14	6.06	5.99	5.90	5.89	5.85	5.78	5.80	5.77	5.75	5.67	5.71	5.73
HD072505	9.27	8.53	7.64	6.89	6.58	6.43	6.19	6.00	5.90	5.82	5.71	5.70	5.65	5.56	5.59	5.55	5.51	5.41	5.46	5.47
HD074088	10.85	9.96	8.74	7.71	7.30	7.03	6.64	6.39	6.21	5.99	5.83	5.72	5.55	5.43	5.37	5.29	5.23	5.11	5.10	5.07
HD074721	9.73	8.69	8.57	8.52	8.63	8.63	8.68	8.72	8.77	8.86	8.88	8.93	8.98	9.03	9.07	9.11	9.12	9.08	9.07	9.13
HD076291	8.46	7.81	6.98	6.31	6.02	5.88	5.65	5.48	5.38	5.29	5.20	5.18	5.13	5.05	5.06	5.02	4.99	4.91	4.93	4.94
HD076932	6.92	6.54	6.24	6.01	5.91	5.84	5.77	5.71	5.67	5.65	5.61	5.60	5.59	5.58	5.57	5.57	5.58	5.56	5.56	5.58
HD078479	10.30	9.52	8.61	7.84	7.52	7.37	7.11	6.93	6.82	6.73	6.62	6.61	6.56	6.46	6.49	6.45	6.41	6.31	6.36	6.37
HD079349	12.58	11.68	10.46	9.44	9.07	8.82	8.44	8.21	8.05	7.81	7.69	7.58	7.37	7.26	7.20	7.14	7.09	6.96	6.95	6.93
HD079469	4.54	3.71	3.63	3.61	3.75	3.78	3.85	3.90	3.95	4.04	4.05	4.10	4.15	4.20	4.26	4.31	4.36	4.35	4.37	4.44
HD080607	10.90	10.44	9.85	9.40	9.24	9.17	9.04	8.92	8.86	8.80	8.73	8.72	8.70	8.66	8.66	8.66	8.67	8.62	8.66	8.69
HD082395	7.43	6.86	6.12	5.51	5.24	5.11	4.92	4.75	4.64	4.56	4.45	4.42	4.37	4.30	4.31	4.28	4.26	4.19	4.25	4.28
HD083212	10.62	10.07	9.43	8.93	8.64	8.45	8.26	8.11	7.98	7.87	7.75	7.68	7.62	7.56	7.51	7.48	7.46	7.40	7.41	7.42
HD085380	7.71	7.29	6.88	6.62	6.52	6.46	6.38	6.31	6.26	6.23	6.17	6.15	6.13	6.12	6.11	6.12	6.15	6.13	6.15	6.18
HD086322	9.34	8.77	8.02	7.42	7.16	7.03	6.85	6.69	6.59	6.50	6.39	6.36	6.31	6.24	6.25	6.21	6.20	6.12	6.16	6.18
HD086986	9.13	8.09	7.93	7.86	7.94	7.93	7.96	7.99	8.02	8.07	8.06	8.09	8.11	8.14	8.17	8.20	8.21	8.16	8.16	8.21
HD090862	12.34	11.53	10.43	9.50	9.13	8.91	8.59	8.37	8.21	8.03	7.87	7.79	7.66	7.55	7.51	7.46	7.41	7.31	7.32	7.32
HD093329	9.92	8.86	8.71	8.65	8.73	8.72	8.76	8.79	8.84	8.91	8.92	8.97	9.01	9.05	9.09	9.12	9.13	9.08	9.08	9.11
HD094028	9.12	8.77	8.54	8.38	8.29	8.22	8.16	8.11	8.06	8.03	7.98	7.96	7.94	7.92	7.92	7.92	7.93	7.92	7.95	7.98
HD095241	7.31	6.89	6.51	6.25	6.13	6.06	5.98	5.91	5.87	5.83	5.78	5.76	5.74	5.73	5.72	5.72	5.74	5.71	5.72	5.75
HD095735	10.63	9.93	9.29	8.34	8.12	7.76	7.37	7.17	7.01	6.55	6.62	6.27	5.83	5.77	5.59	5.51	5.47	5.36	5.31	5.31
HD095849	9.01	8.27	7.34	6.58	6.27	6.11	5.87	5.69	5.57	5.47	5.35	5.32	5.25	5.15	5.17	5.13	5.10	5.00	5.05	5.07
HD096446	6.43	6.34	6.35	6.41	6.52	6.58	6.66	6.75	6.81	6.90	6.95	7.01	7.08	7.14	7.20	7.25	7.32	7.35	7.39	7.46
HD097633	4.23	3.25	3.13	3.09	3.21	3.23	3.29	3.34	3.40	3.49	3.50	3.55	3.60	3.65	3.71	3.75	3.77	3.73	3.74	3.79
HD099648	7.25	6.74	6.01	5.47	5.20	5.06	4.89	4.75	4.65	4.57	4.47	4.44	4.40	4.33	4.34	4.32	4.31	4.24	4.30	4.33
HD101013	8.51	8.03	7.34	6.68	6.38	6.24	6.07	5.93	5.85	5.79	5.70	5.70	5.66	5.59	5.62	5.59	5.55	5.47	5.52	5.54
HD102212	7.95	7.09	5.89	4.93	4.57	4.29	3.95	3.75	3.59	3.30	3.19	3.04	2.78	2.69	2.60	2.53	2.51	2.40	2.38	2.38
HD102780	12.38	11.47	10.23	9.17	8.77	8.48	8.10	7.87	7.71	7.46	7.34	7.23	7.00	6.90	6.83	6.76	6.70	6.59	6.57	6.55

Table A.2 Continuation

Star name	Alh1	Alh2	Alh3	Alh4	Alh5	Alh6	Alh7	Alh8	Alh9	Alh10	Alh11	Alh12	Alh13	Alh14	Alh15	Alh16	Alh17	Alh18	Alh19	Alh20
HD105546	10.01	9.57	9.21	8.94	8.78	8.66	8.56	8.47	8.39	8.33	8.25	8.21	8.17	8.14	8.12	8.11	8.12	8.10	8.11	8.14
HD105740	10.52	10.04	9.38	8.86	8.62	8.49	8.30	8.16	8.06	7.97	7.88	7.83	7.77	7.71	7.68	7.65	7.64	7.57	7.56	7.56
HD106304	9.98	9.00	8.90	8.87	8.97	8.97	9.03	9.07	9.13	9.22	9.23	9.29	9.34	9.39	9.44	9.48	9.50	9.45	9.45	9.49
HD106516	7.11	6.71	6.44	6.25	6.18	6.12	6.07	6.02	5.98	5.96	5.91	5.90	5.88	5.87	5.87	5.88	5.90	5.89	5.90	5.93
HD107582	9.49	9.16	8.79	8.49	8.37	8.30	8.21	8.13	8.07	8.03	7.97	7.94	7.91	7.90	7.89	7.88	7.89	7.87	7.88	7.91
HD108945	6.48	5.53	5.34	5.25	5.36	5.39	5.42	5.44	5.49	5.58	5.58	5.63	5.68	5.73	5.78	5.83	5.88	5.86	5.86	5.92
HD109995	8.66	7.63	7.48	7.42	7.52	7.51	7.56	7.60	7.65	7.73	7.74	7.78	7.83	7.87	7.91	7.95	7.96	7.91	7.91	7.95
HD110885	10.45	9.95	9.63	9.40	9.27	9.17	9.08	8.99	8.92	8.86	8.80	8.76	8.72	8.69	8.68	8.67	8.69	8.66	8.67	8.70
HD111464	10.16	9.36	8.31	7.45	7.07	6.85	6.53	6.31	6.16	6.03	5.89	5.84	5.75	5.64	5.62	5.56	5.51	5.39	5.39	5.38
HD111515	9.56	9.22	8.77	8.41	8.26	8.18	8.07	7.98	7.93	7.89	7.83	7.81	7.79	7.78	7.76	7.75	7.76	7.72	7.72	7.74
HD111721	9.53	9.14	8.74	8.38	8.18	8.06	7.93	7.82	7.73	7.65	7.56	7.51	7.47	7.43	7.40	7.38	7.38	7.34	7.35	7.37
HD111786	7.15	6.41	6.20	6.09	6.14	6.11	6.11	6.11	6.12	6.14	6.11	6.12	6.12	6.13	6.15	6.17	6.20	6.20	6.21	6.25
HD113002	10.36	9.92	9.48	9.12	8.94	8.83	8.72	8.62	8.54	8.48	8.41	8.38	8.34	8.31	8.29	8.27	8.27	8.22	8.22	8.23
HD113092	8.53	7.83	6.89	6.11	5.76	5.57	5.31	5.12	4.98	4.85	4.72	4.65	4.57	4.48	4.45	4.40	4.36	4.28	4.28	4.27
HD114330	5.29	4.30	4.21	4.19	4.31	4.34	4.38	4.39	4.44	4.53	4.54	4.59	4.64	4.69	4.75	4.80	4.84	4.80	4.83	4.90
HD114710	5.50	5.12	4.71	4.44	4.35	4.28	4.20	4.12	4.08	4.04	3.98	3.96	3.95	3.93	3.92	3.93	3.96	3.93	3.95	3.99
HD115617	6.29	5.91	5.40	5.02	4.88	4.81	4.69	4.58	4.51	4.46	4.39	4.36	4.34	4.31	4.30	4.29	4.32	4.29	4.31	4.34
HD117880	10.13	9.10	8.99	8.94	9.03	9.02	9.06	9.08	9.12	9.19	9.19	9.22	9.26	9.30	9.35	9.39	9.41	9.37	9.38	9.43
HD118055	11.63	10.95	10.21	9.62	9.26	9.02	8.79	8.61	8.44	8.29	8.14	8.05	7.96	7.88	7.82	7.77	7.75	7.67	7.66	7.67
HD121146	9.39	8.65	7.76	7.02	6.74	6.60	6.33	6.15	6.03	5.92	5.80	5.77	5.70	5.62	5.62	5.58	5.55	5.46	5.49	5.50
HD122064	9.05	8.44	7.65	6.96	6.79	6.71	6.41	6.22	6.11	6.02	5.92	5.88	5.82	5.76	5.76	5.74	5.73	5.67	5.70	5.73
HD122956	9.30	8.80	8.26	7.81	7.54	7.36	7.19	7.03	6.91	6.80	6.69	6.61	6.55	6.49	6.44	6.40	6.39	6.34	6.34	6.34
HD124186	9.40	8.59	7.62	6.82	6.49	6.34	6.07	5.87	5.75	5.66	5.54	5.52	5.45	5.35	5.37	5.34	5.29	5.18	5.23	5.24
HD124425	7.09	6.58	6.25	6.04	5.97	5.91	5.86	5.81	5.78	5.76	5.71	5.71	5.70	5.69	5.69	5.70	5.74	5.72	5.74	5.77
HD124547	8.18	7.44	6.46	5.61	5.25	5.05	4.73	4.52	4.37	4.23	4.09	4.04	3.94	3.85	3.84	3.80	3.75	3.65	3.69	3.71
HD126511	10.07	9.65	9.09	8.67	8.52	8.44	8.32	8.22	8.15	8.10	8.03	8.01	7.98	7.95	7.94	7.93	7.95	7.91	7.93	7.96
HD126614	10.76	10.25	9.62	9.16	8.98	8.89	8.75	8.62	8.57	8.52	8.47	8.47	8.46	8.42	8.44	8.43	8.44	8.38	8.41	8.43
HD128000	9.71	8.83	7.63	6.62	6.25	6.02	5.64	5.41	5.24	5.03	4.89	4.80	4.62	4.50	4.47	4.41	4.37	4.26	4.29	4.29
HD128279	9.21	8.83	8.57	8.34	8.19	8.08	7.98	7.90	7.81	7.74	7.66	7.62	7.57	7.54	7.52	7.50	7.49	7.46	7.48	7.51
HD128801	9.46	8.58	8.51	8.51	8.64	8.66	8.72	8.77	8.82	8.89	8.90	8.95	8.99	9.04	9.09	9.13	9.16	9.13	9.14	9.21
HD128987	8.85	8.46	7.93	7.55	7.39	7.31	7.19	7.07	7.01	6.97	6.90	6.89	6.86	6.84	6.83	6.82	6.86	6.82	6.84	6.88
HD132345	9.15	8.33	7.35	6.56	6.22	6.06	5.80	5.61	5.49	5.40	5.28	5.27	5.20	5.09	5.12	5.08	5.03	4.91	4.97	4.98
HD132475	9.60	9.23	8.98	8.77	8.67	8.59	8.52	8.45	8.39	8.34	8.28	8.25	8.21	8.20	8.18	8.17	8.18	8.16	8.17	8.21
HD134113	9.45	9.08	8.75	8.50	8.39	8.31	8.23	8.16	8.11	8.07	8.02	7.99	7.97	7.95	7.94	7.93	7.95	7.92	7.93	7.95
HD134439	10.48	10.17	9.73	9.36	9.22	9.14	9.01	8.90	8.84	8.78	8.72	8.68	8.65	8.63	8.61	8.60	8.60	8.56	8.56	8.59
HD134440	11.26	10.88	10.34	9.89	9.71	9.62	9.42	9.28	9.18	9.10	9.01	8.95	8.90	8.85	8.83	8.80	8.80	8.75	8.75	8.78
HD138716	7.04	6.47	5.72	5.12	4.88	4.76	4.55	4.39	4.29	4.21	4.12	4.09	4.05	3.99	3.99	3.97	3.96	3.91	3.94	3.97
HD140232	6.91	6.09	5.84	5.69	5.77	5.76	5.77	5.77	5.79	5.86	5.83	5.85	5.88	5.90	5.93	5.96	6.00	5.99	6.00	6.04
HD141851	6.11	5.22	5.03	4.95	5.04	5.04	5.07	5.10	5.13	5.19	5.17	5.20	5.23	5.26	5.30	5.34	5.37	5.36	5.37	5.42
HD142703	7.11	6.43	6.24	6.11	6.13	6.08	6.08	6.08	6.09	6.12	6.11	6.13	6.15	6.17	6.20	6.21	6.24	6.23	6.24	6.27

Table A.2 Continuation

Star name	Alh1	Alh2	Alh3	Alh4	Alh5	Alh6	Alh7	Alh8	Alh9	Alh10	Alh11	Alh12	Alh13	Alh14	Alh15	Alh16	Alh17	Alh18	Alh19	Alh20
HD142860	4.93	4.50	4.19	3.98	3.91	3.85	3.79	3.73	3.70	3.69	3.65	3.65	3.64	3.64	3.66	3.66	3.69	3.68	3.71	3.77
HD143459	6.43	5.49	5.39	5.35	5.45	5.46	5.50	5.55	5.60	5.68	5.68	5.72	5.76	5.81	5.85	5.88	5.89	5.84	5.83	5.88
HD145328	7.15	6.58	5.84	5.23	4.99	4.87	4.68	4.54	4.44	4.35	4.26	4.23	4.18	4.11	4.11	4.09	4.07	3.99	4.02	4.03
HD146051	6.81	5.91	4.68	3.65	3.27	2.99	2.63	2.42	2.25	1.96	1.83	1.69	1.42	1.30	1.23	1.16	1.12	0.99	0.99	0.99
HD146233	6.90	6.53	6.08	5.76	5.63	5.56	5.45	5.36	5.32	5.29	5.24	5.23	5.21	5.20	5.20	5.20	5.24	5.21	5.24	5.28
HD147550	7.17	6.26	6.14	6.08	6.17	6.18	6.22	6.25	6.30	6.37	6.37	6.40	6.44	6.48	6.52	6.56	6.58	6.53	6.53	6.58
HD148293	8.06	7.38	6.52	5.85	5.56	5.42	5.21	5.05	4.94	4.86	4.75	4.73	4.68	4.59	4.61	4.58	4.55	4.46	4.51	4.52
HD148513	9.24	8.36	7.22	6.25	5.87	5.66	5.32	5.10	4.94	4.79	4.65	4.60	4.48	4.36	4.36	4.30	4.24	4.11	4.14	4.13
HD149382	8.32	8.38	8.47	8.56	8.71	8.80	8.91	9.00	9.10	9.22	9.30	9.39	9.47	9.55	9.64	9.70	9.78	9.84	9.91	9.99
HD160346	8.83	8.30	7.56	6.95	6.78	6.70	6.46	6.29	6.19	6.10	6.01	5.96	5.90	5.84	5.81	5.79	5.79	5.73	5.74	5.75
HD160922	5.91	5.42	5.10	4.89	4.84	4.78	4.73	4.69	4.67	4.68	4.64	4.65	4.65	4.66	4.67	4.67	4.71	4.69	4.70	4.73
HD161770	10.96	10.56	10.27	10.04	9.90	9.77	9.65	9.54	9.45	9.38	9.29	9.24	9.19	9.15	9.12	9.10	9.10	9.06	9.06	9.08
HD163346	8.44	7.57	7.26	7.01	6.94	6.83	6.73	6.64	6.57	6.53	6.45	6.43	6.39	6.35	6.34	6.33	6.33	6.27	6.29	6.32
HD163641	6.90	6.19	6.12	6.10	6.19	6.20	6.24	6.29	6.35	6.43	6.46	6.51	6.56	6.62	6.67	6.70	6.73	6.70	6.71	6.75
HD163810	10.69	10.38	10.09	9.86	9.75	9.66	9.58	9.49	9.44	9.40	9.34	9.32	9.29	9.28	9.27	9.27	9.29	9.27	9.29	9.33
HD164257	7.81	6.84	6.72	6.65	6.72	6.74	6.75	6.77	6.82	6.89	6.90	6.94	6.98	7.01	7.05	7.08	7.09	7.03	7.03	7.07
HD164402	5.53	5.49	5.53	5.58	5.63	5.67	5.72	5.77	5.81	5.86	5.89	5.92	5.97	6.02	6.06	6.10	6.15	6.17	6.21	6.28
HD164967	8.29	7.35	7.16	7.07	7.17	7.15	7.18	7.21	7.24	7.31	7.29	7.32	7.34	7.38	7.42	7.45	7.48	7.46	7.45	7.49
HD165195	10.11	9.39	8.71	8.17	7.79	7.52	7.26	7.05	6.87	6.70	6.55	6.44	6.34	6.26	6.18	6.13	6.09	6.02	6.00	6.00
HD165341	5.98	5.55	4.96	4.49	4.32	4.24	4.08	3.93	3.86	3.79	3.71	3.69	3.65	3.62	3.61	3.60	3.62	3.58	3.61	3.64
HD166229	8.40	7.69	6.82	6.09	5.80	5.66	5.42	5.25	5.15	5.07	4.97	4.97	4.91	4.83	4.85	4.81	4.77	4.67	4.71	4.72
HD166283	8.91	8.05	7.82	7.68	7.76	7.72	7.72	7.71	7.73	7.79	7.75	7.77	7.79	7.82	7.85	7.88	7.92	7.90	7.91	7.96
HD166991	7.89	6.98	6.77	6.67	6.78	6.77	6.81	6.84	6.88	6.95	6.93	6.97	7.00	7.04	7.08	7.12	7.16	7.14	7.14	7.19
HD167105	9.96	8.93	8.81	8.77	8.89	8.89	8.94	8.97	9.02	9.11	9.12	9.17	9.22	9.27	9.32	9.37	9.39	9.35	9.36	9.43
HD167278	9.21	8.75	8.46	8.28	8.24	8.18	8.14	8.09	8.07	8.07	8.04	8.05	8.05	8.06	8.07	8.08	8.12	8.10	8.14	8.18
HD167946	8.11	7.28	7.18	7.14	7.26	7.26	7.30	7.34	7.38	7.46	7.45	7.49	7.53	7.58	7.63	7.67	7.71	7.69	7.70	7.76
HD169191	8.35	7.67	6.72	5.96	5.63	5.45	5.18	4.98	4.85	4.72	4.59	4.54	4.47	4.37	4.36	4.33	4.30	4.23	4.26	4.27
HD170737	9.79	9.40	8.91	8.50	8.32	8.21	8.08	7.96	7.87	7.79	7.70	7.66	7.61	7.57	7.54	7.52	7.52	7.48	7.48	7.49
HD170973	7.00	6.26	6.21	6.18	6.28	6.38	6.39	6.42	6.48	6.56	6.57	6.62	6.66	6.71	6.77	6.82	6.85	6.82	6.84	6.90
HD172230	8.42	7.56	7.27	7.10	7.13	7.11	7.10	7.10	7.13	7.19	7.17	7.20	7.24	7.26	7.29	7.31	7.34	7.29	7.28	7.31
HD172506	9.04	8.38	8.13	7.97	7.97	7.93	7.92	7.91	7.91	7.94	7.91	7.93	7.94	7.95	7.97	8.00	8.04	8.03	8.06	8.10
HD173158	11.33	10.63	9.67	8.95	8.50	8.17	7.82	7.54	7.38	7.23	7.03	6.94	6.82	6.69	6.63	6.55	6.50	6.35	6.36	6.34
HD174240	7.18	6.22	6.09	6.04	6.15	6.16	6.21	6.25	6.30	6.39	6.39	6.43	6.48	6.52	6.57	6.61	6.64	6.60	6.60	6.64
HD174959	6.26	5.79	5.79	5.83	5.95	6.00	6.07	6.13	6.18	6.26	6.29	6.34	6.39	6.44	6.50	6.55	6.61	6.61	6.64	6.72
HD174966	8.85	8.07	7.82	7.67	7.71	7.67	7.66	7.64	7.65	7.69	7.66	7.67	7.69	7.71	7.74	7.77	7.81	7.80	7.82	7.87
HD175156	5.60	5.14	5.09	5.06	5.07	5.04	5.05	5.06	5.06	5.08	5.06	5.07	5.08	5.10	5.12	5.14	5.15	5.12	5.15	5.21
HD175305	8.66	8.26	7.88	7.55	7.37	7.26	7.14	7.04	6.96	6.90	6.83	6.81	6.77	6.74	6.73	6.71	6.71	6.68	6.69	6.72
HD175545	10.40	9.68	8.78	8.05	7.75	7.60	7.33	7.15	7.03	6.94	6.84	6.81	6.76	6.67	6.68	6.64	6.61	6.51	6.53	6.53
HD175640	6.68	6.01	5.97	5.97	6.09	6.12	6.18	6.23	6.28	6.35	6.36	6.41	6.45	6.50	6.56	6.60	6.65	6.63	6.66	6.72
HD175674	10.03	9.27	8.27	7.40	7.03	6.86	6.58	6.38	6.24	6.13	5.98	5.95	5.86	5.74	5.77	5.72	5.66	5.54	5.61	5.63

Table A.2 Continuation

Star name	Alh1	Alh2	Alh3	Alh4	Alh5	Alh6	Alh7	Alh8	Alh9	Alh10	Alh11	Alh12	Alh13	Alh14	Alh15	Alh16	Alh17	Alh18	Alh19	Alh20
HD175805	8.95	8.46	8.07	7.83	7.74	7.66	7.59	7.53	7.50	7.48	7.43	7.43	7.42	7.41	7.42	7.43	7.48	7.46	7.48	7.52
HD176232	7.03	6.29	5.99	5.85	5.89	5.87	5.87	5.86	5.88	5.94	5.92	5.95	5.98	6.01	6.05	6.09	6.14	6.13	6.14	6.20
HD181720	9.05	8.68	8.34	8.07	7.96	7.89	7.81	7.74	7.69	7.65	7.59	7.56	7.54	7.52	7.51	7.50	7.52	7.49	7.51	7.53
HD183324	6.77	5.88	5.69	5.60	5.73	5.72	5.76	5.80	5.85	5.94	5.94	5.98	6.02	6.07	6.12	6.16	6.21	6.21	6.22	6.27
HD183915	10.29	9.72	8.89	8.06	7.67	7.48	7.24	7.04	6.92	6.81	6.67	6.64	6.55	6.45	6.47	6.42	6.36	6.26	6.32	6.34
HD184266	8.92	8.34	8.07	7.87	7.75	7.64	7.55	7.46	7.39	7.34	7.28	7.24	7.21	7.19	7.17	7.17	7.17	7.15	7.16	7.20
HD185144	6.42	6.03	5.46	5.01	4.85	4.77	4.62	4.49	4.42	4.35	4.27	4.24	4.21	4.17	4.15	4.14	4.16	4.12	4.13	4.15
HD185351	7.33	6.83	6.15	5.63	5.41	5.29	5.12	4.97	4.88	4.81	4.71	4.69	4.65	4.59	4.59	4.57	4.57	4.52	4.55	4.58
HD187111	10.37	9.75	9.04	8.48	8.14	7.89	7.66	7.46	7.30	7.15	7.01	6.91	6.81	6.73	6.66	6.62	6.59	6.52	6.51	6.50
HD188262	9.50	8.85	8.51	8.16	7.97	7.82	7.66	7.51	7.42	7.35	7.24	7.21	7.16	7.09	7.10	7.08	7.06	6.98	7.03	7.05
HD190073	8.71	7.85	7.73	7.69	7.77	7.76	7.80	7.81	7.84	7.81	7.87	7.88	7.89	7.91	7.94	7.96	7.89	7.91	7.91	7.96
HD190360	7.40	6.98	6.43	6.04	5.88	5.80	5.69	5.59	5.53	5.48	5.41	5.39	5.36	5.33	5.32	5.31	5.32	5.28	5.30	5.32
HD191277	8.47	7.72	6.80	6.05	5.75	5.60	5.34	5.15	5.04	4.95	4.85	4.83	4.77	4.68	4.69	4.66	4.62	4.53	4.56	4.56
HD194453	7.51	6.65	6.57	6.55	6.65	6.68	6.73	6.79	6.85	6.95	6.97	7.03	7.09	7.14	7.20	7.24	7.26	7.22	7.22	7.27
HD195434	11.34	10.91	10.32	9.81	9.64	9.54	9.32	9.17	9.08	8.99	8.92	8.87	8.80	8.75	8.72	8.69	8.68	8.63	8.61	8.61
HD196218	8.58	8.14	7.80	7.57	7.50	7.44	7.38	7.33	7.29	7.26	7.21	7.19	7.17	7.16	7.16	7.17	7.20	7.18	7.20	7.24
HD196426	6.55	5.97	5.94	5.96	6.08	6.12	6.20	6.27	6.34	6.42	6.46	6.52	6.57	6.62	6.69	6.73	6.77	6.76	6.78	6.84
HD196662	5.38	4.94	4.95	5.00	5.11	5.17	5.24	5.29	5.36	5.45	5.49	5.55	5.60	5.66	5.73	5.78	5.84	5.85	5.89	5.97
HD196725	9.47	8.66	7.53	6.62	6.18	5.94	5.61	5.38	5.22	5.08	4.91	4.86	4.75	4.62	4.62	4.57	4.51	4.38	4.42	4.43
HD196892	9.27	8.89	8.62	8.42	8.34	8.27	8.21	8.16	8.11	8.08	8.02	8.00	7.98	7.96	7.96	7.95	7.97	7.95	7.96	7.99
HD197177	8.01	7.49	6.74	6.18	5.91	5.76	5.59	5.44	5.34	5.25	5.14	5.12	5.06	4.99	4.99	4.97	4.95	4.87	4.92	4.94
HD198809	6.42	5.97	5.39	4.96	4.76	4.66	4.52	4.40	4.33	4.26	4.17	4.15	4.11	4.07	4.07	4.05	4.06	4.01	4.04	4.07
HD200081	9.84	9.23	8.72	8.32	8.15	8.04	7.91	7.80	7.72	7.66	7.56	7.54	7.49	7.44	7.44	7.42	7.43	7.37	7.39	7.42
HD201091	8.09	7.48	6.56	5.75	5.61	5.50	5.11	4.89	4.75	4.63	4.55	4.47	4.37	4.30	4.25	4.22	4.20	4.13	4.11	4.11
HD201377	7.74	6.88	6.66	6.54	6.63	6.61	6.64	6.65	6.68	6.73	6.71	6.73	6.76	6.78	6.82	6.85	6.89	6.88	6.89	6.94
HD201601	5.80	5.13	4.80	4.63	4.68	4.65	4.64	4.63	4.64	4.69	4.65	4.66	4.68	4.71	4.74	4.77	4.82	4.81	4.82	4.87
HD203638	8.28	7.57	6.71	5.98	5.68	5.54	5.31	5.14	5.03	4.95	4.84	4.82	4.77	4.67	4.70	4.67	4.63	4.53	4.58	4.60
HD204041	7.51	6.67	6.46	6.34	6.43	6.40	6.42	6.44	6.48	6.55	6.54	6.57	6.61	6.64	6.68	6.71	6.74	6.72	6.72	6.76
HD204155	9.68	9.31	8.98	8.71	8.60	8.52	8.44	8.37	8.33	8.31	8.27	8.26	8.25	8.24	8.23	8.23	8.24	8.21	8.21	8.23
HD204543	10.23	9.71	9.20	8.81	8.56	8.39	8.24	8.11	7.99	7.90	7.80	7.74	7.68	7.63	7.59	7.57	7.56	7.52	7.52	7.54
HD205202	9.19	8.63	8.38	8.21	8.16	8.11	8.07	8.03	8.01	8.00	7.96	7.96	7.95	7.95	7.96	7.96	7.98	7.96	7.98	8.00
HD205811	7.11	6.22	6.05	5.98	6.10	6.10	6.15	6.21	6.27	6.38	6.38	6.44	6.49	6.54	6.60	6.64	6.69	6.66	6.66	6.70
HD210807	6.87	6.40	5.75	5.26	5.02	4.89	4.74	4.59	4.51	4.43	4.35	4.33	4.29	4.24	4.25	4.23	4.22	4.17	4.22	4.26
HD212516	12.98	12.05	10.79	9.74	9.35	9.01	8.65	8.44	8.27	7.93	7.82	7.64	7.31	7.21	7.10	7.01	6.96	6.83	6.80	6.79
HD217107	7.91	7.47	6.90	6.49	6.32	6.24	6.12	6.01	5.96	5.93	5.87	5.87	5.86	5.83	5.83	5.82	5.84	5.79	5.80	5.82
HD217357	11.08	10.41	9.51	8.59	8.43	8.23	7.77	7.51	7.33	7.12	7.04	6.89	6.70	6.60	6.53	6.49	6.46	6.39	6.36	6.36
HD221377	8.60	8.10	7.85	7.68	7.63	7.58	7.54	7.51	7.48	7.47	7.43	7.42	7.41	7.41	7.41	7.42	7.44	7.42	7.44	7.47
HD224926	5.25	4.78	4.78	4.83	4.96	5.02	5.09	5.15	5.21	5.29	5.32	5.38	5.43	5.48	5.55	5.60	5.66	5.67	5.71	5.78
HD284248	10.17	9.79	9.58	9.42	9.35	9.27	9.22	9.16	9.12	9.09	9.04	9.02	9.01	9.00	9.00	9.00	9.03	9.02	9.05	9.09
HD93521	6.44	6.46	6.56	6.69	6.80	6.90	7.00	7.09	7.18	7.28	7.36	7.44	7.52	7.59	7.67	7.73	7.80	7.86	7.92	7.98

Table A.2 Continuation

Star name	Alh1	Alh2	Alh3	Alh4	Alh5	Alh6	Alh7	Alh8	Alh9	Alh10	Alh11	Alh12	Alh13	Alh14	Alh15	Alh16	Alh17	Alh18	Alh19	Alh20
HR0753	8.07	7.55	6.81	6.21	6.07	6.02	5.74	5.57	5.48	5.40	5.33	5.30	5.26	5.22	5.21	5.20	5.19	5.13	5.14	5.17
HR8086	9.09	8.42	7.52	6.62	6.48	6.27	5.82	5.57	5.39	5.19	5.13	4.98	4.81	4.73	4.65	4.61	4.58	4.51	4.48	4.49
HZ44	10.99	11.11	11.23	11.36	11.47	11.57	11.66	11.76	11.86	11.98	12.07	12.15	12.24	12.33	12.40	12.48	12.55	12.62	12.69	12.76
MMJ6476	12.76	11.96	11.69	11.52	11.54	11.50	11.47	11.46	11.48	11.53	11.52	11.54	11.57	11.59	11.62	11.63	11.66	11.64	11.63	11.66
MMJ6490	11.89	10.96	10.77	10.67	10.77	10.75	10.79	10.83	10.88	10.98	10.98	11.03	11.08	11.12	11.17	11.20	11.23	11.20	11.19	11.23
P041c	13.40	13.01	12.56	12.26	12.13	12.05	11.96	11.88	11.84	11.81	11.77	11.75	11.74	11.73	11.72	11.72	11.74	11.71	11.72	11.72
V*BNVul	12.90	11.85	11.61	11.43	11.33	11.16	11.04	10.95	10.89	10.84	10.74	10.68	10.63	10.60	10.55	10.52	10.46	10.38	10.37	10.39
V*GKCom	10.74	9.75	8.66	8.00	7.63	7.08	6.90	6.80	6.57	5.98	5.94	5.50	4.73	4.75	4.43	4.26	4.28	4.04	3.96	3.97

Table A.3 AB colors of the E/S0 template in the ALHAMBRA system at diffferent redshifts; r is the SLOAN band.

z	Alh1-r	Alh2-r	Alh3-r	Alh4-r	Alh5-r	Alh6-r	Alh7-r	Alh8-r	Alh9-r	Alh10-r
0.00	2.26	1.84	1.26	0.77	0.55	0.45	0.26	0.15	-0.01	-0.09
0.05	2.38	2.12	1.46	0.98	0.56	0.44	0.32	0.14	0.03	-0.12
0.10	2.41	2.11	1.84	1.14	0.68	0.39	0.31	0.18	0.00	-0.11
0.15	2.53	2.19	1.90	1.39	0.89	0.46	0.25	0.20	0.01	-0.14
0.20	2.80	2.24	1.95	1.74	1.01	0.65	0.30	0.11	0.09	-0.13
0.25	3.00	2.39	2.00	1.69	1.32	0.79	0.44	0.13	-0.01	-0.07
0.30	3.26	2.61	2.02	1.75	1.52	0.92	0.61	0.21	-0.05	-0.14
0.35	3.55	2.77	2.14	1.75	1.45	1.31	0.63	0.37	-0.03	-0.23
0.40	3.81	2.96	2.29	1.72	1.46	1.22	0.92	0.39	0.06	-0.27
0.45	3.96	3.13	2.34	1.73	1.36	1.10	1.01	0.42	0.10	-0.29
0.50	3.95	3.28	2.42	1.79	1.24	1.03	0.76	0.68	-0.02	-0.27
0.55	3.85	3.41	2.55	1.81	1.21	0.91	0.71	0.51	0.13	-0.32
0.60	3.70	3.45	2.71	1.89	1.29	0.81	0.62	0.38	0.33	-0.35
0.65	3.56	3.39	2.85	2.01	1.33	0.81	0.53	0.34	0.09	-0.11
0.70	3.46	3.26	2.93	2.14	1.36	0.88	0.42	0.23	-0.00	-0.09
0.75	3.48	3.21	3.00	2.38	1.56	0.99	0.53	0.23	0.04	-0.22
0.80	3.53	3.19	3.01	2.59	1.77	1.12	0.72	0.24	0.04	-0.18
0.85	3.54	3.16	2.93	2.66	1.95	1.26	0.76	0.32	-0.01	-0.18
0.90	3.55	3.15	2.85	2.67	2.13	1.42	0.85	0.44	-0.05	-0.23
0.95	3.53	3.14	2.78	2.61	2.24	1.57	0.98	0.48	0.02	-0.29
1.00	3.47	3.12	2.72	2.49	2.26	1.72	1.09	0.53	0.12	-0.35
1.05	3.36	3.07	2.66	2.36	2.20	1.81	1.19	0.60	0.11	-0.34
1.10	3.20	2.98	2.58	2.23	2.06	1.80	1.28	0.65	0.08	-0.30
1.15	3.02	2.85	2.49	2.10	1.88	1.72	1.33	0.69	0.10	-0.35
1.20	2.83	2.71	2.40	2.00	1.72	1.60	1.32	0.77	0.14	-0.40
1.25	2.64	2.55	2.30	1.91	1.57	1.43	1.26	0.82	0.17	-0.39
1.30	2.43	2.36	2.17	1.80	1.43	1.24	1.13	0.81	0.20	-0.39
1.35	2.23	2.16	2.01	1.70	1.31	1.06	0.96	0.74	0.25	-0.38
1.40	2.03	1.97	1.85	1.59	1.21	0.91	0.78	0.65	0.27	-0.35
1.45	1.85	1.79	1.70	1.49	1.12	0.81	0.62	0.53	0.25	-0.29
1.50	1.69	1.63	1.56	1.40	1.06	0.73	0.50	0.40	0.21	-0.22
1.55	1.56	1.50	1.44	1.31	1.02	0.69	0.43	0.28	0.16	-0.17
1.60	1.47	1.40	1.34	1.24	1.01	0.68	0.40	0.20	0.11	-0.13
1.65	1.40	1.33	1.27	1.19	1.00	0.70	0.41	0.17	0.05	-0.10
1.70	1.35	1.27	1.21	1.14	0.99	0.73	0.43	0.17	0.01	-0.10
1.75	1.31	1.22	1.16	1.10	0.98	0.76	0.47	0.19	-0.02	-0.11
1.80	1.28	1.18	1.11	1.06	0.96	0.78	0.51	0.22	-0.03	-0.14
1.85	1.25	1.14	1.07	1.01	0.93	0.79	0.55	0.25	-0.02	-0.17
1.90	1.23	1.10	1.02	0.96	0.89	0.78	0.58	0.29	0.00	-0.20
1.95	1.23	1.05	0.97	0.91	0.85	0.75	0.59	0.32	0.02	-0.22
2.00	1.23	1.01	0.91	0.85	0.79	0.71	0.58	0.34	0.03	-0.22
2.05	1.24	0.96	0.85	0.78	0.73	0.66	0.55	0.35	0.05	-0.22
2.10	1.25	0.91	0.79	0.72	0.66	0.61	0.52	0.34	0.06	-0.22
2.15	1.23	0.90	0.73	0.65	0.60	0.55	0.47	0.33	0.07	-0.22
2.20	1.20	0.90	0.68	0.59	0.53	0.48	0.42	0.30	0.08	-0.21
2.25	1.17	0.90	0.63	0.53	0.47	0.43	0.37	0.28	0.09	-0.19
2.30	1.14	0.92	0.59	0.48	0.42	0.37	0.33	0.25	0.09	-0.17
2.35	1.12	0.95	0.56	0.44	0.37	0.32	0.28	0.21	0.08	-0.15
2.40	1.11	0.96	0.58	0.41	0.33	0.28	0.24	0.18	0.07	-0.13
2.45	1.11	0.95	0.61	0.38	0.29	0.24	0.20	0.15	0.06	-0.11
2.50	1.13	0.95	0.65	0.36	0.27	0.21	0.17	0.13	0.05	-0.09

Table A.3 Continuation

z	Alh11-r	Alh12-r	Alh13-r	Alh14-r	Alh15-r	Alh16-r	Alh17-r	Alh18-r	Alh19-r	Alh20-r
0.00	-0.20	-0.26	-0.39	-0.41	-0.43	-0.51	-0.54	-0.63	-0.66	-0.63
0.05	-0.20	-0.31	-0.37	-0.46	-0.54	-0.50	-0.61	-0.61	-0.72	-0.76
0.10	-0.25	-0.31	-0.42	-0.49	-0.55	-0.66	-0.63	-0.69	-0.74	-0.77
0.15	-0.24	-0.37	-0.42	-0.53	-0.61	-0.62	-0.77	-0.75	-0.77	-0.86
0.20	-0.26	-0.34	-0.47	-0.52	-0.63	-0.70	-0.72	-0.86	-0.87	-0.84
0.25	-0.27	-0.37	-0.46	-0.58	-0.63	-0.73	-0.80	-0.82	-0.94	-0.99
0.30	-0.22	-0.40	-0.51	-0.59	-0.71	-0.74	-0.86	-0.92	-0.95	-1.01
0.35	-0.28	-0.38	-0.54	-0.64	-0.74	-0.85	-0.87	-0.99	-1.04	-1.09
0.40	-0.43	-0.45	-0.59	-0.72	-0.82	-0.89	-1.01	-1.03	-1.15	-1.19
0.45	-0.54	-0.66	-0.66	-0.84	-0.96	-1.04	-1.13	-1.24	-1.25	-1.35
0.50	-0.64	-0.82	-0.91	-0.93	-1.12	-1.21	-1.29	-1.38	-1.48	-1.48
0.55	-0.62	-0.92	-1.09	-1.15	-1.18	-1.36	-1.45	-1.52	-1.60	-1.71
0.60	-0.59	-0.92	-1.18	-1.32	-1.36	-1.39	-1.58	-1.67	-1.73	-1.80
0.65	-0.70	-0.88	-1.22	-1.43	-1.55	-1.57	-1.64	-1.80	-1.88	-1.94
0.70	-0.63	-0.94	-1.19	-1.50	-1.68	-1.76	-1.76	-1.87	-2.01	-2.09
0.75	-0.24	-0.92	-1.09	-1.40	-1.67	-1.80	-1.87	-1.87	-2.01	-2.12
0.80	-0.31	-0.58	-1.11	-1.28	-1.60	-1.79	-1.93	-1.98	-1.97	-2.12
0.85	-0.45	-0.42	-1.01	-1.29	-1.51	-1.79	-1.97	-2.10	-2.12	-2.11
0.90	-0.41	-0.62	-0.65	-1.31	-1.46	-1.71	-2.00	-2.14	-2.24	-2.26
0.95	-0.46	-0.67	-0.71	-1.08	-1.54	-1.65	-1.96	-2.19	-2.31	-2.39
1.00	-0.52	-0.67	-0.93	-0.88	-1.52	-1.71	-1.91	-2.19	-2.38	-2.49
1.05	-0.62	-0.78	-0.96	-1.08	-1.22	-1.81	-1.93	-2.17	-2.43	-2.57
1.10	-0.75	-0.89	-1.04	-1.28	-1.24	-1.62	-2.08	-2.19	-2.45	-2.67
1.15	-0.78	-1.04	-1.19	-1.35	-1.55	-1.48	-2.11	-2.33	-2.48	-2.72
1.20	-0.74	-1.16	-1.31	-1.46	-1.69	-1.71	-1.90	-2.48	-2.56	-2.73
1.25	-0.80	-1.18	-1.46	-1.60	-1.74	-1.97	-1.89	-2.34	-2.73	-2.80
1.30	-0.87	-1.17	-1.60	-1.74	-1.90	-2.04	-2.18	-2.16	-2.77	-2.97
1.35	-0.89	-1.25	-1.63	-1.91	-2.04	-2.15	-2.39	-2.34	-2.55	-3.11
1.40	-0.88	-1.32	-1.60	-2.02	-2.18	-2.31	-2.45	-2.65	-2.54	-2.94
1.45	-0.85	-1.32	-1.67	-2.03	-2.31	-2.41	-2.55	-2.76	-2.80	-2.78
1.50	-0.81	-1.28	-1.71	-1.98	-2.40	-2.52	-2.66	-2.77	-3.01	-2.93
1.55	-0.71	-1.21	-1.67	-1.99	-2.36	-2.61	-2.73	-2.86	-3.00	-3.16
1.60	-0.58	-1.11	-1.58	-1.98	-2.24	-2.62	-2.78	-2.90	-3.00	-3.21
1.65	-0.46	-0.97	-1.46	-1.90	-2.21	-2.50	-2.81	-2.92	-3.05	-3.13
1.70	-0.37	-0.81	-1.33	-1.78	-2.17	-2.37	-2.78	-2.93	-3.04	-3.15
1.75	-0.31	-0.66	-1.19	-1.65	-2.07	-2.33	-2.65	-2.94	-3.04	-3.16
1.80	-0.27	-0.55	-1.02	-1.51	-1.95	-2.27	-2.51	-2.90	-3.05	-3.14
1.85	-0.26	-0.47	-0.86	-1.37	-1.82	-2.17	-2.46	-2.75	-3.05	-3.14
1.90	-0.28	-0.43	-0.74	-1.22	-1.69	-2.05	-2.42	-2.62	-3.00	-3.15
1.95	-0.32	-0.42	-0.67	-1.07	-1.57	-1.93	-2.34	-2.59	-2.85	-3.16
2.00	-0.37	-0.44	-0.62	-0.95	-1.44	-1.82	-2.24	-2.57	-2.74	-3.09
2.05	-0.41	-0.49	-0.61	-0.88	-1.31	-1.72	-2.14	-2.50	-2.74	-2.95
2.10	-0.44	-0.54	-0.62	-0.83	-1.19	-1.61	-2.04	-2.41	-2.72	-2.88
2.15	-0.46	-0.59	-0.66	-0.81	-1.11	-1.48	-1.95	-2.32	-2.65	-2.88
2.20	-0.46	-0.63	-0.72	-0.81	-1.05	-1.36	-1.84	-2.22	-2.57	-2.85
2.25	-0.45	-0.65	-0.76	-0.83	-1.01	-1.27	-1.72	-2.13	-2.48	-2.78
2.30	-0.44	-0.65	-0.80	-0.87	-0.99	-1.21	-1.59	-2.02	-2.37	-2.70
2.35	-0.42	-0.64	-0.83	-0.91	-0.99	-1.16	-1.48	-1.90	-2.27	-2.59
2.40	-0.39	-0.62	-0.83	-0.94	-1.00	-1.12	-1.39	-1.76	-2.17	-2.48
2.45	-0.35	-0.59	-0.81	-0.96	-1.03	-1.10	-1.33	-1.63	-2.04	-2.38
2.50	-0.31	-0.55	-0.78	-0.96	-1.04	-1.10	-1.27	-1.53	-1.89	-2.26

Table A.4 AB colors of the Sbc template in the ALHAMBRA system at diffferent redshifts; r is the SLOAN band.

z	Alh1-r	Alh2-r	Alh3-r	Alh4-r	Alh5-r	Alh6-r	Alh7-r	Alh8-r	Alh9-r	Alh10-r
0.00	1.64	1.20	0.87	0.60	0.45	0.36	0.20	0.11	0.01	-0.08
0.05	1.83	1.41	0.96	0.69	0.45	0.34	0.26	0.09	0.01	-0.08
0.10	2.01	1.59	1.13	0.75	0.50	0.33	0.24	0.15	-0.02	-0.09
0.15	2.16	1.74	1.32	0.87	0.59	0.35	0.23	0.13	0.04	-0.12
0.20	2.25	1.91	1.48	1.04	0.63	0.43	0.22	0.12	0.03	-0.08
0.25	2.28	2.02	1.60	1.20	0.76	0.47	0.29	0.10	0.00	-0.08
0.30	2.29	2.09	1.75	1.33	0.91	0.55	0.35	0.14	-0.01	-0.11
0.35	2.27	2.11	1.85	1.45	1.04	0.70	0.36	0.21	-0.02	-0.13
0.40	2.23	2.09	1.89	1.56	1.15	0.80	0.47	0.20	0.04	-0.16
0.45	2.17	2.03	1.87	1.61	1.22	0.88	0.55	0.24	0.02	-0.17
0.50	2.09	1.95	1.81	1.60	1.28	0.91	0.63	0.32	-0.02	-0.17
0.55	1.99	1.86	1.72	1.56	1.29	0.96	0.66	0.35	0.01	-0.23
0.60	1.89	1.77	1.63	1.48	1.27	0.99	0.67	0.39	0.06	-0.25
0.65	1.77	1.65	1.51	1.38	1.21	0.98	0.69	0.38	0.08	-0.24
0.70	1.63	1.52	1.39	1.25	1.11	0.92	0.68	0.37	0.09	-0.25
0.75	1.50	1.40	1.27	1.14	1.00	0.85	0.66	0.38	0.05	-0.22
0.80	1.38	1.28	1.16	1.03	0.90	0.77	0.61	0.38	0.06	-0.22
0.85	1.26	1.17	1.05	0.93	0.80	0.68	0.55	0.36	0.08	-0.25
0.90	1.17	1.07	0.96	0.84	0.71	0.60	0.49	0.33	0.09	-0.21
0.95	1.09	0.97	0.87	0.75	0.63	0.52	0.42	0.28	0.09	-0.19
1.00	1.03	0.89	0.79	0.68	0.56	0.45	0.35	0.24	0.07	-0.16
1.05	1.00	0.83	0.72	0.62	0.51	0.40	0.30	0.20	0.06	-0.14
1.10	1.00	0.80	0.67	0.58	0.47	0.36	0.26	0.17	0.05	-0.12
1.15	1.01	0.78	0.64	0.54	0.44	0.34	0.24	0.14	0.04	-0.10
1.20	1.03	0.79	0.62	0.52	0.42	0.32	0.22	0.13	0.03	-0.09
1.25	1.05	0.81	0.61	0.49	0.40	0.31	0.21	0.12	0.02	-0.09
1.30	1.08	0.84	0.61	0.48	0.39	0.30	0.21	0.11	0.01	-0.08
1.35	1.12	0.87	0.62	0.47	0.37	0.29	0.20	0.11	0.01	-0.08
1.40	1.15	0.90	0.65	0.47	0.36	0.28	0.20	0.11	0.01	-0.08
1.45	1.19	0.93	0.67	0.47	0.35	0.27	0.20	0.11	0.01	-0.08
1.50	1.22	0.96	0.71	0.48	0.34	0.26	0.19	0.11	0.01	-0.08
1.55	1.25	1.00	0.74	0.50	0.34	0.25	0.19	0.10	0.01	-0.08
1.60	1.29	1.03	0.77	0.52	0.34	0.24	0.18	0.10	0.01	-0.08
1.65	1.33	1.07	0.80	0.55	0.35	0.24	0.17	0.10	0.01	-0.08
1.70	1.36	1.10	0.84	0.59	0.37	0.24	0.16	0.10	0.01	-0.07
1.75	1.40	1.14	0.87	0.62	0.39	0.24	0.16	0.09	0.02	-0.07
1.80	1.44	1.17	0.91	0.65	0.41	0.25	0.15	0.09	0.02	-0.07
1.85	1.47	1.21	0.94	0.69	0.45	0.26	0.16	0.08	0.01	-0.06
1.90	1.52	1.25	0.98	0.72	0.48	0.29	0.16	0.08	0.01	-0.06
1.95	1.58	1.28	1.01	0.76	0.51	0.31	0.17	0.08	0.01	-0.06
2.00	1.65	1.32	1.05	0.79	0.55	0.34	0.19	0.08	0.00	-0.06
2.05	1.73	1.35	1.08	0.82	0.58	0.37	0.20	0.08	0.00	-0.06
2.10	1.81	1.39	1.11	0.85	0.61	0.40	0.23	0.09	-0.00	-0.07
2.15	1.87	1.45	1.14	0.88	0.64	0.43	0.25	0.10	-0.01	-0.08
2.20	1.90	1.51	1.17	0.91	0.66	0.45	0.28	0.11	-0.01	-0.08
2.25	1.92	1.58	1.20	0.94	0.69	0.48	0.30	0.12	-0.01	-0.09
2.30	1.95	1.65	1.22	0.96	0.71	0.50	0.32	0.14	-0.01	-0.10
2.35	1.97	1.72	1.24	0.98	0.73	0.52	0.33	0.16	-0.01	-0.11
2.40	1.99	1.77	1.29	1.00	0.74	0.53	0.35	0.17	-0.00	-0.12
2.45	2.02	1.78	1.35	1.01	0.76	0.54	0.36	0.18	0.00	-0.13
2.50	2.05	1.80	1.41	1.02	0.77	0.56	0.37	0.19	0.01	-0.14

Table A.4 Continuation

z	Alh11-r	Alh12-r	Alh13-r	Alh14-r	Alh15-r	Alh16-r	Alh17-r	Alh18-r	Alh19-r	Alh20-r
0.00	-0.16	-0.22	-0.28	-0.33	-0.37	-0.41	-0.45	-0.50	-0.55	-0.60
0.05	-0.17	-0.24	-0.30	-0.36	-0.41	-0.45	-0.49	-0.53	-0.56	-0.60
0.10	-0.18	-0.26	-0.33	-0.39	-0.45	-0.49	-0.53	-0.57	-0.60	-0.64
0.15	-0.19	-0.26	-0.34	-0.41	-0.47	-0.52	-0.57	-0.61	-0.64	-0.67
0.20	-0.22	-0.28	-0.35	-0.43	-0.50	-0.55	-0.60	-0.65	-0.69	-0.72
0.25	-0.20	-0.31	-0.37	-0.44	-0.52	-0.58	-0.64	-0.68	-0.73	-0.76
0.30	-0.18	-0.30	-0.40	-0.46	-0.53	-0.59	-0.66	-0.71	-0.76	-0.80
0.35	-0.22	-0.28	-0.42	-0.50	-0.56	-0.62	-0.69	-0.75	-0.80	-0.84
0.40	-0.26	-0.33	-0.39	-0.54	-0.61	-0.66	-0.73	-0.79	-0.85	-0.89
0.45	-0.32	-0.40	-0.47	-0.54	-0.69	-0.74	-0.79	-0.85	-0.91	-0.96
0.50	-0.38	-0.48	-0.56	-0.62	-0.70	-0.83	-0.88	-0.93	-0.99	-1.05
0.55	-0.37	-0.56	-0.65	-0.73	-0.79	-0.85	-0.99	-1.04	-1.08	-1.14
0.60	-0.43	-0.58	-0.74	-0.82	-0.90	-0.94	-1.03	-1.15	-1.19	-1.23
0.65	-0.52	-0.63	-0.82	-0.93	-1.01	-1.07	-1.12	-1.21	-1.32	-1.36
0.70	-0.54	-0.73	-0.84	-1.04	-1.14	-1.19	-1.26	-1.31	-1.40	-1.50
0.75	-0.51	-0.79	-0.94	-1.07	-1.24	-1.31	-1.38	-1.43	-1.48	-1.57
0.80	-0.52	-0.77	-1.02	-1.13	-1.31	-1.41	-1.49	-1.56	-1.60	-1.64
0.85	-0.49	-0.76	-1.03	-1.21	-1.31	-1.49	-1.59	-1.66	-1.72	-1.75
0.90	-0.47	-0.73	-0.98	-1.25	-1.39	-1.47	-1.66	-1.74	-1.80	-1.86
0.95	-0.49	-0.69	-0.97	-1.22	-1.44	-1.54	-1.68	-1.81	-1.89	-1.93
1.00	-0.44	-0.69	-0.93	-1.17	-1.44	-1.58	-1.67	-1.84	-1.94	-2.01
1.05	-0.38	-0.66	-0.85	-1.13	-1.36	-1.59	-1.72	-1.80	-1.97	-2.05
1.10	-0.33	-0.58	-0.85	-1.05	-1.30	-1.50	-1.73	-1.83	-1.92	-2.07
1.15	-0.28	-0.50	-0.77	-0.98	-1.24	-1.43	-1.68	-1.82	-1.90	-2.03
1.20	-0.25	-0.44	-0.68	-0.94	-1.12	-1.36	-1.57	-1.81	-1.92	-1.97
1.25	-0.22	-0.38	-0.60	-0.85	-1.07	-1.27	-1.49	-1.70	-1.89	-1.99
1.30	-0.20	-0.34	-0.52	-0.76	-1.02	-1.15	-1.42	-1.61	-1.83	-1.95
1.35	-0.18	-0.30	-0.46	-0.67	-0.92	-1.12	-1.31	-1.52	-1.70	-1.93
1.40	-0.17	-0.28	-0.42	-0.60	-0.83	-1.04	-1.22	-1.46	-1.63	-1.80
1.45	-0.17	-0.26	-0.38	-0.54	-0.74	-0.94	-1.18	-1.31	-1.56	-1.72
1.50	-0.17	-0.25	-0.36	-0.49	-0.67	-0.85	-1.09	-1.27	-1.46	-1.63
1.55	-0.17	-0.25	-0.34	-0.46	-0.61	-0.77	-1.00	-1.23	-1.34	-1.57
1.60	-0.17	-0.24	-0.33	-0.43	-0.57	-0.71	-0.92	-1.13	-1.32	-1.44
1.65	-0.16	-0.24	-0.32	-0.41	-0.53	-0.65	-0.84	-1.04	-1.25	-1.38
1.70	-0.16	-0.24	-0.32	-0.40	-0.50	-0.61	-0.77	-0.96	-1.16	-1.35
1.75	-0.15	-0.23	-0.31	-0.39	-0.48	-0.58	-0.72	-0.88	-1.07	-1.26
1.80	-0.15	-0.23	-0.31	-0.38	-0.46	-0.55	-0.67	-0.82	-0.99	-1.17
1.85	-0.14	-0.22	-0.30	-0.37	-0.45	-0.53	-0.64	-0.77	-0.92	-1.09
1.90	-0.14	-0.21	-0.29	-0.37	-0.44	-0.51	-0.61	-0.72	-0.86	-1.01
1.95	-0.14	-0.21	-0.29	-0.36	-0.44	-0.50	-0.59	-0.69	-0.81	-0.94
2.00	-0.13	-0.20	-0.28	-0.36	-0.43	-0.49	-0.57	-0.66	-0.76	-0.89
2.05	-0.13	-0.20	-0.27	-0.35	-0.42	-0.48	-0.56	-0.64	-0.73	-0.84
2.10	-0.13	-0.20	-0.27	-0.35	-0.42	-0.48	-0.55	-0.62	-0.71	-0.80
2.15	-0.14	-0.20	-0.27	-0.34	-0.42	-0.48	-0.55	-0.61	-0.69	-0.77
2.20	-0.14	-0.20	-0.27	-0.34	-0.42	-0.48	-0.55	-0.61	-0.68	-0.76
2.25	-0.15	-0.21	-0.28	-0.34	-0.42	-0.48	-0.55	-0.61	-0.67	-0.74
2.30	-0.17	-0.22	-0.28	-0.35	-0.42	-0.48	-0.55	-0.61	-0.67	-0.74
2.35	-0.18	-0.24	-0.29	-0.36	-0.43	-0.49	-0.56	-0.62	-0.68	-0.74
2.40	-0.20	-0.25	-0.31	-0.37	-0.44	-0.50	-0.57	-0.63	-0.69	-0.74
2.45	-0.22	-0.27	-0.33	-0.39	-0.45	-0.51	-0.58	-0.64	-0.70	-0.75
2.50	-0.23	-0.29	-0.35	-0.40	-0.47	-0.52	-0.59	-0.65	-0.71	-0.77

Table A.5 AB colors of the Im template in the ALHAMBRA system at diffferent redshifts; r is the SLOAN band.

z	Alh1-r	Alh2-r	Alh3-r	Alh4-r	Alh5-r	Alh6-r	Alh7-r	Alh8-r	Alh9-r	Alh10-r
0.00	0.75	0.55	0.39	0.27	-0.00	0.16	0.13	0.06	-0.00	-0.05
0.05	1.01	0.60	0.42	0.30	0.18	-0.09	0.11	0.07	0.01	-0.06
0.10	1.06	0.83	0.46	0.33	0.22	0.10	-0.12	0.07	0.03	-0.04
0.15	1.15	1.01	0.65	0.44	0.30	0.20	0.09	-0.10	0.07	0.03
0.20	1.19	1.07	0.93	0.47	0.35	0.26	0.16	0.01	-0.07	0.04
0.25	1.20	1.12	0.98	0.64	0.43	0.29	0.21	0.13	-0.17	0.01
0.30	1.20	1.13	1.02	0.89	0.44	0.34	0.24	0.15	0.07	-0.22
0.35	1.14	1.10	1.01	0.87	0.55	0.37	0.21	0.14	0.04	-0.06
0.40	1.06	1.02	0.96	0.85	0.72	0.32	0.22	0.09	0.02	-0.07
0.45	1.01	0.98	0.93	0.85	0.71	0.54	0.15	0.11	0.01	-0.09
0.50	0.96	0.94	0.90	0.83	0.72	0.61	0.26	0.16	-0.01	-0.08
0.55	0.89	0.87	0.85	0.80	0.71	0.60	0.51	0.08	0.01	-0.11
0.60	0.81	0.79	0.77	0.73	0.66	0.57	0.46	0.23	-0.03	-0.14
0.65	0.72	0.70	0.68	0.65	0.59	0.52	0.42	0.33	-0.08	-0.15
0.70	0.62	0.60	0.58	0.56	0.52	0.46	0.38	0.27	0.14	-0.27
0.75	0.53	0.51	0.49	0.47	0.44	0.39	0.33	0.23	0.13	-0.23
0.80	0.44	0.41	0.39	0.37	0.35	0.31	0.26	0.18	0.07	-0.03
0.85	0.34	0.31	0.29	0.27	0.25	0.22	0.18	0.11	0.02	-0.08
0.90	0.31	0.27	0.25	0.23	0.21	0.19	0.15	0.10	0.02	-0.08
0.95	0.28	0.24	0.22	0.19	0.18	0.16	0.13	0.09	0.02	-0.07
1.00	0.27	0.22	0.19	0.16	0.15	0.13	0.11	0.07	0.02	-0.06
1.05	0.26	0.20	0.16	0.14	0.12	0.11	0.09	0.06	0.02	-0.05
1.10	0.27	0.19	0.15	0.12	0.10	0.09	0.07	0.05	0.01	-0.04
1.15	0.28	0.19	0.14	0.11	0.09	0.07	0.06	0.04	0.01	-0.03
1.20	0.29	0.20	0.13	0.10	0.08	0.06	0.05	0.03	0.01	-0.03
1.25	0.31	0.21	0.14	0.10	0.07	0.06	0.04	0.03	0.01	-0.02
1.30	0.33	0.23	0.14	0.09	0.07	0.05	0.04	0.02	0.01	-0.02
1.35	0.35	0.25	0.16	0.10	0.07	0.05	0.03	0.02	0.01	-0.02
1.40	0.37	0.27	0.17	0.10	0.07	0.05	0.03	0.02	0.00	-0.01
1.45	0.39	0.29	0.19	0.11	0.07	0.05	0.03	0.02	0.00	-0.01
1.50	0.42	0.31	0.21	0.12	0.07	0.05	0.03	0.01	0.00	-0.01
1.55	0.44	0.33	0.23	0.14	0.08	0.05	0.03	0.01	0.00	-0.01
1.60	0.47	0.36	0.25	0.16	0.09	0.05	0.03	0.02	0.00	-0.01
1.65	0.49	0.38	0.27	0.17	0.10	0.05	0.03	0.02	0.00	-0.01
1.70	0.52	0.40	0.29	0.19	0.11	0.06	0.03	0.02	0.00	-0.01
1.75	0.54	0.42	0.31	0.21	0.12	0.07	0.04	0.02	0.00	-0.01
1.80	0.56	0.45	0.33	0.23	0.14	0.08	0.04	0.02	0.00	-0.01
1.85	0.59	0.47	0.35	0.25	0.15	0.09	0.04	0.02	0.00	-0.01
1.90	0.62	0.49	0.37	0.27	0.17	0.10	0.05	0.02	-0.00	-0.02
1.95	0.67	0.51	0.39	0.28	0.19	0.11	0.06	0.02	-0.00	-0.02
2.00	0.73	0.53	0.41	0.30	0.20	0.12	0.06	0.02	-0.00	-0.02
2.05	0.80	0.55	0.43	0.32	0.22	0.14	0.07	0.03	-0.00	-0.02
2.10	0.87	0.57	0.45	0.33	0.23	0.15	0.08	0.03	-0.00	-0.02
2.15	0.91	0.62	0.46	0.35	0.24	0.16	0.09	0.04	-0.00	-0.03
2.20	0.93	0.68	0.48	0.36	0.26	0.17	0.10	0.04	-0.01	-0.03
2.25	0.95	0.73	0.49	0.37	0.27	0.18	0.11	0.05	-0.01	-0.04
2.30	0.97	0.80	0.51	0.39	0.28	0.19	0.12	0.05	-0.00	-0.04
2.35	0.99	0.87	0.52	0.40	0.29	0.20	0.13	0.06	-0.00	-0.05
2.40	1.01	0.91	0.57	0.41	0.30	0.21	0.13	0.06	-0.00	-0.05
2.45	1.04	0.92	0.62	0.42	0.30	0.21	0.14	0.07	-0.00	-0.05
2.50	1.07	0.94	0.68	0.42	0.31	0.22	0.14	0.07	0.00	-0.06

Table A.5 Continuation

z	Alh11-r	Alh12-r	Alh13-r	Alh14-r	Alh15-r	Alh16-r	Alh17-r	Alh18-r	Alh19-r	Alh20-r
0.00	-0.09	-0.13	-0.16	-0.19	-0.21	-0.23	-0.25	-0.27	-0.30	-0.32
0.05	-0.10	-0.14	-0.17	-0.21	-0.23	-0.25	-0.27	-0.29	-0.31	-0.33
0.10	-0.10	-0.13	-0.17	-0.21	-0.24	-0.26	-0.29	-0.31	-0.32	-0.34
0.15	-0.04	-0.08	-0.12	-0.16	-0.20	-0.22	-0.25	-0.27	-0.29	-0.31
0.20	0.00	-0.06	-0.10	-0.14	-0.18	-0.21	-0.24	-0.26	-0.28	-0.30
0.25	0.01	-0.03	-0.08	-0.13	-0.17	-0.20	-0.23	-0.26	-0.28	-0.30
0.30	0.01	-0.02	-0.06	-0.12	-0.17	-0.20	-0.23	-0.26	-0.29	-0.31
0.35	-0.30	-0.07	-0.10	-0.14	-0.20	-0.24	-0.27	-0.30	-0.33	-0.35
0.40	-0.21	-0.38	-0.18	-0.20	-0.25	-0.29	-0.34	-0.37	-0.40	-0.42
0.45	-0.15	-0.36	-0.37	-0.24	-0.27	-0.31	-0.36	-0.40	-0.43	-0.45
0.50	-0.17	-0.21	-0.54	-0.35	-0.30	-0.33	-0.37	-0.42	-0.45	-0.48
0.55	-0.17	-0.26	-0.33	-0.61	-0.35	-0.38	-0.41	-0.44	-0.49	-0.52
0.60	-0.22	-0.29	-0.36	-0.46	-0.72	-0.44	-0.47	-0.50	-0.54	-0.58
0.65	-0.29	-0.33	-0.42	-0.47	-0.61	-0.83	-0.55	-0.57	-0.60	-0.64
0.70	-0.31	-0.41	-0.45	-0.54	-0.58	-0.75	-0.86	-0.66	-0.67	-0.71
0.75	-0.30	-0.45	-0.51	-0.58	-0.66	-0.68	-1.00	-0.86	-0.76	-0.77
0.80	-0.47	-0.47	-0.59	-0.64	-0.71	-0.77	-0.86	-1.15	-0.88	-0.87
0.85	-0.41	-0.55	-0.63	-0.72	-0.76	-0.84	-0.89	-0.99	-1.28	-0.97
0.90	-0.15	-0.58	-0.59	-0.72	-0.78	-0.83	-0.90	-0.94	-1.06	-1.33
0.95	-0.17	-0.32	-0.67	-0.68	-0.79	-0.82	-0.90	-0.96	-0.99	-1.12
1.00	-0.15	-0.22	-0.64	-0.63	-0.77	-0.84	-0.88	-0.95	-1.00	-1.02
1.05	-0.13	-0.22	-0.28	-0.73	-0.72	-0.83	-0.88	-0.93	-1.00	-1.04
1.10	-0.11	-0.19	-0.27	-0.60	-0.70	-0.76	-0.88	-0.91	-0.98	-1.03
1.15	-0.09	-0.17	-0.26	-0.30	-0.78	-0.71	-0.84	-0.92	-0.94	-1.01
1.20	-0.08	-0.14	-0.22	-0.30	-0.49	-0.82	-0.78	-0.90	-0.95	-0.97
1.25	-0.06	-0.12	-0.19	-0.28	-0.33	-0.73	-0.75	-0.82	-0.93	-0.97
1.30	-0.05	-0.10	-0.16	-0.24	-0.33	-0.35	-0.82	-0.78	-0.88	-0.95
1.35	-0.05	-0.08	-0.14	-0.21	-0.29	-0.34	-0.66	-0.80	-0.81	-0.92
1.40	-0.04	-0.07	-0.12	-0.18	-0.25	-0.33	-0.36	-0.86	-0.75	-0.84
1.45	-0.03	-0.06	-0.10	-0.15	-0.22	-0.29	-0.35	-0.48	-0.88	-0.80
1.50	-0.03	-0.05	-0.09	-0.13	-0.19	-0.25	-0.34	-0.36	-0.76	-0.82
1.55	-0.03	-0.05	-0.07	-0.11	-0.16	-0.22	-0.30	-0.37	-0.39	-0.89
1.60	-0.03	-0.04	-0.07	-0.10	-0.14	-0.19	-0.26	-0.34	-0.38	-0.54
1.65	-0.02	-0.04	-0.06	-0.09	-0.13	-0.17	-0.23	-0.30	-0.37	-0.38
1.70	-0.02	-0.04	-0.05	-0.08	-0.11	-0.15	-0.20	-0.26	-0.33	-0.38
1.75	-0.03	-0.04	-0.05	-0.07	-0.10	-0.13	-0.18	-0.23	-0.30	-0.36
1.80	-0.03	-0.04	-0.05	-0.07	-0.09	-0.12	-0.16	-0.21	-0.27	-0.33
1.85	-0.03	-0.04	-0.05	-0.06	-0.09	-0.11	-0.14	-0.19	-0.24	-0.30
1.90	-0.03	-0.04	-0.05	-0.06	-0.08	-0.10	-0.13	-0.17	-0.22	-0.27
1.95	-0.03	-0.04	-0.05	-0.06	-0.08	-0.10	-0.12	-0.16	-0.20	-0.24
2.00	-0.03	-0.04	-0.06	-0.07	-0.08	-0.09	-0.12	-0.15	-0.18	-0.22
2.05	-0.04	-0.05	-0.06	-0.07	-0.08	-0.09	-0.11	-0.14	-0.17	-0.21
2.10	-0.04	-0.05	-0.06	-0.07	-0.08	-0.10	-0.11	-0.14	-0.16	-0.19
2.15	-0.04	-0.06	-0.07	-0.08	-0.09	-0.10	-0.11	-0.13	-0.16	-0.18
2.20	-0.05	-0.06	-0.07	-0.08	-0.09	-0.10	-0.12	-0.13	-0.15	-0.18
2.25	-0.06	-0.07	-0.08	-0.09	-0.10	-0.11	-0.12	-0.14	-0.16	-0.18
2.30	-0.06	-0.08	-0.09	-0.10	-0.11	-0.12	-0.13	-0.14	-0.16	-0.18
2.35	-0.07	-0.08	-0.10	-0.11	-0.12	-0.13	-0.14	-0.15	-0.16	-0.18
2.40	-0.08	-0.09	-0.11	-0.12	-0.13	-0.14	-0.15	-0.16	-0.17	-0.18
2.45	-0.08	-0.10	-0.12	-0.13	-0.14	-0.15	-0.16	-0.17	-0.18	-0.19
2.50	-0.09	-0.11	-0.13	-0.14	-0.15	-0.16	-0.17	-0.18	-0.19	-0.20

Table A.6 AB colors of the SB2 template in the ALHAMBRA system at diffferent redshifts; r is the SLOAN band.

z	Alh1-r	Alh2-r	Alh3-r	Alh4-r	Alh5-r	Alh6-r	Alh7-r	Alh8-r	Alh9-r	Alh10-r
0.00	0.54	0.47	0.38	0.34	-0.34	0.30	0.30	0.26	0.24	-0.37
0.05	0.52	0.21	0.19	0.10	0.07	-0.66	0.05	0.05	-0.00	-0.03
0.10	0.54	0.49	0.13	0.20	0.10	-0.05	-0.64	0.08	0.07	0.01
0.15	0.90	0.70	0.49	0.37	0.32	0.29	0.10	-0.44	0.26	0.23
0.20	1.01	0.78	0.80	0.37	0.41	0.32	0.30	-0.04	-0.29	0.30
0.25	1.00	0.97	0.73	0.55	0.44	0.41	0.31	0.31	-0.51	0.24
0.30	1.01	1.01	0.79	0.79	0.39	0.42	0.37	0.32	0.29	-0.48
0.35	0.87	0.88	0.83	0.59	0.39	0.34	0.28	0.20	0.19	0.01
0.40	0.69	0.68	0.69	0.47	0.46	0.11	0.09	0.08	-0.01	-0.02
0.45	0.66	0.64	0.64	0.60	0.36	0.41	-0.07	0.05	0.02	-0.06
0.50	0.65	0.64	0.63	0.64	0.42	0.40	0.08	0.09	0.04	-0.04
0.55	0.65	0.60	0.59	0.59	0.54	0.31	0.39	-0.01	-0.01	-0.01
0.60	0.62	0.55	0.52	0.54	0.53	0.36	0.22	0.11	-0.04	-0.06
0.65	0.58	0.52	0.49	0.49	0.48	0.44	0.15	0.28	-0.12	-0.09
0.70	0.57	0.53	0.44	0.41	0.45	0.45	0.31	0.13	0.23	-0.27
0.75	0.51	0.46	0.39	0.38	0.37	0.37	0.36	0.08	0.16	-0.19
0.80	0.43	0.40	0.33	0.30	0.27	0.27	0.28	0.17	-0.03	0.07
0.85	0.33	0.32	0.27	0.17	0.16	0.18	0.18	0.16	-0.12	-0.03
0.90	0.29	0.29	0.25	0.17	0.16	0.14	0.13	0.15	0.04	-0.15
0.95	0.21	0.27	0.24	0.19	0.13	0.09	0.13	0.12	0.10	-0.17
1.00	0.13	0.22	0.22	0.16	0.08	0.07	0.08	0.05	0.08	-0.03
1.05	0.08	0.16	0.16	0.13	0.06	0.05	-0.02	0.04	0.03	0.02
1.10	0.06	0.11	0.16	0.13	0.08	-0.01	-0.00	0.02	-0.01	0.02
1.15	0.08	0.06	0.16	0.15	0.09	0.00	0.04	-0.04	0.03	0.00
1.20	0.12	0.06	0.14	0.14	0.10	0.05	-0.01	-0.00	0.02	-0.02
1.25	0.14	0.05	0.11	0.15	0.12	0.10	-0.02	0.03	-0.02	0.01
1.30	0.19	0.07	0.07	0.17	0.14	0.08	0.04	0.03	-0.02	0.01
1.35	0.17	0.10	0.04	0.14	0.14	0.10	0.10	-0.03	-0.00	0.00
1.40	0.12	0.12	0.04	0.11	0.14	0.12	0.07	-0.00	0.03	-0.06
1.45	0.09	0.15	0.04	0.07	0.15	0.12	0.07	0.05	-0.02	-0.02
1.50	0.06	0.16	0.05	0.03	0.12	0.12	0.09	0.07	-0.06	0.00
1.55	0.12	0.11	0.08	0.01	0.09	0.10	0.10	0.03	-0.01	-0.01
1.60	0.16	0.07	0.08	-0.00	0.05	0.11	0.07	0.04	0.04	-0.07
1.65	0.19	0.05	0.11	-0.01	0.01	0.09	0.09	0.05	0.03	-0.08
1.70	0.19	0.04	0.12	-0.00	-0.02	0.07	0.07	0.07	-0.01	-0.04
1.75	0.16	0.07	0.06	0.03	-0.04	0.02	0.07	0.04	0.01	0.00
1.80	0.15	0.09	0.01	0.02	-0.07	-0.03	0.05	0.03	0.01	-0.03
1.85	0.18	0.13	-0.01	0.04	-0.06	-0.07	0.03	0.02	0.02	-0.05
1.90	0.21	0.14	-0.03	0.07	-0.05	-0.07	-0.01	0.03	0.01	-0.03
1.95	0.24	0.13	0.02	0.04	-0.01	-0.09	-0.05	0.03	0.02	-0.01
2.00	0.33	0.12	0.06	-0.00	0.00	-0.09	-0.07	0.02	0.00	0.01
2.05	0.39	0.16	0.10	-0.03	0.03	-0.07	-0.08	-0.02	0.03	-0.00
2.10	0.45	0.19	0.13	-0.04	0.07	-0.04	-0.09	-0.04	0.03	0.02
2.15	0.50	0.25	0.15	-0.01	0.07	-0.00	-0.07	-0.05	0.05	0.02
2.20	0.53	0.31	0.14	0.07	0.03	0.04	-0.05	-0.06	0.02	0.05
2.25	0.56	0.40	0.16	0.12	0.01	0.06	-0.03	-0.06	-0.00	0.05
2.30	0.58	0.47	0.20	0.15	-0.00	0.11	-0.00	-0.05	-0.02	0.07
2.35	0.61	0.53	0.23	0.17	-0.01	0.10	0.05	-0.04	-0.04	0.05
2.40	0.64	0.58	0.28	0.17	0.04	0.07	0.07	-0.02	-0.04	0.02
2.45	0.67	0.60	0.34	0.17	0.10	0.04	0.09	0.00	-0.05	0.00
2.50	0.72	0.62	0.44	0.17	0.14	-0.01	0.12	0.02	-0.04	-0.02

Table A.6 Continuation

z	Alh11-r	Alh12-r	Alh13-r	Alh14-r	Alh15-r	Alh16-r	Alh17-r	Alh18-r	Alh19-r	Alh20-r
0.00	0.07	0.07	0.03	-0.02	-0.04	-0.06	-0.10	-0.21	-0.25	-0.36
0.05	-0.69	-0.32	-0.16	-0.22	-0.25	-0.28	-0.31	-0.33	-0.39	-0.49
0.10	-0.01	-0.61	-0.34	-0.13	-0.20	-0.20	-0.27	-0.29	-0.29	-0.34
0.15	0.19	0.17	-0.06	-0.57	0.08	-0.06	-0.02	-0.09	-0.09	-0.12
0.20	0.23	0.22	0.20	-0.15	-0.56	0.17	-0.02	0.02	-0.04	-0.06
0.25	0.31	0.24	0.23	0.21	0.18	-0.72	0.15	-0.02	0.01	-0.00
0.30	0.29	0.29	0.24	0.22	0.21	0.21	-0.62	0.18	0.02	-0.02
0.35	-0.65	0.16	0.16	0.10	0.09	0.07	0.08	-0.85	-0.09	-0.08
0.40	-0.28	-0.82	-0.03	-0.04	-0.09	-0.10	-0.12	-0.12	-1.01	-0.34
0.45	-0.07	-0.50	-0.72	-0.07	-0.08	-0.13	-0.15	-0.16	-0.15	-1.06
0.50	-0.04	-0.09	-1.01	-0.26	-0.08	-0.09	-0.14	-0.15	-0.17	-0.16
0.55	-0.10	-0.09	-0.24	-0.99	-0.15	-0.11	-0.14	-0.18	-0.19	-0.22
0.60	-0.08	-0.18	-0.17	-0.36	-1.09	-0.21	-0.16	-0.21	-0.24	-0.25
0.65	-0.11	-0.20	-0.18	-0.22	-0.54	-1.18	-0.23	-0.23	-0.27	-0.29
0.70	-0.13	-0.16	-0.27	-0.24	-0.29	-0.70	-1.04	-0.26	-0.27	-0.31
0.75	-0.17	-0.24	-0.23	-0.34	-0.32	-0.36	-1.26	-0.71	-0.33	-0.34
0.80	-0.39	-0.32	-0.31	-0.40	-0.39	-0.42	-0.62	-1.43	-0.50	-0.42
0.85	-0.40	-0.38	-0.40	-0.42	-0.53	-0.49	-0.53	-0.76	-1.53	-0.58
0.90	-0.07	-0.48	-0.42	-0.46	-0.45	-0.56	-0.53	-0.58	-0.81	-1.58
0.95	-0.11	-0.11	-0.60	-0.49	-0.48	-0.50	-0.60	-0.57	-0.61	-0.86
1.00	-0.24	-0.13	-0.58	-0.45	-0.51	-0.53	-0.62	-0.60	-0.62	-0.65
1.05	-0.27	-0.26	-0.16	-0.65	-0.58	-0.58	-0.57	-0.69	-0.65	-0.68
1.10	-0.10	-0.32	-0.19	-0.58	-0.50	-0.57	-0.59	-0.60	-0.72	-0.67
1.15	-0.01	-0.21	-0.30	-0.20	-0.70	-0.54	-0.57	-0.60	-0.69	-0.69
1.20	0.01	-0.09	-0.35	-0.20	-0.26	-0.76	-0.60	-0.60	-0.59	-0.72
1.25	0.01	-0.02	-0.19	-0.31	-0.21	-0.67	-0.52	-0.57	-0.60	-0.60
1.30	-0.01	0.00	-0.08	-0.33	-0.21	-0.17	-0.68	-0.57	-0.60	-0.59
1.35	-0.02	0.00	-0.03	-0.17	-0.34	-0.22	-0.60	-0.55	-0.63	-0.60
1.40	0.02	-0.02	-0.00	-0.09	-0.35	-0.23	-0.20	-0.76	-0.55	-0.58
1.45	-0.00	-0.03	-0.01	-0.03	-0.18	-0.38	-0.21	-0.23	-0.79	-0.58
1.50	-0.07	0.00	-0.04	-0.02	-0.10	-0.34	-0.29	-0.22	-0.71	-0.55
1.55	-0.07	-0.03	-0.06	-0.04	-0.06	-0.19	-0.38	-0.26	-0.22	-0.80
1.60	-0.04	-0.10	-0.02	-0.06	-0.05	-0.06	-0.39	-0.31	-0.27	-0.29
1.65	-0.01	-0.10	-0.04	-0.08	-0.06	-0.07	-0.20	-0.44	-0.29	-0.26
1.70	-0.07	-0.08	-0.09	-0.05	-0.08	-0.07	-0.13	-0.31	-0.43	-0.29
1.75	-0.13	-0.05	-0.13	-0.07	-0.12	-0.08	-0.10	-0.22	-0.46	-0.32
1.80	-0.11	-0.10	-0.13	-0.10	-0.13	-0.12	-0.11	-0.12	-0.34	-0.49
1.85	-0.06	-0.14	-0.10	-0.17	-0.08	-0.16	-0.12	-0.13	-0.23	-0.46
1.90	-0.02	-0.16	-0.08	-0.14	-0.11	-0.14	-0.13	-0.12	-0.14	-0.29
1.95	-0.05	-0.10	-0.12	-0.12	-0.18	-0.07	-0.16	-0.12	-0.12	-0.25
2.00	-0.05	-0.03	-0.18	-0.08	-0.18	-0.12	-0.15	-0.14	-0.14	-0.15
2.05	-0.03	-0.04	-0.14	-0.13	-0.13	-0.18	-0.10	-0.15	-0.13	-0.13
2.10	0.00	-0.06	-0.06	-0.14	-0.09	-0.17	-0.11	-0.14	-0.14	-0.13
2.15	0.02	-0.04	-0.00	-0.16	-0.07	-0.13	-0.14	-0.07	-0.14	-0.10
2.20	0.02	0.00	-0.03	-0.10	-0.09	-0.08	-0.15	-0.09	-0.12	-0.12
2.25	0.05	0.02	-0.02	-0.03	-0.15	-0.05	-0.13	-0.13	-0.06	-0.13
2.30	0.04	0.05	-0.01	0.01	-0.13	-0.08	-0.09	-0.13	-0.08	-0.11
2.35	0.06	0.04	0.02	-0.01	-0.06	-0.12	-0.05	-0.14	-0.10	-0.04
2.40	0.06	0.07	0.05	-0.01	0.02	-0.13	-0.07	-0.07	-0.14	-0.07
2.45	0.09	0.05	0.06	0.01	0.00	-0.07	-0.08	-0.04	-0.13	-0.10
2.50	0.07	0.08	0.04	0.03	-0.02	0.03	-0.14	-0.04	-0.09	-0.13

Table A.7 AB colors of the SB3 template in the ALHAMBRA system at diffferent redshifts; r is the SLOAN band.

z	Alh1-r	Alh2-r	Alh3-r	Alh4-r	Alh5-r	Alh6-r	Alh7-r	Alh8-r	Alh9-r	Alh10-r
0.00	1.15	0.82	0.57	0.42	0.32	0.30	0.27	0.16	0.09	-0.20
0.05	1.21	0.89	0.55	0.36	0.24	0.15	0.15	0.11	-0.00	-0.07
0.10	1.21	1.04	0.67	0.39	0.26	0.14	0.10	0.11	0.01	-0.07
0.15	1.03	1.13	0.86	0.51	0.29	0.17	0.08	0.05	0.04	-0.05
0.20	1.02	1.05	1.02	0.64	0.35	0.21	0.11	0.03	-0.00	-0.00
0.25	1.05	0.96	1.07	0.82	0.49	0.26	0.16	0.06	-0.04	-0.03
0.30	1.08	0.96	0.97	0.96	0.61	0.35	0.18	0.10	0.00	-0.09
0.35	1.07	0.98	0.87	0.98	0.74	0.51	0.23	0.11	0.00	-0.09
0.40	1.03	0.96	0.84	0.85	0.85	0.56	0.32	0.11	0.01	-0.09
0.45	0.99	0.91	0.81	0.69	0.83	0.70	0.36	0.16	-0.02	-0.10
0.50	0.91	0.85	0.77	0.65	0.69	0.69	0.45	0.25	-0.03	-0.14
0.55	0.81	0.77	0.69	0.61	0.50	0.64	0.54	0.24	0.01	-0.18
0.60	0.69	0.67	0.60	0.53	0.38	0.45	0.48	0.26	0.07	-0.20
0.65	0.62	0.56	0.51	0.45	0.35	0.22	0.40	0.31	0.03	-0.18
0.70	0.63	0.45	0.41	0.33	0.26	0.17	0.17	0.24	0.13	-0.22
0.75	0.53	0.39	0.35	0.29	0.23	0.15	-0.01	0.20	0.11	-0.14
0.80	0.48	0.44	0.29	0.27	0.19	0.09	0.05	0.02	0.11	0.01
0.85	0.43	0.43	0.28	0.22	0.17	0.13	0.05	-0.11	0.10	0.02
0.90	0.45	0.40	0.30	0.24	0.20	0.14	0.03	-0.01	-0.04	0.06
0.95	0.39	0.42	0.39	0.23	0.22	0.11	0.12	0.03	-0.13	0.08
1.00	0.36	0.41	0.41	0.24	0.21	0.18	0.13	0.02	-0.02	-0.05
1.05	0.33	0.42	0.38	0.30	0.22	0.21	0.09	0.10	0.02	-0.13
1.10	0.34	0.38	0.39	0.37	0.22	0.16	0.17	0.11	0.00	-0.05
1.15	0.35	0.29	0.35	0.34	0.17	0.17	0.17	0.04	0.04	-0.04
1.20	0.45	0.24	0.31	0.30	0.20	0.15	0.08	0.06	0.03	-0.08
1.25	0.48	0.25	0.29	0.30	0.27	0.12	0.09	0.08	0.02	-0.05
1.30	0.57	0.25	0.23	0.28	0.26	0.09	0.12	0.08	-0.02	-0.02
1.35	0.55	0.31	0.17	0.24	0.24	0.15	0.09	0.01	0.02	-0.03
1.40	0.44	0.40	0.16	0.23	0.23	0.21	0.01	0.05	0.05	-0.08
1.45	0.39	0.47	0.19	0.19	0.23	0.22	0.08	0.07	-0.01	-0.02
1.50	0.31	0.51	0.21	0.16	0.20	0.21	0.18	0.02	-0.02	-0.01
1.55	0.40	0.44	0.30	0.10	0.20	0.17	0.19	-0.01	0.03	-0.01
1.60	0.42	0.35	0.34	0.10	0.15	0.16	0.17	0.03	0.01	-0.07
1.65	0.46	0.32	0.39	0.12	0.11	0.15	0.17	0.09	-0.06	-0.04
1.70	0.44	0.25	0.44	0.14	0.07	0.16	0.07	0.14	-0.06	-0.03
1.75	0.35	0.31	0.37	0.22	0.02	0.09	0.10	0.10	-0.02	-0.05
1.80	0.34	0.34	0.28	0.26	0.03	0.05	0.09	0.11	0.04	-0.13
1.85	0.35	0.36	0.25	0.29	0.05	0.03	0.11	0.02	0.08	-0.11
1.90	0.38	0.36	0.17	0.40	0.07	-0.01	0.04	0.05	0.06	-0.06
1.95	0.41	0.30	0.24	0.33	0.15	-0.05	-0.01	0.04	0.07	-0.02
2.00	0.48	0.26	0.27	0.21	0.19	-0.04	-0.02	0.05	-0.03	0.03
2.05	0.55	0.29	0.28	0.19	0.21	0.01	-0.05	-0.00	0.00	0.01
2.10	0.63	0.31	0.31	0.11	0.34	0.07	-0.09	-0.03	0.01	0.01
2.15	0.68	0.37	0.34	0.15	0.34	0.13	-0.07	-0.01	0.06	-0.01
2.20	0.71	0.46	0.27	0.27	0.26	0.22	-0.00	-0.03	0.04	0.01
2.25	0.74	0.55	0.28	0.31	0.22	0.25	0.08	-0.06	-0.00	0.04
2.30	0.76	0.62	0.31	0.31	0.17	0.39	0.10	-0.06	-0.01	0.04
2.35	0.78	0.69	0.32	0.32	0.12	0.37	0.16	-0.03	-0.02	0.06
2.40	0.79	0.73	0.37	0.31	0.18	0.27	0.22	0.02	-0.05	-0.00
2.45	0.82	0.74	0.45	0.25	0.26	0.20	0.27	0.07	-0.10	-0.03
2.50	0.85	0.75	0.53	0.24	0.27	0.12	0.40	0.09	-0.10	-0.04

Table A.7 Continuation

z	Alh11-r	Alh12-r	Alh13-r	Alh14-r	Alh15-r	Alh16-r	Alh17-r	Alh18-r	Alh19-r	Alh20-r
0.00	-0.03	0.03	-0.06	-0.11	-0.18	-0.24	-0.31	-0.41	-0.45	-0.47
0.05	-0.38	-0.20	-0.12	-0.19	-0.25	-0.30	-0.38	-0.42	-0.55	-0.59
0.10	-0.14	-0.44	-0.28	-0.18	-0.23	-0.30	-0.34	-0.43	-0.45	-0.52
0.15	-0.11	-0.18	-0.38	-0.53	-0.22	-0.25	-0.34	-0.38	-0.44	-0.49
0.20	-0.12	-0.16	-0.22	-0.48	-0.52	-0.25	-0.30	-0.39	-0.40	-0.46
0.25	-0.04	-0.16	-0.20	-0.27	-0.32	-0.74	-0.28	-0.32	-0.40	-0.43
0.30	-0.08	-0.08	-0.20	-0.24	-0.30	-0.34	-0.71	-0.31	-0.36	-0.40
0.35	-0.12	-0.13	-0.14	-0.26	-0.30	-0.34	-0.39	-0.82	-0.42	-0.40
0.40	-0.17	-0.20	-0.21	-0.22	-0.34	-0.36	-0.42	-0.46	-0.87	-0.57
0.45	-0.19	-0.27	-0.28	-0.26	-0.35	-0.42	-0.45	-0.50	-0.53	-0.88
0.50	-0.24	-0.30	-0.39	-0.36	-0.37	-0.44	-0.52	-0.54	-0.61	-0.62
0.55	-0.27	-0.37	-0.44	-0.48	-0.47	-0.47	-0.55	-0.63	-0.64	-0.68
0.60	-0.35	-0.42	-0.50	-0.57	-0.61	-0.60	-0.60	-0.68	-0.76	-0.78
0.65	-0.40	-0.49	-0.57	-0.64	-0.72	-0.74	-0.73	-0.71	-0.82	-0.88
0.70	-0.41	-0.55	-0.63	-0.72	-0.78	-0.85	-0.86	-0.86	-0.83	-0.93
0.75	-0.32	-0.55	-0.68	-0.74	-0.83	-0.86	-0.95	-0.92	-0.95	-0.92
0.80	-0.31	-0.46	-0.65	-0.75	-0.81	-0.89	-0.96	-0.97	-0.96	-1.01
0.85	-0.22	-0.36	-0.59	-0.73	-0.81	-0.88	-0.95	-1.03	-1.03	-1.02
0.90	-0.03	-0.31	-0.45	-0.67	-0.79	-0.83	-0.92	-0.96	-1.04	-1.05
0.95	0.00	-0.10	-0.41	-0.55	-0.72	-0.81	-0.86	-0.94	-0.97	-1.06
1.00	0.06	-0.04	-0.29	-0.42	-0.64	-0.74	-0.83	-0.89	-0.96	-0.99
1.05	0.07	0.02	-0.08	-0.37	-0.50	-0.70	-0.79	-0.84	-0.92	-0.97
1.10	-0.06	0.05	-0.04	-0.26	-0.38	-0.56	-0.74	-0.83	-0.86	-0.94
1.15	-0.22	0.03	-0.04	-0.11	-0.41	-0.49	-0.69	-0.80	-0.88	-0.91
1.20	-0.14	-0.17	-0.03	-0.10	-0.22	-0.51	-0.59	-0.80	-0.88	-0.92
1.25	-0.08	-0.27	-0.02	-0.08	-0.16	-0.40	-0.50	-0.68	-0.83	-0.92
1.30	-0.13	-0.17	-0.21	-0.07	-0.14	-0.21	-0.50	-0.59	-0.77	-0.86
1.35	-0.14	-0.14	-0.36	-0.07	-0.13	-0.19	-0.42	-0.50	-0.65	-0.85
1.40	-0.06	-0.17	-0.21	-0.27	-0.11	-0.16	-0.24	-0.53	-0.58	-0.72
1.45	-0.05	-0.16	-0.15	-0.35	-0.10	-0.12	-0.21	-0.28	-0.60	-0.64
1.50	-0.10	-0.08	-0.20	-0.24	-0.29	-0.12	-0.18	-0.25	-0.50	-0.52
1.55	-0.11	-0.09	-0.20	-0.20	-0.42	-0.17	-0.16	-0.25	-0.30	-0.59
1.60	-0.06	-0.14	-0.14	-0.24	-0.29	-0.38	-0.17	-0.22	-0.29	-0.35
1.65	-0.03	-0.16	-0.13	-0.24	-0.22	-0.45	-0.22	-0.20	-0.25	-0.33
1.70	-0.11	-0.10	-0.17	-0.19	-0.28	-0.29	-0.41	-0.20	-0.25	-0.31
1.75	-0.13	-0.08	-0.22	-0.18	-0.30	-0.26	-0.49	-0.26	-0.23	-0.29
1.80	-0.08	-0.12	-0.18	-0.17	-0.28	-0.32	-0.35	-0.48	-0.24	-0.26
1.85	-0.06	-0.17	-0.12	-0.25	-0.20	-0.32	-0.30	-0.52	-0.30	-0.27
1.90	-0.10	-0.15	-0.11	-0.24	-0.20	-0.31	-0.34	-0.36	-0.51	-0.26
1.95	-0.19	-0.11	-0.21	-0.18	-0.28	-0.23	-0.37	-0.32	-0.54	-0.43
2.00	-0.15	-0.13	-0.22	-0.17	-0.30	-0.23	-0.36	-0.40	-0.39	-0.61
2.05	-0.08	-0.19	-0.17	-0.20	-0.24	-0.30	-0.28	-0.40	-0.35	-0.51
2.10	0.00	-0.22	-0.11	-0.23	-0.16	-0.31	-0.26	-0.35	-0.40	-0.35
2.15	0.02	-0.12	-0.13	-0.20	-0.16	-0.24	-0.27	-0.27	-0.40	-0.34
2.20	0.03	-0.03	-0.21	-0.13	-0.21	-0.15	-0.30	-0.23	-0.34	-0.39
2.25	0.05	0.02	-0.19	-0.11	-0.20	-0.13	-0.26	-0.27	-0.26	-0.37
2.30	0.01	0.04	-0.10	-0.14	-0.18	-0.20	-0.19	-0.27	-0.23	-0.33
2.35	-0.02	0.01	-0.01	-0.20	-0.11	-0.21	-0.16	-0.29	-0.25	-0.26
2.40	0.01	0.06	-0.01	-0.17	-0.12	-0.21	-0.18	-0.23	-0.29	-0.25
2.45	0.03	-0.03	0.02	-0.12	-0.20	-0.12	-0.24	-0.15	-0.31	-0.28
2.50	0.03	-0.04	-0.01	-0.03	-0.26	-0.12	-0.24	-0.18	-0.27	-0.32

Table A.8 AB colors of the Scb template in the ALHAMBRA system at diffferent redshifts; r is the SLOAN band.

z	Alh1-r	Alh2-r	Alh3-r	Alh4-r	Alh5-r	Alh6-r	Alh7-r	Alh8-r	Alh9-r	Alh10-r
0.00	1.31	0.96	0.70	0.48	0.30	0.29	0.18	0.08	0.00	-0.07
0.05	1.46	1.12	0.77	0.55	0.36	0.21	0.21	0.09	0.00	-0.07
0.10	1.49	1.28	0.89	0.60	0.40	0.25	0.13	0.12	0.00	-0.08
0.15	1.53	1.36	1.06	0.70	0.47	0.29	0.17	0.06	0.03	-0.07
0.20	1.57	1.40	1.22	0.82	0.52	0.36	0.19	0.07	0.00	-0.06
0.25	1.60	1.42	1.24	0.97	0.62	0.40	0.26	0.10	-0.05	-0.05
0.30	1.61	1.45	1.27	1.11	0.73	0.46	0.30	0.14	0.00	-0.13
0.35	1.60	1.45	1.27	1.10	0.85	0.56	0.31	0.18	0.00	-0.11
0.40	1.56	1.43	1.26	1.09	0.93	0.62	0.37	0.16	0.03	-0.13
0.45	1.50	1.40	1.24	1.07	0.90	0.73	0.40	0.18	0.02	-0.14
0.50	1.41	1.34	1.20	1.03	0.87	0.72	0.49	0.25	-0.02	-0.14
0.55	1.32	1.26	1.15	0.99	0.82	0.68	0.57	0.25	0.00	-0.19
0.60	1.21	1.16	1.07	0.94	0.77	0.63	0.50	0.33	0.03	-0.21
0.65	1.10	1.05	0.98	0.87	0.71	0.57	0.45	0.32	0.04	-0.19
0.70	0.98	0.94	0.88	0.79	0.65	0.51	0.38	0.26	0.12	-0.22
0.75	0.88	0.84	0.79	0.72	0.60	0.46	0.33	0.21	0.08	-0.17
0.80	0.78	0.75	0.71	0.65	0.55	0.42	0.29	0.17	0.04	-0.07
0.85	0.70	0.67	0.63	0.58	0.50	0.39	0.27	0.14	0.02	-0.11
0.90	0.66	0.62	0.59	0.54	0.47	0.38	0.27	0.14	0.02	-0.11
0.95	0.63	0.57	0.54	0.49	0.44	0.36	0.26	0.14	0.01	-0.10
1.00	0.61	0.52	0.49	0.45	0.40	0.34	0.25	0.14	0.01	-0.10
1.05	0.59	0.49	0.44	0.41	0.36	0.31	0.24	0.14	0.02	-0.11
1.10	0.59	0.46	0.40	0.37	0.33	0.28	0.22	0.14	0.02	-0.10
1.15	0.59	0.44	0.36	0.33	0.29	0.25	0.20	0.13	0.02	-0.10
1.20	0.60	0.44	0.33	0.29	0.26	0.22	0.18	0.12	0.02	-0.09
1.25	0.62	0.44	0.31	0.26	0.23	0.19	0.16	0.10	0.02	-0.08
1.30	0.64	0.45	0.30	0.23	0.20	0.17	0.13	0.09	0.02	-0.07
1.35	0.66	0.47	0.31	0.21	0.18	0.15	0.12	0.08	0.02	-0.06
1.40	0.68	0.50	0.32	0.20	0.16	0.13	0.10	0.07	0.02	-0.05
1.45	0.71	0.52	0.34	0.20	0.14	0.12	0.09	0.06	0.02	-0.04
1.50	0.74	0.56	0.37	0.21	0.13	0.11	0.08	0.05	0.01	-0.04
1.55	0.78	0.59	0.40	0.23	0.13	0.09	0.07	0.04	0.01	-0.03
1.60	0.81	0.62	0.43	0.25	0.14	0.09	0.07	0.04	0.01	-0.03
1.65	0.85	0.66	0.46	0.28	0.15	0.08	0.06	0.04	0.01	-0.03
1.70	0.89	0.69	0.50	0.31	0.16	0.09	0.06	0.04	0.01	-0.03
1.75	0.92	0.73	0.53	0.35	0.19	0.09	0.05	0.03	0.01	-0.03
1.80	0.96	0.77	0.57	0.38	0.21	0.11	0.05	0.03	0.01	-0.02
1.85	1.00	0.81	0.61	0.42	0.24	0.12	0.06	0.03	0.01	-0.02
1.90	1.04	0.84	0.64	0.45	0.28	0.14	0.06	0.02	0.00	-0.02
1.95	1.10	0.88	0.68	0.49	0.31	0.17	0.08	0.03	0.00	-0.02
2.00	1.16	0.91	0.71	0.52	0.34	0.19	0.09	0.03	-0.00	-0.02
2.05	1.24	0.94	0.75	0.55	0.37	0.22	0.11	0.03	-0.01	-0.03
2.10	1.32	0.97	0.78	0.58	0.40	0.25	0.13	0.04	-0.01	-0.03
2.15	1.36	1.03	0.81	0.61	0.43	0.28	0.15	0.05	-0.01	-0.04
2.20	1.39	1.09	0.83	0.64	0.45	0.30	0.17	0.06	-0.01	-0.05
2.25	1.41	1.15	0.85	0.66	0.48	0.32	0.19	0.07	-0.01	-0.06
2.30	1.43	1.22	0.87	0.69	0.50	0.34	0.21	0.08	-0.01	-0.07
2.35	1.45	1.29	0.89	0.70	0.52	0.36	0.23	0.10	-0.01	-0.07
2.40	1.46	1.33	0.94	0.72	0.53	0.37	0.24	0.11	-0.01	-0.08
2.45	1.48	1.34	0.99	0.73	0.55	0.39	0.25	0.12	-0.00	-0.09
2.50	1.51	1.35	1.05	0.74	0.56	0.40	0.26	0.13	-0.00	-0.10

Table A.8 Continuation

z	Alh11-r	Alh12-r	Alh13-r	Alh14-r	Alh15-r	Alh16-r	Alh17-r	Alh18-r	Alh19-r	Alh20-r
0.00	-0.12	-0.16	-0.19	-0.22	-0.23	-0.24	-0.25	-0.26	-0.27	-0.29
0.05	-0.14	-0.19	-0.23	-0.26	-0.28	-0.30	-0.31	-0.32	-0.33	-0.34
0.10	-0.15	-0.21	-0.26	-0.30	-0.33	-0.35	-0.37	-0.38	-0.39	-0.40
0.15	-0.15	-0.21	-0.27	-0.32	-0.36	-0.39	-0.41	-0.43	-0.44	-0.45
0.20	-0.14	-0.22	-0.28	-0.33	-0.38	-0.41	-0.45	-0.47	-0.49	-0.50
0.25	-0.14	-0.21	-0.29	-0.34	-0.40	-0.44	-0.48	-0.51	-0.53	-0.55
0.30	-0.12	-0.21	-0.28	-0.36	-0.41	-0.46	-0.50	-0.54	-0.57	-0.59
0.35	-0.22	-0.21	-0.31	-0.37	-0.44	-0.49	-0.54	-0.58	-0.62	-0.65
0.40	-0.24	-0.32	-0.31	-0.41	-0.48	-0.54	-0.59	-0.64	-0.68	-0.71
0.45	-0.26	-0.37	-0.41	-0.43	-0.53	-0.58	-0.65	-0.69	-0.74	-0.77
0.50	-0.30	-0.39	-0.53	-0.51	-0.56	-0.64	-0.70	-0.76	-0.80	-0.84
0.55	-0.30	-0.45	-0.54	-0.66	-0.62	-0.69	-0.77	-0.83	-0.88	-0.92
0.60	-0.35	-0.47	-0.60	-0.68	-0.80	-0.75	-0.83	-0.89	-0.95	-1.00
0.65	-0.41	-0.50	-0.65	-0.75	-0.84	-0.93	-0.89	-0.98	-1.03	-1.08
0.70	-0.43	-0.57	-0.67	-0.82	-0.90	-0.99	-1.05	-1.03	-1.11	-1.16
0.75	-0.38	-0.60	-0.72	-0.83	-0.96	-1.02	-1.15	-1.14	-1.15	-1.23
0.80	-0.41	-0.57	-0.76	-0.85	-0.99	-1.08	-1.16	-1.28	-1.23	-1.26
0.85	-0.32	-0.54	-0.75	-0.89	-0.97	-1.10	-1.19	-1.27	-1.38	-1.32
0.90	-0.20	-0.49	-0.66	-0.87	-0.99	-1.05	-1.20	-1.27	-1.34	-1.45
0.95	-0.22	-0.35	-0.64	-0.81	-0.98	-1.06	-1.17	-1.28	-1.34	-1.41
1.00	-0.22	-0.31	-0.57	-0.73	-0.95	-1.06	-1.14	-1.27	-1.35	-1.41
1.05	-0.21	-0.32	-0.40	-0.72	-0.86	-1.05	-1.15	-1.22	-1.35	-1.42
1.10	-0.21	-0.31	-0.42	-0.61	-0.82	-0.97	-1.14	-1.23	-1.30	-1.42
1.15	-0.21	-0.31	-0.41	-0.49	-0.80	-0.90	-1.10	-1.22	-1.28	-1.38
1.20	-0.20	-0.30	-0.40	-0.50	-0.64	-0.90	-1.02	-1.21	-1.30	-1.34
1.25	-0.19	-0.29	-0.39	-0.49	-0.57	-0.80	-0.97	-1.13	-1.27	-1.36
1.30	-0.18	-0.28	-0.38	-0.47	-0.58	-0.63	-0.95	-1.06	-1.24	-1.33
1.35	-0.16	-0.26	-0.36	-0.45	-0.55	-0.63	-0.82	-1.01	-1.13	-1.31
1.40	-0.14	-0.24	-0.34	-0.44	-0.53	-0.61	-0.68	-0.98	-1.07	-1.21
1.45	-0.13	-0.22	-0.32	-0.41	-0.50	-0.59	-0.68	-0.77	-1.06	-1.13
1.50	-0.11	-0.19	-0.29	-0.39	-0.48	-0.56	-0.65	-0.72	-0.94	-1.08
1.55	-0.09	-0.17	-0.26	-0.36	-0.45	-0.53	-0.62	-0.71	-0.75	-1.06
1.60	-0.08	-0.15	-0.23	-0.33	-0.42	-0.50	-0.59	-0.67	-0.75	-0.85
1.65	-0.07	-0.13	-0.21	-0.30	-0.39	-0.47	-0.56	-0.64	-0.72	-0.77
1.70	-0.07	-0.11	-0.18	-0.27	-0.36	-0.44	-0.53	-0.60	-0.68	-0.76
1.75	-0.06	-0.10	-0.16	-0.24	-0.33	-0.41	-0.50	-0.57	-0.65	-0.72
1.80	-0.06	-0.09	-0.14	-0.21	-0.30	-0.37	-0.46	-0.54	-0.61	-0.69
1.85	-0.05	-0.09	-0.13	-0.19	-0.27	-0.34	-0.43	-0.51	-0.59	-0.65
1.90	-0.05	-0.08	-0.12	-0.17	-0.24	-0.31	-0.40	-0.48	-0.56	-0.62
1.95	-0.05	-0.08	-0.11	-0.16	-0.22	-0.28	-0.37	-0.45	-0.53	-0.59
2.00	-0.05	-0.08	-0.11	-0.15	-0.20	-0.26	-0.34	-0.42	-0.50	-0.57
2.05	-0.05	-0.08	-0.11	-0.14	-0.19	-0.24	-0.31	-0.39	-0.47	-0.54
2.10	-0.05	-0.08	-0.11	-0.14	-0.18	-0.22	-0.29	-0.36	-0.44	-0.51
2.15	-0.06	-0.08	-0.11	-0.14	-0.17	-0.21	-0.27	-0.34	-0.41	-0.48
2.20	-0.07	-0.08	-0.11	-0.14	-0.17	-0.21	-0.26	-0.32	-0.39	-0.46
2.25	-0.08	-0.09	-0.12	-0.15	-0.17	-0.21	-0.25	-0.31	-0.38	-0.44
2.30	-0.09	-0.11	-0.13	-0.15	-0.18	-0.21	-0.25	-0.30	-0.36	-0.43
2.35	-0.11	-0.12	-0.14	-0.17	-0.19	-0.22	-0.25	-0.30	-0.35	-0.41
2.40	-0.12	-0.14	-0.15	-0.18	-0.20	-0.23	-0.26	-0.30	-0.35	-0.41
2.45	-0.14	-0.16	-0.17	-0.19	-0.22	-0.24	-0.27	-0.31	-0.35	-0.40
2.50	-0.15	-0.18	-0.19	-0.21	-0.24	-0.26	-0.29	-0.32	-0.36	-0.40

Table A.9 Physical parameters of the 288 stars from the NGSL.

Star	SP Type	T_{eff} NGSL	T_{eff} QFA	T_{eff} ec.	*logg* NGSL	*logg* QFA	$[Fe/H]$ NGSL	$[Fe/H]$ QFA	E(B-V) NGSL	E(B-V) QFA
Agk+81266	B2	22000	80000	41014	Nan	6.624	Nan	Nan	Nan	0 (+/- 0.003)
BD+413306	K0V [1]	5047	5500	5540	4.3	4.5	-0.6	0.3	0.003	0.08 (+/- 0.009)
BD-122669	A5 [2]	6939	7000	6513	4.05	4	-1.5	-2	0.02	0 (+/- 0.01)
BD+092860	F8IIIwle	5471	5750	5717	2.75	2.5	-1.8	-1	0.017	0.04 (+/- 0.009)
BD+174708	sdF8 [2]	6018	6500	6146	3.9	4.5	-1.6	-1.5	0.003	0.02 (+/- 0.009)
BD+174708	sdF8[2]	6018	6250	6054	3.9	4	-1.6	-1.5	0.003	0 (+/- 0.01)
BD+292091	F5 [1]	5758	6000	5808	4.5	5	-1.9	-1.5	0.004	0 (+/- 0.007)
BD+423607	F3 [1]	5676	6250	5982	3.9	5	-1.9	-2	0.017	0 (+/- 0.007)
BD+442051	M2.0V [1]	3943	3750	3773	4.9	1.5	-0.6	-0.3	0.002	0 (+/- 0.08)
BD+511696	sdG0 [1]	5636	6000	5823	4.6	5	-1.3	-1	0.007	0.04 (+/- 0.01)
BD+592723	F2[2]	6104	6250	6029	4.04	4	-1.7	-2	0.02	0.03 (+/- 0.01)
BD+720094	sdF2[1]	6244	6250	6084	4.2	4	-1.7	-1.5	0.06	0 (+/- 0.009)
BD+284211	Op[20]	46572	100.000	43777	6.2	6.7	Nan	Nan	0.09	0 (+/- 0.007)
BD+75325	O5pv	30044	40000	40668	3	4.5	Nan	0	Nan	0 (+/- 0.01)
CD-259286	A5[3]	6712	6500	6328	3	2.5	-1.4	-1.5	0.09	0.12 (+/- 0.008)
CD-3018140	F8[1]	6322	6750	6323	4	4.5	-2	-3	0.03	0.03 (+/- 0.004)
CD-621346	G5	5481	5250	5522	3.2	2	-1.3	-1	0.03	0 (+/- 0.01)
Feige110	DA[20]	42300	55000	32245	5.95	6.5	Nan	Nan	Nan	0 (+/- 0.01)
Feige34	DO[20]	80000	140.000	41511	5	7.8	Nan	Nan	Nan	0.06 (+/- 0.01)
G019-013	K5V [4]	4396	4250	4526	4.7	3.5	-0.4	-0.2	0	0 (+/- 0.03)
G021-024	K5 [5]	4198	4250	4260	4.8	3.5	-0.8	0.3	0	0 (+/- 0.03)
G029-023	F5[1]	6043	6500	6124	3.8	4.5	-1.8	-2	0.02	0.05 (+/- 0.01)
G114-26	F3 [2]	5876	6250	6027	4.1	4.5	-1.8	-1.5	0	0.03 (+/- 0.01)
G115-58	sdG[1]	6209	6250	5959	4.2	4	-0.6	-2	0.004	0 (+/- 0.02)
G12-21	F2[1]	6067	6250	6077	4.3	4.5	-1.3	-1.5	0.004	0.04 (+/- 0.007)
G13-35	sdF5 [1]	6146	6250	6079	4.2	4	-1.6	-1.5	0.007	0 (+/- 0.007)
G169-28	Nan [1]	5913	6000	5828	4.2	4.5	-0.4	-1	0.014	0 (+/- 0.01)
G17-25	F8[4]	5111	5500	5458	4.4	4	-1.3	-0.2	0.02	0.04 (+/- 0.01)
G18-39	G0 [1]	6024	6500	6245	4	4.5	-1.3	-1	0.008	0.07 (+/- 0.01)
G18-54	sdF7 [2]	5859	6250	6056	4.2	4.5	-1.45	-1	0.014	0.06 (+/- 0.01)
G180-24	F5 [1]	6013	6250	6032	3.8	4	-1.5	-1	0.002	0 (+/- 0.01)
G187-40	G0 [1]	5753	6250	5953	3.4	5	-0.9	-1	0.012	0.04 (+/- 0.007)
G188-22	F8 [4]	5904	6250	6059	3.7	4.5	-1.3	-1.5	0.01	0.04 (+/- 0.008)
G188-30	sdG2 [1]	5254	5750	5700	4.5	4	-1.7	-0.5	0.01	0.03 (+/- 0.01)
G191b2b	DAw[20]	55932	65000	38791	7.5	7.695	Nan	Nan	0.6	0 (+/- 0.001)

Table A.9 Continuation

Star	SP Type	T_{eff} NGSL	T_{eff} QFA	T_{eff} ec.	*logg* NGSL	*logg* QFA	$[Fe/H]$ NGSL	$[Fe/H]$ QFA	E(B-V) NGSL	E(B-V) QFA
G192-43	sdF2 [1]	6163	6500	6207	4.2	4.5	-1.4	-1.5	0.018	0.04 (+/- 0.01)
G194-22	sdF6 [1]	6102	6250	6123	4.3	4.5	-1.5	-1.5	0.005	0 (+/- 0.006)
G196-48	G [2]	5689	6000	5926	3.4	4	-1.7	-1.5	Nan	0.05 (+/- 0.01)
G20-15	F8 [1]	5745	6500	6226	3.8	4.5	-1.9	-1	0.088	0.22 (+/- 0.02)
G202-65	sdF3 [2]	6849	7000	6609	4.4	4.5	-1.2	-3	0	0 (+/- 0.01)
G231-52	G1 [1]	5400	6000	5827	3.9	5	-1.7	-1	0.026	0.07 (+/- 0.01)
G234-28	G0 [2]	6011	6250	6081	3.9	4.5	-1.05	-1.5	0.01	0.04 (+/- 0.006)
G24-3	sdF8 [1]	5949	6250	6084	4.2	4.5	-1.5	-1.5	0.009	0.05 (+/- 0.008)
G243-62	K2 [1]	4721	5500	5525	4.6	4.5	-1.7	0.2	0.07	0.12 (+/- 0.02)
G260-36	K2 [1]	4901	5250	5245	2.6	4.5	0.1	0.5	0.02	0.04 (+/- 0.01)
G262-14	G8 [2]	5066	5500	5561	4.2	4.5	0.18	-0.1	0.019	0.1 (+/- 0.01)
G63-26	sdF [1]	5760	6500	6165	4.2	4.5	-1.5	-1.5	0	0.05 (+/- 0.02)
G88-27	sdF8 [1]	6086	6500	6176	4.1	4.5	-1.7	-1	0	0.04 (+/- 0.01)
GJ825	M0V [10]	3784	4000	3944	4.8	3.5	-0.7	0	0	0 (+/- 0.05)
GL109	M3.5V [10]	3373	3350	3589	Nan	5	-0.21	0	Nan	0 (+/- 0.12)
GL15B	M6.0V [10]	3518	3750	3675	5.1	1.5	-0.9	0	0	0 (+/- 0.09)
HD000319	A1V [9]	8381	8250	8350	3.9	4	-0.6	-1.5	0.012	0 (+/- 0.02)
HD001461	G0V [1]	5770	6000	5894	4.3	4.5	0.2	0.3	0.013	0.06 (+/- 0.01)
HD002857	A2 [7]	7892	10000	9495	2.7	3.5	-1.4	-1.5	0.04	0.13 (+/- 0.01)
HD004727	B5V+ [2]	13352	16000	13888	3.9	4	0.005	-0.5	0.02	0.03 (+/- 0.006)
HD004813	F7IV [5]	6217	6500	6184	4.4	4.5	-0.1	-0.1	0.002	0.05 (+/- 0.01)
HD005256	G5 [1]	5278	5500	5522	3.8	3.5	-0.6	-0.2	0.011	0.026 (+/- 0.008)
HD005395	G8IIIb [6]	4825	5000	5012	2.5	2	-0.5	-0.3	0	0 (+/- 0.02)
HD005544	K0IIIp	4583	4750	4882	1.7	2	-0.5	-0.1	Nan	0.07 (+/- 0.02)
HD005916	G8III-IV	4930	5250	5337	2	2.5	-0.6	-0.3	0.015	0.08 (+/- 0.01)
HD006229	G5IIIw [7]	5281	5750	5777	2.5	3	-0.8	-0.3	0.01	0.13 (+/- 0.02)
HD006734	K0IV [1]	4986	5500	5422	3.5	4	-0.4	0.2	0.04	0.09 (+/- 0.01)
HD006755	F8V [1]	5162	5500	5528	2.7	3	-1.5	-1	0.03	0.08 (+/- 0.008)
HD008724	G5	4639	5500	5417	1.4	3	-1.8	-0.5	0.06	0.28 (+/- 0.02)
HD009051	G7IIIw	4930	5500	5424	2.2	2.5	-1.6	-0.5	0.01	0.11 (+/- 0.01)
HD010780	K0V [8]	5355	5500	5390	4.5	4	0.07	0.3	0.008	0.02 (+/- 0.008)
HD012533	K3IIb [4]	4296	4250	4275	1.2	0.5	-0.1	-0.3	Nan	0 (+/- 0.03)
HD015089	A5p [9]	8785	9000	8932	4.1	4	0.7	1	0	0 (+/- 0.02)

Table A.9 Continuation

Star	SP Type	T_{eff} NGSL	T_{eff} QFA	T_{eff} ec.	*logg* NGSL	*logg* QFA	$[Fe/H]$ NGSL	$[Fe/H]$ QFA	E(B-V) NGSL	E(B-V) QFA
HD016031	F0V [1]	6145	6500	6243	4	4.5	-1.8	-1.5	0.004	0.04 (+/- 0.006)
HD017072	G2w	5497	6000	5898	2.3	3	-1	-0.3	0.02	0.12 (+/- 0.01)
HD017361	K1.5III [1]	4615	4750	4733	2.6	2	0.02	-0.1	0.02	0 (+/- 0.02)
HD017925	K1V [11]	5169	5500	5374	4.5	5	0.06	0.3	Nan	0.09 (+/- 0.01)
HD018078	A0p	8720	8250	8248	3.4	2.5	0.95	1	Nan	0.11 (+/- 0.03)
HD018769	A3m [5]	8544	8250	8241	4.2	4	0.5	-0.5	Nan	0 (+/- 0.01)
HD018907	K2V [1]	5150	5500	5464	3.9	3.5	-0.6	-0.1	0.05	0.09 (+/- 0.008)
HD019019	F8 [1]	6074	6500	6143	3.3	4.5	-0.1	0.1	0.006	0.07 (+/- 0.02)
HD019308	G0 [1]	5806	6000	5743	3.8	4	0.07	0.2	0.006	0.03 (+/- 0.01)
HD019445	A4p [5]	6004	6250	6002	4.4	4.5	-1.9	-2	0	0 (+/- 0.008)
HD019656	K0III [4]	4608	4750	4688	2.4	1.5	-0.1	-0.2	Nan	0 (+/- 0.03)
HD019787	K2III [5]	4744	5000	5034	2.7	2.5	0.06	0.1	Nan	0.06 (+/- 0.02)
HD020039	F8 [2]	5203	5500	5482	3.8	3	-0.7	-0.2	0.014	0.02 (+/- 0.01)
HD020630	G5Vv [8]	5683	6000	5881	4.5	4.5	0.09	0.2	0	0.07 (+/- 0.005)
HD021742	K1IV [1]	5108	5250	5297	4.4	4	0.4	0.2	0.003	0 (+/- 0.02)
HD022049	K2Vk [8]	5079	5500	5341	4.6	5	-0.1	0.5	0.013	0.08 (+/- 0.01)
HD022484	F9IV-V [1]	6003	6250	5950	4.1	4	-0.08	0.1	0.003	0 (+/- 0.01)
HD023439	K1V [4]	5043	5750	5726	4.5	5	-1.1	0.1	0.01	0.1 (+/- 0.01)
HD025329	K1V [5]	4806	5250	5279	4.6	4.5	-1.6	-0.2	0.02	0.06 (+/- 0.02)
HD025893	G5 [9]	5143	5500	5394	4.4	4	-0.03	0.3	Nan	0.04 (+/- 0.01)
HD025975	K1III [1]	4868	5000	5024	3.3	2.5	-0.1	-0.1	Nan	0 (+/- 0.02)
HD026297	G5/G6IVw	4474	4750	4694	1	0	-1.7	-1.5	0.012	0.09 (+/- 0.007)
HD027295	B9IV [12]	11463	12500	12851	3.9	4	-0.6	-3	0.005	0 (+/- 0.02)
HD028946	K0 [1]	5279	5500	5426	3.7	4	-0.07	0.1	0.004	0 (+/- 0.01)
HD028978	A2Vs	9045	8750	8892	3.8	3.5	0.08	0.3	0.12	0 (+/- 0.01)
HD029574	G9IIIw [5]	4221	4750	4730	0.4	0	-1.8	-1.5	0.05	0.33 (+/- 0.02)
HD030834	K3III	4242	4250	4258	1.6	1	-0.3	-0.3	0.03	0.08 (+/- 0.02)
HD031219	F8 [1]	6099	6500	6079	3.4	5	0.3	0.3	0.02	0.06 (+/- 0.009)
HD033793	sdM1.0 [5]	4155	3750	3770	4.9	1.5	-0.7	-0.3	Nan	0 (+/- 0.08)
HD034078	O9.5Ve [9]	33917	32000	20747	4	4.5	0	-1	0.5	0.5 (+/- 0.02)
HD034797	B8/B9IV[12]	12799	13000	12690	4.2	4.5	0.01	1	Nan	0 (+/- 0.01)
HD036702	K0	4889	4750	4607	0.9	0	-2	-1.5	0.03	0.13 (+/- 0.01)
HD037202	B2IV[13]	21306	19000	14712	3.1	2.5	0	-3	0.07	0 (+/- 0.03)
HD037216	G5V	5384	5500	5465	3.9	3.5	-0.05	0.1	0.005	0 (+/- 0.009)
HD037763	K2III [4]	4634	4750	4710	2.9	3	0.3	0.3	Nan	0 (+/- 0.02)

Table A.9 Continuation

Star	SP Type	T_{eff} NGSL	T_{eff} QFA	T_{eff} ec.	*logg* NGSL	*logg* QFA	$[Fe/H]$ NGSL	$[Fe/H]$ QFA	E(B-V) NGSL	E(B-V) QFA
HD037828	K0	4452	4750	4871	1.2	0.5	-1.5	-1	0.06	0.13 (+/- 0.02)
HD038237	A3	8176	8000	8252	3.9	4	-0.9	0	Nan	0 (+/- 0.02)
HD038510	F5/F6V [1]	5989	6250	6019	4.2	4	-0.8	-0.3	0.001	0.03 (+/- 0.01)
HD039587	G0V [2]	5930	6250	5970	4.5	4.5	-0.01	0.1	0.002	0.05 (+/- 0.01)
HD039833	G0III	5819	6250	5945	4	4.5	0.13	0.3	0.012	0.08 (+/- 0.009)
HD040573	A0	10084	10500	9558	4.1	4	-0.4	-2.5	Nan	0 (+/- 0.01)
HD041357	A4m [2]	8070	7500	7043	3.7	3.5	0.2	-0.5	Nan	0 (+/- 0.01)
HD041661	F2 [9]	6578	6750	6406	4.1	3.5	0.04	0.1	0.013	0.06 (+/- 0.01)
HD041667	G8V	4756	5250	5322	1.9	2	-1.1	-0.3	0.03	0.19 (+/- 0.01)
HD044007	G5IV:w	4926	5250	5329	2.5	2	-1.5	-1	0.05	0.09 (+/- 0.008)
HD045282	G0	5280	5750	5661	3.4	3	-1.4	-0.5	0.02	0.07 (+/- 0.01)
HD047839	O7Ve [9]	30976	33000	25381	3.5	4.5	-0.06	0.2	0.06	0.03 (+/- 0.006)
HD048279	O8V [4]	36650	34000	26478	3.9	4.5	0.05	-1.5	0.44	0.34 (+/- 0.02)
HD050420	A9III [5]	6947	7250	7046	3.2	3	0.07	-0.3	0.02	0.09 (+/- 0.01)
HD055496	GII:wp [6]	4928	5000	5010	2.4	2	-1	-0.3	0.04	0 (+/- 0.02)
HD057727	G8III	4875	5500	5397	2.8	3.5	-0.1	0.3	Nan	0.12 (+/- 0.02)
HD058551	F6V [1]	6223	6500	6123	4.2	4.5	-0.5	-0.3	0	0 (+/- 0.01)
HD060319	F8 [1]	5912	6250	5967	3.9	4	-0.8	-0.3	0.01	0 (+/- 0.01)
HD061064	F6III[14]	6560	6750	6467	3.3	3.5	0.2	-0.1	0.01	0.04 (+/- 0.009)
HD062412	K1III	4726	5000	5000	2.4	2	-0.5	-0.1	0.01	0 (+/- 0.02)
HD063077	F9V [1]	5778	6250	6077	4	4.5	-0.9	-0.3	Nan	0.04 (+/- 0.008)
HD063791	G0	4826	5500	5542	1.7	2.5	-1.7	-0.5	0.04	0.22 (+/- 0.01)
HD064412	G0 [1]	5644	6000	5823	3.6	4	-0.4	-0.2	0.003	0 (+/- 0.01)
HD065228	F7/F8II	5924	6000	5856	2.3	2	0.3	0.1	0.14	0.11 (+/- 0.01)
HD065354	K3III	4052	4000	3864	0.8	0	-0.7	-0.3	0.17	0 (+/- 0.02)
HD065714	G8III	4898	5000	4937	2.1	2	0.2	0.1	0.04	0 (+/- 0.03)
HD067390	F2[14]	7073	7250	6822	3.6	3.5	-0.7	0	0.04	0.05 (+/- 0.01)
HD068988	G0	5886	6000	5822	4	4	0.3	0.3	0.002	0.05 (+/- 0.01)
HD071160	K3/K4III [4]	4112	4000	4073	0.9	0.5	-0.6	-0.3	0.08	0 (+/- 0.02)
HD072184	K2III [2]	4590	4750	4758	2.6	2.5	0.12	0.2	0.002	0 (+/- 0.02)
HD072324	G9III	4764	5250	5173	2.1	3	0.01	0.3	0.006	0.09 (+/- 0.03)
HD072505	K0III	4559	4750	4619	2.4	2.5	0.12	0.3	Nan	0 (+/- 0.03)
HD074088	K4III	4781	4000	3977	2.1	0.5	-1	-0.5	Nan	0.1 (+/- 0.04)
HD074721	A0V [7]	8877	9500	10557	3.6	3.5	-1	-3	0.03	0.04 (+/- 0.02)
HD076291	K1IV	4529	4750	4722	2.5	2.5	-0.1	0.1	Nan	0 (+/- 0.02)

Table A.9 Continuation

Star	SP Type	T_{eff} NGSL	T_{eff} QFA	T_{eff} ec.	*logg* NGSL	*logg* QFA	$[Fe/H]$ NGSL	$[Fe/H]$ QFA	E(B-V) NGSL	E(B-V) QFA
HD076932	G2V [1]	5902	6250	6063	4.1	4.5	-0.8	-0.5	0.01	0.03 (+/- 0.01)
HD078479	K3III	4420	4750	4779	2.4	2.5	0.3	0.3	Nan	0.09 (+/- 0.04)
HD079349	K7IV	4142	4000	3899	1.1	1	-0.4	0.1	0.11	0 (+/- 0.04)
HD079469	B9.5V [1]	10482	10500	10071	4.1	4	-0.1	0.5	0.01	0 (+/- 0.009)
HD080607	G5 [4]	5520	5500	5448	4.3	3.5	0.4	0.3	0	0 (+/- 0.01)
HD082395	K0III [5]	4716	5000	5044	2.5	2.5	-0.2	0.1	Nan	0.09 (+/- 0.03)
HD083212	G8IIIw	4603	5000	5009	1.4	0.5	-1.5	-1	0.04	0.15 (+/- 0.01)
HD085380	F8V	6278	6500	6162	4.2	4.5	0.2	0.2	0.002	0.08 (+/- 0.008)
HD086322	K1III	4673	5000	5057	2.4	2.5	-0.2	0.1	Nan	0.08 (+/- 0.02)
HD086986	A1V [7]	8126	7750	7480	3.2	3	-1.6	-3	0.03	0 (+/- 0.02)
HD090862	K2	4249	4000	4075	0.9	0.5	-0.6	-0.5	0.03	0 (+/- 0.02)
HD093329	A0 [7]	8194	9250	10106	2.9	3.5	-1.3	-0.3	0.03	0.08 (+/- 0.02)
HD094028	F4V [1]	6033	6250	6069	4.1	4.5	-1.4	-1.5	0.002	0.02 (+/- 0.008)
HD095241	F9V [2]	5903	6000	5936	3.9	3.5	-0.2	-0.2	Nan	0.03 (+/- 0.004)
HD095735	M2.0V [10]	3682	3500	3718	4.9	4	-0.4	-0.5	0.01	0 (+/- 0.1)
HD095849	K3III	4418	4500	4565	2	1.5	0.14	-0.1	Nan	0 (+/- 0.03)
HD096446	B2IIIp [15]	18932	29000	27259	4.2	5	-0.6	-0.5	0.09	0.11 (+/- 0.01)
HD097633	A2V [5]	9161	9250	9799	3.6	3.5	0.04	0.5	0.01	0 (+/- 0.01)
HD099648	G8Iab [4]	4876	5250	5172	2.2	2.5	-0.01	0.2	0.05	0.09 (+/- 0.02)
HD101013	G9III [2]	4701	4750	4919	2.5	2	-0.1	-0.1	0.03	0 (+/- 0.03)
HD102212	M1III [16]	3892	4000	3893	1.2	0.5	-0.1	-0.5	0	0 (+/- 0.07)
HD102780	K2	4215	4000	3799	0.5	1	-0.6	0.2	0.04	0 (+/- 0.05)
HD105546	G2IIIw [7]	5193	5750	5649	2.4	2.5	-1.4	-0.5	0.005	0.08 (+/- 0.009)
HD105740	G5	4804	5000	5166	2.4	2	-0.6	-0.3	0.02	0.09 (+/- 0.01)
HD106304	B9V	9696	9500	9663	3.6	3.5	-1.6	-0.5	Nan	0 (+/- 0.02)
HD106516	F9V [2]	6134	6500	6255	4.3	4.5	-0.7	-0.5	0.01	0.04 (+/- 0.009)
HD107582	G2V [2]	5637	5750	5731	4.4	4	-0.6	-0.3	0.01	0 (+/- 0.009)
HD108945	A2pv[12]	8909	9000	8895	3.7	4	0.2	0.5	0	0 (+/- 0.01)
HD109995	A0p [7]	8551	9500	10029	3.3	3.5	-1.5	-3	0.005	0.06 (+/- 0.02)
HD110885	G0	5696	5750	5767	2.6	2.5	-1.1	-1	0.006	0.06 (+/- 0.008)
HD111464	K3III	4207	4250	4274	1	1	-0.7	-0.3	0.1	0.06 (+/- 0.03)
HD111515	G8V [1]	5420	5750	5688	4.5	4	-0.5	0.1	0.009	0.03 (+/- 0.01)
HD111721	G6V [1]	4979	5750	5685	2.8	3.5	-1.5	-0.3	0.02	0.16 (+/- 0.01)
HD111786	A0III [5]	8162	7750	7216	4	4	-1.45	-3	0.023	0.05 (+/- 0.01)
HD113002	K0 [1]	5192	5750	5741	2.7	3.5	-0.8	-0.2	0.02	0.12 (+/- 0.01)

Table A.9 Continuation

Star	SP Type	T_{eff} NGSL	T_{eff} QFA	T_{eff} ec.	*logg* NGSL	*logg* QFA	$[Fe/H]$ NGSL	$[Fe/H]$ QFA	E(B-V) NGSL	E(B-V) QFA
HD113092	K2III	4378	4250	4355	2	1	-0.6	-0.5	0.024	0 (+/- 0.02)
HD114330	A1IVs+ [4]	9529	9500	9087	3.7	3.5	-0.09	1	0.022	0 (+/- 0.01)
HD114710	G0V [1]	5956	6250	6030	4.4	4.5	0.08	0.1	0.005	0.05 (+/- 0.007)
HD115617	G7V [1]	5562	5750	5631	4.4	4	0	0.2	0.01	0.04 (+/- 0.007)
HD117880	B9IV/V	9231	9250	8871	3.5	3.5	-1.4	-1	0.08	0.04 (+/- 0.008)
HD118055	K0w	4330	4750	4713	0.8	0	-1.9	-1.5	0.05	0.2 (+/- 0.02)
HD121146	K2IV [1]	4521	4500	4581	2.5	2	-0.1	-0.1	0.002	0 (+/- 0.02)
HD122064	K3V [1]	4746	5000	5041	4.5	5	0.2	0.5	Nan	0.08 (+/- 0.02)
HD122956	G6IV/Vw	4646	5000	5057	1.4	1	-1.8	-1	0.04	0.13 (+/- 0.007)
HD124186	K4III	4303	4500	4489	2.3	2	0.3	0.2	0	0 (+/- 0.03)
HD124425	F6V [2]	6419	6750	6415	3.8	4	0.06	0.1	0.002	0.07 (+/- 0.008)
HD124547	K3III [2]	4227	4250	4200	1.7	1.5	-0.04	-0.2	Nan	0 (+/- 0.02)
HD126511	G5 [1]	5399	5500	5501	3.8	3.5	0.08	0.2	0.01	0 (+/- 0.009)
HD126614	K0V+MV [4]	5434	5500	5379	4.2	3	0.6	0.5	0.03	0 (+/- 0.02)
HD128000	K5III	4042	4000	3936	1.6	0.5	-0.06	-0.2	Nan	0 (+/- 0.03)
HD128279	G0 [1]	5244	5500	5610	2.8	3.5	-2.1	-2	0.045	0.05 (+/- 0.009)
HD128801	B9	10161	10000	9137	3.6	3.5	-1.4	-1	0.026	0 (+/- 0.008)
HD128987	G8Vk [8]	5588	5750	5601	4.6	4	0.04	0.3	0.011	0.03 (+/- 0.008)
HD132345	K3IIICN [4]	4361	4750	4778	2.1	2.5	0.24	0.5	0	0.12 (+/- 0.04)
HD132475	F5/F6V [5]	5687	6000	5972	3.8	4	-1.5	-1	0.02	0.05 (+/- 0.01)
HD134113	F9V [2]	5721	6000	5951	4.1	4	-0.7	-0.3	0.006	0.04 (+/- 0.008)
HD134439	K2V[1]	5016	5500	5489	4.5	3.5	-1.5	-0.1	0.008	0 (+/- 0.02)
HD134440	K2V [5]	4829	5500	5437	4.6	4.5	-1.4	0.1	0	0.12 (+/- 0.01)
HD138716	K1IV [1]	4787	5000	4886	3.3	3	-0.1	0.2	0.02	0 (+/- 0.02)
HD140232	A2m	8162	8000	7329	4.3	4	0.5	0	Nan	0 (+/- 0.01)
HD141851	A3Vn [9]	8355	8250	8236	3.9	4	-1.2	-3	0.27	0 (+/- 0.009)
HD142703	A2Ib/II [5]	7627	7250	6880	4	3.5	-1.2	-3	0.04	0 (+/- 0.02)
HD142860	F6IV [5]	6309	6500	6111	4.2	4.5	-0.2	-0.3	0.002	0 (+/- 0.01)
HD143459	A0Vs	9373	9750	9840	3.8	3.5	-0.9	-1.5	0.11	0.06 (+/- 0.02)
HD145328	K1III-IV [5]	4713	4750	4935	2.8	2.5	-0.2	-0.2	Nan	0 (+/- 0.02)
HD146051	M0.5III [5]	3770	3750	3831	1.2	0.5	-0.01	-0.3	0.015	0 (+/- 0.05)
HD146233	G2Va [5]	5834	6000	5716	4.3	4	0.06	0.2	0.005	0 (+/- 0.01)
HD147550	B9V [1]	9939	10500	10078	3.6	4	-0.1	-0.1	Nan	0.09 (+/- 0.01)
HD148293	K2III	4563	4750	4747	2.4	2	0.1	-0.1	Nan	0 (+/- 0.03)
HD148513	K4III	4281	4250	4098	2.1	1.5	-0.17	0.5	0	0 (+/- 0.03)

Table A.9 Continuation

Star	SP Type	T_{eff} NGSL	T_{eff} QFA	T_{eff} ec.	*logg* NGSL	*logg* QFA	$[Fe/H]$ NGSL	$[Fe/H]$ QFA	E(B-V) NGSL	E(B-V) QFA
HD149382	B5	24439	45000	33467	5.5	6.723	-1.3	Nan	0.08	0 (+/- 0.01)
HD160346	K3V [2]	4850	5000	5159	4.5	4.5	-0.05	0.2	0.02	0.06 (+/- 0.02)
HD160922	F4V [2]	6543	6750	6376	4.2	4.5	0.07	-0.1	0.001	0.02 (+/- 0.009)
HD161770	G0 [1]	5369	6000	5917	4.2	4	-1.9	-1	0.07	0.19 (+/- 0.009)
HD163346	A3	6915	7500	6959	3.1	3.5	-0.13	0	Nan	0.34 (+/- 0.02)
HD163641	B9III	10686	11500	12129	3.8	4	-0.02	0.3	Nan	0.07 (+/- 0.02)
HD163810	G3V [9]	5470	6000	5851	4.2	4.5	-1.4	-1	0.014	0.04 (+/- 0.009)
HD164257	A0 [17]	9327	9750	10053	3.2	3.5	0.34	1	Nan	0.11 (+/- 0.02)
HD164402	B0Iab/Ib [2]	17776	31000	23545	4.1	4	Nan	-0.5	0.22	0.24 (+/- 0.008)
HD164967	A0	9094	8250	8237	3.4	4	-0.6	-2.5	Nan	0 (+/- 0.01)
HD165195	K3p [5]	4482	4750	4697	1	0	-2.2	-2	0.11	0.29 (+/- 0.01)
HD165341	K0V [2]	5100	5500	5377	4.6	4.5	-0.07	0.2	0.016	0.04 (+/- 0.01)
HD166229	K2.5III [1]	4554	4750	4707	2.5	2.5	0.06	0.3	Nan	0 (+/- 0.03)
HD166283	A0	8368	8250	8303	3.7	4	-1	0	Nan	0.06 (+/- 0.01)
HD166991	A2	9062	8500	8298	3.9	4	-0.6	-0.5	Nan	0 (+/- 0.01)
HD167105	A0 [7]	9078	9000	9220	2.9	3.5	-1.4	0	0.038	0 (+/- 0.01)
HD167278	F2 [9]	6541	6750	6312	4.2	4.5	-0.15	-0.3	Nan	0 (+/- 0.008)
HD167946	A0	9942	10500	9497	3.5	4	-0.16	-1	Nan	0.05 (+/- 0.009)
HD169191	K3III	4331	4500	4538	2.1	1.5	-0.18	-0.2	Nan	0.07 (+/- 0.02)
HD170737	G8III-IV [2]	5192	5500	5600	3	3.5	-0.7	-0.2	0.03	0.12 (+/- 0.007)
HD170973	A0sp[12]	10431	11500	10813	3.6	3.5	0.8	1	0.05	0.08 (+/- 0.02)
HD172230	A5	7848	7750	8236	3	3.5	0.5	0.2	Nan	0.06 (+/- 0.02)
HD172506	F2	7042	7250	6755	4.3	4	-0.12	-1	Nan	0 (+/- 0.007)
HD173158	K0	4497	6250	5739	1	5	-0.6	1	Nan	0.8 (+/- 0.05)
HD174240	A1V	9403	9000	8964	3.9	3.5	-0.4	0.3	Nan	0 (+/- 0.02)
HD174959	B6IV	13786	14000	11992	3.8	4	-0.45	-0.1	0.04	0.04 (+/- 0.006)
HD174966	A3[14]	7625	7750	6902	3.9	4	-1.4	-0.5	Nan	0 (+/- 0.01)
HD175156	B3II	15486	16000	13784	3.6	3.5	0.4	-1	0.33	0.34 (+/- 0.009)
HD175305	G5III [1]	5027	5750	5630	2.5	3.5	-1.5	-0.3	0.02	0.09 (+/- 0.008)
HD175545	K2III	4443	4500	4578	2.6	2	0.16	-0.1	Nan	0 (+/- 0.02)
HD175640	B9III	11367	12000	11112	3.8	4	-0.3	0.1	0.044	0.06 (+/- 0.006)
HD175674	K3IIICN [9]	4281	4500	4689	1.8	2	-0.1	0.3	Nan	0.16 (+/- 0.04)
HD175805	F8 [4]	6300	6750	6283	4.1	4.5	0.11	0.2	0.011	0.08 (+/- 0.006)
HD176232	F0spe[12]	7752	7750	8508	4	4	0.24	0	0.038	0 (+/- 0.01)
HD181720	G1V [1]	5785	6000	5946	4.1	4	-0.6	-0.2	Nan	0.04 (+/- 0.008)

Table A.9 Continuation

Star	SP Type	T_{eff} NGSL	T_{eff} QFA	T_{eff} ec.	*logg* NGSL	*logg* QFA	$[Fe/H]$ NGSL	$[Fe/H]$ QFA	E(B-V) NGSL	E(B-V) QFA
HD183324	A0V[14]	9378	9250	8909	4.2	4.5	-1.3	-3	0.028	0 (+/- 0.01)
HD183915	Kp [18]	4295	4500	4544	1.4	1.5	-0.4	-0.2	Nan	0.08 (+/- 0.04)
HD184266	F2V [7]	5780	6000	5902	2.4	2	-1.5	-1	0.05	0.09 (+/- 0.01)
HD185144	K0V	5312	5500	5454	4.5	4.5	-0.2	0.2	0.003	0.04 (+/- 0.006)
HD185351	G9IIIbCN	4820	5250	5226	3.1	3	-0.04	0.2	0	0.07 (+/- 0.02)
HD187111	G8wv	4417	5250	5258	0.8	1	-1.8	-0.5	0.06	0.42 (+/- 0.02)
HD188262	G0	5279	6750	6226	4.5	3	-0.7	0.2	0	0.38 (+/- 0.04)
HD190073	A2IVe [18]	7502	9750	9562	3.5	2	-2.9	-3	0.002	0.18 (+/- 0.03)
HD190360	G7IV-V [4]	5336	5500	5541	4.2	3	0.2	0.1	0.008	0 (+/- 0.01)
HD191277	K3III	4394	4500	4589	2.5	2	0.09	-0.1	Nan	0 (+/- 0.03)
HD194453	A0	10098	10500	10546	3.2	4	0.05	0.5	Nan	0 (+/- 0.02)
HD195434	K0 [2]	4943	5250	5393	4.6	5	-0.7	-0.2	Nan	0.13 (+/- 0.01)
HD196218	F8	6232	6500	6268	4.2	4.5	-0.1	-0.1	0.003	0.06 (+/- 0.008)
HD196426	B8IIIp	9510	13000	11819	3.8	4	-0.2	-0.1	Nan	0 (+/- 0.01)
HD196662	B7III [9]	14339	15000	13690	3.6	4	0.1	-0.2	0.025	0.029 (+/- 0.006)
HD196725	K3Iab	4134	4250	4188	1.1	0.5	-0.2	-0.3	Nan	0.1 (+/- 0.02)
HD196892	F6V [1]	6002	6250	6173	4.1	4.5	-0.8	-1	0.006	0.05 (+/- 0.006)
HD197177	G8IIb [9]	4903	5250	5209	2.1	2.5	0.13	0.3	0.006	0.13 (+/- 0.02)
HD198809	G7III [5]	5126	5500	5477	2.8	3	-0.07	0.1	0	0.08 (+/- 0.02)
HD200081	G0	5242	6250	6033	3.2	4.5	-0.3	0.1	Nan	0.22 (+/- 0.03)
HD201091	K5V [8]	4221	4500	4566	4.5	4.5	-0.26	0.1	0.06	0 (+/- 0.02)
HD201377	A3	8343	8000	8382	3.9	4	-0.4	-1	Nan	0 (+/- 0.009)
HD201601	A9p [9]	7681	8000	8671	3.7	4.5	0.2	0.3	0.003	0.04 (+/- 0.008)
HD203638	K0III [5]	4558	4750	4848	2.2	2.5	0.1	0.3	0.01	0.07 (+/- 0.03)
HD204041	A1IV	8488	8000	8237	4.1	4	-0.8	-2.5	0.025	0 (+/- 0.02)
HD204155	G5 [1]	5843	6000	5864	4.1	4	-0.7	-0.3	0.002	0 (+/- 0.01)
HD204543	G0	4853	5250	5263	1.3	1	-1.8	-1	0.03	0.14 (+/- 0.01)
HD205202	F2 [1]	6614	6750	6486	3	4	-0.5	-1	0.008	0.04 (+/- 0.009)
HD205811	A2V [4]	8512	10000	10232	4	4.5	-0.3	-0.5	Nan	0 (+/- 0.02)
HD210807	G7II-III	4952	5500	5299	2.3	3	-0.2	0.3	0.034	0.09 (+/- 0.02)
HD212516	K5 [5]	3386	3750	3694	0.5	0.5	-0.6	-0.2	0.05	0 (+/- 0.06)
HD217107	G8IV	5572	6000	5754	4.3	4.5	0.3	0.5	0.007	0.07 (+/- 0.02)
HD217357	K7+Vk [1]	4094	4000	4081	4.8	2.5	-0.9	-0.1	0	0 (+/- 0.03)
HD221377	F7Vw [9]	6294	6750	6528	3.8	4	-0.8	-0.5	0.006	0.06 (+/- 0.01)
HD224926	B7III-IV [5]	12834	14000	12272	3.8	4	0.3	0.2	Nan	0.02 (+/- 0.006)

Table A.9 Continuation

Star	SP Type	T_{eff} NGSL	T_{eff} QFA	T_{eff} ec.	*logg* NGSL	*logg* QFA	$[Fe/H]$ NGSL	$[Fe/H]$ QFA	E(B-V) NGSL	E(B-V) QFA
HD284248	F2 [1]	6035	6250	6024	4.2	4	-1.6	-1.5	0.01	0 (+/- 0.008)
HD93521	O9Vp	25416	30000	24967	4	3.5	Nan	0.3	0.04	0 (+/- 0.02)
HR0753	K3V [4]	4915	5000	5075	4.6	5	-0.06	0.2	0.01	0 (+/- 0.02)
HR8086	K7V [10]	4166	4000	4138	4.5	3	-0.4	-0.2	0.06	0 (+/- 0.04)
HZ44	B2 [20]	27110	37500	35726	Nan	4.5	Nan	0	Nan	0 (+/- 0.01)
MMJ6476	A4	7300	7750	8314	Nan	4	Nan	0	Nan	0.07 (+/- 0.02)
MMJ6490	A2V	6456	8500	8920	3.9	4	0.02	0	0.03	0 (+/- 0.02)
P041C	Nan	5789	6000	5773	3.9	4	0.02	0.1	0.03	0 (+/- 0.01)
V*BNVul	A9.2 [3]	5119	7000	6941	2.4	2	-1.3	-3	0.27	0.41(+/- 0.03)
V*GKCom	M3 [16]	4385	3350	3494	Nan	4.5	-1.9	0	0.04	0 (+/- 0.12)

1. High proper-motion star
2. Spectroscopy Binary
3. Variable Star of RR Lyr type
4. Star in double system
5. Variable star
6. Peculiar star
7. Horizontal Branch Star
8. Variable of BY Dra type
9. Double or multiple star
10. Flare star
11. Variable of RS CVn type
12. Variable Star of alpha2 CVn type
13. Be star
14. Variable Star of delta Sct type
15. Variable Star of beta Cep type
16. Semi-regular pulsating Star
17. Ellipsoidal variable Star
18. Carbon Star
19. Emission-line Star
20. White Dwarf